University of Padova
Department of Physics and Astronomy “Galileo Galilei”
PhD course in Physics
2026

Disordered models in community ecology

PhD candidate
Francesco Ferraro

Supervisors
Prof. Sandro Azaele
Prof. Amos Maritan

Qualunque cosa sia il destino,
abita nelle montagne che abbiamo sopra la testa.
– Paolo Cognetti

Abstract

Disordered models, high-dimensional systems with random parameters, are relevant to community ecology for two main reasons. First, they generate empirical predictions: if these match observations, it suggests that detailed properties are unnecessary to explain community patterns; conversely, discrepancies signal the presence of non-random features or the need for alternative modeling assumptions. Second, disordered systems function as null models upon which specific structure can be imposed and its effects quantified. Motivated by this relevance, in this thesis we review foundational disordered ecological models and extend them to study the impact of ecologically realistic features on community stability, structure, and dynamics. We demonstrate that time-varying interactions can stabilize complexity, promote coexistence, and give rise to abundance distributions that better match experimental data. We also establish that introducing a non-linear saturating response resolves non-physical unbounded population growth. Furthermore, we show that the interplay of memory effects and community heterogeneity can lead to both periodic and aperiodic persistent fluctuations in species abundances. Overall, this thesis adds instruments to the theoretician's toolkit potentially useful for understanding the functioning of ecological communities and complex systems in general.

Acknowledgments

What an adventure! It is with a heart brimming with gratitude that I would like to thank all the extraordinary people who made this experience so rich with joy and meaning.

First and foremost, I wish to sincerely thank Amos and Sandro. From the very moment you welcomed me into the lab, you supported me, inspired me to produce my best work, and gave me the opportunity to conduct research that is as important as it is beautiful. I am deeply indebted for everything you taught me, both scientifically and personally. Your creativity, your integrity, your insightful and precise feedback, and your constant encouragement were the driving force behind this work. A special thank you also goes to Samir, who contributed so much through his brilliant ideas and inspiring, unwavering optimism. I am incredibly grateful to you all for cultivating a group where doing research has been such an enriching journey.

I warmly thank Maria Chiara Angelini and Tobias Galla for taking the time to carefully read this thesis and for valuable comments that have significantly improved it.

I would like to take this opportunity to also thank Stefano Allesina for so kindly hosting me in his lab in Chicago. Thank you for the great conversations and for sharing your insights and expertise.

I am deeply grateful for the company of all the members of LIPh, past and present, with whom I had the pleasure of sharing the highs and lows of this path. Special thanks go to Alice, Andrea, Clelia, Davide, Elisa, Fabione, Federico, Giorgio, Jack, Jacopo, Marcello and Marika. Thank you for all the great times, for the countless laughs, and for making the heavy days feel so much lighter. My heartfelt thanks go to Ema, Luca, Marco and Tom for our collaborations, which filled these years with the joy of shared discovery. I must reserve a very special mention for Christian il Saggio: grazie per avermi supportato, e sopportato, con imperitura pazienza.

To all my oldest friends, I still cannot believe how incredibly lucky I am to have you in my life. Your unconditional love and support mean more to me than I can ever fully express. A very special thank you to Ale, Ave, Fabi, Fiore, Gaia, Gallo, Isabella, Matte, Oni, Pigi, Silvia, Veronica and Zara.

Carlo and Miz, thank you for giving me a second wind, and letting me believe once more.

Finally, my deepest gratitude goes to my family: mom, dad, Benedetta and Gianluca.
I owe you everything. I love you, and this is for you.

Contents

Introduction

An estimated 9 million species inhabit Earth today [149, 274]. A primary goal of ecology is to understand the origin [17, 93] and consequences [31, 97] of this immense biodiversity, as well as to ensure its maintenance [57]. The fraction of the global pool of species inhabiting a specific local region is termed an ecological community. While communities exhibit profound heterogeneity, resulting in classification into over thirty biomes [29], they are not unstructured collections of organisms [37, 100]. Indeed, despite their substantial environmental and compositional differences, ecological communities display recurrent statistical regularities. All communities share some stylized properties: the stable coexistence of multiple species, heavy-tailed abundance distributions, the prevalence of rare species alongside a few dominant ones, and large abundance fluctuations [302]. At a quantitative level, these regularities manifest as robust macroecological patterns [147]. For instance, bacterial communities display universal forms for abundance fluctuations and mean distributions, as well as precise scaling behaviors [218].

The existence of non-trivial regularities amidst the diversity and complexity of ecological communities suggests the presence of underlying universal principles. Detailing such principles could enable, on a fundamental level, the explanation and prediction of macroecological patterns. Moreover, in an applied context, identifying the laws governing community structure and dynamics would facilitate the interpretation and contextualization of monitoring data. This capability, in turn, is essential for forecasting the future state of communities and enabling their control toward desired conditions.

To approach the theoretical modeling of ecological communities, two different perspectives can be adopted. The traditional ecological approach is typically mechanistic, focuses on a limited number of variables, and usually aims to describe a specific type of community. A textbook example is that removing sea otters from a kelp forest leads to a sea urchin population explosion and the disappearance of kelp [34]. While mechanistically precise, and often more useful in applied ecological practice, this approach struggles to explain universal community properties. The alternative is the complex systems approach, which deals with high-dimensional models and is often probabilistic in nature. An example is the classical prediction that highly diverse or numerous communities should be inherently less stable [31] (see Section 1.1).

An unavoidable limitation of high-dimensional models is that only their broad features can be constrained by ecological or mathematical arguments. For example, a dynamical model for species abundances results in the generalized Lotka-Volterra (GLV) equations following the assumption of multiplicative growth combined with a linear dependence of per-capita growth rates on species abundances. However, in this specific example, the parameters specifying the precise interactions between species are prohibitively numerous, often practically unknowable, or even conceptually ill-defined. These difficulties are ubiquitous in high-dimensional modeling. A possible way to circumvent these limitations is to adopt a disordered system perspective. This entails assuming

that unknown model parameters are drawn from random distributions characterized by a limited number of statistical properties. The resulting models can then be proficiently analyzed employing statistical mechanics tools originating from spin-glass physics [61, 260].

As mentioned in the abstract, disordered models are relevant to theoretical community ecology for two main reasons. First, they have the capacity to generate testable empirical predictions. These include the relationship between diversity and stability [31], macroecological patterns such as abundance distributions [186, 199], and the emergence of distinct dynamical regimes like the transition from stable fixed points to chaos [271, 281]. If these predictions align with empirical observations, it suggests that the disordered perspective is informative and possibly sufficient. This supports the parsimonious hypothesis that detailed biological and ecological structure is unnecessary to explain community patterns. Conversely, systematic deviations signal the relevance of non-random features or indicate the need for alternative modeling assumptions. Second, disordered systems serve as null models upon which additional structure can be superimposed [296]. By comparing the predictions of a structured model to the random one, the specific impact of particular features can be isolated. For instance, the linear null model introduced by May can be extended to incorporate structural constraints to analyze their effect on stability [153] (see Section 1.1).

Motivated by this twofold relevance, in this thesis we study disordered models of ecological communities. It focuses specifically on extending simple models to incorporate realistic ecological features and analyzing their impact on community stability, structure, and dynamics. The content is exclusively theoretical, with the sole exception of Section 4.6. Chapter 1 contains a brief review of the ideas and tools used to study disordered models. The main focus is on the GLV equations, a foundational model of community dynamics which is particularly amenable to a disordered system treatment. Chapter 2 introduces stochastic interactions, termed annealed disorder, into a linear model and provides its exact solution. Chapter 3 exploits these results to analyze the impact of time-varying interactions on the stability of a generic complex system. Chapter 4 introduces annealed disorder into the GLV equations and details the resulting community properties. Chapter 5 modifies the GLV model by incorporating a more realistic non-linear response. Chapter 6 develops general tools for the analysis of disordered models with time delays, which are then applied to the GLV equations to study the effects of memory on dynamical properties of complex ecological communities. In Chapter 7 the same methodologies are applied to a random neural network model with time delays. We conclude with general remarks on the work. A short appendix pays homage to the scientific achievements and civic stature of Vito Volterra.

Chapter 1

Disordered models in community ecology: a brief review

This chapter reviews disordered models employed in community ecology, establishing the theoretical basis for the subsequent chapters. We begin by illustrating May's model, which introduced disordered modeling into ecology to investigate the relationship between complexity and stability. We then focus on the generalized Lotka-Volterra (GLV) equations with random interactions, a foundational non-linear model for the dynamics of multi-species communities. We first examine the equilibrium properties of the random GLV model. This includes a detailed analysis of the unique fixed point phase using the cavity method, as well as a characterization of the multiple equilibria phase. We then address the dynamical properties of the random GLV model via Dynamical Mean-Field Theory. Finally, we survey extended GLV models and disordered consumer-resource models to provide a broader overview in the landscape of disordered ecological models.

1.1 May's disordered linear model

The seminal contribution of May [31] can be considered the introduction of the methods of high-dimensional disordered systems into theoretical ecology. Before this point, ecological theory had largely relied on the analysis of low-dimensional models or specific structural configurations. This methodological advance emerged in the context of one of the central themes of community ecology, which is the relationship between the complexity and stability of communities. Ecologists of the mid-twentieth century expected increased stability in structurally complex communities relative to simple ones. This expectation is intuitively appealing, given the astonishing diversity of natural ecosystems, and is consistent with worldwide efforts to reverse biodiversity loss [137, 269]. While initial theoretical and experimental evidence supported this view [13, 14, 17, 18, 22], this consensus was later disputed from various perspectives [19, 20, 23, 26]. As May observed, "simple mathematical models with many species are in general less stable than the corresponding simple mathematical models with few species" [98].

The work of May must be understood within the context of this debate regarding complexity and stability. He investigated the linear stability of a community composed of S interacting species,

This chapter is based on a review article currently being prepared in collaboration with Tommaso Jack Leonardi. As a co-first author, I shared responsibility for conducting the literature review, structuring the conceptual narrative, and preparing the text.

each with abundance x_i. Positing that the state of the community is fully determined by abundances, he assumed their dynamics follows a set of first-order differential equations:

$$\dot{x}_i = f_i(x_1, \ldots, x_S), \tag{1.1}$$

where f_i are non-linear functions. May focused on the linear stability of an equilibrium point of these dynamics. Small deviations $\delta x_i = x_i - x_i^*$ from equilibrium evolve under the linear dynamics

$$\delta\dot{x}_i = \sum_j J_{ij}\delta x_j, \tag{1.2}$$

where of course

$$J_{ij} = \frac{\partial f_i}{\partial x_j}(x^*) \tag{1.3}$$

is the Jacobian matrix evaluated at the equilibrium under consideration. In ecological literature, this is referred to as the community matrix [27, 98]. The entry J_{ij} quantifies the effect of the abundance of species j on the growth of species i near equilibrium. The equilibrium is linearly stable to perturbations if all eigenvalues of this matrix have negative real part.

To proceed, specifying the community dynamics seems inevitable. This corresponds to defining f_i, which subsequently determines J_{ij}. However, a functional choice for f_i alone could not suffice, as the Jacobian might depend heavily on specific parameter values. Furthermore, even with defined parameters, the dynamics could display multiple equilibria. While a systematic exploration of stability is viable for small systems, it becomes intractable as the number of species grows.

Confronted with this formidable predicament, May assumed each entry of the Jacobian matrix to be drawn randomly. This approach is expected to be informative in the limit of a large number of species. On a fundamental level, moreover, this limit allows one to isolate the effects of system structure, that is, the functional form of f_i, on stability independently of specific system size.

May assumed that, due to self-regulation, each species returns to its equilibrium abundance with a characteristic timescale, fixed by setting $J_{ii} = -1$ uniformly across species. Off-diagonal entries J_{ij} are then sampled from a distribution with zero mean and variance σ^2, with some entries set to zero to give the model a connectance C (fraction of non-zero entries). The circular law [24, 55, 145], a fundamental result in random matrix theory, describes the distribution of eigenvalues for such matrices. In the limit of large S, the eigenvalues in the complex plane are uniformly supported in a circle centered at $(-1, 0)$ with radius

$$R = \sigma\sqrt{SC}. \tag{1.4}$$

This spectral radius R is sometimes termed "complexity" in the ecological literature [180]. Based on this, May concluded that the community is stable only if the complexity satisfies the bound

$$R < 1. \tag{1.5}$$

This result suggests that complexity is detrimental to stability, a conclusion that ran contrary to the prevailing ecological intuition of the time. The tension between this theoretical finding and empirical observations sparked the complexity-stability debate [54, 78, 94, 159], which remains an active area of research [171, 184, 197, 243, 292].

It would be clearly naïve to infer from this result that less complex ecosystems are favored in nature, given the strong underlying assumption of random interactions. Real ecological communities

are not randomly assembled, but are shaped by a multitude of ecological and evolutionary mechanisms [148, 200, 219]. A possible interpretation of May's result is that real ecosystems persist due to specific non-random, stabilizing features. Such features can be imposed onto the disordered null model to assess their impact on stability. As May noted, "The task, therefore, is to elucidate the devious strategies which make for stability in enduring natural systems" [98].

For instance, a correlations between reciprocal interaction strengths can be incorporated into May's model by setting $\text{corr}(J_{ij}, J_{ji}) = \gamma$. Ecologically, $\gamma < 0$ represents a community dominated by predator-prey pairs, while $\gamma > 0$ indicates a prevalence of competitive and mutualistic pairs. The circular law generalizes to the elliptic law for such matrices [62], modifying the complexity bound to $(1 + \gamma)R < 1$. This yields a non-trivial hierarchy of stability, where predator-prey communities are predicted to be more stable than unstructured ones, which in turn are more stable than mixture communities [153].

In a similar vein, numerous extensions beyond May's null model have been considered. These include interaction structures [153, 181, 245], degree heterogeneity [192], self-regulation [165, 185], delayed interactions [111, 252, 275], dispersal [177, 214], time variability [52, 105, 206, 227, 237], modularity [178], and higher-order interactions [187], see for example [286] for a review. In this spirit, Chapter 3 extends May's model to incorporate time-varying interactions and analyzes their impact on stability. For comparisons with experimental data, see for instance [47, 66, 69, 79, 104, 130, 172, 180, 255].

It is crucial to remember that the Jacobian is derived from the linearization of a specific dynamics. Consequently, the community matrix inherits a precise structure from the underlying non-linear equations. Assuming this matrix to be random is therefore questionable, as such a matrix does not necessarily correspond to any dynamical system near a feasible equilibrium. Moreover, even if the linearized model were to represent valid dynamics near an equilibrium, it would yield information only on local linear stability. Natural communities, however, may persist in limit cycles or chaotic non-equilibrium states, and other definitions of stability might apply [286].

To address these concerns, non-linear analogs of May's model have been proposed [109, 125, 175, 232, 242, 258, 270, 326]. An alternative, more ecologically informed approach is to specify a functional form for the community dynamics. The canonical candidate for this is the generalized Lotka-Volterra model, as discussed in the next section.

1.2 Disordered generalized Lotka-Volterra equations

The disordered linear model considered by May presents some critical drawbacks which limit its ecological interpretability. To address these issues, a possibility is to move beyond the linear model and define a specific functional form for the community dynamics. Any choice of a dynamical model aimed at describing the evolution of an ecological community must first identify the variables of interest. Clearly, such a choice should reflect quantities that can be experimentally measured, ensuring the model is empirically testable. As ecological data primarily consist of species abundances, measured as the number of individuals or biomass [129, 160, 238], the standard approach is to posit that the state and dynamics of a community are fully determined by the abundances of focal species. The effects of external variables are either encoded in the parameters, or explicitly included as model extensions or noise. While alternative state variables such as resources, energy fluxes, and functional roles have been studied [95, 107], the role of abundance itself remains a core component to be understood [147].

The foundational model for the dynamics of an interacting community is provided by the

generalized Lotka-Volterra (GLV) equations [1, 2, 3, 5, 6, 7, 87]:

$$\dot{x}_i = r_i x_i \left(1 + \sum_{j=1}^{S} \alpha_{ij} x_j \right). \tag{1.6}$$

Here, x_i denotes the abundance of species i, out of S species, r_i represents its intrinsic growth rate, and α_{ij} quantifies the effect of species j on the growth of species i. Although the model assumes that interspecific influences on growth rates are linear, it can still represent a broad range of interaction types. We assume self-regulation via a negative diagonal term α_{ii}, which yields logistic growth for each species in isolation. We set the unit of abundance for each x_i by fixing

$$\alpha_{ii} = -1, \tag{1.7}$$

and for simplicity, we further assume $r_i = 1$ for all species.

The properties of the GLV equations for generic α_{ij} have been detailed extensively [87]. For a small number of species, a systematic exploration of the parameter space, classifying equilibria and dynamical regimes, is viable. However, as the number of species increases, this approach becomes prohibitively taxing, making a disordered systems perspective more informative. Consequently, we treat the unspecified parameters α_{ij} as random variables. We note that randomness is introduced here in a different manner than in May's disordered null model. While May imposed randomness directly on the Jacobian, which represents the linearized dynamics only near an equilibrium, here we assume randomness in the interaction coefficients themselves. This approach maintains a global non-linear dynamical model, rather than a local linear approximation.

We assume that interaction parameters are independent and that their statistical properties are fully determined at large S by the first two cumulants:

$$\begin{aligned} \text{mean}(\alpha_{ij}) &= \mu/S, \\ \text{var}(\alpha_{ij}) &= \sigma^2/S. \end{aligned} \tag{1.8}$$

The parameter μ determines the typical sign and strength of interactions: a positive μ implies a community with cooperative tendencies, whereas a negative μ indicates a predominantly competitive community. The parameter σ sets the degree of heterogeneity in the interactions, and in the limit $\sigma = 0$ the model becomes homogeneous.

Introducing statistical variation allows for heterogeneity in interactions, which can be related to the concept of species' niche space [168, 189]. Heterogeneity captures, for instance, fitness differences in a shared environment or non-uniform competition and mutualism arising from specific traits. This contrasts with neutral theory and facilitates the comparison of their respective empirical predictions [163, 174].

The scaling of the cumulants in Eq. (1.8) ensures that abundances remain finite in the $S \to \infty$ limit and allows for a meaningful comparison between self-regulation and interspecific interactions. We assume a distribution for the interactions such that only their first two cumulants dominate at large S. The more general, non-Gaussian case has been considered in [282, 316]. We also note that some studies have explored the regime of strong interactions, where the interaction term dominates significantly at large S [246, 247, 293, 315]. We further note that the scaling in Eq. (1.8) leads to interaction parameters that are not easily interpretable at the microscopic level, as is typically the case in disordered systems theory. For example, any specific α_{ij} yields a vanishing contribution to the interaction term at large S. Another consequence of this scaling is that, at leading order in S,

any specific α_{ij} is positive or negative with equal probability, regardless of μ. This indicates that the interaction parameters acquire meaning at the community level only, specifically through their collective contribution within the summation term.

In this framework, the random interaction parameters α_{ij} are quenched variables. This implies that the fluctuations of α_{ij} occur on a timescale far slower than the dynamics of the system itself. If the interactions were to fluctuate on a timescale comparable to the system dynamics, the disorder would be termed "annealed" in the terminology of spin glass theory. Models with annealed disorder are discussed in Chapters 2, 3 and 4.

1.2.1 Equilibrium properties

Depending on the specific values of the interaction parameters α_{ij}, the non-linear GLV equations Eq. (1.6) can exhibit a diverse range of dynamics: convergence to a fixed point, limit cycles, chaos, or unbounded growth. As a starting point, we analyze the properties of the equilibria as the statistics of the interaction matrix are varied. The number of equilibria and their stability provide foundational information regarding the dynamics displayed by the GLV system. The equilibria of the GLV equations are, of course, the abundances x_i satisfying

$$x_i \left(1 - x_i + \sum_{j \neq i} \alpha_{ij} x_j \right) = 0. \tag{1.9}$$

We restrict our analysis to the biologically relevant case of non-negative abundances. Because the non-negative orthant is an invariant set of the dynamics, any trajectory initialized with positive abundances remains positive at all times [87]. At equilibrium, each species satisfies either $x_i = 0$ or $1 - x_i + \sum_{j \neq i} \alpha_{ij} x_j = 0$. As each of the S species is subject to this binary condition, there exist exactly 2^S possible support sets. Provided the interaction matrix is non-singular, a condition met almost surely in the random case, each subset yields a unique linear system with a single mathematical solution. Consequently, the GLV equations admit a maximum of 2^S theoretical equilibria. In practice, this total is reduced because many solutions produce non-physical negative abundances. Explicitly determining the equilibria of the GLV equations and deriving their stability constitutes a Linear Complementarity Problem [279], the complexity of which scales exponentially with the number of species.

A significant simplification arises in the disordered case. In the limit $S \to \infty$, we expect the dynamical behavior to depend on the statistical properties of the interaction matrix only, and that self-averaging observables will provide a complete description of any typical realization of the system.

In the limit $\sigma = 0$ the model is homogeneous. For $\mu < 1$, all species coexist and reach a unique, globally stable fixed point. Conversely, for $\mu > 1$, cooperative interactions overwhelm self-regulation, causing abundances to grow without bound in finite time. By continuity, we expect that for small interaction heterogeneity σ the GLV equations will retain this behavior. This is formalized in [279], where it is shown that weak heterogeneity preserves the existence of a feasible equilibrium, which is guaranteed to be unique and globally stable [41, 87, 203].

1.2.1.1 Unique fixed point assumption and cavity method

Within the assumption of a unique fixed point, we expect for large S by central limit arguments that the interaction term $\sum_{j \neq i} \alpha_{ij} x_j$ will be Gaussian, since our scaling regulates fluctuations of

individual contributions. Once its statistics are known, then by employing Eq. (1.9) one can obtain the statistics of the fixed point. Unfortunately, it appears not straightforward to obtain the statistics of this interaction since α_{ij} and x_j are in principle correlated. The cavity method can be used to circumvent this obstacle, by showing that for large S this correlation is negligible. The statistics of the interaction term thus ultimately arises from the distributions of α_{ij} and of x_j independently. Using properties of the distribution of x_j at equilibrium for its own definition gives expressions that must be solved self-consistently.

The cavity method was originally introduced to derive equilibrium properties of the mean-field Sherrington-Kirkpatrick model of a spin-glass without resorting to the replica trick [59]. The method in the present case allows to compute the statistics of the fixed point by adding one species to an assembled community and assuming that, since the community is large, the resulting statistics are unchanged. It is particularly simple to state fully here, since in the language of spin-glasses we are working with a zero-temperature (without noise) and fully connected (all species pairs have non-zero interaction) model, and moreover within a replica-symmetric (RS) ansatz, which we will show to be correct up to intermediate values of the interaction heterogeneity σ, precisely up to the same bound obtained by May in his disordered linear model.

We now outline the procedure. Suppose we have a community at equilibrium, to which we add a new species $i = 0$ with interactions induced $\{\alpha_{0i}\}$ and felt $\{\alpha_{i0}\}$. Our objective is to obtain the value of the equilibrium abundance x_0 once the system has re-equilibrated. The equilibrium value of x_0 satisfies

$$x_0 \left(1 - x_0 + \sum_j \alpha_{0j} x_j \right) = 0, \tag{1.10}$$

and it either becomes extinct or gains a finite abundance. As anticipated, one would like to use the central limit theorem to give an estimate of the interaction term, however it is impeded by the fact that α_{0j} and x_j are formally correlated. We show that this correlation is in fact of the order of a single interaction, by propagating the perturbative effect of the cavity species.

If a small perturbation ξ_i is added to a non-extinct species as

$$1 - x_i + \sum_{j \neq i} \alpha_{ij} x_j + \xi_i = 0, \tag{1.11}$$

then the equilibrium abundances change as $x_i \to x_i + \sum_j v_{ij} \xi_j$, where the response field is $v_{ij} = \partial x_i / \partial \xi_j |_{\xi=0}$. This equation gives $\mathcal{O}(v_{ii}) \sim 1$ while $\mathcal{O}(v_{ij})|_{i \neq j} \sim 1/S$. In this way we see that the addition of species 0 adjusts the abundance of species j with the perturbation due to the new interaction $\xi_i = \alpha_{i0} x_0$, giving as follows for the community

$$x_j = x_{j \backslash 0} + \sum_k v_{jk} \alpha_{k0} x_0, \tag{1.12}$$

where $x_{j\backslash 0}$ is its abundance before the insertion of the new species. This correction itself cannot cause extinction of species j since alone it has order $1/S$, whereas all surviving equilibrium abundances $x_{j\backslash 0}$ are finite. In a similar way it does not bring the species back from extinction, and so the extinct proportion of species remains the same.

Inserting these shifted abundances into our expression for the abundance of the introduced species itself we get

$$x_0 \left(1 - x_0 + \sum_j \alpha_{0j} x_{j \backslash 0} + x_0 \sum_{jk} v_{jk} \alpha_{0j} \alpha_{k0} \right) = 0. \tag{1.13}$$

Now, the first sum in the bracket is clearly composed of independent variables α_{0j} and $x_{j\setminus 0}$. The second sum can only contribute for $j = k$ as $v_{j\neq k} \ll v_{jj}$ and only if there are finite correlations of $\langle \alpha_{0j}\alpha_{j0}\rangle - \langle \alpha_{0j}\rangle\langle \alpha_{j0}\rangle = \gamma\sigma^2/S$. Taking into account these for completeness, defining $\chi = \langle v_{jj}\rangle$, we have

$$x_0\left(1 - x_0 + \frac{1}{S}\sum_j \mu x_{j\setminus 0} + \frac{1}{\sqrt{S}}\sum_j \sigma x_{j\setminus 0}z + \frac{x_0}{S}\sum_j v_{jj}\gamma\sigma^2\right) = 0, \tag{1.14}$$

which results in

$$x_0\left(1 - x_0 + \mu M + \sigma\sqrt{q}z + x_0\chi\gamma\sigma^2\right) = 0, \tag{1.15}$$

where $M = \langle x_{j\setminus 0}\rangle$ and $q = \langle x^2_{j\setminus 0}\rangle$ and z is a zero-mean, unit-variance Gaussian variable. From this condition on x_0 it follows that the equilibrium abundance must be be

$$x(z) = \max\left(0, \frac{1 + \mu M + \sigma\sqrt{q}z}{1 - \gamma\sigma^2\chi}\right). \tag{1.16}$$

We notice that we omit the subscript 0 since this species, after it is inserted and it has reached equilibrium, is statistically identical to all other species. This is the crucial observation of the cavity method. Another point of view is that one can also imagine taking an assembled community and removing a species, thus creating a cavity, hence the name of the method. To compute the equilibrium abundance after the insertion one could follow the same reasoning as before. In any case, the conclusion is that the distribution of any species in an assembled community will be given by Eq. (1.16).

1.2.1.2 Unique fixed point properties

The regime in which the system possesses a unique, globally stable fixed point corresponds to a phase of replica symmetry. This means that for any given realization of the disorder, the system converges to the same equilibrium regardless of initial conditions. Furthermore, while specific equilibrium abundances differ across realizations of α_{ij}, their statistical properties are self-averaging. The self-consistent cavity Eq. (1.16) determines the statistics of the equilibrium abundances, providing a complete characterization of the community structure. The Species Abundance Distribution (SAD) is a truncated Gaussian, with a probability mass at zero representing extinct species.

The equilibrium will be strictly positive for values of $z > -\Delta$, where

$$\Delta = \frac{1 + \mu M}{\sigma\sqrt{q}}. \tag{1.17}$$

For $\gamma = 0$, the moments of $x(z)$ are then given by

$$\langle x^k\rangle = (\sigma\sqrt{q})^k w_k(\Delta), \tag{1.18}$$

with

$$w_k(\Delta) = \int_{-\Delta}^{\infty} dz \frac{e^{-z^2/2}}{\sqrt{2\pi}}(z + \Delta)^k. \tag{1.19}$$

Since $q = \langle x^2\rangle$, from Eq. (1.18) it follows that $1 = \sigma^2 w_2(\Delta)$ and thus $\Delta = w_2^{-1}(1/\sigma^2)$. With Δ known, all properties of equilibrium can be obtained. The fraction of non-extinct species in the

community ϕ, the mean abundance M and the second moment q are

$$\begin{aligned} \phi &= w_0(\Delta), \\ M &= \frac{w_1(\Delta)}{\Delta - \mu w_1(\Delta)}, \\ q &= \frac{1}{\sigma^2(\Delta - \mu w_1(\Delta))^2}. \end{aligned} \tag{1.20}$$

These relations can be generalized in a straightforward way to the case $\gamma \neq 0$.

1.2.1.3 Unbounded growth

Inspecting Eq. (1.20) reveals that for specific parameter combinations, the mean abundance and second moment diverge. For $\gamma = 0$, the condition for this divergence is given by $\Delta - \mu w_1(\Delta) = 0$. This defines a critical boundary in the μ-σ plane, generalizing the $\mu = 1$ limit of the homogeneous model. Beyond this line, the unique fixed point is lost to unbounded growth. This phase is non-physical, as real biological populations are inevitably limited by finite resources or higher-order self-regulation mechanisms. Introducing a saturating response in the GLV equations can eliminate this divergent regime [226], see also Chapter 5.

1.2.1.4 Unique fixed point stability

As previously discussed, the unique fixed point assumption is expected to hold in the limit of weak heterogeneity. However, as the variance of the interactions increases, disorder and frustration are expected to play a dominant role, inducing complex behaviors analogous to those found in other spin glass models [61, 260]. The assumption of a unique, stable fixed point breaks down at a critical threshold of heterogeneity. Specifically, instability emerges precisely when the surviving community reaches the critical complexity predicted by the May bound.

The Jacobian of the GLV equations evaluated at a generic equilibrium $\{x_i\}$ is given by

$$J_{ij} = \begin{cases} 1 - 2x_i + \sum_k \alpha_{ik} x_k & i = j \\ x_i \alpha_{ij} & i \neq j \end{cases} . \tag{1.21}$$

From this equation we see that each row corresponding to an extinct species has zero entries for all columns except for the one on the diagonal. Moreover, since the linearized dynamics for extinct species is explicitly given by

$$\delta \dot{x}_i = \left(1 + \sum_{j \neq i} \alpha_{ij} x_j^*\right) \delta x_i \tag{1.22}$$

we see that, if the equilibrium is linearly stable, $J_{ii} = 1 + \sum_j \alpha_{ij} x_j$ must be negative for all extinct species. We can thus rearrange the Jacobian into a block triangular form, separating surviving and extinct species:

$$J = \begin{pmatrix} J' & B \\ 0 & D \end{pmatrix}. \tag{1.23}$$

Here, J' is the Jacobian restricted to the community of non-extinct species, and D is the diagonal block corresponding to extinct species. Since the entries of D are negative, the linear stability

is controlled entirely by the reduced Jacobian J'. The block B does not affect stability. For the surviving species, the equilibrium condition implies that the reduced Jacobian takes the simple form

$$J'_{ij} = x_i(\alpha_{ij} - \delta_{ij}). \tag{1.24}$$

In the case of the specific equilibrium implied by the unique fixed point assumption, the bulk of the spectrum of the interaction matrix restricted to non-extinct species obeys the universality principle. This non-trivial result is demonstrated in [257], and implies that this bulk is distributed uniformly in a circle centered at the origin with radius $\sigma\sqrt{\phi}$. It is interesting to note that the outlier of the reduced interaction matrix does not depend on its mean alone, as universality would dictate [257]. Since the equilibrium abundances of surviving species are strictly positive by definition, we have that

$$\text{sign}(\det J'_{ij}) = \text{sign}(\det(\alpha_{ij} - \delta_{ij})). \tag{1.25}$$

Consequently, the transition from stability to instability for the system J' coincides with the point at which a single eigenvalue of the matrix $\alpha_{ij} - \delta_{ij}$ crosses the imaginary axis. Thus, the change in stability of J' takes place exactly when the shifted interaction matrix becomes unstable. Given that universality holds for α_{ij}, stability is lost when the spectral radius of α equals unity, that is, $\sigma\sqrt{\phi} = 1$. This recovers the May bound, derived here for the subset of surviving species.

We can determine the critical heterogeneity using the cavity solution from the previous section. For $\gamma = 0$, recalling that $\phi = w_0(\Delta)$ and that the variance closure is $1 = \sigma^2 w_2(\Delta)$, the stability condition becomes $w_0(\Delta) = w_2(\Delta)$. Using the properties of the Gaussian integrals $w_k(\Delta)$, this equality holds only when $\Delta = 0$. This implies that at the transition, the fraction of surviving species is $\phi = w_0(0) = 1/2$. Substituting this into the May bound yields the critical value $\sigma = \sqrt{2}$. Thus, at this value of heterogeneity, the unique fixed point of the random GLV equations loses linear stability. In fact, this point also represents, non-trivially, loss of replica symmetry, that is, global stability, as well as loss of uniqueness. The argument can be generalized to the case $\gamma \neq 0$, yielding

$$\sigma = \frac{\sqrt{2}}{1+\gamma}. \tag{1.26}$$

This instability can also be understood from a dynamical point of view, see Section 1.2.2.2. To sum up, the phase diagram for the system is the one reported in Figure 1.1.

1.2.1.5 Multiple equilibria

Upon the breakdown of stability, the assumption of a unique equilibrium is no longer valid. Beyond the critical threshold, the system enters a phase where the dynamics may settle into one of many alternative stable states, or exhibit complex non-equilibrium behaviors such as high-dimensional chaos. This phase is termed Multiple Attractors (MA). Qualitatively, increasing γ tends to reduce volatility for a finite number of species, as in the limit of symmetric interactions $\gamma = 1$ the GLV equations admit a Lyapunov function, see Section 1.2.1.6.

While the unique equilibrium phase can be comprehensively characterized by its distribution, describing the multiple attractor phase is significantly more challenging. It requires quantifying the number of equilibria, their diversity, and their stability properties. Quantitative results in this regime can be obtained by employing more sophisticated techniques from the theory of disordered systems. The application of these methods to ecological models is particularly significant because, for generic asymmetric interactions, the GLV equations represent a non-conservative system. Unlike

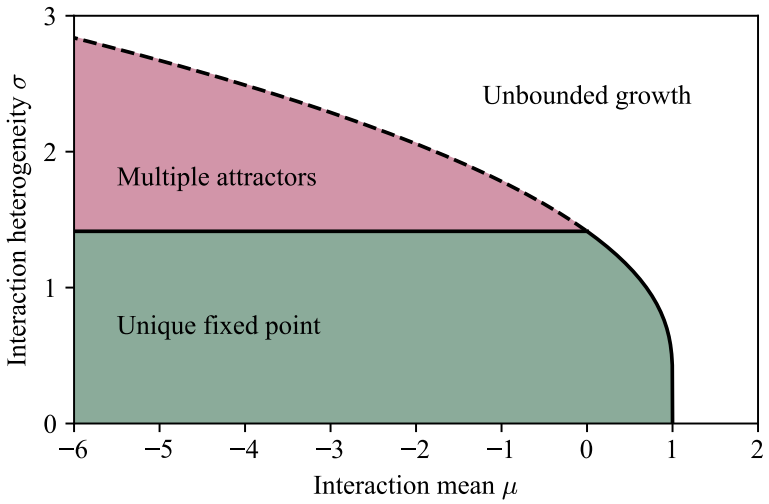

Figure 1.1: Phase diagram of the GLV equations Eq. (1.6) as a function of the interaction statistics, defined in Eq. (1.8). In the UFP phase, the model possesses a unique and stable fixed point, reached from any initial condition. The SAD is a truncated Gaussian, see Eq. (1.16), with parameters obtained as in Section 1.2.1.2. In the MA phase, multiple fixed points exist. The dynamics may settle into one of the multiple attractors or persist in non-equilibrium fluctuations. In the third phase, abundances grow without bound in finite time. The dashed line separating the MA and UG phases is approximate, obtained as the analytic continuation of the boundary separating the UFP and UG phases. The diagram shown is for asymmetric interactions $\gamma = 0$.

equilibrium settings, the dynamics cannot be described as gradient descent on an energy landscape, requiring a generalization of standard analysis.

The replicated Kac-Rice method enables the determination of the typical number of equilibria in a high-dimensional random dynamical system. The starting point is the Kac formula [8]

$$Z = \int dx_1 \dots dx_S \, \delta(f_1) \dots \delta(f_S) \left| \det \left(\frac{\partial f_i}{\partial x_j} \right) \right| . \tag{1.27}$$

This integral counts the number of zeros of the functions f_i within the region of integration. When f_i depend on random parameters, Rice extended this result to derive an expression for the average number of zeros [10]. This extension is known as the Kac-Rice formula.

We specialize the Kac-Rice formula to count the equilibria of the GLV equations. Analogous to what happens in the unique fixed point phase, as discussed in Section 1.2.1.4, the linear stability of an uninvadable equilibrium is determined solely by its complexity $\phi\sigma^2$, see [272] for details. Consequently, counting the number of equilibria as a function of their diversity ϕ is essential for understanding their stability properties. Defining the per-capita growth rates as $g_i = 1 - x_i + \sum_{j \neq i} \alpha_{ij} x_j$, for a given realization of the disordered interaction parameters α_{ij}, the number of equilibria $Z(\phi)$ at a given fraction ϕ of non-extinct species is given by

$$Z(\phi) = \sum_{I : |I| = \phi S} \int \prod_i dx_i \prod_{i \in I} \theta(x_i) \delta(g_i) \prod_{i \notin I} \delta(x_i) \theta(-g_i) \left| \det \left(\frac{\partial g_i}{\partial x_j} \right) \right| . \tag{1.28}$$

Here, the summation extends over all possible subsets of species I with a number $|I| = \phi S$ of species present. The terms inside the integral enforce the various constraints. Specifically, for

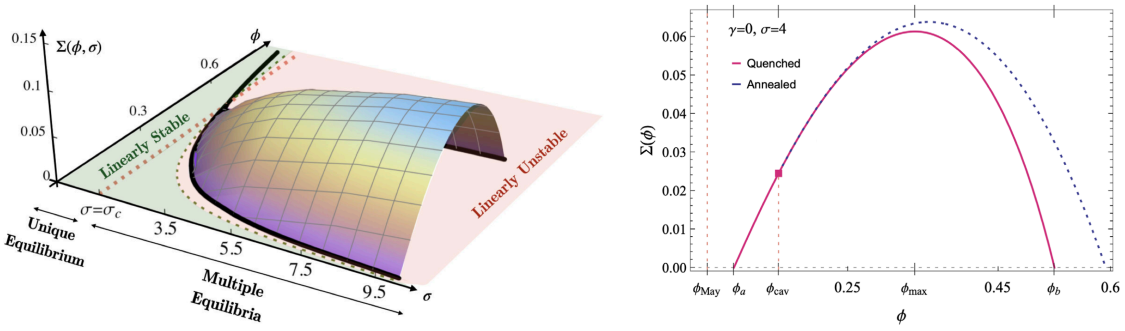

Figure 1.2: Left: Quenched complexity $\Sigma(\phi, \sigma)$ of uninvadable equilibria for $\gamma = 0$ within the replica-symmetric ansatz. Black lines indicate vanishing complexity. In the red area the richness ϕ predicts equilibria which are linearly unstable. Since the complexity is non-zero only in this region, it implies that in typical realizations of the disordered GLV equations all equilibria in the MA phase are expected to be linearly unstable. Right: A section of the plot on the left for a fixed value $\sigma = 4$. The complexity is positive only for $\phi > \phi_{\text{May}}$, indicating also in this case that all equilibria are unstable. The plot further shows comparison with the annealed complexity, see [271, 272] for more details. Taken from [271, 272]

the surviving species, the delta functions $\delta(g_i)$ enforce the equilibrium condition $g_i = 0$, while the Heaviside functions $\theta(x_i)$ ensure positive abundances. Conversely, for the extinct species ($i \notin I$), the delta functions $\delta(x_i)$ enforce zero abundance. Finally, the term $\theta(-g_i)$ imposes the uninvadability condition $g_j < 0$, which ensures that the equilibrium is stable against invasions by absent species.

The total number of equilibria in the multiple attractor phase is expected to scale exponentially with the number of species S. This is motivated by the analysis of the symmetric limit $\gamma = 1$, where the existence of an energy function enables the application of established spin-glass techniques, see Section 1.2.1.6. It also corresponds to the general phenomenology of glassy systems [61]. While the exact number of equilibria is a random variable that depends on the specific realization of the interaction parameters α_{ij}, the associated intensive quantity, which is the logarithm of this number normalized by S, is expected to be self-averaging. Consequently, it suffices to compute the average of this intensive quantity over the disorder to characterize the typical properties of the system.

This average is the so-called quenched complexity:

$$\Sigma(\phi) = \lim_{S\to\infty} \frac{\langle \log Z(\phi) \rangle}{S}. \tag{1.29}$$

To compute the average of the logarithm, it is convenient to employ the replica method

$$\langle \log Z(\phi) \rangle = \lim_{n\to 0} \frac{\langle Z(\phi)^n \rangle - 1}{n}, \tag{1.30}$$

which requires calculating the n-th moment of the number of equilibria. To achieve this, one introduces n replicas of the system. While these replicas are initially independent, averaging over the common disordered interactions induces an effective coupling between them.

This coupling between replicas can be summarized with order parameters of mean abundance and growth rate per replica, and the overlaps of abundance, growth rate, and abundance-growth rate. As usual in replica calculations, to proceed one must specify the structure of these order parameters. The only structure that has been considered is the replica-symmetric one, detailed in [271, 272]. Within this ansatz, replicas are treated as equivalent and the only parameters necessary specify

intra-replica or inter-replica properties. From the theory of conservative spin-glasses, it is known that more complicated variational ansätze might describe the macroscopic behavior of disordered models. The replica-symmetric assumption should therefore be confirmed via a stability analysis, which is currently lacking. Under the assumption of replica symmetry, the n-th moment can be expressed as an integral over the order parameters X

$$\langle Z(\phi)^n \rangle = \int dX \exp\left(nSA(X,\phi)\right), \tag{1.31}$$

where the explicit form of the action $A(X,\phi)$ is given in [271, 272]. In the $S \to \infty$ limit, the integral is dominated by the saddle point X^*, to be determined self-consistently, yielding the complexity

$$\Sigma(\phi) = A(X^*,\phi). \tag{1.32}$$

The behavior of the complexity is illustrated in Figure 1.2. As anticipated, the complexity is strictly positive, confirming the existence of an exponentially large number of equilibria. Crucially, the entire region where the complexity is non-zero corresponds to diversity values ϕ that exceed the linear stability threshold. Consequently, all typical uninvadable equilibria are expected to be linearly unstable. This suggests a complex dynamical evolution, potentially involving heteroclinic networks, where the system transiently approaches an equilibrium before being repelled along unstable directions. Future investigations should address the validity of the replica-symmetric ansatz in this regime, as well as clarify the role of invadable equilibria in shaping the resulting dynamics.

1.2.1.6 The symmetric case

It is instructive to examine in detail the special case in which the interaction matrix is symmetric, meaning that $\alpha_{ij} = \alpha_{ji}$ for all species pairs [196, 229]. Under this condition, the influence of species j on the growth of species i exactly mirrors the influence of species i on species j. Such perfect reciprocity is unlikely to hold in real ecological communities, although it can serve as an effective approximation for systems dominated by predominantly mutualistic or predominantly competitive interactions. Moreover, symmetry introduces substantial mathematical simplifications, which motivates a dedicated discussion of this regime.

The microscopic symmetry guaranteed by reciprocal interactions generally allows derivation from a Lyapunov function. This holds true for the GLV equations. Indeed, it is easily shown that there exists a Lyapunov function if and only if the interaction matrix is symmetric. This Lyapunov function is

$$H = \sum_i \left(x_i - \frac{1}{2}x_i^2\right) - \frac{1}{2}\sum_{i\neq j} \alpha_{ij} x_i x_j. \tag{1.33}$$

GLV trajectories will follow the gradient of this energy function as

$$\dot{x}_i = x_i \frac{\partial H}{\partial x_i}. \tag{1.34}$$

To characterize the multiple equilibria phase, one can then employ standard theoretical tools developed for equilibrium spin-glass systems.

Averaging the replicated partition function and taking the saddle point contribution, the single-body, effective Hamiltonian can be found as

$$H_{\text{eff}} = \sum_a \left(x^a - \frac{1}{2}(x^a)^2 \right) + \mu \sum_a m_a x^a - \beta\sigma^2 \sum_{a<b} q_{ab} x^a x^b - \frac{1}{2}\beta\sigma^2 \sum_a q_{aa}(x^a)^2. \quad (1.35)$$

Here the order parameters are mean abundance m_a for replica a and the replica overlaps q_{ab}. At saddle point these order parameters satisfy self-consistency equations determined by these definitions, averaged over the effective system.

As in Section 1.2.1.5, one first considers the replica-symmetric ansatz $q_{aa} = q_D$, $q_{ab} = q_0$, $m_a = m$. This allows writing down self-consistency equations for these parameters, which can be numerically solved to obtain the distribution of the abundances at equilibrium. Taking the limit $q_D - q_0 \to 0$ one obtains the same results of the cavity method presented above for $\gamma = 1$. Indeed, it is well established that a replica-symmetric ansatz yields the correct results for a system displaying an unique equilibrium. This corresponds to a phase in which the disordered component of the energy is dominated by the external potential, here due to the logistic growth term.

However, a stability analysis inspecting the replicon eigenvalue shows the replica-symmetric ansatz is not sufficient for a description of the system for the whole phase diagram. By increasing σ the model undergoes a phase transition at $\sigma = 1/\sqrt{2}$ and this simple, paramagnetic scenario is no longer applicable. One therefore assumes replica symmetry is broken and proceeds to investigate the one-step replica symmetry breaking ansatz. An analysis of the stability of this ansatz shows it also loses stability, yet with a replicon eigenvalue of reduced magnitude.

This hints strongly at the fact that any finite k-RSB is unstable in this system, and that the complete FRSB must be considered to describe the correct thermodynamical properties. This is not automatic after the replica-symmetric ansatz is shown to lose stability, as the p-spin spherical spin-glass for example is described fully by a 1-RSB [280]. The fact that replica-symmetry is broken yields two main consequences. First, the number of equilibria is expected to be exponential in the number of species. Second, they are all marginally stable [61]. The fact that equilibria in this regime are found numerically to be marginally stable would appear to confirm the full RSB is necessary, as it alone has this property.

Being marginally stable for the entire extended region implies the May bound $\sigma^2\phi = 1/4$ is satisfied in this whole phase and not just at the boundary. This can be interpreted as how, above the threshold of diversity set by May bound, randomly-assembled ecological communities are able to restore stability by dynamically reducing the coexisting species up until marginality. Marginality also implies critical properties such as slow relaxation and strong response, characteristic of strongly correlated and spin-glass phases.

1.2.2 Dynamical properties

In the previous sections, we analyzed the properties of the equilibria of the GLV equations with disordered interactions. However, since the assumption of a unique stable fixed point is not valid across the entire parameter space, a purely static analysis provides an incomplete picture. Moreover, from an ecological perspective, empirical communities are rarely static: they frequently exhibit complex non-equilibrium behaviors, ranging from periodic fluctuations to chaos [89, 133]. Consequently, in this section, we detail the dynamical properties of the GLV system.

The out-of-equilibrium dynamics of Eq. (1.6) present a rich phenomenology in the MA phase. While analyzing high-dimensional non-linear dynamics is generally analytically intractable, we

expect that an effective dimensional reduction, analogous to the methods previously used for statics, is possible. Dynamical Mean-Field Theory (DMFT) is the tool allowing this reduction [46, 50, 199, 289].

1.2.2.1 Dynamical Mean-Field Theory

In Eq. (1.6), each interaction term $\sum_{j\neq i}\alpha_{ij}x_j(t)$ is a time-dependent random variable, since the interactions α_{ij} are disordered, and moreover is Gaussian, by central limit theorem arguments. The intuitive picture behind DMFT is that all these interaction terms can be exchanged with a single, statistically equivalent Gaussian stochastic process.

To derive the DMFT equations, one can employ a dynamic variant of the cavity method [61, 211] or use generating functional techniques [32, 39, 40, 44, 289]. The resulting effective single-species process is given, in the case of uncorrelated couplings $\gamma = 0$, by

$$\dot{x}(t) = x(t)\left[1 - x(t) + \eta(t)\right], \tag{1.36}$$

where $\eta(t)$ is a Gaussian process with statistics fixed by

$$\begin{aligned} \langle\eta(t)\rangle &= \mu\langle x(t)\rangle, \\ \langle\eta(t)\eta(t')\rangle_c &= \sigma^2\langle x(t)x(t')\rangle. \end{aligned} \tag{1.37}$$

The averages in Eq. (1.37) are understood to be over all realizations of the noise in Eq. (1.36) and the notation $\langle\ldots\rangle_c$ indicates the connected correlation function.

The DMFT equation is stochastic, non-Markovian, and self-consistent. These properties arise as a consequence of the dimensional reduction. Stochasticity arises as a substitute for the disordered realization of the interaction parameters, while non-Markovianity appears as the interactions between species are exchanged with couplings between different times. The self-consistency is analogous to the one appearing in static mean-field methods.

We observe that while the noise $\eta(t)$ is Gaussian, the resulting abundance process $x(t)$ is generally non-Gaussian due to the non-linearity of the dynamics. The Gaussian nature of $\eta(t)$ follows strictly from the scaling of the interaction parameters together with the assumption that only the first two cumulants of α_{ij} dominate at large S. If this assumption were relaxed, $\eta(t)$ would depend on higher-order statistics of $x(t)$, see [282, 316] for more details on this.

When a correlation γ between reciprocal interactions is included, the DMFT equation generalizes to include an explicit memory kernel [199, 289]:

$$\dot{x}(t) = x(t)\left[1 - x(t) + \gamma\sigma^2\int_0^t dt' G(t,t')x(t') + \eta(t)\right]. \tag{1.38}$$

Here, $G(t,t')$ is the response function, defined as the linear response of the mean abundance at time t to a perturbation in growth rate at time t':

$$G(t,t') = \frac{\delta\langle x(t)\rangle}{\delta\eta(t')}. \tag{1.39}$$

It can be shown analytically that the response function satisfies the boundary condition $G(t,t) = \langle x(t)\rangle$ [211]. Furthermore, the integrated stationary response satisfies $\int_0^\infty d\tau G(\tau) = \chi$, where χ corresponds to the static susceptibility derived via the cavity method, see below. A simple approximation for the stationary response function that respects these constraints is an exponential decay: $G(\tau) = \langle x\rangle\exp(-\langle x\rangle\tau/\chi)$. This approximation is employed for example in Chapter 6.

1.2.2.2 Unique fixed point properties via DMFT

DMFT provides an alternative derivation of the static results previously obtained via the cavity method. We assume that the dynamics in Eq. (1.36) reach a stable fixed point, such that $x(t) \to x$ as $t \to \infty$. Under this assumption, Eq. (1.37) implies that the stochastic process $\eta(t)$ reduces to a static Gaussian variable η [199, 289], with statistics:

$$\begin{aligned} \text{mean}(\eta) &= \mu\langle x\rangle, \\ \text{var}(\eta) &= \sigma\langle x^2\rangle. \end{aligned} \tag{1.40}$$

Assuming time-translational invariance at stationarity, such that $G(t,t') = G(t-t')$, the fixed point equation becomes, from Eq. (1.38), $x(1 - x + \gamma\sigma^2\chi x + \eta) = 0$, where $\chi = \int_0^\infty dt G(t)$ represents the static susceptibility. This yields

$$x = \max\left(0, \frac{1+\eta}{1-\gamma\sigma^2\chi}\right), \tag{1.41}$$

which coincides with Eq. (1.16). The static susceptibility must satisfy the self-consistency condition $\chi = \partial\langle x\rangle/\partial\eta$ [199, 289].

DMFT also allows us to deepen our understanding of the previous result on the loss of validity of the UFP assumption from a dynamical perspective. We inspect the autocorrelation at stationarity and see at a specific value of heterogeneity this object is no longer well-defined, indicating that the system is linearly unstable. In general, divergence of autocorrelation does not correspond exactly with linear instability [316]. For the GLV equations with Gaussian disorder, however, it can be explicitly shown through probing the stability of the reduced interaction matrix alone that investigating the autocorrelation is sufficient. This dynamical method can also detect the loss of validity of the UFP assumption also in other situations, see Chapter 6.

To formally derive the stability condition, we introduce a small white noise perturbation $\xi(t)$ in the growth rate to the DMFT equation as

$$\dot{x}(t) = x(t)\left[1 - x(t) + \eta(t) + \xi(t)\right], \tag{1.42}$$

and study the resulting fluctuations about the fixed point $\delta x(t) = x(t) - x$. We look at the autocorrelation $\delta C(t) = \langle \delta x(t)\delta x(0)\rangle$ at stationarity. The transform of this autocorrelation is

$$\delta C(\omega) = \frac{B(\omega)}{1 - \sigma^2 B(\omega)}, \tag{1.43}$$

where

$$B(\omega) = \langle \left| \frac{i\omega}{x} + 1 - \gamma\sigma^2 G(\omega) \right|^{-2} \rangle. \tag{1.44}$$

The fixed point is linearly unstable if perturbations fail to decay, which corresponds to a divergence in $\delta C(\omega)$. This occurs if there exists a frequency ω such that the denominator vanishes, $1 - \sigma^2 B(\omega) = 0$. For the GLV equations, the function $B(\omega)$ is monotonically decreasing with ω, meaning the instability first occurs at the static limit $\omega = 0$. Evaluating the condition at zero frequency yields the critical boundary

$$\sigma = \frac{\sqrt{2}}{1+\gamma}, \tag{1.45}$$

which is the May bound found before.

Thus, the dynamical analysis confirms that beyond this critical heterogeneity, perturbations at any point in time will not decay, signaling the breakdown of the unique stable equilibrium and the onset of more complex dynamics.

1.2.2.3 Persistent species turnover

Having established that the unique equilibrium assumption breaks down beyond the May bound, we now turn to the dynamical behavior in the MA phase.

In the case $\gamma < 1$ the dynamics in this phase is expected to be chaotic. As discussed in Section 1.2.1.5, we expect an exponentially large number (in the number of species) of equilibria, all of which are predicted to be linearly unstable. Numerical integration of the GLV dynamics beyond the May bound supports this conclusion, revealing a state of persistent non-equilibrium fluctuations. Detailed numerical explorations of this phase are reported in [211], as well as in spatially coupled systems where complex spatiotemporal patterns emerge [225]. In this regime a continuous turnover of species is observed, with populations fluctuating between rarity and dominance.

An analytical description of the MA phase using DMFT is provided in [281]. To analyze this regime, we consider the GLV dynamics within the DMFT framework, in which a small immigration rate λ is added:

$$\dot{x}(t) = x(t)\,[1 - x(t) + \eta(t)] + \lambda. \tag{1.46}$$

We introduce this immigration term since the case $\lambda = 0$ is singular, in the sense that it differs from the limit $\lambda \to 0^+$, as discuss below and in Section 1.2.2.4. Introducing this immigration ensures that all species maintain a minimum abundance λ at all times.

The relevant timescale for the dynamics in this regime is set by $|\log \lambda|$, which represents the characteristic time required for a species to grow from the immigration floor $x \sim \lambda$ to carrying capacity $x \sim O(1)$ under multiplicative growth. By rescaling time and abundance as $s = t/|\log \lambda|$ and $z(s) = \log x(t)/|\log \lambda|$, the dynamics is equivalently described by the reduced equation

$$z'(s) = 1 + \eta(s), \tag{1.47}$$

with the important feature that this process is confined within the interval $-1 \leq z(s) \leq 0$. The boundaries become sharp in the limit $\lambda \to 0^+$. The lower boundary at $z = -1$ corresponds to the immigration floor, while the upper boundary at $z = 0$ corresponds to the self-regulation limit where abundances are $O(1)$. To close the DMFT loop, one must express the self-consistency relations for $\eta(s)$ in terms of $z(s)$. Inverting the coordinate transformation yields $x(s) = \exp(|\log \lambda| z(s))$. While it's clear that $x = 0$ for $z < 0$ in the limit $\lambda \to 0^+$, a more careful analysis is needed for $z = 0$. For $z = 0$, it turns out that $x(s) = 1 + \eta(s)$. The relation of $x(s)$ in terms of $z(s)$ is therefore

$$x(s) = [1 + \eta(s)]\,\theta(z(s)), \tag{1.48}$$

where $\theta(z)$ is the Heaviside theta with the convention $\theta(0) = 1$. Inserting this relation into the DMFT self-consistency equations yields a closed description of the process $z(s)$.

An example of the dynamics of $z(s)$, supplemented with $x(s)$ using Eq. (1.48), is given in Figure 1.3. The variable $z(s)$ alternates between sticking to the boundaries and transiting the intermediate region. In the rescaled time s, the abundance $x(s)$ spends finite intervals either at the extinction floor or at macroscopic abundance. Notably, $x(s)$ appears discontinuous in this rescaled limit, jumping instantaneously from extinction to finite abundance, while returning to zero via a continuous decay.

The properties of the process $z(s)$ suggest two alternative definitions for the fraction of active species at stationarity. The first is the fraction of species with macroscopic abundance, $\phi_{\text{top}} = \text{Prob}(z = 0)$. The second includes rare species lying above the immigration floor, $\phi_{\text{inter}} = 1 - \text{Prob}(z = -1)$. Interestingly, the macroscopic community defined by ϕ_{top} never

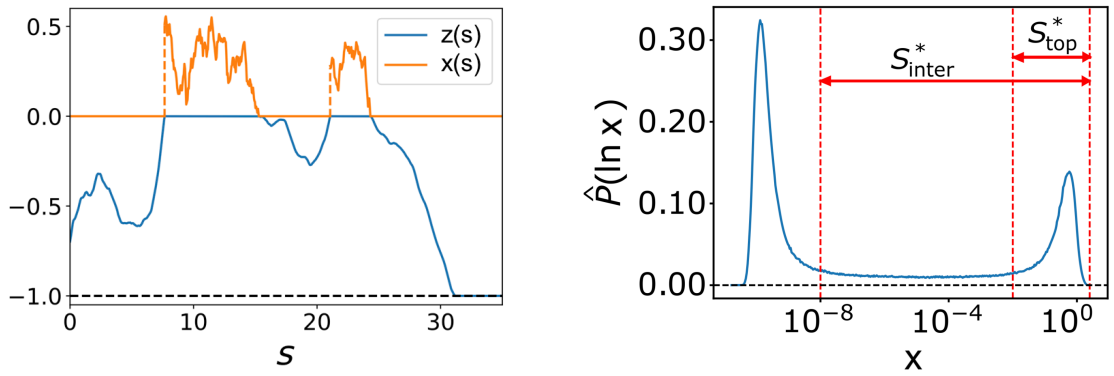

Figure 1.3: Left: Example dynamics of the disordered GLV equations in the MA phase for $\lambda \to 0^+$. The plot shows the trajectories of a representative species $x(s)$ and its rescaling $z(s) = \log x(s)/|\log \lambda|$ in the rescaled time $s = t/|\log \lambda|$. The species displays both positive and vanishing abundance in finite intervals time, and jumps discontinuously from near-extinct to abundant. Right: The corresponding SAD. Taken from [281].

violates the May bound. Specifically, $\sigma^2\phi_{\text{top}} < 1$ at all times. This implies that the instantaneous sub-community of abundant species is always linearly stable. However, the global equilibrium is continuously destabilized by the invasion of rare species, driving the persistent turnover.

From the distribution of z in the intermediate region, one can derive the SAD for rare species. Transforming back to the original variable x, the distribution takes the form:

$$P(x) = \frac{1}{x|\log\lambda|} h\left(\frac{\log x}{|\log\lambda|}\right), \tag{1.49}$$

where $h(z)$ is a dimensionless scaling function. This form provides a theoretical mechanism for the emergence of a power-law abundance distributions, with an exponent of -1, see Figure 1.3.

Finally, we consider the case of strictly $\lambda = 0$. The preceding analysis implies that the characteristic timescale diverges, leading to a dynamical slowing down, see next section. A logarithmic rescaling of time $s = \log t$ allows for a closed description of $z(s)$ in this limit, where the hard wall at $z = -1$ is replaced by a soft quadratic potential extending over $z < 0$.

The work [281] also presents a thorough analysis of finite-S effects and small but finite λ. Importantly, these predictions are found to be robust for generic correlations $-1 < \gamma < 1$.

1.2.2.4 Aging by near-extinction

As discussed in the previous section, the GLV model with random interactions exhibits a dynamical slowing down throughout the MA phase when $\lambda = 0$. Consequently, the system fails to settle into a stationary state, continuing to evolve indefinitely, a phenomenon termed "aging". However, we note that the origin of aging in this context differs fundamentally from the mechanisms typically observed in spin glasses [72, 81, 196, 229, 250] or critical systems [42, 75, 114, 166]. Rather than arising from a rugged landscape with marginally stable minima, aging in the GLV framework is conjectured to be driven by the presence of robust heteroclinic orbits connecting unstable fixed points, analogous to behavior observed in certain low-dimensional dynamical systems [38, 77, 85].

To investigate this phenomenon in the high-dimensional limit, the authors of [256] proposed an

exactly solvable population dynamics model defined by

$$\dot{x}_i(t) = x_i(t)[1 - x_i(t)] \sum_{j=1}^{S} \alpha_{ij} x_j(t), \tag{1.50}$$

where $x_i \in [0, 1]$ and the statistics of the matrix are $\langle \alpha_{ij} \rangle = 0$ and $\langle \alpha_{ij}^2 \rangle = 1/S$. Unlike the GLV model, which possesses a highly complex fixed-point structure, this formulation imposes two absorbing boundaries $x_i = 0$ and $x_i = 1$ for each variable. This structure allows for the isolation of dynamics driven by near-extinction and saturation processes while maintaining analytical tractability.

The dynamics are characterized by variables spending exponentially long periods near the absorbing boundaries, creating population near-extinctions and blooms. These timescales grow concurrently with the age of the system. The autocorrelation function $C(t, t')$ displays aging behavior, taking the scaling form, as $t' \to \infty$

$$C(t' + \tau, t') \sim \hat{C}(\log(1 + \tau/t')), \tag{1.51}$$

indicating that the correlation time scales linearly with the system age t'. By employing the coordinate transformation $u_i(t) = \log[x_i(t)/(1 - x_i(t))]$ and rescaling time to logarithmic coordinates $s = \log t$, the dynamics can be mapped onto a time-translation-invariant process. In this representation, the mean-square displacement grows ballistically, $\langle u(t)^2 \rangle \sim t^2$. At long times, the probability distribution concentrates exponentially onto the boundaries, explicitly $\lim_{t\to\infty} P_t(x) = \frac{1}{2}[\delta(x) + \delta(x - 1)]$.

This reveals that the aging mechanism differs fundamentally from that of reciprocal glassy systems. In traditional spin glasses, aging is associated with the system exploring marginally stable fixed points. An analysis of the stability spectrum of the visited fixed points of Eq. (1.50) shows that approximately 14% of directions are unstable. Thus, the system evolves through a sequence of saddles that are exponentially rare compared to typical fixed points, which possess 50% unstable directions, yet are distinct from the marginally stable states that govern the dynamics of physical glasses.

1.2.2.5 Low-heterogeneity DMFT

We can derive a small σ, approximated DMFT equation by expanding the noise $\eta(t)$ at lowest order in σ. At $\sigma = 0$ the system is homogeneous, meaning all species follow identical dynamics, and consequently $\langle x(t)x(t') \rangle = x(t)x(t') + \text{h.o.t.}$, so that the autocorrelation of the noise at lowest order is given by $\langle \eta(t)\eta(t') \rangle_c = \sigma^2 \langle x(t)x(t') \rangle = \sigma^2 \langle x(t) \rangle \langle x(t') \rangle + \text{h.o.t.}$. Therefore we can approximate the noise at small σ as

$$\eta(t) \approx \mu \langle x(t) \rangle + \sigma z \langle x(t) \rangle, \tag{1.52}$$

where z is a quenched Gaussian variable with zero mean and unit variance. This expansion is generically valid for the DMFT equation associated to any disordered dynamical system. Moreover, it is expected to hold not only at low heterogeneity, but whenever correlations between $x(t)$ and $x(t')$ can be neglected. In the specific case of the GLV equations the approximation yields

$$\dot{x}(t) = x(t) \left[1 - x(t) + (\mu + \sigma z) \langle x(t) \rangle \right]. \tag{1.53}$$

This approximation has been employed for instance in [282] and also in Chapters 6 and 7.

1.2.2.6 Numerical solution of DMFT

It can be instructive to detail a numerical procedure for solving the DMFT Eq. (1.36). A celebrated approach, proposed in [70], essentially constructs the moments of $\eta(t)$ sequentially timestep by timestep. An alternative method, proposed in [211], construct the whole trajectory at once. We detail the latter method.

In the case of uncorrelated reciprocal interactions $\gamma = 0$, the problem reduces to finding a fixed point for the statistical moments of the noise $\eta(t)$. First, one defines the simulation window $[0, T]$ and introduces a discrete time grid t_i on it. The iterative strategy is the following.

1. Propose an initial guess for the mean and the covariance matrix of the noise $\eta(t)$. The mean will be a one-dimensional vector $M_i = \langle \eta(t_i) \rangle$ and the correlation matrix a two-dimensional matrix $C_{ij} = \langle \eta(t_i)\eta(t_j) \rangle$. Results are numerically found to be robust to the choice of initialization.

2. Generate a realization of $\eta(t)$ with this mean and correlation. Operatively, this is done by performing the Cholesky decomposition of the matrix C into $C = LL^T$, generating independent Gaussian variables z_i, and computing $\eta_i = M_i + \sum_j L_{ij} z_j$, which will be a sample path.

3. For each sample path of $\eta(t)$, numerically integrate the DMFT equation. Standard schemes such as RK4(5) are suitable for this purpose.

4. Repeat steps 2 and 3 a number of N_{trajs} times, obtaining multiple samples of $x(t)$

5. From the ensemble of N_{traj} trajectories $x(t)$, compute the new first two moments of the abundance, $\langle x(t) \rangle$ and $\langle x(t)x(t') \rangle$. Use the self-consistency equations to calculate the updated mean and covariance for the noise. To aid stability, a soft-update is often employed.

6. Repeat steps 2-5 until convergence is reached.

For further details on this iterative implementation, we refer to [211], which also details how to obtain the self-consistent memory kernel in the case $\gamma \neq 0$.

We note that a rigorous analysis of these numerical schemes is currently lacking. Open questions remain regarding the conditions for global convergence, the optimal choice of initial guesses, and the dependence of convergence speed on system parameters.

1.3 Extended generalized Lotka-Volterra models

We briefly survey here extensions of the disordered GLV model.

A fundamental question is whether the specific choice of the GLV functional form limits the generality of predictions. In [195], a comprehensive numerical exploration is presented, covering various extensions such as different interaction types, functional responses, network structures, and trait distributions. A key finding of this work is that macroscopic properties of the community are largely insensitive to microscopic details, suggesting that the disordered GLV model suffices to capture the essential phenomenology of complex ecosystems in many regimes.

In the specific case of symmetric interactions $\gamma = 1$ with demographic noise, it is shown in [196, 229] that the system can be mapped analytically to an equilibrium Hamiltonian, as discussed in Section 1.2.1.6. This mapping allows for a rigorous application of standard disordered systems

tools. This results in a comprehensive characterization of the MA phase, including the prediction of a so-called Gardner phase. In this phase, the basin of attraction of the stable state fractures into a hierarchical, fractal-like structure of marginally stable sub-basins, implying that the community becomes critically sensitive to perturbations and structural changes.

The baseline model assumes Gaussian-distributed interactions, but empirical interaction might deviate from this assumption. The effects of non-Gaussian interactions, which includes sparse matrices and strictly competitive or cooperative regimes, are detailed in [282, 316]. These studies highlight how deviations from Gaussianity can lead to additional phases, such as a Griffiths phase, where rare, strongly interacting species clusters dominate the macroscopic dynamics.

To address the non-physical unbounded growth observed in the linear GLV model at highly heterogeneous or cooperative couplings, modifications to the functional response have been proposed. An analytical study of GLV equations with a saturating response is provided in [226], see also Chapter 5. These non-linearities effectively cap population growth, eliminating the divergent phase and stabilizing the system at high interaction strengths. The role of the Allee effect, in which growth rates become negative at low densities, is explored in [244].

The standard framework relies on the assumption that interspecific interactions remain constant over time, acting as quenched disorder. However, in natural settings, interaction strengths fluctuate due to factors such as environmental stochasticity, seasonality, or behavioral plasticity. To capture this, the GLV model can be extended to include time-varying, or "annealed", interactions [188, 236, 254, 287, 314, 323]. This extension can alter community properties and is one of the two main focuses of this thesis. We introduce annealed disorder in a linear model in Chapter 2, employ it to discuss implications of time-varying interactions in the context of the diversity-stability debate in Chapter 3, and investigate the GLV equations with annealed disorder in Chapter 4.

Beyond the functional form, the effect of the topology of the interaction network has been investigated. Random heterogeneous network structures are explored in [278, 298, 317, 320], revealing how connectivity patterns influence stability and macroecological patterns. Furthermore, extensions to higher-order interactions are discussed in [299]. The assumption of a linear growth rate are addressed in works on sublinear growth [291, 295], which show that this can substantially improve stability and even reverse the classical diversity-stability relationship.

A rapidly growing body of literature continues to refine and expand the disordered GLV framework. Relevant contributions include studies on spatial coupling and meta-communities [225, 266, 294, 319, 307], evolutionary dynamics and niche construction [264, 290], and many other generalizations [207, 233, 262, 268, 276, 277, 301, 303, 310, 330, 322].

1.4 Disordered consumer-resource model

While the GLV equations provide a foundational phenomenological framework for studying community dynamics, they essentially treat species interactions as direct pairwise effects. In empirical settings, however, species rarely interact directly. Instead, they compete for shared resources, consume one another, or exchange metabolic byproducts. Consumer-resource models (CRM) offer a mechanistic description of these processes by explicitly including the dynamics of the resources alongside that of species abundances. In this formulation, the growth rate of a species is determined by its harvest of various resources according to a consumption matrix, minus a maintenance cost. Concurrently, the resources are depleted by the consumers and replenished through intrinsic growth or chemostat dynamics.

The classic MacArthur CRM [28, 67] describes the dynamics of S species $x_i(t)$ competing for

R resources $r_\alpha(t)$ as

$$\begin{aligned} \dot{x}_i &= x_i \left(\sum_\alpha c_{i\alpha} w_\alpha r_\alpha - m_i \right), \\ \dot{r}_\alpha &= r_\alpha \left(K_\alpha - r_\alpha - \sum_i c_{i\alpha} x_i \right). \end{aligned} \tag{1.54}$$

Here, $c_{i\alpha}$ represents the rate at which species i consumes resource α, and w_α denotes the energy content or quality of that resource. The term m_i corresponds to the maintenance cost or mortality rate of species i. For the resources, we assume a logistic growth law characterized by a carrying capacity K_α.

In the limit where resource dynamics are fast compared to species dynamics, one can solve for the equilibrium r^*_α and substitute it back into the consumer equation. This adiabatic elimination yields effective GLV equations with an interaction matrix $\alpha_{ij} = -\sum_\alpha w_\alpha c_{i\alpha} c_{j\alpha}$. Crucially, the resulting interactions are symmetric and strictly competitive. This contrasts to the random GLV model discussed previously, in which interactions are generally asymmetric or mutualistic [318].

As in previous sections, a disordered system perspective is expected to be informative in the high-dimensional limit. We posit that the metabolic parameters appearing in Eq. (1.54) are randomly distributed independent variables. Specifically, we consider the standard scaling for the first two cumulants of the consumption rates as mean$(c_{i\alpha}) = \mu_c/S$ and var$(c_{i\alpha}) = \sigma_c^2/S$, while the maintenance costs and carrying capacities are drawn from distributions with means m, K and variances σ_m^2, σ_K^2 respectively.

Using the cavity [194] or generating-functional [231] methods, one can derive the properties of the stationary state. Within a replica-symmetric ansatz, the equilibrium distributions for species and resources decouple into truncated Gaussian forms

$$\begin{aligned} x(z_1) &= \max\left(0, \frac{g + \sigma_g z_1}{\sigma_c^2 \xi \chi}\right), \\ r(z_2) &= \max\left(0, \frac{K_{\text{eff}} + \sigma_{K_{\text{eff}}} z_2}{1 - \sigma_c^2 \nu}\right). \end{aligned} \tag{1.55}$$

Here $g = \mu_c s \langle r \rangle - m$ and $K_{\text{eff}} = K - \mu_c \langle x \rangle$ represent the effective growth rate and effective capacity. The parameters σ_g and $\sigma_{K_{\text{eff}}}$ are the corresponding standard deviations, while χ and ν denote the static growth-rate susceptibilities of the resources and the species respectively. The parameter $\xi = R/S$ is the resource-species ratio of the system, and z_1, z_2 are independent standard Gaussian variables. These distributions obey the same truncated form found for the GLV equation in the UFP phase, see Eq. (1.16). Interestingly, the question of whether the replica-symmetric ansatz remains stable for all parameter values remains open. Beyond static properties, the dynamical evolution can be explored using DMFT, as detailed in [216, 231].

The connection between ecological dynamics and constrained optimization has been recently explored. It has been shown that the Lyapunov function of the symmetric CRM maps onto a convex optimization problem, suggesting that ecosystems self-organize to minimize an effective energy function [205, 209]. This duality provides rigorous bounds on the maximum biodiversity the system can support.

Furthermore, extensions of the model given by Eq. (1.54) have been proposed to incorporate more realistic metabolic processes. Standard competition models are limited by the competitive exclusion principle, which bounds the number of surviving species by the number of resources.

However, including cross-feeding, where species secrete metabolic byproducts that serve as resources for others, fundamentally alters this constraint [208, 313]. These studies reveal that metabolic trade-offs and cross-feeding networks can stabilize high-diversity communities well beyond classical limits.

While the classical MacArthur model implies symmetric interactions, introducing specific non-reciprocal couplings between species and resources leads to more complex dynamical behavior [284]. Such extensions bridge the gap between the purely competitive MacArthur limit and the diverse dynamical regimes observed in the random GLV framework, including chaos and persistent turnover [191, 212, 215].

Complementing the static perspective, the role of temporal variability in consumption traits has been investigated, employing the annealed disorder framework. The work [323] highlights the limitations of assuming static consumption matrices. By modeling metabolic strategies as fluctuating stochastic variables, rather than quenched parameters, this approach demonstrates that the system can display more realistic macroecological patterns. This dynamic adaptation naturally generates skewed abundance distributions, characterized by many rare species and few common ones. Consequently, functional diversity and realistic rarity patterns can arise solely from the temporal fluctuations of metabolic activities, without relying on fine-tuned heterogeneity in the underlying resource preferences.

Chapter 2

Linear system with annealed disorder

The standard assumption in disordered models is that interactions remain constant over time, acting as quenched disorder. However, in realistic settings, this assumption might not be applicable. In this chapter, we introduce "annealed" disorder, which consists of interactions varying stochastically in time as Ornstein-Uhlenbeck processes. Employing an extended Dynamical Mean-Field Theory that accommodates annealed disorder, we find the exact solution of a linear model. Our analysis yields analytical results for the non-stationary autocorrelation, the stationary variance, the power spectral density, and the phase diagram of the model. Some unexpected features emerge upon changing the correlation time of the interactions. The stationary variance of the system and the critical variance of the disorder are generally found to be non-monotonic functions of the correlation time of the interactions. We also find that a re-entrant phase transition can take place when this correlation time is varied.

2.1 Introduction

As exemplified in Chapter 1, assuming disordered interactions between degrees of freedom effectively lowers the dimensionality of complex system models and allows analytical progress. However, in empirical systems, interactions may not be strictly quenched. For example, synaptic plasticity in neuronal populations consists of long-term potentiation or depression, resulting in temporal fluctuations in interaction strength between neurons [99, 221]. In an ecological setting, it is known that the strength of interactions between species can fluctuate on a timescale comparable to that of population dynamics [161, 170, 204, 222].

For this reason, we consider in this chapter interactions consisting of Ornstein-Uhlenbeck processes with a characteristic correlation time τ. We dub this type of disorder "annealed", in contrast to quenched disorder. We tackle the problem of finding the exact solution of a linear interacting system with annealed disorder. We solve this model for all values of the correlation time τ of the disorder by employing DMFT, which is tailored here for the case of annealed interactions.

We show that DMFT leads to a stochastic differential equation that is formally equivalent to that of a one-dimensional Ornstein-Uhlenbeck process, with the difference that the DMFT process is driven by a noise which is self-consistent and colored. The DMFT process is Gaussian, and its

This chapter is based on: Francesco Ferraro et al. "Exact solution of dynamical mean-field theory for a linear system with annealed disorder". In: *Journal of Statistical Mechanics: Theory and Experiment* 2025.2 (2025), p. 023301. As a co-first author, I shared equal responsibility for designing and conducting the theoretical and numerical analyses and preparing the text and figures.

first two moments can be exactly determined. We are thus able to obtain analytical results for the non-stationary autocorrelation, the stationary variance, and the power spectral density. Unlike the one-dimensional Ornstein-Uhlenbeck process, driven by simple white noise, the DMFT process displays a non-trivial phase diagram. A stationary state is not reached if the mean or variance of the random interactions exceed some critical value, which we are also able to determine analytically.

Despite the simplicity of the model considered here, interesting features arise as the correlation time of the couplings is varied. The stationary variance of the process and the critical variance of the disorder are generally found to be non-monotonic functions of the correlation time of the interactions τ. We also find that in some cases a re-entrant phase transition takes place in τ. These features are found to be a consequence of the specific way in which our model interpolates between the white-noise and quenched limits.

This chapter is organized as follows: in Section 2.2 we present the model; in Section 2.3 we present its DMFT equation, which is solved in Section 2.4; in Section 2.5 we derive the phase diagram of the model; in Section 2.6 simplified results in the limit of white-noise and quenched disorder are given; we conclude with a summary of the results and possibilities for further research. In Chapter 3, the framework of annealed disorder is employed to investigate the effect of temporal variability in interactions on the stability of general complex systems, while in Chapter 4 this framework is introduced into the GLV equations.

2.2 Model

We consider a system with N degrees of freedom that interact linearly

$$\dot{x}_i(t) = h - kx_i(t) + \sum_{j \neq i} \alpha_{ij}(t) x_j(t). \tag{2.1}$$

Here h and k are fixed parameters and the annealed disorder $\alpha_{ij}(t)$ is Gaussian colored noise. Explicitly, it is given by

$$\alpha_{ij}(t) = \frac{\mu}{N} + \frac{\sigma}{\sqrt{N}} z_{ij}(t), \tag{2.2}$$

where μ and σ are fixed parameters, and $z_{ij}(t)$ are independent Ornstein-Uhlenbeck processes with

$$\begin{aligned} \langle z_{ij}(t) \rangle &= 0, \\ \langle z_{ij}(t) z_{ij}(t') \rangle &= Q(t - t'), \end{aligned} \tag{2.3}$$

where

$$Q(t) = \frac{1 + 2\tau/\tau_0}{2\tau} \exp(-|t|/\tau). \tag{2.4}$$

The initial conditions for $z_{ij}(t)$ are drawn from the stationary distribution. The noise amplitude in Eq. (2.4) as a function of τ is one of the possible choices such that in the limit $\tau \to 0$ the annealed disorder becomes white noise, while in the limit $\tau \to \infty$ we recover the case of quenched disorder. The time scale τ_0 is introduced for simple dimensionality reasons, and in the following we set $\tau_0 = 1$ without loss of generality. We note that our choice for the noise amplitude is different from the standard in the colored-noise literature [60, 76]. With the standard choice, the noise vanishes in the limit $\tau \to \infty$, while with our choice $Q(t) \to 1$ in this limit, so that z_{ij} becomes a quenched Gaussian variable with zero mean and unit variance. Clearly, there are many possible choices for $Q(t)$ that interpolate between the white and quenched limits. As a consequence, some details of our results depend on this specific choice.

Figure 2.1 shows examples of the dynamics of the system upon varying the correlation time τ.

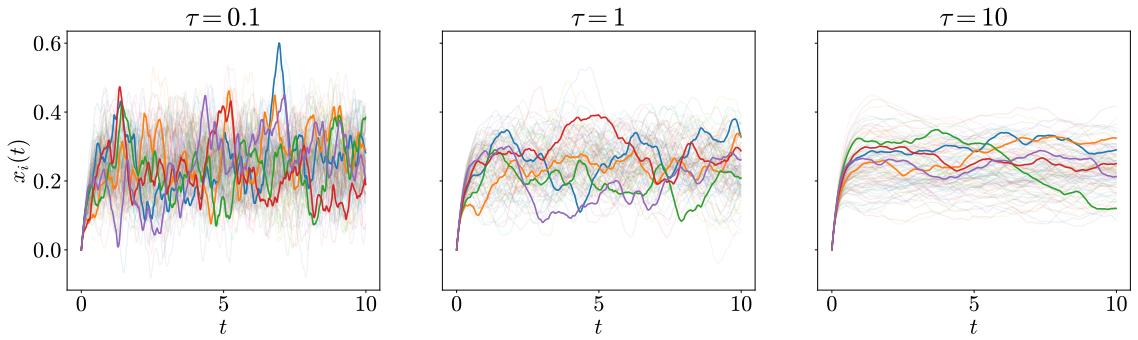

Figure 2.1: Example of trajectories of the linear system Eq. (2.1) for different values of the correlation time τ of the annealed disorder. In each plot five trajectories chosen at random are highlighted. The model has been simulated with $N = 1000$, $h = 1$, $k = 4$, $\mu = 0$, $\sigma = 1$, and initial condition $x_i(0) = 0$ for all i.

2.3 Dynamical Mean-Field Theory

In order to solve the linear system Eq. (2.1) we employ DMFT. The DMFT equation for the linear system Eq. (2.1) is derived using generating functionals in Appendix A of [308], although we note that it could be derived also using the dynamical cavity method [61, 211]. The DMFT equation associated to Eq. (2.1) is the following stochastic differential equation for a representative degree of freedom of the system $x(t)$:

$$\dot{x}(t) = h - kx(t) + \mu\langle x(t)\rangle + \sigma\eta(t). \tag{2.5}$$

In this equation $\eta(t)$ is colored, non-stationary, Gaussian noise with mean and correlations given self-consistently by

$$\begin{aligned} \langle \eta(t)\rangle &= 0, \\ \langle \eta(t)\eta(t')\rangle &= Q(t-t')\langle x(t)x(t')\rangle, \end{aligned} \tag{2.6}$$

where the averages $\langle x(t)\rangle$ and $\langle x(t)x(t')\rangle$ are understood to be over solutions of Eq. (2.5). We note that the difference with the quenched case lies in the presence of the correlation function $Q(t)$ in the correlations of $\eta(t)$.

Eq. (2.5) is formally equivalent to the stochastic differential equation of a one-dimensional Ornstein-Uhlenbeck process, with the important difference that the DMFT process is driven by a noise that is both self-consistent and colored. As shown in the following, this makes the DMFT process fundamentally different from an Ornstein-Uhlenbeck process. For example, the DMFT process displays a non-trivial phase diagram, in contrast with that of the Ornstein-Uhlenbeck process, which invariably settles into a stationary state.

2.4 Exact solution of Dynamical Mean-Field Theory

To solve the DMFT equation we start by noticing that the formal solution of Eq. (2.5) is

$$x(t) = x_0 e^{-kt} + \int_0^t ds e^{-k(t-s)} \left[h + \mu\langle x(s)\rangle + \sigma\eta(s)\right], \tag{2.7}$$

assuming a fixed initial condition x_0 at $t = 0$. This equation shows that the process $x(t)$, being a linear combination of the Gaussian process $\eta(t)$ at different times, is itself a Gaussian

process. The process $x(t)$ is therefore completely specified by its mean $\langle x(t)\rangle$ and autocorrelation $C(t,t') = \langle x(t)x(t')\rangle - \langle x(t)\rangle\langle x(t')\rangle$. In the rest of this section we derive and solve closed equations for the mean and autocorrelation, thus exactly solving the DMFT equation Eq. (2.5).

We also notice that, since $x(t)$ is a Gaussian process with a fixed initial condition, its single-time probability distribution is given by a Gaussian

$$P(x,t) = \frac{1}{\sqrt{2\pi C(t,t)}} \exp\left[-\frac{(x - \langle x(t)\rangle)^2}{2C(t,t)}\right]. \tag{2.8}$$

2.4.1 Mean

The time evolution of the mean is simply found by taking the average of Eq. (2.5)

$$\frac{d\langle x(t)\rangle}{dt} = h - (k-\mu)\langle x(t)\rangle, \tag{2.9}$$

which has solution

$$\langle x(t)\rangle = x_0 e^{-(k-\mu)t} + \frac{h}{k-\mu}\left[1 - e^{-(k-\mu)t}\right]. \tag{2.10}$$

For the stationary state of the system to be reached we have the necessary condition

$$\mu < k, \tag{2.11}$$

and when the stationary state is reached its mean is given by

$$\langle x\rangle_{\rm st} = \frac{h}{k-\mu}. \tag{2.12}$$

2.4.2 Autocorrelation

To get a closed equation for the auto-correlation function we rewrite Eq. (2.5) as

$$\sigma\eta(t) = \dot{x}(t) + kx(t) - h - \mu\langle x(t)\rangle. \tag{2.13}$$

By averaging the product $\sigma^2\eta(t)\eta(t')$, using Eq. (2.6), and performing simple manipulations, assuming $t \neq t'$, we get the following PDE for the autocorrelation

$$\left[\partial_t\partial_{t'} + k(\partial_t + \partial_{t'}) + k^2 - \sigma^2 Q(t-t')\right] C(t,t') = f(t,t'), \tag{2.14}$$

where

$$f(t,t') = \sigma^2 Q(t-t')\langle x(t)\rangle\langle x(t')\rangle. \tag{2.15}$$

This equation for $C(t,t')$ is valid only for $t \neq t'$ since it is derived under this assumption. For example, $\langle \dot{x}(t)\dot{x}(t')\rangle = \partial_t\partial_{t'}\langle x(t)x(t')\rangle$ is true only if $t \neq t'$. As a consequence, one cannot set $t = t'$ to get a closed equation for the variance $C(t,t)$. However, the trajectories $x(t)$ are continuous, as implied by Eq. (2.5), and thus $C(t,t')$ is continuous in both t and t'. Therefore one can extend the solution for of Eq. (2.14) also to $t = t'$. Since we assume the initial condition $x(0) = x_0$ to be fixed, the PDE must be solved with the boundary conditions $C(t,0) = 0$ and $C(0,t') = 0$. The solution is found using the Riemann method in Appendix 2.8.1 and is

$$C(t,t') = e^{-k(t+t')} \int_0^t ds \int_0^{t'} ds' e^{k(s+s')} A(s,s';t,t') f(s,s'), \tag{2.16}$$

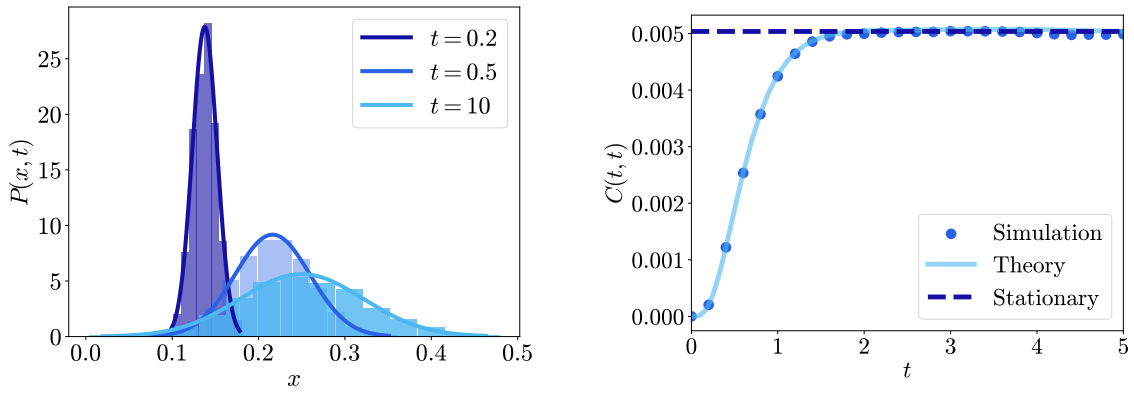

Figure 2.2: Left: Comparison between the single-time probability distribution of $x(t)$ Eq. (2.8), with mean and variance given by Eq. (2.10) and Eq. (2.16), and numerical simulations. The parameters are $N = 1000$,, $h = 1$, $k = 4$, $\mu = 0$, $\sigma = 1$, and $\tau = 1$. Right: Comparison between the time evolution of the variance of $x(t)$, found analytically by setting $t = t'$ in Eq. (2.16), and numerical simulations with the same parameters as in the left panel. Each simulated point is the result of 100 iterations.

where $A(s, s'; t, t')$ is the Riemann function of the PDE, see Eq. (2.35).

Comparisons between this analytical result and the numerical integration of Eq. (2.1) are given in Figure 2.2. Even if derived only for $t \neq t'$, we observe numerically that Eq. (2.16) gives the correct result also for $t = t'$, as anticipated.

2.4.3 Stationary autocorrelation and variance

The process $x(t)$ is stationary for sufficiently long times, that is, for $t \gg 1/(k - \mu)$, and its autocorrelation depends only on the difference $t - t'$. Thus at stationarity $C(t, t') = C_{\rm st}(t - t')$ and the PDE Eq. (2.14) reduces to an ODE

$$-\ddot{C}_{\rm st}(t) + \left[k^2 - \sigma^2 Q(t)\right] C_{\rm st}(t) = \sigma^2 Q(t) \langle x \rangle_{\rm st}^2, \tag{2.17}$$

Here, the derivative is with respect to the difference $t - t'$, which we renamed t. The boundary conditions of this ODE are $\dot{C}_{\rm st}(0) = 0$ and $C_{\rm st}(\infty)$ is finite. The first condition follows from the fact that $C_{\rm st}(t)$ is even and that we assume it to be differentiable in $t = 0$. We note however that $C_{\rm st}(t)$ is actually non-analytic at $t = 0$ for $\tau = 0$. This is in turn due to the fact that in this limit the noise $z_{ij}(t)$ is white. Upon increasing τ, the δ-function appearing in the correlation of the noise is smeared out, and so is the non-analyticity in the correlation $C_{st}(t)$ of the process $x(t)$. The second boundary condition arises from the fact that we assume $x(t)$ to remain bounded. The ODE Eq. (2.17) is solved with standard methods in Appendix 2.8.2.

The solution of the ODE for which the boundary conditions are satisfied has initial condition $C_{\rm st}(0)$, which is the stationary variance $\sigma^2_{\rm st} = \langle x^2 \rangle_{\rm st} - \langle x \rangle^2_{\rm st}$, given by

$$\sigma^2_{\rm st} = \left[\frac{{}_1F_2\left(n; n+1, 2n+1; -\lambda^2/4\right)}{2{}_0F_1\left(2n; -\lambda^2/4\right) - {}_0F_1\left(2n+1; -\lambda^2/4\right)} - 1 \right] \langle x \rangle^2_{\rm st}, \tag{2.18}$$

where

$$\begin{aligned} n &= k\tau, \\ \lambda &= \sqrt{2\tau(1+2\tau)}\sigma, \end{aligned} \tag{2.19}$$

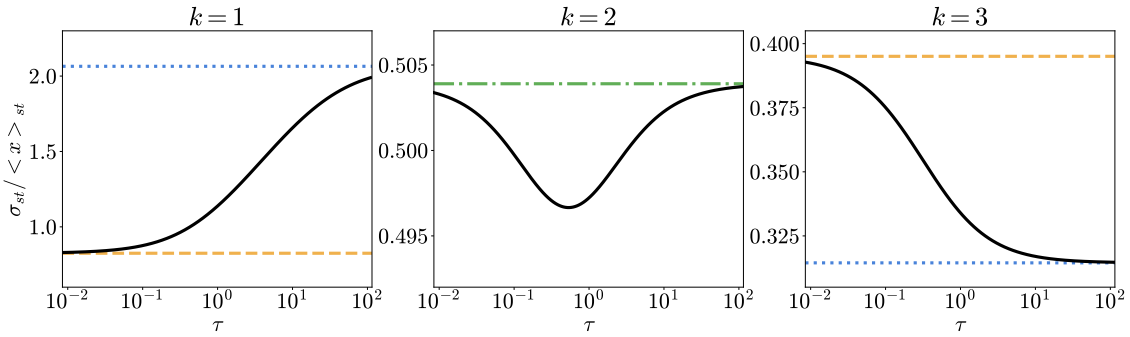

Figure 2.3: The stationary variance of $x(t)$, given by Eq. (2.18), as a function of τ for different values of k, at fixed $\sigma = 0.9$. The dependence of $\sigma_{\rm st}$ on τ can also be non-monotonic for other values of k, not just for $k = 2$ (not shown here). The orange (dashed) line is the value of the stationary variance for $\tau \to 0$, the blue (dotted) line is the one for $\tau \to \infty$. For $k = 2$ the two lines coincide (green, dashed-dotted line).

and ${}_pF_q$ is the generalized hypergeometric function [123]. Notice that the dependence on μ and h in $\sigma_{\rm st}$ is factorized into the stationary mean $\langle x \rangle_{\rm st} = h/(k - \mu)$.

An example of the dependence of $\sigma_{\rm st}$ on the parameters of the model is given in Figure 2.3. Interestingly, $\sigma_{\rm st}$ can be a monotonically increasing or decreasing function of τ, depending on the values of k and σ. For some values of the parameters the dependence of $\sigma_{\rm st}$ on τ can also be non-monotonic. Although not shown in Figure 2.3, we found that this non-monotonic dependence of $\sigma_{\rm st}$ on τ takes place not only for $k = 2$, but also for values near $k = 2$. More precisely, for the values of the parameters chosen in the figure, the non-monotonicity is present from approximately $k = 1.9$ to $k = 2.1$. The range of values of k for which this non-monotonicity is present does not change significantly when σ is varied. We notice that upon increasing τ the stationary variance can either increase or decrease. This follows from the fact that in the white-noise limit this quantity is smaller or greater than the value in the quenched limit depending on the value of k, see Section 2.6. The dependence of $\sigma_{\rm st}$ on τ is therefore generally non-monotonic. We note that the details of the non-monotonic behavior displayed by $\sigma_{\rm st}$ depends on the specific way the prefactor in Eq. (2.4) interpolates between the white and quenched limits.

Eq. (2.18) also allows us to derive the phase diagram of the model, as discussed in the next section.

The explicit expression for $C_{\rm st}(t)$ is reported in Appendix 2.8.2, see Eq. (2.46). It turns out that $C_{\rm st}(t) > 0$ at all times for any value of the parameters. Moreover, the characteristic timescale of the autocorrelation is

$$\tau_c = \frac{\int_0^\infty dt C_{\rm st}(t)}{C_{\rm st}(0)} = 1/k + \tau. \tag{2.20}$$

We verified this relation by performing the numerical integration in the numerator for different values of τ while fixing all the other parameters. We notice that the characteristic timescale τ_c of the process is given by the sum of the two timescales present in the system. This suggests that an estimation of this correlation time could be obtained also in non-linear systems by summing an intrinsic timescale, if known, and the correlation time τ.

Figure 2.4 shows comparisons between the analytical and numerical stationary autocorrelation.

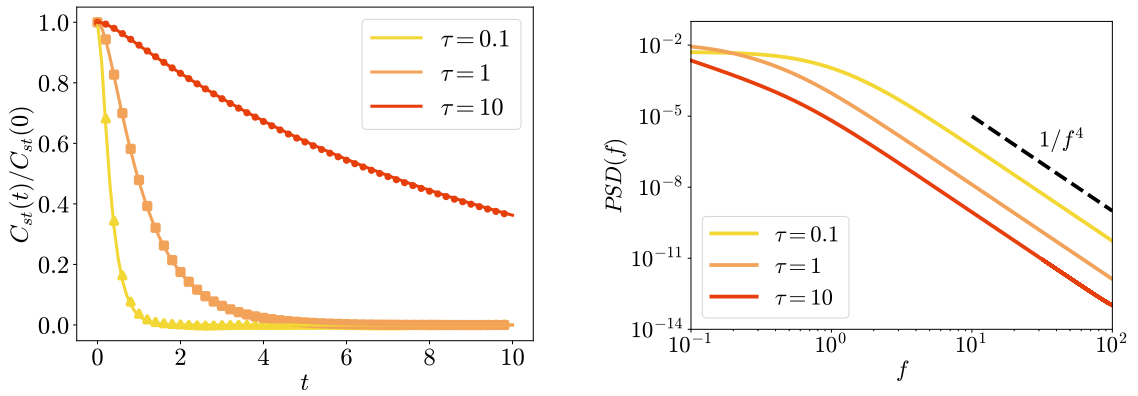

Figure 2.4: Left: Comparison between the analytical result and numerics for the stationary autocorrelation of $x(t)$ for different τ. Solid lines are obtained using Eq. (2.46), while markers indicate numerical simulations. The parameters are $N = 1000$, $h = 1$, $k = 4$, $\mu = 0$, and $\sigma = 1$. Right: Power spectral density of $x(t)$ for different values τ. Lines were obtaining by performing numerically the Fourier transform of Eq. (2.46). The parameters are $h = 1$, $k = 4$, $\mu = 0$, and $\sigma = 1$.

2.4.4 Power spectral density

The power spectral density of the process $x(t)$ can be found as the Fourier transform of the stationary autocorrelation. We found no simple expression for the power spectral density, but we verified that it decays as $1/f^4$ at high frequencies by computing numerically the Fourier transform. This is shown in Figure 2.4.

We explain heuristically the exponent of this decay by observing that in the linear equation Eq. (2.1) the process $x_i(t)$ is essentially the time integration of the Ornstein-Uhlenbeck noise $\alpha_{ij}(t)$, which has a power spectral density that decays as $1/f^2$ at high frequencies. The time integration includes a further factor $1/f^2$, which leads to the decay $1/f^4$.

2.5 Phase diagram

In this section, we discuss the phases of the linear system as a function of the mean μ and the variance σ of the disorder.

As already discussed in the previous section, for the system to reach the stationary state, we have the necessary condition $\mu < k$.

Furthermore, the stationary variance σ^2_{st} must be finite. By numerical investigation, we observe that increasing σ in Eq. (2.18), while keeping k and τ fixed, a critical σ_c is reached such that for $\sigma > \sigma_c$ the stationary variance diverges. This is the smallest σ_c for which the denominator in Eq. (2.18) vanishes. Thus, we get the following equation for the critical value σ_c

$$ {}_2F_1(2k\tau; -\tau(1+2\tau)\sigma_c^2/2) - {}_0F_1(1+2k\tau; -\tau(1+2\tau)\sigma_c^2/2) = 0. \tag{2.21} $$

This relation can also be simplified using relations between the hypergeometric function and the Bessel functions $J_n(x)$ (see Eq. 9.1.69 of [30])

$$ 2nJ_{2n}(\lambda_c) - \lambda_c J_{2n-1}(\lambda_c) = 0, \tag{2.22} $$

where n and λ_c are defined in Eq. (2.19) and are evaluated at the critical σ_c. Notice that σ_c does not depend neither on h nor on μ. Numerical simulations confirm that for $\sigma < \sigma_c$ the system

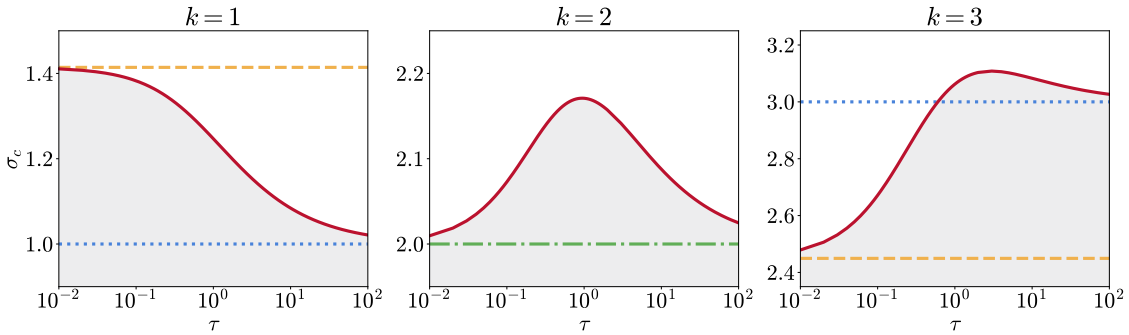

Figure 2.5: The critical value σ_c as a function of τ for different values of k, found as the solution of Eq. (2.22). For $\sigma < \sigma_c$ the system reaches a stationary state (darker region). For $\sigma > \sigma_c$ the variance diverges. The horizontal orange (dashed) line is the value of σ_c for $\tau \to 0$, while the blue (dotted) line is the one for $\tau \to \infty$. For $k = 2$ the two lines coincide (green, dashed-dotted line).

reaches the stationary state, while for $\sigma > \sigma_c$ the variance of the trajectories at fixed time diverges exponentially and a stationary state is not reached.

Figure 2.5 shows σ_c as a function of τ for different values of k. Interestingly, the dependence of σ_c on τ can be both increasing or decreasing. Moreover, it is not necessarily monotonic, displaying in some cases a re-entrant phase transition in τ. This means that at fixed σ, increasing τ can sometimes move the system from a phase in which the stationary state is not reached, to a phase in which it is reached, and finally to a phase where it is not reached again. We believe this non-monotonicity is also due to the non-monotonicity of the noise amplitude Q as a function of τ.

Similarly to what happens to the stationary variance, we also notice that for $k < 2$ the critical σ_c at $\tau = 0$ is larger than the critical σ_c at $\tau = \infty$, while for $k > 2$ the opposite is true. At $k = 2$ the two values coincide, but the dependence of σ_c on τ is nevertheless non-trivial.

In conclusion, the phase diagram of the system is the one reported in Figure 2.6. In the phase in which only the variance diverges the average of the trajectories at a fixed time $\langle x(t) \rangle$ reaches the stationary value given by equation Eq. (2.12). The variance of the trajectories at fixed time $\langle x(t)^2 \rangle - \langle x(t) \rangle^2$, on the other hand, diverges exponentially as t grows. In the phase in which both the mean and the variance diverge both of these quantities diverge exponentially as t grows.

2.6 White-noise and quenched limits

The previous results simplify in the limits $\tau \to 0$ and $\tau \to \infty$.

In the white-noise limit, the noise $\eta(t)$ in the DMFT equation Eq. (2.5) becomes white, although with an amplitude which is self-consistent and time-dependent

$$\langle \eta(t)\eta(t') \rangle = \langle x(t)^2 \rangle \delta(t - t'). \tag{2.23}$$

In this limit a simple expression for the equal-time average of the noise $\eta(t)$ and the process $x(t)$ can be easily found

$$\langle x(t)\eta(t) \rangle = \frac{1}{2}\sigma \langle x(t)^2 \rangle, \tag{2.24}$$

which allows us to write a simple equation for the evolution of the variance $s^2(t) = \langle x(t)^2 \rangle - \langle x(t) \rangle^2$

$$\frac{ds^2(t)}{dt} = \sigma^2 \langle x(t) \rangle^2 - (2k - \sigma^2) s^2(t). \tag{2.25}$$

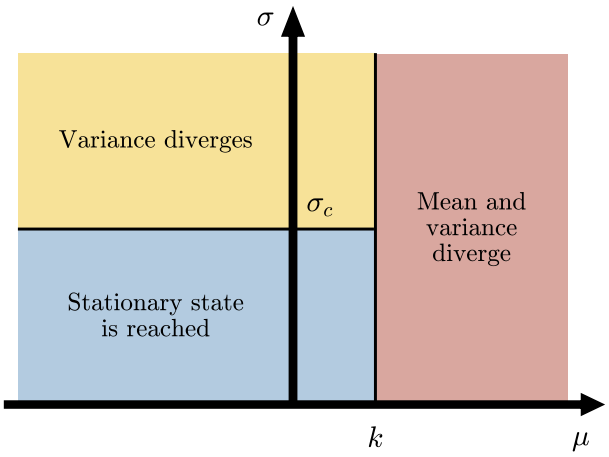

Figure 2.6: The phase diagram of the model as a function of the mean and the variance of the annealed disorder. For $\mu < k$ and $\sigma < \sigma_c$ the system reaches a stationary state, in which the stationary distribution is a Gaussian. For $\mu < k$ and $\sigma > \sigma_c$ this Gaussian has a finite mean but its variance diverges. For $\mu > k$ both the mean and the variance of this Gaussian diverge.

From this equation, we read explicitly that

$$\sigma_c = \sqrt{2k}, \tag{2.26}$$

and, when stationarity is reached, the variance is

$$\sigma^2_{\rm st} = \frac{\sigma^2}{2k - \sigma^2} \langle x \rangle^2_{\rm st}. \tag{2.27}$$

This result can also be derived by taking the $\tau \to 0$ limit of Eq. (2.18). The stationary auto-correlation is also simply

$$C_{\rm st}(t) = \sigma^2_{\rm st} \exp(-k|t|). \tag{2.28}$$

As anticipated, in this limit the stationary autocorrelation $C_{\rm st}(t)$ is continuous but not analytic for $t = 0$.

In the quenched limit the mean and the correlation of the noise in the DMFT equation Eq. (2.5) reads

$$\langle \eta(t)\eta(t') \rangle = \langle x(t)x(t') \rangle. \tag{2.29}$$

The stationary variance can be obtained either by taking the limit $\tau \to \infty$ of Eq. (2.18) or by a fixed-point ansatz in the DMFT equation Eq. (2.5). It is given by

$$\sigma^2_{\rm st} = \frac{\sigma^2}{k^2 - \sigma^2} \langle x \rangle^2_{\rm st}, \tag{2.30}$$

so that the critical σ is simply

$$\sigma_c = k. \tag{2.31}$$

This critical σ_c could also be obtained by applying the circular law [24, 55, 145].

2.7 Discussion

In this chapter, we studied a disordered linear system in which interactions are not fixed in time but vary stochastically with a correlation time τ. We dubbed this type of disorder "annealed". By employing DMFT, tailored for the case of annealed disorder, we were able to find the exact solution of the system in the limit of a large number of degrees of freedom.

DMFT leads to an equation similar to the stochastic differential equation of an Ornstein-Uhlenbeck process, with the crucial difference that it is driven by a noise which is self-consistent and colored. This difference makes analytical results much more challenging and gives rise to non-trivial behaviors. We derived equations for the mean and autocorrelation of the DMFT process and solved them. Since this process is Gaussian, this solves exactly the model. The exact solution allowed us to derive the phase diagram of the linear system. We found that if the mean or variance of the interactions exceeds a critical threshold, the system does not reach a stationary state. Interestingly, our findings reveal that the critical variance value σ_c depends in a non-trivial way on the correlation time τ of the annealed disorder. Furthermore, when the stationary state is reached, we have shown that its variance also varies in a non-monotonic way depending on τ. We interpreted these features as a consequence of the fact that our noise amplitude interpolates between white-noise and quenched disorder.

We foresee a number of possible extensions in the context of the linear model studied in this work. Firstly, we assumed that the interaction parameters $\alpha_{ij}(t)$ to be independent of each other, but a correlation between pairs of couplings [186, 199] or a hierarchical structure [268] could be introduced. For example, human microbiomes exhibit both taxonomic and functional organization far more intricate than the corresponding null models consisting of completely uncorrelated species or functions [273, 285]. Moreover, we assumed the model to be fully connected, but, as has been shown recently [278, 298, 320], the DMFT approach can also be applied to situations in which a network structure is present in the interactions. It would also be interesting to investigate the effect of non-Gaussian interactions on the emerging properties of these systems [282, 316].

More broadly, the framework of annealed disorder considered in this work could be applied to any many-body system in which interactions can be modeled as random, but not static. Investigating the impact of annealed disorder on the properties of the diverse number of models that have been treated so far in the limit of quenched disorder would be a compelling research avenue. The DMFT equation can be obtained for a large class of non-linear systems by straightforward extensions of the generating functional formalism employed in [308]. Still, obtaining analytical results is more challenging in non-linear systems because the DMFT process will generally be non-Gaussian. Moreover, the exact solution of the model studied in this work substantially depends on the linearity of the system. This enables the derivation of closed-form equations for the first moments of the process, but this will generally not be the case in non-linear systems. We explore a non-linear application in Chapter 4, where the framework of annealed disorder is introduced into the GLV equations.

Finally, exploring how a combination of quenched and annealed disorder can produce emergent patterns observed in physical or biological systems could yield valuable insight to bridge the gap between theoretical models and real-world systems. In Appendix 2.8.3, we show how the methods developed in this chapter can be extended to investigate a linear system in which interactions are a combination of quenched and annealed disorder.

2.8 Appendix

2.8.1 Solution of PDE for autocorrelation

In this appendix we solve the PDE Eq. (2.14).

Consider the transformation $C(t,t') = e^{-k(t+t')}D(t,t')$. The equation for $D(t,t')$ is the simpler PDE

$$\left[\partial_t\partial_{t'} - \sigma^2 Q(t-t')\right] D(t,t') = e^{k(t+t')} f(t,t'), \tag{2.32}$$

together with the boundary conditions $D(t,0) = 0$ and $D(0,t') = 0$. To solve this inhomogeneous PDE we use the Riemann method [263]. In the present case it amounts to finding the Riemann function $A(s,s';t,t')$, which is defined as the solution of the homogeneous PDE

$$\left[\partial_s\partial_{s'} - \sigma^2 Q(s-s')\right] A(s,s';t,t') = 0, \tag{2.33}$$

together with the boundary conditions $A(s,t';t,t') = 1$ and $A(t,s';t,t') = 1$. We call $A_0(s,s';t,t')$ the solution of the PDE for $s > s'$. In this region we have that $Q(s-s') = (1+2\tau)\,/\,(2\tau)\, e^{-(s-s')/\tau}$. The PDE for A_0 can be solved by performing the change of variables $u = e^{-s/\tau}$, $u' = e^{s'/\tau}$ and using the known solution [263] of equation $(\partial_u\partial_{u'} + c)A_0(u,u') = 0$. The result is

$$A_0(s,s';t,t') = J_0\left(\lambda\sqrt{(e^{-s/\tau} - e^{-t/\tau})(e^{s'/\tau} - e^{t'/\tau})}\right), \tag{2.34}$$

where $\lambda = \sqrt{2\tau(1+2\tau)}\sigma$. Similarly, for $s < s'$, the solution of Eq. (2.33) is $A_0(-s,-s';-t,-t')$. It is then clear that the Riemann function of the PDE is

$$A(s,s';t,t') = \theta(s-s')A_0(s,s';t,t') + \theta(s'-s)A_0(-s,-s';-t,-t'). \tag{2.35}$$

Using the Riemann formula the solution of Eq. (2.32) is

$$D(t,t') = \int_0^t ds \int_0^{t'} ds' e^{k(s+s')} A(s,s';t,t') f(s,s'). \tag{2.36}$$

In terms of $C(t,t')$ one immediately concludes that the solution of Eq. (2.14) is Eq. (2.16).

2.8.2 Solution of ODE for stationary autocorrelation

In this appendix we solve the ODE Eq. (2.17).

It is simpler to solve for the function $E(t) = \langle x(t)x(0)\rangle_{\rm st} = C_{\rm st}(t) + \langle x\rangle_{\rm st}^2$. The ODE for $E(t)$ is

$$-\ddot{E}(t) + \left[k^2 - \sigma^2 Q(t)\right] E(t) = k^2\langle x\rangle_{\rm st}^2. \tag{2.37}$$

With the change of variable $z = \lambda e^{-t/2\tau}$, $\lambda = \sqrt{2\tau(1+2\tau)}\sigma$ the homogeneous equation becomes

$$z^2 E''(z) + zE'(z) + \left[z^2 - (2k\tau)^2\right] E(z) = 0, \tag{2.38}$$

which is Bessel differential equation. Two independent solutions are then

$$\begin{aligned} u_1(t) &= J_{2k\tau}(\lambda e^{-t/2\tau}), \\ u_2(t) &= Y_{2k\tau}(\lambda e^{-t/2\tau}). \end{aligned} \tag{2.39}$$

Since the Wronskian of $u_1(t)$ and $u_2(t)$ is $W = 1/\pi\tau$, the general solution of Eq. (2.37) is, by the method of variation of parameters,

$$E(t) = c_1 u_1(t) + c_2 u_2(t) + \pi\tau k^2 \langle x\rangle_{\rm st}^2 \left[u_2(t)U_1(t) - u_1(t)U_2(t)\right], \tag{2.40}$$

where

$$\begin{aligned} U_1(t) &= \int dt\, u_1(t) \\ &= -\frac{(\lambda/2)^{2k\tau}}{k\Gamma(1+2k\tau)} e^{-kt}\, {}_1F_2(k\tau; 1+2k\tau, 1+k\tau; -(\lambda/2)^2 e^{-t/\tau}) \end{aligned} \tag{2.41}$$

and

$$\begin{aligned} U_2(t) &= \int dt\, u_2(t) \\ &= \frac{(\lambda/2)^{2k\tau}\cos(2\pi k\tau)\Gamma(-2k\tau)}{\pi k} e^{-kt}\, {}_1F_2(k\tau; 1+2k\tau, 1+k\tau; -(\lambda/2)^2 e^{-t/\tau}) \\ &\quad - \frac{(\lambda/2)^{-2k\tau}\Gamma(2k\tau)}{\pi k} e^{kt}\, {}_1F_2(-k\tau; 1-2k\tau, 1-k\tau; -(\lambda/2)^2 e^{-t/\tau}). \end{aligned} \tag{2.42}$$

The primitive functions were found with the substitution $z = \lambda e^{-t/2\tau}$ and using known integrals of Bessel functions.

We now impose the boundary conditions. The asymptotic behavior of each piece of Eq. (2.40) at long time is

$$\begin{aligned} u_1(t) &\sim \frac{(\lambda/2)^{2k\tau}}{\Gamma(1+2k\tau)} e^{-kt}, \\ u_2(t) &\sim -\frac{\Gamma(2k\tau)(\lambda/2)^{-2k\tau}}{\pi} e^{kt}, \\ u_1(t)U_2(t) &\sim -\frac{1}{2\pi k^2\tau}, \\ u_2(t)U_1(t) &\sim \frac{1}{2\pi k^2\tau}, \end{aligned} \tag{2.43}$$

from which we get, if we want $E(\infty)$ to be finite, that $c_2 = 0$. With this condition, we also get $E(\infty) = \langle x\rangle_{\rm st}^2$. Imposing $E'(0) = 0$ we get the condition

$$c_1 = -\frac{1}{2}\langle x\rangle_{\rm st}^2 (a+b), \tag{2.44}$$

with

$$\begin{aligned} a &= (\lambda/2)^{-2k\tau}\Gamma(1+2k\tau)\, {}_1F_2(-k\tau; 1-2k\tau, 1-k\tau; -(\lambda/2)^2), \\ b &= (\lambda/2)^{2k\tau}\Gamma(1-2k\tau)\frac{kJ_{-2k\tau}(\lambda) + \lambda J_{-2k\tau+1}(\lambda)/2\tau}{kJ_{2k\tau}(\lambda) - \lambda J_{2k\tau-1}(\lambda)/2\tau} \\ &\quad \times {}_1F_2(k\tau; 1+k\tau, 1+2k\tau; -(\lambda/2)^2). \end{aligned} \tag{2.45}$$

With all this, the solution of Eq. (2.17) is

$$C_{\rm st}(t) = c_1 u_1(t) + \pi\tau k^2 \langle x\rangle_{\rm st}^2 \left[u_2(t)U_1(t) - u_1(t)U_2(t)\right] - \langle x\rangle_{\rm st}^2. \tag{2.46}$$

Setting $t = 0$ and after some manipulations (done with FullSimplify on Mathematica 13.2) one gets Eq. (2.18) of the main text.

2.8.3 Linear system with a combination of quenched and annealed disorder

In this appendix, we show how the methods developed in this chapter can be extended to determine the stability properties of a linear system in which interactions are a combination of quenched and annealed disorder.

We consider the linear model

$$\dot{x}_i(t) = -x_i(t) + \sum_{j \neq i} M_{ij}(t) x_j(t), \tag{2.47}$$

where the interaction matrix $M_{ij}(t)$ is given by

$$M_{ij}(t) = A_{ij} + B_{ij}(t). \tag{2.48}$$

Here, A_{ij} represents the quenched component and $B_{ij}(t)$ the annealed one. Both matrices have connectivity C, meaning that individual entries are set to zero with probability $1 - C$. We employ the normalization

$$\begin{aligned} \langle A_{ij}^2 \rangle &= (1-\lambda)\sigma^2, \\ \langle B_{ij}(t) B_{ij}(t') \rangle &= \lambda \sigma^2 Q(t-t'), \\ Q(t) &= e^{-|t|/\tau}. \end{aligned} \tag{2.49}$$

Notice that $Q(t)$ has a slightly different definition with respect to the main text of this chapter. The parameter $\lambda \in [0, 1]$ interpolates between quenched and annealed disorder. For $\lambda = 0$, the matrix $M_{ij}(t)$ is fully quenched, while for $\lambda = 1$ it is fully annealed. With this choice, the community matrix $M_{ij}(t)$ maintains the fixed variance

$$\langle M_{ij}(t)^2 \rangle = \sigma^2 \tag{2.50}$$

at any instant t for any value of λ and τ. We note that for $\tau \to \infty$, the term $B_{ij}(t)$ becomes quenched, while for $\tau \to 0$ it vanishes.

The DMFT equation is given by

$$\dot{x}(t) = -x(t) + \sqrt{1-\lambda} R \eta(t) + \sqrt{\lambda} R \xi(t), \tag{2.51}$$

where $R = \sigma\sqrt{NC}$ is the spectral radius of the interaction matrix at any fixed time. We omit the full derivation of the DMFT equation, which can be obtained using the generating functional formalism [289, 308] or the dynamical cavity method [211]. The Gaussian noises $\eta(t)$ and $\xi(t)$ have zero mean and correlations

$$\langle \eta(t)\eta(t') \rangle = \langle x(t)x(t') \rangle, \tag{2.52}$$

$$\langle \xi(t)\xi(t') \rangle = Q(t-t') \langle x(t)x(t') \rangle. \tag{2.53}$$

Importantly, the noises are independent of each other, meaning $\langle \eta(t)\xi(t') \rangle = 0$ for all t, t'. The method to determine stability from the DMFT Eq. (2.51) is similar to that presented in the main text. We introduce an external field h to ensure a non-zero stationary state and derive a closed equation for the autocorrelation of $x(t)$. By taking the stationary limit, we obtain an equation for the stationary autocorrelation. Solving this allows us to compute the stationary variance of $x(t)$ (at $t = 0$). Finally, we identify the stability boundary by finding the parameters for which this stationary variance diverges.

We begin by noticing that taking the average of Eq. (2.51) we have

$$\frac{d\langle x(t)\rangle}{dt} = -\langle x(t)\rangle + h. \tag{2.54}$$

From this we see that $\langle x\rangle_{\rm st} = h$.

To find a closed equation for the autocorrelation $C(t,t') = \langle x(t)x(t')\rangle$, we first rewrite Eq. (2.51) as

$$\sqrt{1-\lambda}R\eta(t) + \sqrt{\lambda}R\xi(t) = \dot{x}(t) + x(t) - h, \tag{2.55}$$

and consider the average for $t \neq t'$. Squaring the expression, averaging over the noise, and applying Eq. (2.52) and Eq. (2.53), we obtain

$$\begin{aligned}
&\langle\left[\sqrt{1-\lambda}R\eta(t) + \sqrt{\lambda}R\xi(t)\right]\left[\sqrt{1-\lambda}R\eta(t') + \sqrt{\lambda}R\xi(t')\right]\rangle \\
&= (1-\lambda)R^2\langle x(t)x(t')\rangle + \lambda R^2 Q(t-t')\langle x(t)x(t')\rangle \\
&= \langle[\dot{x}(t) + x(t) - h]\left[\dot{x}(t') + x(t') - h\right]\rangle \\
&= \partial_t\partial_{t'}\langle x(t)x(t')\rangle + \partial_t\langle x(t)x(t')\rangle + \partial_{t'}\langle x(t)x(t')\rangle + \langle x(t)x(t')\rangle \\
&\quad - h\partial_t\langle x(t)\rangle - h\partial_{t'}\langle x(t')\rangle - h\langle x(t)\rangle - h\langle x(t')\rangle + h^2.
\end{aligned} \tag{2.56}$$

The second and fourth line of this equation yield a closed equation for $C(t,t')$.

We assume that the process $x(t)$ reaches a stationary state at long times $t \gg 1$, such that $C(t,t') = C_{\rm st}(t-t')$. In this limit, time-translation invariance implies for example $\partial_t C_{\rm st}(t-t') = -\partial_{t'}C_{\rm st}(t-t')$. Combining this with Eq. (2.54) yields a closed equation for the stationary autocorrelation:

$$-\ddot{C}_{\rm st}(t) + \left[1 - (1-\lambda)R^2 - \lambda R^2 Q(t)\right] C_{\rm st}(t) = h^2. \tag{2.57}$$

We introduce the parameters

$$\alpha^2 = 1 - (1-\lambda)R^2, \tag{2.58}$$

$$\beta^2 = \lambda R^2. \tag{2.59}$$

We note that α^2 remains positive within the stability region, so that thus α is real, which ensures that the special functions involved below are also real. Applying the change of variables $z = 2\tau\beta e^{-t/2\tau}$ leads to the equivalent homogeneous ODE

$$z^2 C''_{\rm st}(z) + zC'_{\rm st}(z) + \left[z^2 - (2\tau\alpha)^2\right] C_{\rm st}(z) = 0, \tag{2.60}$$

which is Bessel differential equation. Two independent solutions to the homogeneous part of Eq. (2.57) are

$$\begin{aligned}
u_1(t) &= J_{2\tau\alpha}(2\tau\beta e^{-t/2\tau}), \\
u_2(t) &= Y_{2\tau\alpha}(2\tau\beta e^{-t/2\tau}).
\end{aligned} \tag{2.61}$$

Given that the Wronskian of $u_1(t)$ and $u_2(t)$ is $1/\pi\tau$, the general solution to Eq. (2.57) can be written as

$$C_{\rm st}(t) = c_1 u_1(t) + c_2 u_2(t) + \pi\tau h^2[u_2(t)U_1(t) - u_1(t)U_2(t)], \tag{2.62}$$

where $U_1(t)$ and $U_2(t)$ are the antiderivatives of $u_1(t)$ and $u_2(t)$, respectively. We impose the boundary conditions, which are $C'_{\rm st}(0) = 0$, due to time-reversal symmetry, and that $C_{\rm st}(\infty)$ is

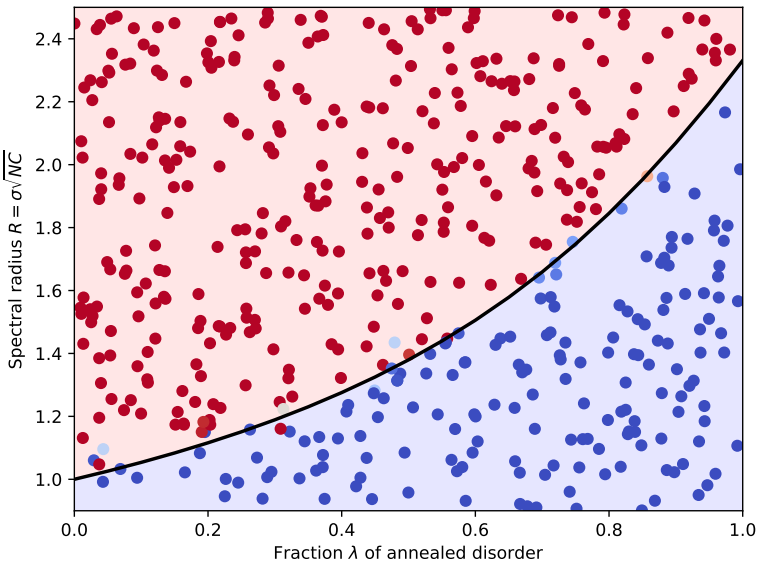

Figure 2.7: Comparison of analytical results and numerical simulations of a linear system with a combination of quenched and annealed disorder. Each point is the result of a simulation of the linear system Eq. (2.47) for a matrix A such that $\langle A_{ij}^2 \rangle = (1-\lambda)\sigma^2$ and $\langle B_{ij}(t)^2 \rangle = \lambda\sigma^2$. The number of degrees of freedom is $N = 200$, the connectivity is $C = 1$ and the correlation time is $\tau = 0.25$. The color of each point indicates whether or not the system reaches the zero fixed point. The black line is the theoretical prediction given by Eq. (2.67).

finite. To apply these, we utilize the asymptotic expansions for $t \to \infty$:

$$\begin{aligned} u_1(t) &\sim \frac{(\tau\beta)^{2\tau\alpha}}{\Gamma(1+2\tau\alpha)} e^{-\alpha t}, \\ u_2(t) &\sim -\frac{\Gamma(2\tau\alpha)(\tau\beta)^{-2\tau\alpha}}{\pi} e^{\alpha t}, \\ u_1(t)U_2(t) &\sim -\frac{1}{2\pi\tau\alpha^2}, \\ u_2(t)U_1(t) &\sim \frac{1}{2\pi\tau\alpha^2}. \end{aligned} \tag{2.63}$$

To ensure a finite result as $t \to \infty$, we must set $c_2 = 0$. Consequently, we obtain

$$C_{\mathrm{st}}(\infty) = \frac{h^2}{\alpha^2} = \frac{h^2}{1-(1-\lambda)R^2}. \tag{2.64}$$

This result implies $C_{\mathrm{st}}(\infty) \neq \langle x \rangle_{\mathrm{st}}^2$, indicating that $x(t)$ does not fully decorrelate from $x(0)$ at long times, except in the fully annealed limit $\lambda = 1$. Finally, imposing $\dot{C}_{\mathrm{st}}(0) = 0$ determines the coefficient c_1, thereby fully specifying the solution $C_{\mathrm{st}}(t)$.

Setting $t = 0$ in the solution yields $C_{\mathrm{st}}(0) = \langle x^2 \rangle_{\mathrm{st}}$. The stationary variance is therefore defined as $\sigma_{\mathrm{st}}^2 = C_{\mathrm{st}}(0) - \langle x \rangle_{\mathrm{st}}^2$. After simplifications (done on Mathematica 13.2.1.0 with FullSimplify), this is

$$\frac{\sigma_{\mathrm{st}}^2}{\langle x \rangle_{\mathrm{st}}^2} = \frac{1}{\alpha^2} \frac{{}_1F_2(\tau\alpha; \tau\alpha+1, 2\tau\alpha+1, -\tau^2\beta^2)}{2\,{}_0F_1(2\tau\alpha, -\tau^2\beta^2) - {}_0F_1(2\tau\alpha+1, -\tau^2\beta^2)} - 1. \tag{2.65}$$

From Eq. (2.65), we observe that the stationary variance diverges when the denominator vanishes:

$$2{}_0F_1(2\tau\alpha, -\tau^2\beta^2) - {}_0F_1(2\tau\alpha + 1, -\tau^2\beta^2) = 0. \tag{2.66}$$

Using Eq. (9.1.69) from Ref. [30], this condition is equivalent to

$$\beta J_{2\tau\alpha-1}(2\tau\beta) - \alpha J_{2\tau\alpha}(2\tau\beta) = 0. \tag{2.67}$$

We recall that α and β are related to the spectral radius R and the annealed disorder fraction λ via Eq. (2.58) and Eq. (2.59). Figure 2.7 presents numerical simulation results that confirm these analytical predictions.

Chapter 3

Will a time-varying complex system be stable?

Randomly-assembled dynamical systems are theoretically predicted to be unstable upon crossing a critical threshold of complexity, as first shown by May and detailed in Section 1.1. Yet, empirical complex systems exhibit remarkable stability, indicating the presence of additional mechanisms playing a stabilizing role. The relation between complexity and stability is typically assessed assuming fixed interactions, whereas real systems often evolve in intrinsically time-dependent states. To understand how this affects stability, we employ the framework of annealed disorder introduced in Chapter 2 to model the parameters obtained after linearizing a general non-autonomous system around its moving equilibrium. This represents the minimal extension of quenched random interactions to time-varying ones. Building on the techniques of Chapter 2, we derive exact stability bounds that generalize complexity theory to dynamically varying systems. Notably, we find that temporal variability allows systems to remain stable even when their instantaneous Jacobian has eigenvalues with positive real part. We illustrate our results in a non-linear neural network model, where our theory applies exactly, and in the generalized Lotka-Volterra equations, where we numerically find that time-varying interactions systematically postpone the onset of replica-symmetry breaking. Overall, our results indicate that temporal variability systematically enhances stability, demonstrating a general mechanism by which complex systems can violate classical complexity limits.

3.1 Introduction

Naïvely, one might expect that a system with more interacting components, or with more diverse and numerous connections, should be more stable. As discussed in Section 1.1, this intuition was challenged by May in his seminal work "Will a large complex system be stable?" [31], which established that complexity can instead beget instability. Much subsequent work has sought to identify which features could reconcile theory with observation. Complexity-stability bounds are usually obtained via local stability analysis around fixed states, with structural constraints imposed on the static coefficients of the resulting linear dynamics to assess whether they enhance or hinder

This chapter is based on: Francesco Ferraro et al. "Will a time-varying complex system be stable?" In: *arXiv preprint arXiv:2603.28464* (2026). As the first author, I was responsible for designing and conducting the theoretical and numerical analyses and preparing the text and figures.

stability relative to a completely random null model.

Still, interactions in complex systems, and consequently their states, are rarely static, as discussed in Section 2.1. Despite the ubiquity of such time-dependent interactions [116, 118, 119, 124, 155, 265], and general results indicating that temporal variability can alter system stability relative to what the instantaneous Jacobian predicts [51, 83, 102], a systematic understanding of how time-varying interactions affect the stability of complex systems remains lacking [4, 36, 52, 105, 206, 227, 237].

In this chapter, we address this gap by assessing the stability of a complex system operating in a time-dependent state. We consider a generic non-autonomous dynamics and linearize it around its moving equilibrium. The resulting parameters are modeled as annealed disorder, introduced in Chapter 2, a natural generalization of quenched random variables to temporally fluctuating ones. Extending slightly the results of Chapter 2, we analytically derive complexity bounds and show that temporal variability systematically enhances the stability of complex systems. Remarkably, we find that a system can remain dynamically stable beyond the May bound, where its instantaneous Jacobian has eigenvalues with positive real part.

We support our analytical results with numerical simulations of two paradigmatic non-linear systems: a neural network model [63], where our linear framework is exact, and the GLV equations [87, 186], a foundational model in theoretical ecology. For the latter, we numerically find that the phenomenology of the linear case persists, that is, temporal variability extends the regime of stability against replica-symmetry breaking.

Our results point to a general principle: time-varying interactions can stabilize complexity. This may ease the long-standing tension between theoretical and empirical stability.

This chapter is organized as follows: in Section 3.2 we present the linear model; in Section 3.3 we analyze its stability properties; in Section 3.4 we compare these results with simulations of non-linear models; we conclude with a summary of the results and possibilities for further research.

3.2 Model

We consider a large system evolving in time following a generic first-order non-autonomous dynamics

$$\dot{x}_i(t) = f_i(\boldsymbol{x}(t), t), \tag{3.1}$$

where $\boldsymbol{x}(t) = (x_1(t), \dots, x_N(t))$ is the state vector of the system, which is composed of $N \gg 1$ degrees of freedom. We assume the existence of a time-dependent equilibrium $\boldsymbol{x}^*(t)$ of Eq. (3.1), which satisfies $f_i(\boldsymbol{x}^*(t), t) = 0$ for all i, t. The Jacobian matrix evaluated at this instantaneous equilibrium is

$$M_{ij}(t) = \frac{\partial f_i}{\partial x_j}(\boldsymbol{x}^*(t), t). \tag{3.2}$$

Small perturbations around the moving equilibrium $\boldsymbol{\delta x}(t) = \boldsymbol{x}(t) - \boldsymbol{x}^*(t)$ evolve according to the linearization of Eq. (3.1):

$$\delta\dot{x}_i(t) = \sum_j M_{ij}(t)\delta x_j(t) + h_i(t), \tag{3.3}$$

where $h_i(t) = -\dot{x}_i^*(t)$. This equation admits a straightforward interpretation. The interaction term describes the linear response around the instantaneous equilibrium, generalizing the usual autonomous case. The forcing term $\boldsymbol{h}(t)$, by contrast, arises in the non-autonomous case from the

drift of $\boldsymbol{x}^*(t)$: as the equilibrium moves, the displacement between the state and moving equilibrium is continuously shifted.

As discussed in Section 1.1, a fundamental complexity-stability bound was first derived by May [31]. He considered a static equilibrium, which implies a constant $M_{ij}(t)$ and $h_i(t) = 0$. He assumed $M_{ii} = -1$ for all i and that the off-diagonal entries of the Jacobian are drawn independently from a random distribution with zero mean. Random matrix theory, in particular the circular law [24, 55, 145], then implies that the spectrum of the Jacobian matrix in the complex plane is uniformly supported on a circle centered in $(-1, 0)$ with radius

$$R = \sigma\sqrt{NC}, \tag{3.4}$$

where σ is the standard deviation of the off-diagonal distribution and C is the connectance (fraction of non-zero entries). From this, May concluded that a complex system becomes linearly unstable whenever

$$R > 1. \tag{3.5}$$

The caricature of a complex systems considered by May serves as a null model that can be extended to determine which features promote or suppress stability [153, 286]. In this spirit, we broaden its scope by promoting the random variables M_{ij} and h_i to annealed disorder, introduced in Chapter 2. This construction yields a natural dynamical counterpart to the static random model of May. Specifically, we set the diagonal entries $M_{ii}(t) = -1$ and take the off-diagonal elements $M_{ij}(t)$ and the forcing terms $h_i(t)$ to be independent Gaussian processes with zero mean and correlations

$$\begin{aligned} \langle M_{ij}(t)M_{ij}(t')\rangle &= \sigma^2 Q(t-t'), \\ \langle h_i(t)h_i(t')\rangle &= \rho^2 Q(t-t'), \\ Q(t) &= e^{-|t|/\tau}, \end{aligned} \tag{3.6}$$

where σ and ρ are fixed parameters, and τ is the correlation time. A fraction of the matrix entries are set to zero at all times, giving the model a connectance C. As in May's original approach, and unlike usual disordered system, we are not rescaling the interactions $M_{ij}(t)$ with the number of degrees of freedom N. This results in an explicit dependence on N in the results that follow.

Note that here the normalization encoded in $Q(t)$ differs slightly from that of Chapter 2. The one chosen here is in order to allow a direct comparison between our model and that of May, in the following sense. The model of May is recovered in the limit $\tau \to \infty$. At finite correlation time, the resulting dynamical system differs from the one of May, but still, at any fixed time, the spectral radius of the Jacobian matrix $M_{ij}(t)$ remains precisely $R = \sigma\sqrt{NC}$ for any value of τ. In particular, for $R > 1$ some eigenvalues of the Jacobian matrix have positive real part. If we choose the normalization of Chapter 2 we would not obtain exactly the spectral radius $R = \sigma\sqrt{NC}$. Another difference between the previous and present chapters is that in Chapter 2 we assumed a quenched forcing $h_i(t) = h$, while here we take it as an annealed variables, as prescribed by Eq. (3.6).

For simplicity of presentation, we consider here the case in which interactions and forcing terms have the same correlation time τ. The general case is detailed in Appendix 3.6.2, where we show that stability is governed solely by the fluctuations of $M_{ij}(t)$. Furthermore, we assume no correlations between the couplings and the fields $h_i(t)$. Since the statistics of the forcing terms do not enter the stability conditions derived below, this assumption is not expected to qualitatively change our conclusions.

3.3 Stability criterion

The linear model defined by Eq. (3.3) and Eq. (3.6) either converges to a stable stationary state or displays diverging solutions. In the former case, fluctuations around the equilibrium remain bounded, indicating a stable system, while in the latter the system is linearly unstable. Rather than solving Eq. (3.3) directly, we follow the same strategy as Chapter 2. We consider the associated DMFT equation, from which we obtain a closed equation for the autocorrelation $C(t,t') = \langle \delta x(t) \delta x(t') \rangle$ and consider its stationary limit $C_{\rm st}(t)$. Solving for $C_{\rm st}(t)$ yields the stationary variance $C_{\rm st}(0)$, whose divergence marks the onset of instability in the system.

The DMFT equation corresponding to the linear model reads

$$\delta \dot{x}(t) = -\delta x(t) + R\eta(t) + h(t), \tag{3.7}$$

where $R = \sigma\sqrt{NC}$, and $\eta(t)$ and $h(t)$ are independent Gaussian noises with zero mean and correlations

$$\begin{aligned} \langle \eta(t)\eta(t') \rangle &= Q(t-t') \langle \delta x(t) \delta x(t') \rangle, \\ \langle h(t)h(t') \rangle &= \rho^2 Q(t-t'). \end{aligned} \tag{3.8}$$

These averages are understood to be over all realizations of $\eta(t)$ and $h(t)$, as usual. The derivation of Eq. (3.7) follows closely the procedure detailed in [300, 308, 323] and is omitted here. We note the DMFT equation implies that stability depends on the same complexity parameter $R = \sigma\sqrt{NC}$ originally identified by May, together with the additional parameters ρ and τ, the latter entering via $Q(t)$.

By multiplying the DMFT equation 3.7 by $h(0)$, taking the stationary average, and using the fact that $\eta(t)$ and $h(t)$ are independent, we obtain a closed equation for the stationary cross-correlation $D(t) = \langle \delta x(t) h(0) \rangle_{\rm st}$, which reads $\dot{D}(t) = -D(t) + \rho^2 Q(t)$. We then rewrite Eq. (3.7) as $R\eta(t) = \delta\dot{x}(t) + \delta x(t) - h(t)$ and average the product $R^2\eta(t)\eta(t')$. After performing straightforward manipulations, taking the stationary limit, and employing the equation for $D(t)$, we find a closed equation for the stationary autocorrelation $C_{\rm st}(t)$:

$$-\ddot{C}_{\rm st}(t) + \left[1 - R^2 Q(t)\right] C_{\rm st}(t) = \rho^2 Q(t). \tag{3.9}$$

Eq. (3.9) is supplemented with the boundary conditions $\dot{C}_{\rm st}(0) = 0$, by time-reversal symmetry, and finite $C_{\rm st}(\infty)$, assuming a bounded stationary state. The solution can be obtained by standard methods (see Appendix 3.6.1). Evaluating $C_{\rm st}(t)$ at $t = 0$ yields the stationary variance of Eq. (3.3):

$$\sigma^2_{\rm st} = \frac{\rho^2}{R^2} \left[\frac{{}_1F_2(\tau; 1+\tau, 1+2\tau; -\tau^2 R^2)}{2\,{}_0F_1(2\tau; -\tau^2 R^2) - {}_0F_1(1+2\tau; -\tau^2 R^2)} - 1 \right], \tag{3.10}$$

where ${}_pF_q$ is the generalized hypergeometric function [123].

The stationary variance diverges whenever the denominator in Eq. (3.10) vanishes, which yields the critical complexity R of the model as a function of the correlation time τ. Using Eq. (9.1.69) of [30], this condition can be rewritten as $RJ_{2\tau-1}(2\tau R) - J_{2\tau}(2\tau R) = 0$, where $J_n(x)$ is the Bessel function. Using then the third line of Eq. (9.1.27) of [30] this condition can be further expressed as

$$J'_{2\tau}(2\tau R) = 0. \tag{3.11}$$

We note that stability is independent of the parameter ρ. Furthermore, in the general case of different correlation timescales for $M_{ij}(t)$ and $h_i(t)$, stability is determined solely by the correlation time of the interaction matrix (see Appendix 3.6.2).

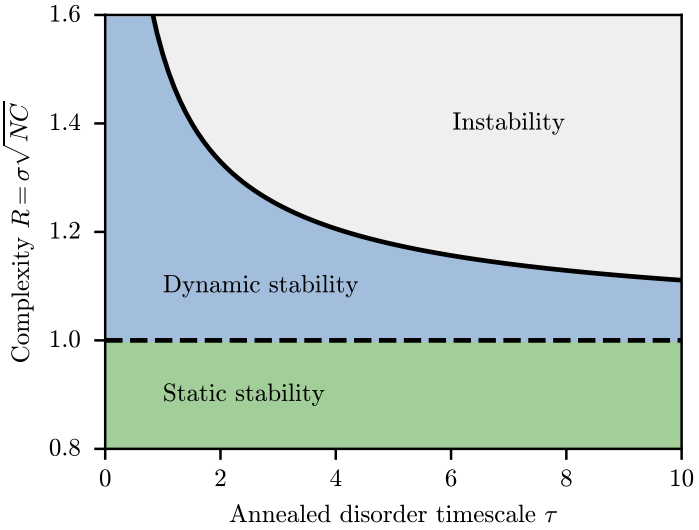

Figure 3.1: Phase diagram of the linear model Eq. (3.3) with annealed interactions as set by Eq. (3.6). Below the bound given by Eq. (3.11) (solid line) the model converges to a stable stationary state, while above it the system is unstable. Below the May bound $R = 1$ (dashed line), all eigenvalues of the instantaneous Jacobian have negative real part and the system exhibits unconditional stability. Above this bound, some eigenvalues of the Jacobian have positive real part, yet the dynamics can be stabilized by sufficiently rapid temporal variability. The critical complexity below which the system remains dynamically stable increases as the scale of temporal variability τ is reduced.

The solution of Eq. (3.11) is shown in Figure 3.1. The critical complexity required for stability is always above the May bound $R = 1$, as it follows from the fact that the smallest zero of $J_n'(x)$ is always larger than n (see Section 15.3 of [9]). This demonstrates that temporal variability systematically promotes stability. In the "Dynamic stability" region, moreover, the system is dynamically stable even though a fraction of the eigenvalues of the instantaneous Jacobian have positive real part. The critical complexity also increases as the timescale of temporal variability τ is reduced, indicating that faster temporal fluctuations further enhance stability.

We can qualitatively explain how time-variability can stabilize a fixed point beyond static bounds, see Figure 3.2. When $R > 1$, the spectrum of $M_{ij}(t)$ has a fraction of eigenvalues with positive real part. However, since the interaction matrix is time-dependent, the corresponding eigenvectors, and thus the directions of the unstable manifold, are continuously changing. Note that Figure 3.2 is strictly schematic, as eigenvectors are generally complex. As these unstable directions shift, the system never spends enough time in any single direction for a perturbation to grow unbounded. Ultimately, this allows the system to remain dynamically stable even when the instantaneous Jacobian would predict static instability.

3.4 Non-linear models

We illustrate our results in simulations of non-linear models. We examine two different settings: a neural network model, where the linear theory applies exactly, and the GLV equations, where temporal fluctuations suppress the onset of replica-symmetry breaking [61, 196, 229].

First, we consider a firing-rate model of a network of N neurons. We assume the synaptic

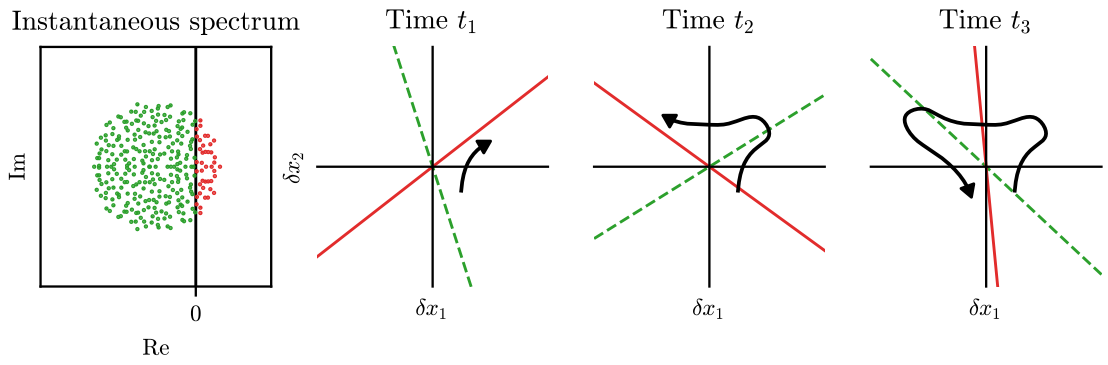

Figure 3.2: Qualitative explanation for the stabilization mechanism in time-varying systems. Left: The instantaneous spectrum of the Jacobian matrix $M_{ij}(t)$ is constant, and a fraction of this spectrum can have positive real part (red points). Right: Dynamics of perturbations at different times (curved arrow). The stable (green dashed lines) and unstable (red solid lines) directions continuously shift as the Jacobian matrix evolves, which effectively averages out the divergence. The panels are illustrative, as eigenvectors are generally complex.

current $x_i(t)$ to evolve according to the non-linear dynamics [63, 173, 201] (see also Chapter 7)

$$\dot{x}_i(t) = -x_i(t) + \sum_{j \neq i} J_{ij}(t)\phi(x_j(t)), \tag{3.12}$$

where the transfer function is, for definiteness, $\phi(x) = \tanh(gx)$. We assume an annealed interaction matrix, with full connectivity $C = 1$ and normalization

$$\langle J_{ij}(t)J_{ij}(t')\rangle = \frac{\sigma^2}{N}Q(t-t'). \tag{3.13}$$

At small heterogeneity σ, the stationary state $x_i(t) = 0$ is stable. Perturbations around this equilibrium follow the linear dynamics

$$\delta\dot{x}_i(t) = -\delta x_i(t) + \sum_{j \neq i} J_{ij}(t)g\delta x_j(t). \tag{3.14}$$

This corresponds exactly to the linear system studied previously via the identification $R = \sigma g$ and $h_i(t) = 0$. This latter condition reflects a time-invariant equilibrium. The stability condition is then given by Eq. (3.11). Numerical simulations confirm the agreement with the theoretical prediction, see Figure 3.3.

Next, we consider an ecological community governed by the GLV equations. The abundance $x_i(t)$ of each species evolves according to (see also Chapter 4)

$$\dot{x}_i(t) = x_i(t)\left[1 - x_i(t) + \sum_{j \neq i} \alpha_{ij}(t)J(x_j(t))\right]. \tag{3.15}$$

To prevent unbounded growth, we introduced a saturating response function $J(x)$, see also Chapters 4 and 5. The interaction matrix is annealed, and normalized as [300]

$$\alpha_{ij}(t) = \frac{\mu}{N} + \frac{\sigma}{\sqrt{N}}z_{ij}(t), \tag{3.16}$$

where $\langle z_{ij}(t)z_{ij}(t')\rangle = Q(t-t')$. For this model, our previously derived linear bound is not expected to hold, as the Jacobian matrix around the instantaneous equilibrium is not described simply by Eq. (3.6), and moreover it is correlated with the external field $h_i(t)$.

To assess whether the community reaches a stable stationary state, we consider two replicas of the community x^a and x^b. The two replicas are subjected to the same realization of the disorder $\alpha_{ij}(t)$ but have different initial conditions. We monitor the distance between replicas defined as

$$d(t) = \frac{1}{N}\sum_i \left[x_i^a(t) - x_i^b(t)\right]^2. \tag{3.17}$$

If $d(t)$ converges to zero, the systems displays replica-symmetry (RS) and reaches a stable stationary state. Conversely, if $d(t)$ remains non-zero, replica-symmetry is broken (RSB). We note that this a "dynamical" form of RSB, different from the one of equilibrium spin-glasses [61, 260]. These two phases are the annealed counterparts of the Unique Fixed Point and Multiple Attractor phases found in the quenched, $\tau \to \infty$ limit [186, 331].

Results from the numerical integration of Eq. (3.15) are shown in Figure 3.4. Both the lower green and intermediate blue regions are RS phases, while in the upper grey region represents the RSB phase. In the lower green region, additionally, the system displays static stability: if the interaction matrix were frozen, the system would settle into a stable fixed point. In the intermediate blue region, the system is only dynamically stable: if the interaction matrix were frozen, the dynamics would be chaotic.

Comparing these results with Figure 3.1 confirms that the phenomenology matches the linear model: time-variability in interactions enhances stability relative to the quenched case by enlarging the region in which replica-symmetry is maintained. We note that the increase in stability is not due to a reduction in the number of surviving species since, as shown in Chapter 4, annealed disorder actually increases the number of surviving species.

3.5 Discussion

We extended the null model of May to accommodate time-dependent interactions by promoting quenched random couplings to annealed stochastic variables. We derived the exact complexity-stability bound of the resulting model, which is given by Eq. (3.11) and shown in Figure 3.1. We highlight two features of this result. First, the stability region expands as the correlation time τ of the annealed disorder decreases, suggesting that rapidly time-varying complex systems are more stable than slowly varying ones. Second, the stability bound is systematically enhanced for any finite τ compared with the classical May bound $R = 1$ recovered in the limit $\tau \to \infty$.

Our results indicate that the stability transition is insensitive to the details of the external forcing $h_i(t)$. Both the analytical bound derived above and its generalization given in Appendix 3.6.2 confirm that the critical threshold is determined exclusively by the properties of the Jacobian matrix $M_{ij}(t)$. The external fields, acting as additive noises, modulate the amplitude of the deviations from equilibrium but do not alter the stability of the system.

We illustrated our results in two paradigmatic non-linear models. In a neural network model, the predicted stability bound and numerical simulations are in agreement, which is expected since for this model the linear framework is exact. In the GLV equations, time-dependent interactions postpone the transition to the replica-symmetry-breaking phase compared to the quenched case. Further properties of the GLV equations with annealed disorder are detailed in Chapter 4. These

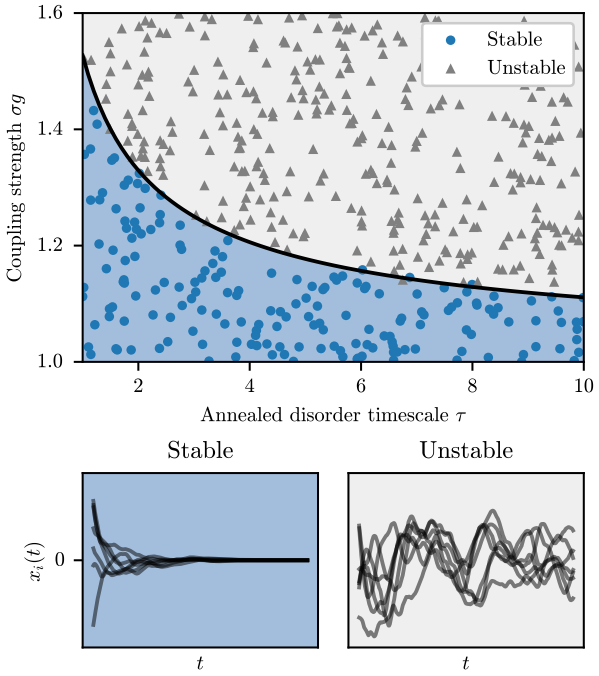

Figure 3.3: Validation of the stability bound in a neural network model with annealed interactions. In the upper panel we compare the critical complexity threshold Eq. (3.11) with $R = \sigma g$ (solid line) with numerical integration of the model Eq. (3.12) for $N = 400$ and interactions given by Eq. (3.13) (circles and triangles). Each realization is classified as stable if it settles into the fixed point $x_i = 0$ or unstable if it reaches a non-zero stationary state. The agreement is excellent, as expected since our stability bound applies exactly to this model. The lower panels qualitative display the dynamics in the two phases.

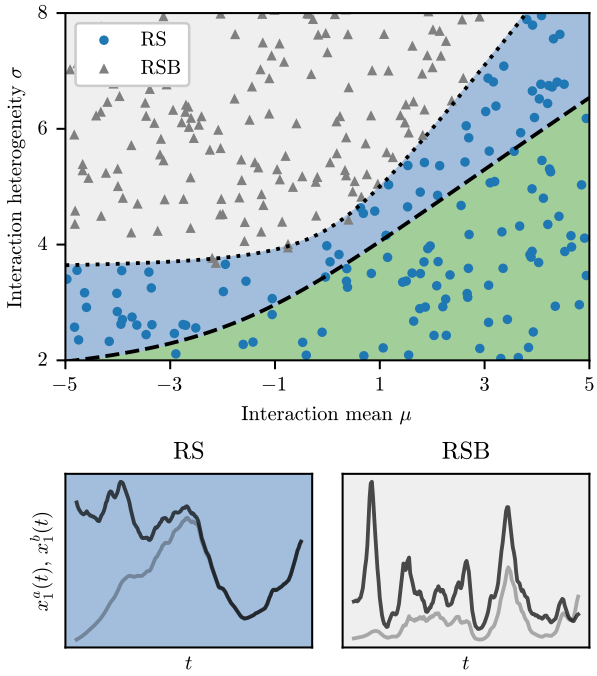

Figure 3.4: Numerical phase diagram of generalized Lotka-Volterra equations with annealed interactions. For each parameter set, we simulate two replicas of the GLV dynamics Eq. (3.15) which share the same disorder realization $\alpha_{ij}(t)$ but start from different initial conditions. The system is classified as replica-symmetric (RS) if the distance $d(t)$ [Eq. (3.17)] vanishes at long times, and replica-symmetry-breaking (RSB) otherwise. The dashed line marks the stability boundary for the quenched case (see Chapter 5), while the dotted line marks the numerical boundary separating the RS and RSB phases. As in Figure 3.1, the lower green region static stability, while the intermediate blue area indicates dynamic stability (see text). Consistent with the linear model, temporal variability extends the stable RS regime beyond the quenched limit. The response function $J(x) = 2x/(2 + x)$ and the correlation time is $\tau = 1$. The lower panels qualitatively show single species trajectories for the two replicas in each phase.

results suggest that the stabilizing effect of temporal variability extends beyond the exactly solvable linear case to more realistic non-linear dynamics. Integrating our annealed disorder framework with the replicated DMFT methods of [201] could allow for an analytical characterization of the replica-symmetry-breaking phase in generic non-linear models with time-varying interactions.

Much like May's original contribution, our linear model represents only a caricature of a complex system. Yet, as detailed in Section 3.3, the stabilization mechanism admits a clear physical interpretation. Empirical complex systems, which do not vary randomly but according to precise functional patterns, may harness this mechanism even more efficiently, potentially achieving stability levels well above the predictions of our null model.

Overall, our results indicate that temporal fluctuations, often regarded as destabilizing, can remarkably act as a stabilizing mechanism in large interacting systems, enabling stability beyond static bounds. Future work should investigate the interplay of annealed disorder with the cornucopia of structural features explored in the context of the complexity-stability debate [153, 286], as well as explore connections to empirical complex systems such as neural dynamics [63], ecological networks [186], or social and economic interactions [146, 210].

3.6 Appendix

3.6.1 Solution of ODE for stationary autocorrelation

In this appendix we solve the ODE Eq. (3.9).

It is simpler to solve for the function $E(t) = C_{\rm st}(t) + \rho^2/R^2$. This function satisfies the ODE

$$-\ddot{E}(t) + \left[1 - R^2 Q(t)\right] E(t) = \frac{\rho^2}{R^2}. \tag{3.18}$$

Consider the change of variables $z = 2\tau R e^{-t/2\tau}$. This yields the equivalent homogeneous ODE

$$z^2 E''(z) + z E'(z) + \left[z^2 - (2\tau)^2\right] E(z) = 0, \tag{3.19}$$

which is Bessel differential equation. Two independent solution of the homogeneous ODE of Eq. (3.18) are then

$$\begin{aligned} u_1(t) &= J_{2\tau}(2\tau R e^{-t/2\tau}), \\ u_2(t) &= Y_{2\tau}(2\tau R e^{-t/2\tau}). \end{aligned} \tag{3.20}$$

Since the Wronskian of $u_1(t)$ and $u_2(t)$ is $1/\pi\tau$ then the general solution of Eq. (3.18) is by the method of variation of parameters

$$E(t) = c_1 u_1(t) + c_2 u_2(t) + \pi\tau \frac{\rho^2}{R^2}[u_2(t)U_1(t) - u_1(t)U_2(t)], \tag{3.21}$$

where $U_1(t)$ and $U_2(t)$ are the primitive functions of $u_1(t)$ and $u_2(t)$ respectively. Explicitly these are

$$\begin{aligned} U_1(t) &= -\frac{(\tau R)^{2\tau}}{\Gamma(1+2\tau)} e^{-t}\, {}_1F_2(\tau; 1+2\tau, 1+\tau; -\tau^2 R^2 e^{-t/\tau}), \\ U_2(t) &= \frac{(\tau R)^{2\tau}\cos(2\pi\tau)\Gamma(-2\tau)}{\pi} e^{-t}\, {}_1F_2(\tau; 1+2\tau, 1+\tau; -\tau^2 R^2 e^{-t/\tau}) \\ &\quad - \frac{(\tau R)^{-2\tau}\Gamma(2\tau)}{\pi} e^{t}\, {}_1F_2(-\tau; 1-2\tau, 1-\tau; -\tau^2 R^2 e^{-t/\tau}). \end{aligned} \tag{3.22}$$

The primitive were found found be with the substitution $z = 2\tau R e^{-t/2\tau}$ and known integrals of Bessel functions. We want to impose the boundary conditions, which are that $\dot{E}(0) = 0$ and that $E(\infty)$ is finite. To do this we use the asymptotic expansions of each term in Eq. (3.21) which are

$$\begin{aligned} u_1(t) &\sim \frac{(\tau R)^{2\tau}}{\Gamma(1+2\tau)} e^{-t}, \\ u_2(t) &\sim -\frac{\Gamma(2\tau)(\tau R)^{-2\tau}}{\pi} e^{t}, \\ u_1(t)U_2(t) &\sim -\frac{1}{2\pi\tau}, \\ u_2(t)U_1(t) &\sim \frac{1}{2\pi\tau}. \end{aligned} \tag{3.23}$$

To have a finite $E(\infty)$ we impose that $c_2 = 0$. With this we also get that $E(\infty) = \rho^2/R^2$. From this we see that $C_{\rm st}(\infty) = 0$, which indicates that the process $x(t)$ decorrelates with itself after a long time, which is expected. Imposing $\dot{E}(0) = 0$ fixes the value of c_1, which is not reported here. This overall fixes the solution $E(t)$ and, consequently, $C_{\rm st}(t)$. Setting $t = 0$ in the solution found one obtains $E(0)$ and consequently the stationary variance $C_{\rm st}(0)$. After simplifications (done on Mathematica 13.2.1.0 with FullSimplify) this is given by Eq. (3.10) of the main text.

3.6.2 Case of different correlation time for Jacobian matrix and external fields

In the main text we assumed for simplicity of presentation that $M_{ij}(t)$ and $h_i(t)$ were colored noises with the same correlation time. We relax here this assumption, by considering the case in which

$$\begin{aligned} \langle M_{ij}(t)M_{ij}(t')\rangle &= \sigma^2 Q(t-t'|\tau_M), \\ \langle h_i(t)h_i(t')\rangle &= \rho^2 Q(t-t'|\tau_h), \end{aligned} \tag{3.24}$$

where $Q(t|\tau) = e^{-|t|/\tau}$.

The procedure to find the stability criterion is analogous to the one presented in the main text. The corresponding DMFT equation remains the same as in the main text and is given by Eq. (3.7), but with noise correlations that generalize to

$$\begin{aligned} \langle \eta(t)\eta(t')\rangle &= Q(t-t'|\tau_M)\langle \delta x(t)\delta x(t')\rangle, \\ \langle h(t)h(t')\rangle &= Q(t-t'|\tau_h). \end{aligned} \tag{3.25}$$

We can follow the same steps of the main text and find the following generalization of Eq. (3.9):

$$-\ddot{C}_{\rm st}(t) + \left[1 - R^2 Q(t|\tau_M)\right] C_{\rm st}(t) = \rho^2 Q(t|\tau_h). \tag{3.26}$$

Two independent solutions of the corresponding homogeneous ODE are given by Eq. (3.20) with the identification $\tau = \tau_M$. Since the Wronskian of $u_1(t)$ and $u_2(t)$ is $1/\pi\tau_M$, by the method of variation of parameters the general solution of Eq. (3.26) is

$$C_{\rm st}(t) = c_1 u_1(t) + c_2 u_2(t) + A_1(t)u_1(t) + A_2(t)u_2(t), \tag{3.27}$$

where

$$\begin{aligned} A_1(t) &= -\pi\tau_M\rho^2\int dt e^{-t/\tau_h}u_2(t) \\ &= \frac{\pi\tau_M\rho^2(\tau_M R)^{-2\tau_M}}{(1-1/\tau_h)\sin(2\pi\tau_M)\Gamma(1-2\tau_M)}e^{(1-1/\tau_h)t} \\ &\quad\times {}_1F_2(-(1-1/\tau_h)\tau_M; 1-2\tau_M, 1-(1-1/\tau_h)\tau_M; -\tau_M^2R^2e^{-t/\tau_M}) \\ &\quad+\frac{\pi\tau_M\rho^2(\tau_M R)^{2\tau_M}}{(1+1/\tau_h)\tan(2\pi\tau_M)\Gamma(1+2\tau_M)}e^{-(1+1/\tau_h)t} \\ &\quad\times {}_1F_2((1+1/\tau_h)\tau_M; 1+2\tau_M, 1+(1+1/\tau_h)\tau_M; -\tau_M^2R^2e^{-t/\tau_M}) \end{aligned} \tag{3.28}$$

and

$$\begin{aligned} A_2(t) &= \pi\tau_M\rho^2\int dt e^{-t/\tau_h}u_1(t) \\ &= -\frac{\pi\tau_M\rho^2(\tau_M R)^{2\tau_M}}{\Gamma(1+2\tau_M)(1+1/\tau_h)}e^{-(1+1/\tau_h)t} \\ &\quad\times {}_1F_2((1+1/\tau_h)\tau_M; 1+2\tau_M, 1+(1+1/\tau_h)\tau_M; -\tau_M^2R^2e^{-t/\tau_M}). \end{aligned} \tag{3.29}$$

These integrals were computed with the substitution $z = 2\tau Re^{-t/2\tau}$ and known integrals of Bessel functions. We want to impose the boundary conditions, which are $\dot{C}_{\rm st}(0) = 0$ and that $C_{\rm st}(\infty)$ is finite. To do this we use the asymptotics of each term appearing in Eq. (3.27) which are

$$\begin{aligned} u_1(t) &\sim \frac{(\tau_M R)^{2\tau_M}}{\Gamma(1+2\tau_M)}e^{-t}, \\ u_2(t) &\sim -\frac{\Gamma(2\tau_M)(\tau_M R)^{-2\tau_M}}{\pi}e^{t}, \\ A_1(t)u_1(t) &\sim \frac{\rho^2}{2(1-1/\tau_h)}e^{-t/\tau_h}, \\ A_2(t)u_2(t) &\sim \frac{\rho^2}{2(1+1/\tau_h)}e^{-t/\tau_h}. \end{aligned} \tag{3.30}$$

To have a finite $C_{\rm st}(\infty)$ we impose that $c_2 = 0$. With this we also get that $C_{\rm st}(\infty) = 0$. Imposing $\dot{C}_{\rm st}(0) = 0$ fixes the value of c_1, which is not reported here. Setting $t = 0$ in the resulting $C_{\rm st}(t)$ one obtaines after simplifications (done on Mathematica 13.2.1.0 with FullSimplify) the following generalization of Eq. (3.10) of the main text:

$$\sigma_{\rm st}^2 = \frac{\rho^2}{1+1/\tau_h}\frac{{}_1F_2((1+1/\tau_h)\tau_M; 1+2\tau_M, 1+(1+1/\tau_h)\tau_M; -\tau_M^2R^2)}{2\,{}_0F_1(2\tau_M; -\tau_M^2R^2) - {}_0F_1(1+2\tau_M; -\tau_M^2R^2)}. \tag{3.31}$$

One can see that setting $\tau_h = \tau_M$ Eq. (3.10) is recovered after manipulations. We also see that the denominator coincides with the one present in Eq. (3.10) with the identification $\tau = \tau_M$. This implies, as mentioned in the main text of this chapter, that stability depends on the correlation time of the interaction matrix only, and the stability criterion remains exactly the same as in the main text, which is given by Eq. (3.11).

Chapter 4

Generalized Lotka-Volterra equations with annealed disorder

The disordered generalized Lotka-Volterra (GLV) model is typically analyzed under the assumption of quenched interactions, as detailed in Chapter 1. However, species interactions can fluctuate due to environmental shifts and evolutionary adaptations on timescales comparable to population dynamics. In this chapter, we incorporate the framework of annealed disorder introduced in Chapter 2 into the GLV equations. By promoting interaction coefficients to stochastic processes, we investigate how temporal variability in species couplings influences community structure. We demonstrate that annealed disorder generates emergent phenomena distinct from the quenched case, yielding species abundance distributions that align more closely with empirical observations. Furthermore, our results indicate that temporal fluctuations in interaction strengths can enhance species coexistence.

4.1 Introduction

Chapter 1 established the GLV equations as a foundational framework for modeling ecological communities. This model maintains analytical tractability while displaying a non-trivial phenomenology and, as discussed previously, is particularly amenable to a disordered system treatment. A central assumption of most analyses in this perspective is that of quenched disorder. This assumption is expected to be valid as long as a clear separation of timescales holds, in which environmental changes and other mechanisms occur so slowly relative to population dynamics that the interaction network can be considered static.

However, this static approximation may not be applicable when describing empirical ecosystems. Ecological interactions are dynamic entities characterized by continuous temporal fluctuations. These can be caused by shifting environmental conditions, seasonal resource availability, and rapid evolutionary adaptations [90, 161, 170]. Evidence suggests that these fluctuations often operate on timescales comparable to the population dynamics themselves [204, 239, 305, 306], thereby violating the assumptions required for the quenched disorder approximation.

To address this limitation, a natural candidate is the framework of annealed disorder introduced in Chapter 2. By promoting the interaction coefficients from static random variables to stochastic

This chapter is based on: Samir Suweis et al. "Generalized lotka-volterra systems with time correlated stochastic interactions". In: *Physical Review Letters* 133.16 (2024), p. 167101. As a co-author, I contributed to the theoretical and numerical analyses and supported the preparation of the text and figures.

processes, we can model the community as a system where environmental stochasticity couples directly to interspecies dynamics.

In this chapter, we study annealed disorder in the GLV equations to investigate how temporal variability in interactions influences community properties. We demonstrate that allowing interactions to fluctuate leads to emergent phenomena distinct from the quenched case, resulting in species abundance distributions that match more closely empirical observations. Moreover, we find that annealed disorder in interaction strengths favors species coexistence.

This chapter is organized as follows: in Section 4.2 we present the model; in Section 4.3 we solve it exactly in the white noise limit; in Section 4.4 we give an approximate solution in the general colored case; in Section 4.5 we analyze the effect of annealed disorder on coexistence; in Section 4.6 we compare predictions to experimental data; we conclude with a summary of the results and possibilities for further research.

4.2 Model

As before, we consider a community of S interacting species whose abundances $x_i(t)$ follow the GLV equations

$$\dot{x}_i(t) = x_i(t)\left[1 - x_i(t) + \sum_{j\neq i} \alpha_{ij}(t) J(x_j(t))\right]. \tag{4.1}$$

We introduced a response $J(x)$, which allows us to model in detail how the abundance of one species affects the growth of another, see also Chapter 5. The linear choice $J(x) = x$ corresponds to a mass-action law and facilitates direct comparison with the standard GLV model. However, as discussed in Section 1.2.1.3, this choice can lead to non-physical unbounded growth of species abundances. To prevent this phenomenon and reflect realistic biological constraints, such as the inability of a predator to process prey instantaneously, one can choose a function $J(x)$ that saturates at large values of its argument. For definiteness, we will consider a Monod-type function, which is analogous to a Holling Type II functional response:

$$J(x) = \frac{x}{1 + hx}. \tag{4.2}$$

The parameter h is known as handling time [241], and sets the saturation level of the interaction. When $h = 0$, we recover the linear interaction model. The quenched counterpart of Eq. (4.1) with a saturating response is studied in Chapter 5.

The interactions in Eq. (4.1) are taken as annealed, in the sense of Chapter 2. To align the annealed model with the quenched one, we employ the following normalization for the interaction coefficients $\alpha_{ij}(t)$:

$$\alpha_{ij}(t) = \frac{\mu}{S} + \frac{\sigma}{\sqrt{S}} z_{ij}(t), \tag{4.3}$$

where μ and σ maintain the same ecological meaning as in Chapter 1. The stochastic components $z_{ij}(t)$ are independent Ornstein-Uhlenbeck processes, characterized by zero mean and autocorrelation

$$\langle z_{ij}(t) z_{ij}(t')\rangle = Q(t - t'), \tag{4.4}$$

where the function $Q(t)$ is defined as

$$Q(t) = \frac{1 + 2\tau/\tau_0}{2\tau} \exp(-|t|/\tau). \tag{4.5}$$

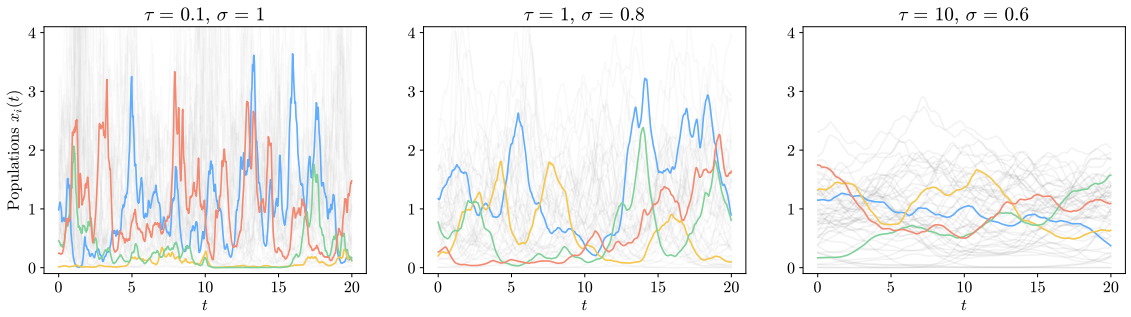

Figure 4.1: Examples of species abundance trajectories obtained via simulation of the annealed GLV equations Eq. (4.1) for $S = 100$, $J(x) = x$ and $\mu = 0$. The panels display different values of the characteristic correlation time τ and noise intensity σ. Fluctuating behavior is instrumental in promoting the coexistence of multiple species within the ecosystem and is present for all ranges of τ.

Here, τ is the correlation time of the fluctuations. As in Chapter 2, the prefactor in Eq. (4.5) is chosen such that the limit $\tau \to \infty$ recovers the standard quenched case, whereas as $\tau \to 0$ the disordered interactions become white noise. The parameter τ_0 is introduced for simple dimensionality reasons, and in the following we set $\tau_0 = 1$ without loss of generality.

Figure 4.1 illustrates the dynamics of the annealed GLV equations for varying correlation times τ. As the correlation time τ is reduced, the increasing time-variability in interactions induces correspondingly more rapid fluctuations in species abundances. We notice that the annealed GLV equations maintain, as in the quenched case, multiplicative growth proportional to current abundance. This implies that for $\tau < \infty$ the continuous variability of the interaction matrix prevents any species from settling into a zero-abundance state. This leads to the absence of true extinctions, except in the limiting case of $\tau \to \infty$.

We analyze the system in the $S \to \infty$ limit employing the associated DMFT equation. As before, this approach allows us to reduce the system to a single effective stochastic process describing the trajectory of a representative species. The DMFT equation corresponding to Eq. (4.1) is obtained employing generating functional techniques in Appendix A of [300], and we omit here the derivation. The result is

$$\dot{x}(t) = x(t)\left[1 - x(t) + \mu\langle J(x(t))\rangle + \sigma\eta(t)\right]. \tag{4.6}$$

Here, $\eta(t)$ is Gaussian noise with zero mean and autocorrelation given self-consistently by

$$\langle \eta(t)\eta(t')\rangle = Q(t-t')\langle J(x(t))J(x(t'))\rangle. \tag{4.7}$$

4.3 Exact stationary distribution in the white noise limit

We first examine the limit in which the timescale of environmental fluctuations becomes negligible compared to the population dynamics. As $\tau \to 0$, the correlation approaches a delta function, $Q(t) \to \delta(t)$. Consequently, the interaction parameters become white noise processes. In this limit, the noise driving the effective DMFT equation retains its self-consistent nature but becomes white as well:

$$\langle \eta(t)\eta(t')\rangle = \delta(t-t')\langle J(x(t))^2\rangle. \tag{4.8}$$

Since the white noise is obtained as the $\tau \to 0$ limit of colored noise, the resulting stochastic differential equation must be interpreted in the Stratonovich sense, rather than Itô or other

interpretations [112, 179].

The time evolution of the probability density function $P(x,t)$ for the representative species is governed by the Fokker-Planck equation associated with the DMFT equation

$$\frac{\partial P(x,t)}{\partial t} = \frac{\partial}{\partial x}\left[-x\Big(1-x+\mu M(t)\Big)P(x,t) + \frac{1}{2}\sigma^2 q(t) x \frac{\partial}{\partial x}\Big(xP(x,t)\Big)\right]. \tag{4.9}$$

The self-consistency of the DMFT process enters the Fokker-Planck equation through the functions

$$\begin{aligned} M(t) &= \langle J(x(t))\rangle, \\ q(t) &= \langle J(x(t))^2\rangle. \end{aligned} \tag{4.10}$$

To obtain the stationary distribution we set $\partial_t P(x,t) = 0$. Solving the resulting equation yields a Gamma distribution:

$$P(x) \propto x^{\delta-1} e^{-\beta x}, \tag{4.11}$$

where the shape δ and the scale β are given by

$$\begin{aligned} \beta &= 2/\sigma^2 q, \\ \delta &= \beta(1+\mu M), \end{aligned} \tag{4.12}$$

where M and q are the stationary values of Eq. (4.10). To relate these parameters to the microscopic ones, we must impose the self-consistencies, by relating M and q back to averages over $P(x)$. In the case of linear interactions $J(x) = x$, imposing them fixes the parameters as

$$\begin{aligned} \beta &= \frac{1}{2}\sigma^2\delta(\delta+1), \\ \delta &= \frac{2}{\sigma^2}(1-\mu) - 1. \end{aligned} \tag{4.13}$$

This result provides a direct link between the microscopic disorder parameters μ and σ and the macroscopic abundance distribution. In the more general case of a Monod response, the self-consistency conditions involve integrals that do not reduce to simple algebraic forms, making the calculation more involved (see Apprendix 4.8.3).

4.4 Approximated stationary distribution in the colored case

Given that the general solution of the effective stochastic process for arbitrary correlation time τ is quite involved already for the linear model, as discussed in Chapter 2, we employ an approximated scheme.

We observe (see Figures 4.5 and 4.6 in Appendix 4.8.1) that at stationarity the connected autocorrelation function of the response $J(x(t))$ can be well-approximated with an exponential decay:

$$\langle J(x(t))J(x(t'))\rangle \approx M^2 + \left(q - M^2\right) e^{-|t-t'|/\tau_x}, \tag{4.14}$$

where τ_x is a characteristic time. If we further approximate this behavior for small time differences $|t-t'| \ll 1$, this simplifies to

$$\langle J(x(t))J(x(t'))\rangle \approx q e^{-\frac{|t-t'|}{\tau_x'}}, \tag{4.15}$$

where we have introduced a renormalized timescale τ'_x defined by

$$\tau'_x = \frac{q}{q - M^2}\tau_x. \tag{4.16}$$

The effective noise $\eta(t)$ driving the DMFT equation then has an exponential correlation function

$$\langle \eta(t)\eta(t')\rangle \approx \frac{1+2\tau}{2\tau} q e^{-\frac{|t-t'|}{\bar{\tau}}}, \tag{4.17}$$

where the effective correlation time $\bar{\tau}$ is

$$\bar{\tau} = \left(\frac{1}{\tau} + \frac{1}{\tau'_x}\right)^{-1}. \tag{4.18}$$

Within this approximation, the noise $\eta(t)$ becomes an Ornstein-Uhlenbeck process. This allows us to further employ a standard approximation for obtaining the stationary distribution of stochastic processes driven by colored Ornstein-Uhlenbeck noise, known as Unified Colored Noise Approximation (UCNA) [60, 76]. To obtain it, we first perform a change of variable in Eq. (4.6) to obtain a stochastic differential equation with additive noise. Explicitly, we consider the substitution $y = \log x$, which transforms Eq. (4.6) into $\dot{y} = 1 - e^y + \mu\langle J(e^{y(t)})\rangle + \sigma\eta(t)$. We can then differentiate this equation with respect to time to explicitly eliminate the colored noise variable, by employing the SDE for the Ornstein-Uhlenbeck noise $\eta(t)$. This transforms the original one-dimensional non-Markovian dynamics into an equivalent two-dimensional Markovian system characterized by an effective inertial term. We then rescale time as $s = \tau^{-1/2}t$ and perform an adiabatic elimination of the acceleration variable in the resulting equation. The procedure effectively reduces the system back to a one-dimensional SDE, but one that is now driven by multiplicative white noise. This procedure is exact in both the limits $\tau \to 0$ and $\tau \to \infty$, see [76] for details on the validity for intermediate values of τ. From the reduced Markovian equation, the corresponding Fokker-Planck equation can be constructed and solved analytically to yield a closed-form expression for the stationary probability distribution. The whole procedure is summarized for the present case by the formula given in Footnote 14 of [60], which yields the approximate stationary distribution of Eq. (4.6):

$$P(x) \propto x^{\delta-1}\left(\frac{1}{\bar{\tau}} + x\right)\exp\left(-\frac{x}{D} - \frac{\bar{\tau}}{2D}(x-\bar{x})^2\right), \tag{4.19}$$

where

$$\begin{aligned} \delta &= \frac{1+\mu M}{D}, \\ D &= \frac{1+2\tau}{2\tau}\bar{\tau}\sigma^2 q, \\ \bar{x} &= 1 + \mu M. \end{aligned} \tag{4.20}$$

We see that the resulting distribution $P(x)$ is essentially an interpolation between the Gamma distribution found in the white noise limit and the Gaussian distribution of the quenched disorder limit in the single equilibrium phase, see Eq. (1.16).

We compare the stationary distribution Eq. (4.19) with the one obtained from direct numerical integration of the GLV equations in Figure 4.2. The agreement is excellent across various values of τ. The parameters were obtained by fitting the auto-correlation function, with errors consistently below 5% (see Appendix 4.8.1.1). We demonstrate that these results hold equally well for the Monod functional response (see Appendix 4.8.1.2). Sensitivity analysis confirms that the analytical solutions robustly match numerical results over a wide parameter range (see Appendix 4.8.4).

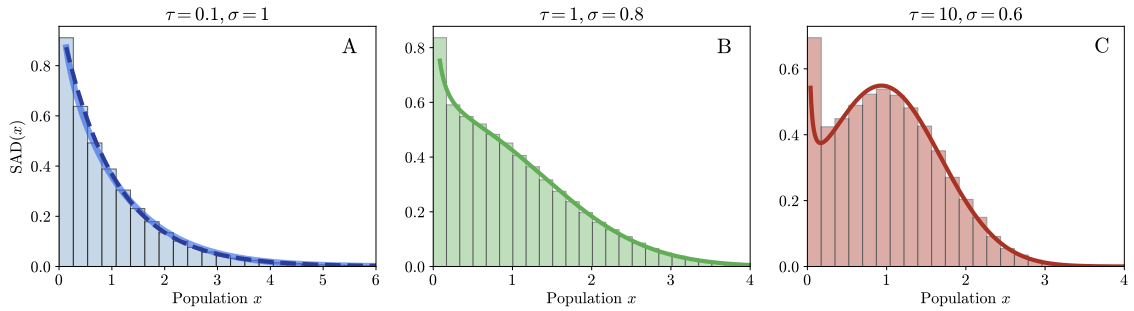

Figure 4.2: Comparison between numerical and analytical Species Abundance Distributions (SADs). The histograms represent the obtained direct simulation of the GLV equations with annealed disorder Eq. (4.1) for $S = 100$ species and linear response $J(x) = x$. Solid lines represent the analytical SADs derived in the text. In panel A the distribution is exact and given by Eq. (4.11). In panels B and C the SADs are approximated using UCNA and given by Eq. (4.19), with parameters obtained by fitting.

4.5 Impact on coexistence

As discussed previously, the introduction of time-dependent fluctuations in interactions is expected to promote species coexistence. This effect arises because the fluctuating interaction matrix prevents any species from reaching the absorbing state at $x = 0$, effectively preventing extinctions for any finite τ.

True extinctions, represented by a discrete mass in $x = 0$, emerge only in the limit $\tau \to \infty$. However, species abundances are discrete, and thus populations become extinct at sufficiently low abundance. To address this, we introduce an extinction threshold x_{th}. Figure 4.3 shows that the fraction of species falling below this threshold is reduced as τ gets smaller. Each point in Figure 4.3 is calculated as $\int_0^{x_{\text{th}}} P(x)dx$, using the analytical distribution Eq. (4.19). The horizontal dashed lines represent the theoretical extinction fraction in the quenched disorder limit, as given by Eq. (1.20).

This supports the implication that stochastic variability promotes coexistence, while slow or static interactions are detrimental to diversity.

4.6 Comparison with empirical data

To address the empirical relevance of our findings, we have analyzed two species abundance datasets: trees from a tropical forest [119] and coral reefs [132]. Figure 4.4 shows the SADs using the Preston (log2) scale, as is customary in this context [174]. The empirical SADs were then compared with the truncated Gaussian and Gamma distributions predicted from the quenched and white annealed GLV, respectively. We find that the empirical SADs are accurately described by the white annealed model, while the quenched model fails to reproduce these patterns. This comparison supports the empirical relevance of our model, demonstrating its applicability to real-world ecological data.

4.7 Discussion

In this chapter, we presented an investigation into the GLV equations with annealed disorder, incorporating finite correlation time as well as a simple saturating response. We have determined

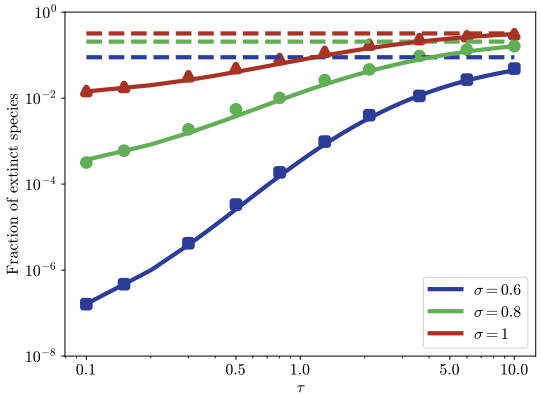

Figure 4.3: Fraction of extinct species at stationarity for $\mu = 0$ and different values of interaction heterogeneity σ as a function of the characteristic fluctuation time (τ). Solid lines are obtained analytically by assuming $\tau_x \propto \tau$ (see Appendix 4.8.2), which allows for a simple estimation of the extinction fraction without fitting model parameters. The dashed lines indicate the quenched limits of the extinct fractions. The extinction threshold is set to $x_{\text{th}} = 10^{-2}$, though the qualitative behavior is independent of this specific value.

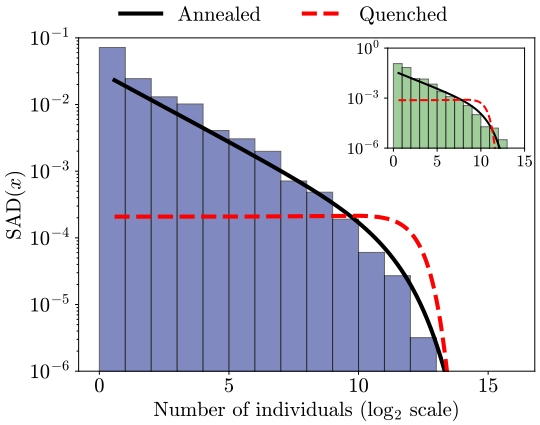

Figure 4.4: Comparison with empirical data. The main panel shows the SAD in the BCI forest. The black line is the fit of the Gamma distribution predicted by the annealed GLV, while the red dashed line is the fit of the Gaussian distribution predicted by quenched GLV. The parameters of the distribution have been estimated by using maximum likelihood. The inset shows the SAD in the Caribbean Coral Reef.

the corresponding DMFT equation, which yields an exact description of the community in the limit of a large number of species. The inclusion of temporal stochastic fluctuations in species interactions has resulted in a diverse range of ecologically significant outcomes.

Firstly, the introduction of annealed disorder in the GLV equations, for any finite correlation time, has exerted a substantial positive influence on the biodiversity of the system. Specifically, when the dynamics of the system converges to the stationary distribution, we observe fluctuations in the dynamics of species populations, where species abundances alternate between high and low values, favoring the coexistence of all species. This is, in fact, a similar outcome to what quenched models find in the chaotic phase [223, 281] when introducing an immigration rate λ, which explicitly prevents extinctions.

Secondly, in the white noise limit, the DMFT leads to the stochastic logistic model, a phenomenological model that proved to be consistent with several macroecological laws in microbial ecosystems [217, 218]. In particular, the analytical species abundance distribution derived from the DMFT follows the Gamma distribution, a widely utilized probability distribution in macroecology [119, 174]. Again, similar truncated fat-tailed distribution has recently been numerically found in the chaotic phase of the quenched GLV [281] and in the GLV with strong interactions [247, 293, 297] with immigration.

Moreover, we have presented a refinement of the model, through the inclusion of a simple response. We have shown that it maintains not only the core phenomenology described above, but also rectifies any non-physical divergences observed in the classic quenched GLV and in the annealed GLV. Thus, it enhances the realism and applicability of the model without sacrificing its fundamental characteristics and predictive capabilities. Further properties of the GLV model with

the same type of saturating response are discussed in Chapter 5.

Various extensions are possible, including the integration of quenched and annealed disorder, the correlations between pairs of interacting species [186, 199] or more complex hierarchical correlation structures [268]. More generally, the methodology presented here can be exploited to study the effect of annealed disorder also in other ecological, and generally non-linear, dynamics [314, 323]. Moreover, to further improve the annealed GLV model, it would be valuable to explore sparse interaction networks instead of the fully connected ones examined here and in previous works [186, 195, 196, 199, 223, 229] for the quenched version.

Finally, as established in Chapter 3, the GLV model with annealed interactions exhibits multiple phases, characterized by either the presence or the breaking of replica symmetry. A detailed characterization of the boundary between these two phases and their properties, for example by employing the replicated DMFT framework developed in [201], represents an important next step. Such an investigation would clarify how temporal variability impacts the stability and properties of high-dimensional ecological landscapes.

4.8 Appendix

4.8.1 Autocorrelation function

In order to test the analytical prediction of the annealed GLV with time correlated stochastic interactions, we first discuss the ansatz on the autocorrelation function from which we then are able to derive the stationary solution $P(x)$ given by Eq. (4.19). Note that the DMFT Eq. (4.6) is the same both for $J(x) = x$ and $J(x) = x/(1 + cx)$, with the only differences being in the self consistence parameters $\langle J(x(t))\rangle$ and $\langle J(x(t))J(x(t'))\rangle$. As a result, the stationary distribution is identical in both cases.

4.8.1.1 Linear functional response

Guided by the empirical behavior of the auto-correlation function, we assume that, at stationarity, it has an exponential-like shape as shown by the red line fit in Figure 4.5

$$\langle x(t)x(t')\rangle \approx e^{-|t-t'|/\tau_x}(q - M^2) + M^2, \tag{4.21}$$

In the time window $|t - t'| \ll \tau_x$ we can approximate the exponential ansatz for the connected autocorrelation function with an exponential ansatz for the non-connected autocorrelation function. Explicitly, we can expand at the first order Eq. (4.21) obtaining

$$\langle x(t)x(t')\rangle \approx q - (q - M^2)|t - t'|/\tau_x \approx qe^{-|t-t'|/\tau'_x}, \tag{4.22}$$

with $\tau'_x = \tau_x q/(q - M^2)$. Thus we can rewrite the auto-correlation of noise $\eta(t)$ as

$$\langle \eta(t)\eta(t')\rangle \approx \sigma^2 C\frac{1 + 2\tau}{2\tau}e^{-|t-t'|/\bar{\tau}}, \tag{4.23}$$

which corresponds to a colored noise with correlation time

$$\bar{\tau} = \left(\frac{1}{\tau} + \frac{1}{\tau'_x}\right)^{-1}. \tag{4.24}$$

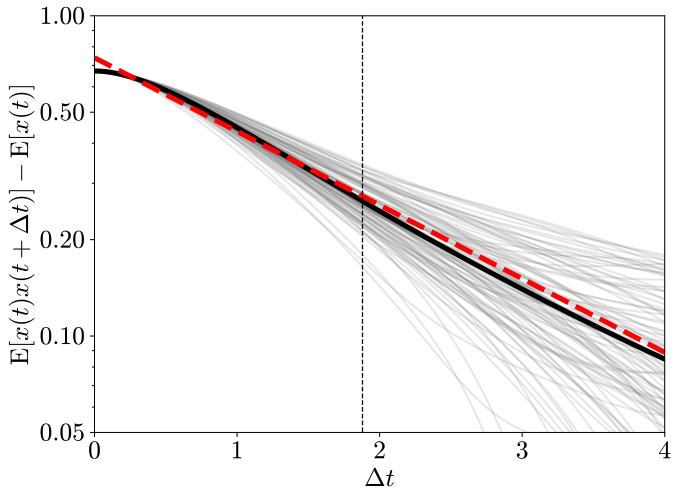

Figure 4.5: Gray lines represent the empirical auto-correlation function for $J(x) = x$ calculated as $\langle x(t)x(t+\Delta t)\rangle - \langle x(t)\rangle^2$ (averaged over t) for each of the species simulated using the annealed GLV, here with $S = 100$, $\tau = 1$, $\mu = 0$ and $\sigma = 0.8$. Black line represents the mean of the auto-correlation, while the thick red line represents the exponential decay given by the ansatz Eq. (4.21). For this set of parameters and for $J(x) = x$, we find $\tau_x = 1.88$, and thus we expect that our ansatz works for $\Delta t < 1.88$, that is, on the left of the vertical line indicating $\Delta t = 2$. A similar procedure has been applied for $J(x) = x/(1 + cx)$, see Figure 4.6.

τ	$\lvert M^{fit} - M^{emp}\rvert / M^{emp}$	$\lvert q^{fit} - q^{emp}\rvert / q^{emp}$	τ_x
10	0.0079	0.015	11.15
1	0.00068	0.015	2.32
0.1	0.00020	0.0024	1.31

Table 4.1: The second and the third columns: Relative error for the M and q parameter obtained by the fit of the correlation with Eq. (4.21) compared with the stationary first and second moment $M^{emp} = \langle x\rangle$ and $q^{emp} = \langle x^2\rangle$ computed from the numerical simulation. Third column: the characteristic decay time τ_x of the correlation function.

The previous two equations become exact both in the $\tau \to 0$ limit leading to $\bar{\tau} = 0$ and so η becomes a white noise and in the $\tau \to \infty$ limit where we expect that also $\tau_x \to \infty$ implying $\bar{\tau} \to \infty$. Given Eq. (4.23), we can use the UCNA approximation [60], specifically footnote 14 of reference [60]. The normalization of $P(x)$ can be found in Eq. (30) of Supplemental Material of [300].

We fit the empirical correlation $\langle x(t)x(t')\rangle$ with Eq. (4.21), obtaining the parameters τ_x, M and q from which we can compute the parameters $\bar{\tau}$ and D.

Thus, we have evaluated the distribution $P(x)$ with the parameters obtained from the fit of the correlation. The result is shown in Figure 4.2.

4.8.1.2 Non-linear Monod functional response

We have repeated the procedure presented in the previous section for the GLV with a Monod response function. We assume that also in this case, at stationarity, the two-points empirical

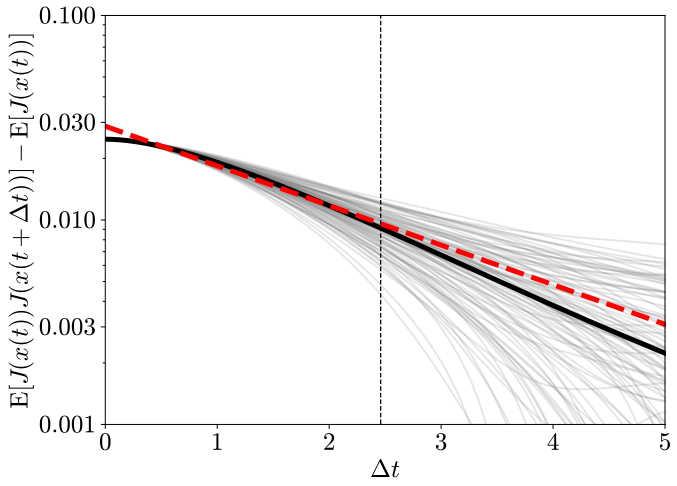

Figure 4.6: Gray lines represent the empirical auto-correlation function for $J(x) = x/(1+cx)$ calculated as $\langle J(x(t))J(x(t+\Delta t))\rangle$ (averaged over t) for each of the species simulated using the annealed GLV, here with $S = 100$, $c = 1$, $\tau = 1$, $\mu = 0$ and $\sigma = 1.5$). Black dots represent the mean of the auto-correlation, while the thick red line represents the exponential decay given by the ansatz Eq. (4.25). For this set of parameters and for $J(x) = x/(1+x)$, we find $\tau_x = 2.46$, and thus we expect that our ansatz works for $\Delta t < 2.46$, i.e., on the left of the vertical line indicating $\Delta t = 2$.

τ	$\lvert M^{fit} - M^{emp}\rvert / M^{emp}$	$\lvert q^{fit} - q^{emp}\rvert / q^{emp}$	τ_x
10	0.0015	0.014	10.23
1	0.0023	0.014	2.46
0.1	$9.078 \cdot 10^{-6}$	0.0033	1.27

Table 4.2: The second and the third columns: Relative error for the M and q parameter obtained by the fit of the correlation with Eq. (4.25) compared with the stationary first and second moment $M^{emp} = \langle J(x)\rangle$ and $q^{emp} = \langle J^2(x)\rangle$ computed from the numerical simulation. Third column: the characteristic decay time τ_x of the correlation function.

correlation function of $J(x)$ has an exponential-like shape, i.e.,

$$\langle J(x(t))J(x(t'))\rangle \approx e^{-|\Delta t|/\tau_x}(q - M^2) + M^2, \tag{4.25}$$

where $J(x = x/(1+cx)$, $M = \langle J(x)\rangle$ and $q = \langle J^2(x)\rangle$. In this case, we fit the correlation $\langle J(x(t))J(x(t'))\rangle$ from the numerical simulation with Eq. (4.25), obtaining the parameters τ_x, M and q from which we can compute the parameters D and $\overline{\tau}$.

Thus, we have evaluated the distribution $P(x)$ with the parameters obtained from the fit of the correlation. The result is shown in Figure 4.7.

Also for this case we have that in the white noise limit $\delta = 2(1+\mu M)/(\sigma^2\Sigma^2)$ with $M = \delta\left(-c + e^{\beta/c}\left(c+\beta+c\delta\right)E_{1+\delta}(\frac{\beta}{c})\right)/c^3$ and $\Sigma = e^{\beta/c}\delta E_{1+\delta}(\frac{\beta}{c})/c$, where the function $E_n(x) = \int_1^\infty e^{-xt}/t^n dt$ is the exponential integral function.

We conclude that the proposed approach works equally well for the GLV with and without the Monod response function and for values of μ that are non-zero, see Appendix 4.8.4 for different values of μ.

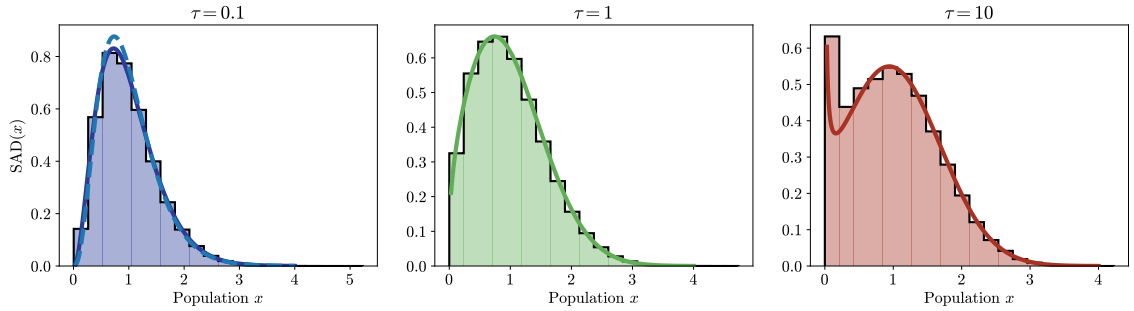

Figure 4.7: Comparison between the numerical equilibrium SAD obtained by simulating the full annealed GLV equation with the Monod function and the theoretical distribution evaluated with the parameters computed by the correlation fit. The analytical solution perfectly describes the numerical simulations. The parameters used are $c = 1$, $\mu = 0$, $\sigma = 1.5$, $\Delta t = 0.01$, $S = 100$ and 100000 time steps. For the case $\tau = 0.1$ we have also plotted $P(x)$ with the parameters computed by solving numerically the self-consistent relations.

4.8.2 Correlation time

In order to compute the stationary distribution $P(x)$, the only missing ingredient is the correlation time τ_x that must be computed by fitting the autocorrelation with the ansatz Eq. (4.21) for the linear response function and Eq. (4.25) for the non-linear Monod response function. Inspired by numerical observation, we assume that the τ_x increases linearly with τ, see Figure 4.8. Therefore, we fit τ_x for given μ and σ, and we assume that the parameters of the fit does not depend too strongly on this specific choice. Indeed, panel A of Figure 4.8 shows that this is a reasonable hypothesis.

Once the correlation time has been determined, we can numerically solve the self-consistent equations to calculate $\langle J(x)\rangle$ and $\langle J(x)^2\rangle$. This will be done for both $J(x) = x$ and $J(x) = x/(1 + cx)$. Using these calculations, we can then determine $\overline{\tau}$ and D, as defined in relation to Eq. (4.19). Figure 4.8 shows the comparison between the numerical simulations and the theoretical prediction obtained by using this assumption. Even if τ_x also depends on μ and σ, this approximation is able to predict the dependence of $\overline{\tau}$, D and the fraction of the extinct species (see Figure 4.3) on τ.

4.8.3 White-noise limit

One simple way to obtain the white noise limit of the AGLV is to take $\overline{\tau} \sim \tau \to 0$. This leads, for $J(x) = x$ to

$$\begin{aligned} \delta &= 2(1 + \mu M^*)/(\sigma^2\langle x^2\rangle), \\ D &= \sigma^2\langle x^2\rangle/2, \end{aligned} \tag{4.26}$$

and to the stationary distribution $P(x)$ that is a Gamma distribution as given by Eq. (4.11).

We can now express these parameters as a function of the interactions mean μ and variance σ^2. In fact, from Eq. (4.26), we can write $\delta = \beta(1 + \mu M)$. At the same time, from the mean of the Gamma distribution Eq. (4.11) we have that $M = \delta/\beta$, and thus $M = 1/(1 - \mu)$. In other words, the existence of $P(x)$ is limited to the region of the $\mu - \sigma$ phase space given by $\mu < 1$.

Similarly, from Eq. (4.11) we also have that $\langle x^2\rangle = \delta(\delta + 1)/\beta^2$. But $\beta = 2/(\sigma^2\langle x^2\rangle$ and thus

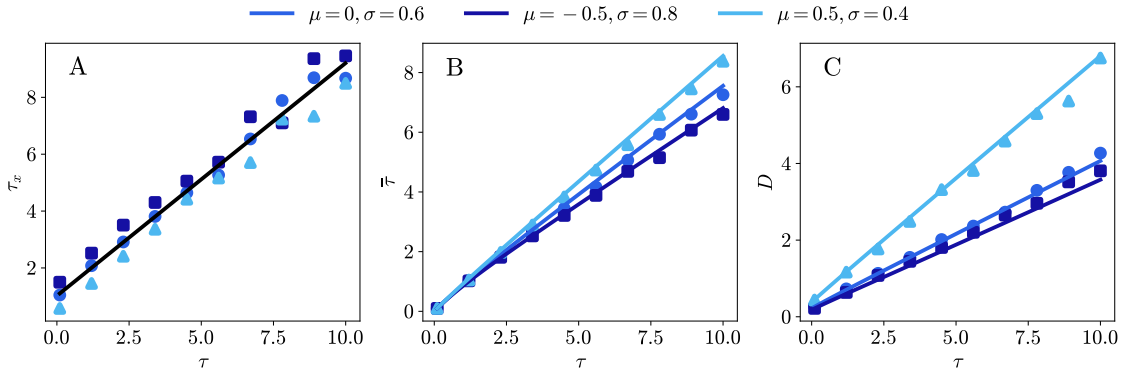

Figure 4.8: A) Solid black line is fit of τ_x for the model with $\mu = 0$ and $\sigma = 0.6$, while markers indicates the correlation time τ_x for different values of the parameters. B-C) Comparison between the theoretical prediction and the numerical simulations for the parameters $\overline{\tau}$ and D. The solid lines are the theoretical prediction computed by using the linear assumption of τ_x, while markers are the numerical simulations. The parameters used are $\Delta t = 0.01$, $S = 100$ species.

we eventually find:

$$\begin{aligned} \beta &= \frac{\sigma^2}{2}\delta(\delta+1), \\ \delta &= \frac{2}{\sigma^2}(1-\mu) - 1, \end{aligned} \tag{4.27}$$

which is Eq. (4.13) ofthe main text.

With the Monod function $J(x) = x/(1+cx)$, the stationary distribution is still given by Eq. (4.11), but the self-consistent relations for the first and the second moments become

$$\begin{aligned} M &= \int_0^\infty J(x)P(x)dx = \frac{\delta\left(-c + e^{\beta/c}\left(c+\beta+c\delta\right)E_{1+\delta}\left(\frac{\beta}{c}\right)\right)}{c^3}, \\ \langle x^2\rangle &= \int_0^\infty J^2(x)P(x)dx = \frac{e^{\beta/c}\delta E_{1+\delta}\left(\frac{\beta}{c}\right)}{c}, \end{aligned} \tag{4.28}$$

where $E_n(x) = \int_1^\infty dt\, t^{-n}\exp(-xt)$ is the exponential integral.

We highlight that the stationary solution given by Eq. (4.11) is actually an exact result that can be obtained without using UCNA, but starting from Eq. (4.6) and taking the limit $\tau \to 0$. In this case, in fact, one can get the DMFT equation through the usual machinery

$$\dot{x}(t) = x(t)[1 - x(t) + \mu M(t) + \sigma\eta(t)], \tag{4.29}$$

with $\langle\eta(t)\eta(t')\rangle = q(t)\delta(t-t')$, $q(t) = \langle J(x(t)^2\rangle$, and the multiplicative noise term $x(t)\eta(t)$ should be interpreted in the Stratonovich sense. From Eq. (4.29), we can derive the corresponding Fokker-Plank equation, the self-consistent equations $M = \langle J(x)\rangle$, $q = \langle J(x)^2\rangle$ and obtain the solution $P(x)$ given by Eq. (4.11).

4.8.4 Sensitivity analysis for different values of interaction mean

We show here the comparison between $P(x)$ obtained through the DMFT and the full numerical simulation of the GLV for different values of μ, to assess the robustness of our approach. The results

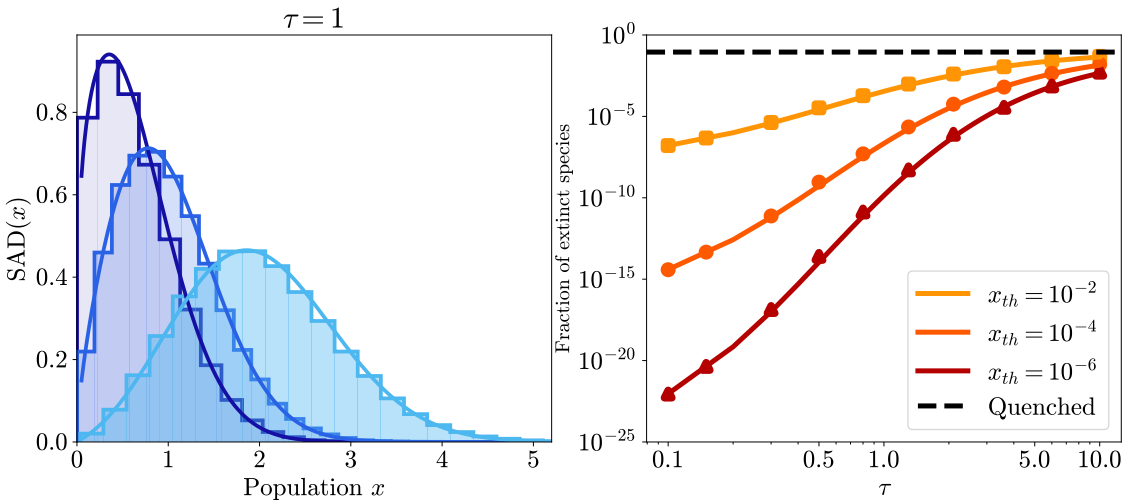

Figure 4.9: Left: comparison between the stationary SAD by simulating the full GLV system for $S = 100$ species and $\tau = 1$, and the analytical prediction obtained by using the linear assumption of τ_x. The values μ and σ are as in Fig. 4.8. Right: Comparison between the fraction of species extinct for different values of x_{th}. The solid lines are the theoretical prediction computed by using the linear assumption of τ_x, while markers are the numerical simulations. The dashed black line is the fraction of extinct species for the quenched case. The parameters used are $\mu = 0$ and $\sigma = 0.6$, $\Delta t = 0.01$, $S = 100$ species.

are summarized in Figure 4.10 Figure 4.11 for $\mu = 0.5$, $\mu = -0.5$ and $J(x) = x$, and Figure 4.12 and Figure 4.13 for $\mu = 0.5$, $\mu = -0.5$ and $J(x) = x/(1 + cx)$. We conclude that our approach works equally well for values of μ that are non-zero and for both choices of $J(x)$.

4.8.5 The stationary state of the white-noise limit for a linear response is not always reached

To make a comparison between GLV with quenched and annealed interactions, we also investigate the phase diagram for the case $\tau = 0$ and $J(x) = x$. Since $\delta > 0$ (see Eq. (4.11)) and $\langle x \rangle > 0$, in order for the stationary solution to exist, we have the conditions $\sigma < \sqrt{2(1-\mu)}$ and $\mu \leq 1$, leading to a upper bound for the phase of the annealed GLV in which the stationary state is reached, as shown in Figure 4.14. However, by solving numerically the self-consistent Eq. (4.6) and also performing the numerical simulation of the GLV equation Eq. (4.1), we find that below this bound, even though a stationary solution exists, it may not be reached. In particular, in the brown region of Figure 4.14, independently of the initial condition for $x(0)$, there is a singularity at finite times, leading to the explosion of the species population. In the light-blue region instead, if we start close to the predicted stationary solution $P(x)$, then we always find that the stationary solution is reached and it coincides with the one predicted by the DMFT Eq. (4.11). However, there is a set of initial conditions (for sufficiently large $x(0)$) for which $x(t)$ may diverge for finite t.

We observed numerically that for some choices of the parameters and initial conditions the stationary state in the white-noise limit and for $J(x) = x$, computed exactly above, is not reached. For fixed μ and σ and a fixed initial condition, that is, $p_0(x) = \delta(x - x_0)$, the dynamics reaches the predicted stationary state only for sufficiently low x_0. Increasing the initial condition always leads to a divergence at finite times. Increasing either μ or σ lowers the initial condition at which the dynamics diverges. The same behavior has been observed with an initial condition drawn from a

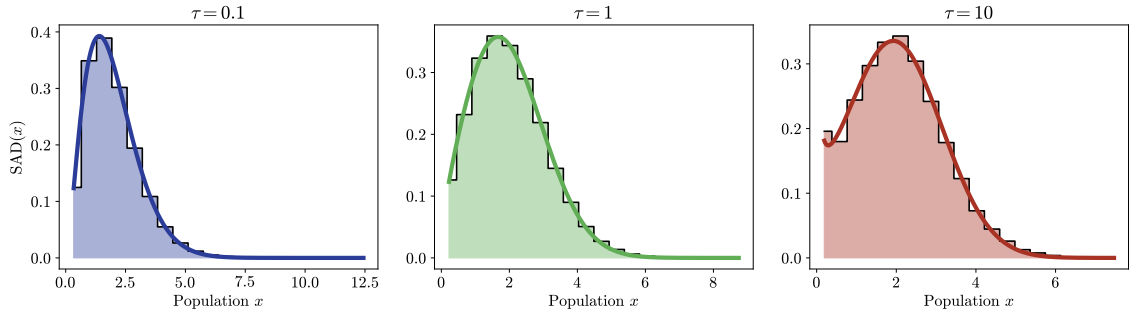

Figure 4.10: Comparison between the numerical equilibrium SAD obtained by simulating the full GLV equation and its fit obtained in the same way as explained in the previous section (and $J(x) = x$). The analytical solution perfectly describes the numerical simulations. The parameters used are $\mu = 0.5$, $\sigma = 0.5$, $\Delta t = 0.01$, $S = 100$ and 50000 timesteps.

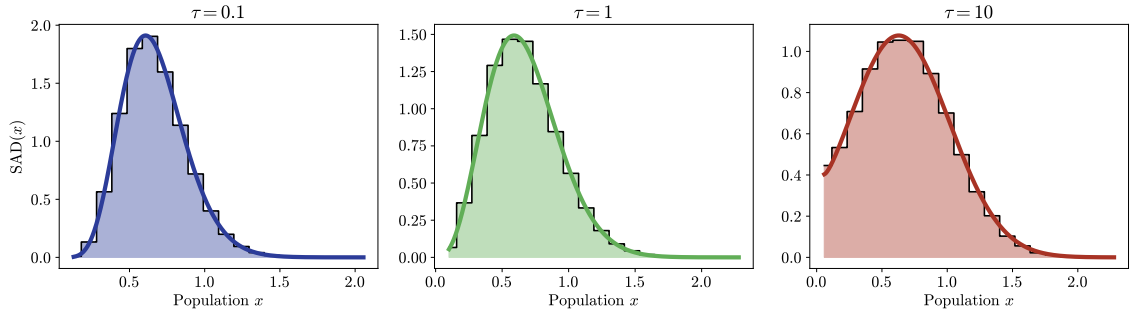

Figure 4.11: Comparison between the numerical equilibrium SAD obtained by simulating the full GLV equation and its fit obtained in the same way as explained in the previous section (and $J(x) = x$). The analytical solution perfectly describes the numerical simulations. The parameters used are $\mu = -0.5$, $\sigma = 0.5$, $\Delta t = 0.01$, $S = 100$ and 50000 timesteps.

uniform distribution.

We highlight that such divergences are not because the DMFT does not hold for a specific set of parameters (in fact simulating both Eq. (4.1) and Eq. (4.6) give rise to the same finite time divergence). Rather, the divergence at finite times and its dependence on initial conditions of the annealed GLV dynamics with $\tau = 0$ are due to unbounded growth of the function $J(x) = x$ in the GLV model and non-linearity of the Fokker-Planck equation [115].

Strictly speaking, given that for any choice of μ and σ we can find initial conditions for which the dynamics diverges, a phase diagram analogous to the one of the quenched $\tau \to \infty$ limit cannot be obtained. We nevertheless analyzed in more depth the case in which the initial condition is drawn from the predicted stationary distribution Eq. (4.11) and obtained the "phase diagram" of Figure 4.14.

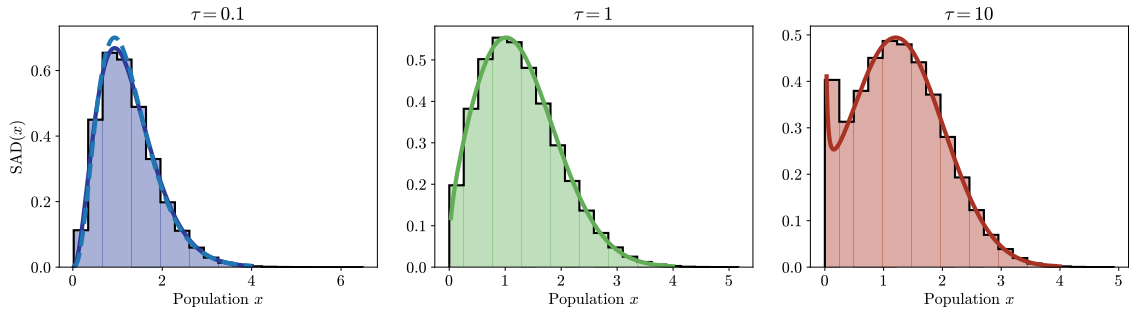

Figure 4.12: Comparison between the numerical equilibrium SAD obtained by simulating the full GLV equation with the Monod function and the theoretical distribution evaluated with the parameters computed by the correlation fit. The analytical solution perfectly describes the numerical simulations. The parameters used are $c = 1$, $\mu = 0.5$, $\sigma = 1.5$, $\Delta t = 0.01$, $S = 100$ and 100000 time steps. For the case $\tau = 0.1$ we have also plotted $P_0^*(x)$ with the parameters obtained by solving numerically the self-consistent relations.

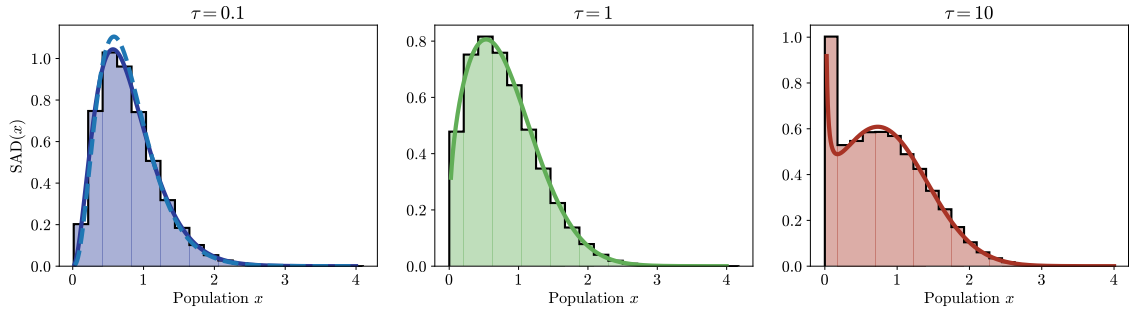

Figure 4.13: Comparison between the numerical equilibrium SAD obtained by simulating the full GLV equation with the Monod function and the theoretical distribution evaluated with the parameters computed by the correlation fit. The analytical solution perfectly describes the numerical simulations. The parameters used are $c = 1$, $\mu = -0.5$, $\sigma = 1.5$, $\Delta t = 0.01$, $S = 100$ and 100000 time steps. For the case $\tau = 0.1$ we have also plotted $P(x)$ with the parameters obtained by solving numerically the self-consistent relations.

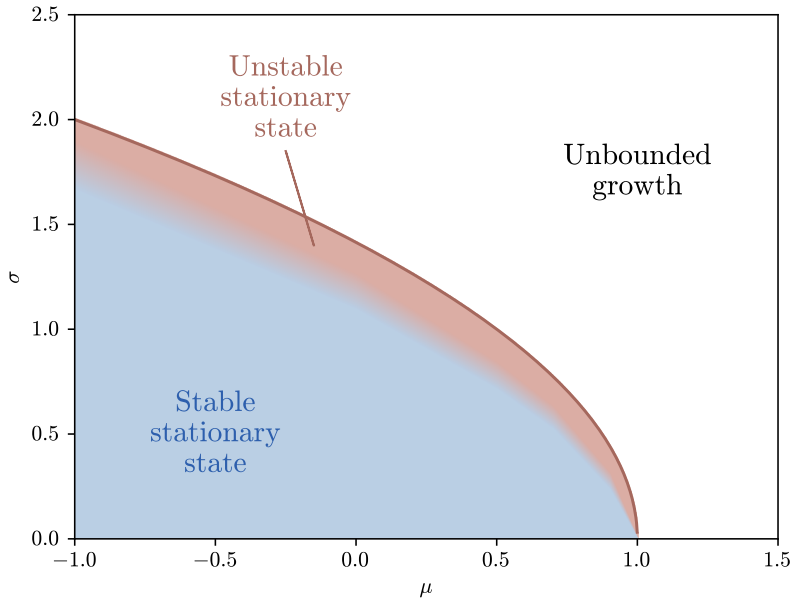

Figure 4.14: Phase diagram for the annealed white noise ($\tau = 0$) case and $J(x) = x$. We show the annealed GLV phase diagram as a function of the mean (μ) and standard deviation (σ) of the species' interaction strengths. In the unbounded growth region, as predicted analytically, the species abundance dynamics diverge for finite times. In the brown region, although the stationary solution of the DMFT equation exists, it is not reachable by the dynamics and we also have a singularity for finite times. In the light-blue region, for initial conditions taken from the stationary distribution Eq. (4.11), a stationary state exists and it corresponds to the Gamma distribution as given by Eq. (4.11). The gradient between the blue and brown regions indicates a region of numerical uncertainty. Divergences and numerical uncertainty are eliminated when $J(x) = x/(1 + cx)$ is considered in the dynamics, and the corresponding phase diagram only displays a stable stationary state.

Chapter 5

Disordered generalized Lotka-Volterra equations with saturating response

As discussed in Chapter 1, the generalized Lotka-Volterra (GLV) equations with quenched disorder suffer from pathological unbounded growth when cooperation or heterogeneity in interactions is sufficiently high. This behavior is a direct consequence of the linear interaction term, which is typically assumed for analytical convenience. This chapter addresses this limitation by introducing a more realistic saturating non-linear response into the disordered GLV equations. We derive analytical expressions for the species abundance distribution in the Unique Fixed Point phase and demonstrate the suppression of unbounded dynamics. Numerical simulations reveal a rich dynamical structure in the Multiple Attractor phase, including a transition between high-dimensional chaotic and low-volatility regimes governed by interaction symmetry. These findings offer a more ecologically realistic foundation for disordered ecosystem models and highlight the critical role of non-linearity and symmetry in shaping the properties of species-rich ecological communities.

5.1 Introduction

The disordered GLV model exhibits three distinct dynamical regimes, as detailed in Chapter 1: global convergence to a unique fixed point (UFP), multiple attractors (MA), and unbounded population growth (UG). In the latter, population abundances diverge in finite time. This ecologically unrealistic outcome stems from a pathology of the GLV model, specifically the assumption that the per-capita growth rate of a species depends linearly on the abundances of other species. This linearity can trigger positive feedback loops when interactions are strongly cooperative or highly heterogeneous, ultimately resulting in unbounded growth. To remedy this limitation, non-linear functional responses can be introduced. Such modifications enhance ecological realism and, indeed, various functional responses have been proposed in the literature to capture the non-linear nature of biological interactions.

Functional responses, which describe how a consumer's feeding rate changes with resource density, play a fundamental role in understanding species interactions and ecosystem dynamics [25, 240]. Holling classified these responses into three main types: Type I (linear), Type II (saturating),

This chapter is based on: Marco Zenari et al. "Generalized Lotka-Volterra systems with quenched random interactions and saturating nonlinear response". In: *Physical Review E* 113.2 (2026), p. 024206. As a co-author, I contributed to the theoretical analyses and supported the preparation of the text.

and Type III (sigmoidal) [25]. Type I responses assume a linear relationship between resource density and consumption rate up to a maximum, while Type II responses show a decelerating intake rate that reaches an asymptote at high resource densities, reflecting handling time limitations. Type III responses exhibit a sigmoid curve, indicating low feeding rates at low resource densities followed by an accelerating phase before reaching saturation.

A recent study extended the disordered GLV equations to include a non-linear response [226]. In that work, a functional response similar to a Holling Type II form was introduced via a saturating feedback function. Similarly, Chapter 3 and 4 introduced a saturating function into the GLV model for the case of annealed interactions. In this chapter, we aim to investigate the dynamics and stability of the GLV model with a non-linear response and quenched interactions. Our approach begins with the derivation of the DMFT equation for the system, which allows us to study the UFP phase and derive the corresponding SAD in a closed form. We then focus on the loss of stability and the emergence of chaos in the MA phase as a function of the mean, variance and correlation of the random interactions. Although the UG phase vanishes as a result of the saturating non-linear response, the MA phase, as also seen in previous work [226], presents two distinct types of dynamics. These are characterized by using the indicators proposed in [226] and two additional quantities: the dimensionality of the dynamics and the maximum Lyapunov exponent.

Overall, this chapter provides a comprehensive understanding of the different phases displayed by disordered GLV equations with saturating responses.

This chapter is organized as follows: in Section 5.2 we present the model; in Section 5.3 we derive a Lyapunov function for its symmetric limit; in Section 5.4 we analyze the model within the unique-fixed-point assumption; in Section 5.5 we discuss the the properties of its multiple attractor phase; we conclude with a summary of the results and possibilities for further research.

5.2 Model

As in previous chapters, we consider a large ecological community composed of S species. We assume that the dynamics of the abundances follow the GLV equations with a non-linear interaction term $J(x)$ introduced as follows:

$$\dot{x}_i = x_i \left[1 - x_i + \sum_{j \neq i} \alpha_{ij} J(x_j) \right] + \lambda. \tag{5.1}$$

The addition of a small migration term λ allows the system to reach a stationary state at long times for all values of the interaction parameters by preventing aging, see Sections 1.2.2.3 and 1.2.2.4.

The function $J(x)$ saturates at large values of its argument and is introduced to capture the non-linear interactions characteristic of biological systems. For definiteness, we consider as in Chapter 3 and 4 a Monod-type response $J(x)$ [12], which is similar to the Holling type II [25] functional response

$$J(x) = \frac{x}{1 + hx}, \tag{5.2}$$

where h is the handling time. We assume a uniform handling time h across all species. This response function behaves linearly for small x and saturates to the value $1/h$ for large values of x. While the results that we obtain depend on our specific choice of the function $J(x)$, the general phenomenology depends only on the saturating character of the response.

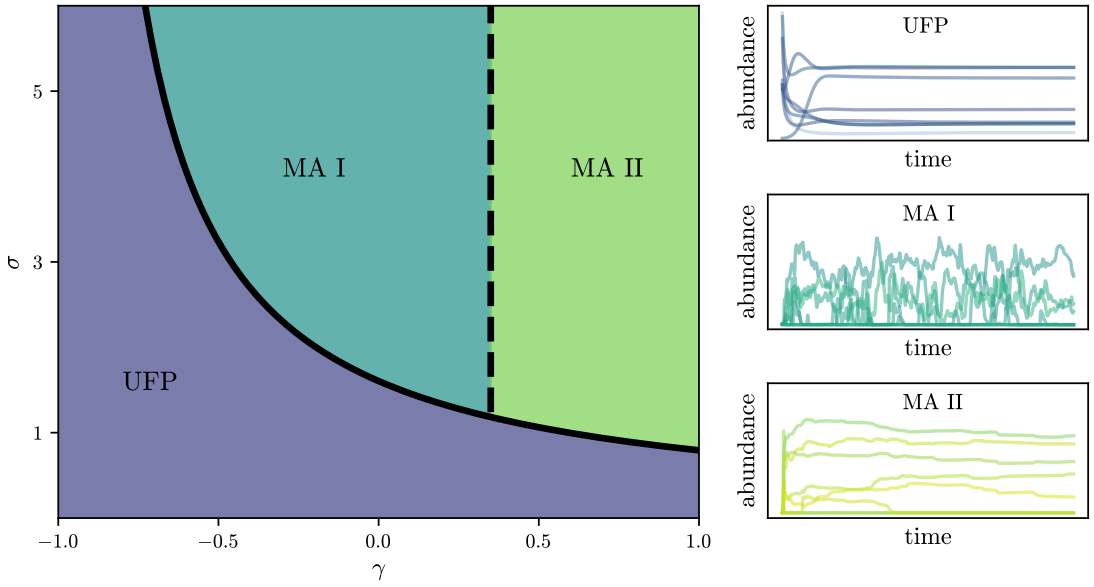

Figure 5.1: Qualitative behavior of the GLV model with saturating non-linear response, as a function of the strength of interactions σ and the correlation parameter γ. The other parameters are set to $\mu = -3$, $h = 0.1$, $\lambda = 10^{-8}$. The insets show the trajectories of 8 random species among the 400 used for the simulations for a total simulation time of 80. The specific values of the parameters used are $\sigma = 5$ and $\gamma = -0.9, 0, 0.9$. The solid line marks the separation of between the Unique Fixed Point phase and the Multiple Attractors phase and is determined from the self-consistent condition Eq. (5.42). The dashed line marks the separation between the qualitatively different behaviors in the multiple attractors phase and is determined approximately with the order parameters shown in Figure 5.4.

The parameters α_{ij} are taken to be randomly distributed as

$$\begin{aligned} \text{mean}(\alpha_{ij}) &= \mu/S, \\ \text{var}(\alpha_{ij}) &= \sigma^2/S, \\ \text{corr}(\alpha_{ij}, \alpha_{ji}) &= \gamma. \end{aligned} \tag{5.3}$$

As discussed in Chapter 1, the specific choice of the distribution from which the parameters are drawn is immaterial, as long as only the first two cumulants dominate at large S. In simulations, they are drawn from a normal distributions with statistics prescribed by Eq. (5.3).

The qualitative behavior of the model as function of interaction statistics is shown in Figure 5.1. Similarly to the standard GLV model, the system exhibits a UFP phase at low interaction strengths and undergoes a transition to the MA phase at a critical interaction strength that can be determined analytically, see below. However, unlike the GLV equations with linear interactions, the inclusion of a saturating response eliminates the non-physical unbounded growth phase present in this model, which emerges for high cooperation and heterogeneity in the interactions, as can be easily demonstrated for a finite number of species. The absence of this unbounded region enables a more comprehensive exploration of the MA phase, where, depending on the correlation parameter γ, two different transient chaotic behaviors are observed. We describe these two regions of the MA phase by quantifying their volatility numerically.

The DMFT equation associated to Eq. (5.1) can be derived with generating functionals or the

dynamical cavity method and reads

$$\dot{x}(t) = x(t)\left[1 - x(t) + \gamma\sigma^2 \int_0^t dt' G(t,t') J(x(t')) + \mu Q(t) + \eta(t)\right] + \lambda. \tag{5.4}$$

In this equation

$$Q(t) = \langle J(x(t)) \rangle, \tag{5.5}$$

$\eta(t)$ is Gaussian noise, which has zero mean and correlations given by

$$\left\langle \eta(t)\eta(t') \right\rangle = \sigma^2 \left\langle J(x(t)) J(x(t')) \right\rangle, \tag{5.6}$$

and

$$G(t,t') = \frac{\delta \langle J(x(t)) \rangle}{\delta \eta(t')}. \tag{5.7}$$

These averages are understood to be over realizations of Eq. (5.4). Thus, as usual, the process defined by Eq. (5.4), Eq. (5.5), Eq. (5.6) and Eq. (5.7) is self-consistent.

5.3 Lyapunov function for symmetric interaction matrix

It is generally expected that the dynamics of systems with reciprocal interactions can be derived from a Lyapunov function, which acts as an energy function in conservative systems. In the context of GLV equations, reciprocity between species corresponds to a symmetric interaction matrix, $\alpha_{ij} = \alpha_{ji}$. While a Lyapunov function for a linear response, $J(x) = x$, was previously established in [196], as discussed in Section 1.2.1.6, we extend this result here to the case of a generic response function $J(x)$.

We consider the following generalization of Eq. (5.1):

$$\dot{x}_i = -x_i \left[f_i(x_i) + \sum_{j \neq i} \alpha_{ij} J_j(x_j) \right] + \lambda_i. \tag{5.8}$$

In this formulation, each species self-regulates via a function $f_i(x_i)$, interacts through a species-specific response function $J_j(x_j)$, and is subject to a species-specific immigration rate λ_i. We assume that the response functions are sufficiently regular and strictly increasing, so that they are invertible and $J_i'(x) > 0$. Assuming a symmetric interaction matrix, not necessarily random, a Lyapunov function for Eq. (5.8) is

$$L = -\sum_i F_i(x_i) - \frac{1}{2} \sum_{i \neq j} \alpha_{ij} J_i(x_i) J_j(x_j) + \sum_i \Lambda_i(x_i), \tag{5.9}$$

where

$$\begin{aligned} F_i(x_i) &= \int^{J_i(x_i)} dy f_i(J_i^{-1}(y)), \\ \Lambda_i(x_i) &= \int^{J(x_i)} dy \frac{\lambda_i}{J_i^{-1}(y)}. \end{aligned} \tag{5.10}$$

This Lyapunov function is similar to the one of Hopfield for a neural network model [53]. To verify that Eq. (5.9) is a Lyapunov function for Eq. (5.8), we note that

$$\frac{\partial L}{\partial x_i} = J_i'(x_i) \frac{\dot{x}_i}{x_i}, \tag{5.11}$$

so that

$$\frac{dL}{dt} = \sum_i J_i'(x_i)\frac{(\dot{x}_i)^2}{x_i} \geq 0. \tag{5.12}$$

Applying this to the specific case of Eq. (5.1), in which $f_i(x) = -1 + x$, $J_j(x) = x/(1 + hx)$, and $\lambda_i = \lambda$, we have that

$$\begin{aligned} F_i(x) &= \frac{1}{h^2}\log(1+hx) - \frac{h+1}{h}\frac{x}{1+hx}, \\ \Lambda_i(x) &= \lambda\left(\frac{1}{1+hx} + \log\frac{x}{1+hx}\right). \end{aligned} \tag{5.13}$$

The existence of a Lyapunov function for the symmetric case $\gamma = 1$ implies that, in this limit, the dynamics inevitably evolves towards the local maxima of L, thus precluding the possibility of limit cycles or chaos. Moreover, it is expected that for values of γ close to 1 and a finite number of species the dynamics will be less volatile.

5.4 Unique fixed point phase

5.4.1 Fixed point ansatz

We begin by assuming that the dynamics defined by Eq. (5.4) reach a fixed point in the long-time behavior and denote $x^* = \lim_{t\to\infty} x(t)$. With this assumption, the Gaussian noise $\eta(t)$ becomes a static Gaussian variable, as implied by Eq. (5.6). Defining it as $\eta^* = \lim_{t\to\infty}\eta(t)$

$$\eta^* = \sigma\sqrt{q}z, \tag{5.14}$$

where

$$q = \langle J(x(z))^2\rangle, \tag{5.15}$$

and z is a zero-mean unit-variance Gaussian random variable. We additionally assume that the response function $G(t,t')$ at stationarity becomes time-translation invariant, $G(t,t') = G(t-t') = G(\tau)$, and define

$$\chi = \int d\tau G(\tau). \tag{5.16}$$

We also define

$$Q^* = \langle J(x(z))\rangle. \tag{5.17}$$

We find that the fixed points of Eq. (5.4) are

$$x^*\left[1 - x^* + \mu Q^* + \gamma\sigma^2\chi J(x^*) + \eta^*\right] = 0. \tag{5.18}$$

The stable solution of Eq. (5.18) is given by

$$x^* = f(\xi)H[\xi], \tag{5.19}$$

where $H[\xi]$ is the Heaviside function. The stability of the zero and non-zero fixed points is analyzed in the next section, see Eq. (5.31), which justifies a posteriori the presence of the Heaviside function, see also [186, 199] for similar calculations. The argument ξ is defined as

$$\xi = 1 + \mu Q^* + \eta^*, \tag{5.20}$$

and the function $f(\xi)$ is given by

$$f(\xi) = \frac{-2\xi}{h\xi - y - \sqrt{(h\xi - y)^2 + 4h\xi}}, \tag{5.21}$$

with $y = 1 - \gamma\sigma^2\chi$. Additional details on the derivation of this solution are provided in Appendix 5.7.1, where it is also explained how to correctly choose the right branch for obtaining the function $f(\xi)$. We note that in the limit $h \to 0$ Eq. (5.19) yields $f(\xi) = \xi/y$ which is the result obtained in [199]. The evaluation of χ can be carried out starting from Eq. (5.16) and noting that, at stationarity, χ is the response of the system to a constant perturbation applied at all previous times [289]. Thus, χ is obtained as the average over the realizations of $x^* = x(z)$ of the derivative of $J(x(z))$ with respect to $\eta^* = \sigma\sqrt{q}z$,

$$\chi = \int Dz \frac{1}{\sqrt{q}\sigma} \frac{\partial J(x(z))}{\partial z}, \tag{5.22}$$

where $Dz = \frac{1}{\sqrt{2\pi}} e^{-\frac{z^2}{2}} dz$ is the Gaussian measure. Computing the derivative, we obtain

$$\chi = \int_{\xi>0} d\xi \; P_\xi(\xi) \frac{1}{(1 + hf(\xi))^2} f'(\xi), \tag{5.23}$$

with $f'(\xi)$ being the derivative respect to ξ of Eq. (5.21) and, as Eq. (5.20) implies, the distribution of ξ is Gaussian, explicitly $\mathcal{N}(1 + \mu Q^*, \sigma^2 q)$.

5.4.2 Species Abundance Distribution

Starting from the stationary solution of DMFT given by Eq. (5.18) we derive the stationary probability distribution for x^*, which corresponds to the SAD. From Eq. (5.19) and the distribution of ξ we obtain

$$\begin{aligned} P_{\text{st}}(x^*) &= \langle \delta(x^* - f(\xi)H(\xi)) \rangle_\xi \\ &= \phi \, \delta(x^*) + P_{\text{surv}}(x^*) H(x^*), \end{aligned} \tag{5.24}$$

where the average is over ξ. The fraction of extinct species is given by

$$\phi = \frac{1}{2} \text{erfc} \left(\frac{m}{\sqrt{2}\nu} \right), \tag{5.25}$$

while the distribution of non-extinct species distribution is:

$$P_{\text{surv}}(x^*) = \frac{\exp\left[-(f^{-1}(x^*) - m)^2 / 2\nu^2\right]}{\sqrt{2\pi}\nu f'(f^{-1}(x^*))}, \tag{5.26}$$

where

$$f^{-1}(x) = x - \gamma\sigma^2\chi J(x) \tag{5.27}$$

(the function f can always be inverted in f^{-1}). The parameters $m = 1 + \mu Q^*$ and $\nu = \sigma\sqrt{q}$ are to be computed self-consistently. Notice that P_{surv} is normalized to $1 - \phi$, the fraction of non-extinct species.

In the specific case $\gamma = 0$ we have $y = 1$, $f^{-1}(x^*) = x^*$ and $f'(\xi) = 1$ and thus the resulting SAD is exactly a truncated Gaussian in Eq. (5.26), as obtained in the linear response case [186, 199]. For $\gamma \neq 0$ the SAD is the pushforward of a Gaussian through $f^{-1}(x)$, but since $f^{-1}(x)$ is linear for large x, the SAD also decays in this case with a Gaussian tail. In Figure 5.2, we show the theoretical prediction together with the histogram of simulation samples for a representative choice of parameters. Results for other parameter choices are provided in Appendix 5.7.2.

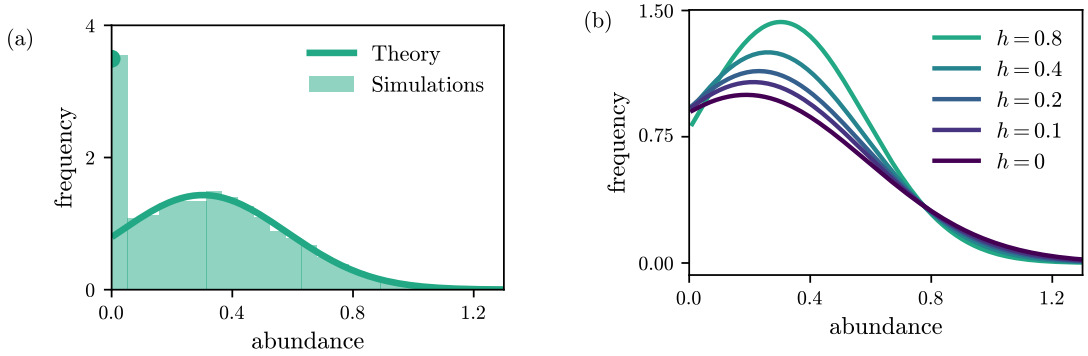

Figure 5.2: Species Abundance Distribution. (a) Comparison between the theoretical species abundance distribution and the histogram of the stationary samples obtained from 10 simulations with 1000 species. The values x^* from the simulations are averaged over the last 5% of the trajectories that last for a total simulation time of 100. The used parameters are $\mu = -3$, $\sigma = 1$, $\gamma = 0$, $h = 0.8$ and $\lambda = 10^{-8}$. The solid line represents the survival distribution $P_{\text{surv}}(x^*)$ while the point at $x^* = 0$ is given by the sum of the probability of extinction ϕ and the fraction of non-extinct species with abundances contained within the first bin, both normalized by the bin length. (b) Comparison among the theoretical species abundance distributions for different values of h. Other parameters are fixed as $\mu = -3$, $\sigma = 1$, $\gamma = 0$ and $\lambda = 10^{-8}$.

5.5 Loss of stability and multiple attractor phase

5.5.1 Linear stability analysis

In this section, we study the stability of the fixed point ansatz with a linear stability analysis following the standard method [71, 199], see also Section 1.2.2.2. We add to the DMFT equation a small white noise $\zeta(t)$

$$\dot{x}(t) = x(t)\left[1 - x(t) + \gamma\sigma^2 \int_0^t dt' G(t,t') J(x(t')) + \mu Q(t) + \eta(t) + \zeta(t)\right], \tag{5.28}$$

and study the resulting deviations $\delta x(t) = x(t) - x^*$ from the stationary solution. At first order the noise is modified to $\eta(t) = \eta^* + \delta\eta(t)$, with

$$\langle \delta\eta(t)\delta\eta(t')\rangle = \sigma^2 \langle (J'^*)^2 \delta x(t)\delta x(t')\rangle, \tag{5.29}$$

where $J'^* \equiv dJ(x)/dx|_{x=x^*}$. The linearized DMFT equation is

$$\begin{aligned} \delta\dot{x}(t) = \delta x(t)[1 - x^* + \gamma\sigma^2 \chi J(x^*) + \mu Q^* + \eta^*] \\ + x^*\Big[- \delta x(t) + \mu\delta Q(t) + \delta\eta(t) + \zeta(t) \\ + \gamma\sigma^2 \int dt' \left(\delta G(t,t') J(x(t')) + G(t,t')\delta J(x(t'))\right)\Big], \end{aligned} \tag{5.30}$$

and it is easy to show that $\delta G(t,t') = 0$ and $\delta Q(t) = 0$, starting from their definition and showing that it can be written as the average of an unperturbed observable multiplied by ζ. Given the independence between the two and the fact that $\langle\zeta\rangle = 0$, the terms mentioned above are zero. The dynamics of small perturbations around $x^* = 0$ thus satisfies

$$\delta\dot{x}(t) = \delta x(t)[1 + \mu Q^* + \eta^*], \tag{5.31}$$

which shows that this fixed point is stable when $\xi = 1 + \mu Q^* + \eta^* < 0$, as anticipated.

The linear dynamics of perturbations around the non-zero fixed point satisfies instead

$$\delta\dot{x}(t) = x^* \left[-\delta x(t) + \gamma\sigma^2 \int dt' G(t,t')\delta J(x(t')) + \delta\eta(t) + \zeta(t) \right]. \tag{5.32}$$

We apply the Fourier transform on both sides, obtaining

$$i\omega\delta\tilde{x}(\omega) = x^*[-\delta\tilde{x}(\omega) + \delta\tilde{\eta}(\omega) + \tilde{\zeta}(\omega) + \gamma\sigma^2\tilde{G}(\omega)\delta\tilde{x}(\omega)J'^*], \tag{5.33}$$

and solving for $\delta\tilde{x}(\omega)$ we get

$$\delta\tilde{x}(\omega) = A(\omega)^{-1}[\delta\tilde{\eta}(\omega) + \tilde{\zeta}(\omega)], \tag{5.34}$$

with

$$A(\omega) = \left[\frac{i\omega}{x^*} + 1 - \gamma\sigma^2\tilde{G}(\omega)J'^* \right]. \tag{5.35}$$

Since ζ is chosen to be a Gaussian white noise, we have

$$\langle\tilde{\zeta}(\omega)\tilde{\zeta}(\omega')\rangle = \epsilon^2\delta(\omega+\omega')2\pi, \tag{5.36}$$

where ϵ is the strength of the Gaussian noise. Regarding $\langle\delta x(t)\delta x(t')\rangle$, since we are around the fixed point, it depends only on $t - t'$, and therefore

$$\langle\delta\tilde{x}(\omega)\delta\tilde{x}(\omega')\rangle = \epsilon^2\delta(\omega+\omega')2\pi\delta\tilde{C}(\omega), \tag{5.37}$$

where $\delta\tilde{C}(\omega)$ can be obtained from Eq. (5.34), Eq. (5.36), Eq. (5.29). Indeed, from Eq. (5.29) and Eq. (5.34) we get

$$\begin{aligned} &\sigma^{-2}\langle\delta\tilde{\eta}(\omega)\delta\tilde{\eta}(\omega')\rangle \\ &= \langle(J'^*)^2\delta\tilde{x}(\omega)\delta\tilde{x}(\omega')\rangle \\ &= D(\omega,\omega')\big[\langle\delta\tilde{\eta}(\omega)\delta\tilde{\eta}(\omega')\rangle + \epsilon^2\delta(\omega+\omega')2\pi\big], \end{aligned} \tag{5.38}$$

where

$$D(\omega,\omega') \equiv \langle(A(\omega)A(\omega'))^{-1}(J'^*)^2\rangle. \tag{5.39}$$

The last equation allows to determine the $\delta\tilde{\eta}$ correlation, which used in eq.(5.34) leads to the final result:

$$\delta\tilde{C}(\omega) = \frac{\langle|A(\omega)|^{-2}\rangle}{1 - \sigma^2 D(\omega,-\omega)}, \tag{5.40}$$

where the $\langle\cdot\rangle$ is an average over the distribution of x^*, with $x^* > 0$. We are in particular interested in the long time response, and we therefore consider $\omega = \omega' = 0$. In this case we obtain that

$$D(0,0) = \Big\langle \frac{(J'^*)^2}{(1 - \gamma\sigma^2\chi J'^*)^2} \Big\rangle, \tag{5.41}$$

where we have used that $\tilde{G}(0) = \chi$. $\delta\tilde{C}(0)$ diverges if the following critical condition is satisfied

$$1 = D(0,0)\sigma^2, \tag{5.42}$$

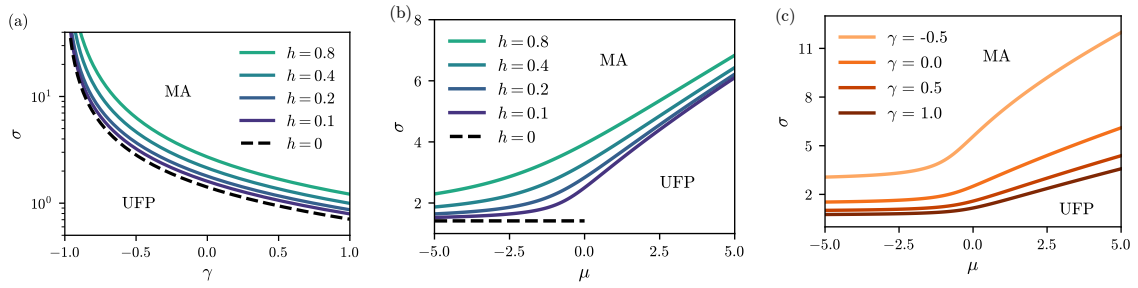

Figure 5.3: Different projections of the phase diagram. The lines separate the Unique Fixed Point phase (below) from the Multiple Attractor phase (above). (a) γ-σ phase diagram with $\mu = -3$. Black dashed line is the result obtained in Ref. [199]. (b) μ-σ phase diagram with $\gamma = 0$. Black dashed line is the result obtained in Ref. [199]. (c) μ-σ phase diagram with $h = 0.1$.

and the averages need to be computed with the stationary distribution of the surviving species

$$P(x^*) = \frac{1}{1-\phi} P_{\text{surv}}(x^*), \tag{5.43}$$

with $x^* > 0$ and the pre-factor $1/(1-\phi)$ guarantees the normalization condition $\int_{x^*>0} dx^* P(x^*) = 1$. The critical condition can be thus rewritten as

$$1 = (1-\phi)\sigma^2 \int_{x^*>0} dx^* P(x^*) (J'^*)^2 \frac{1}{(1-\gamma\sigma^2\chi J'^*)^2}. \tag{5.44}$$

As expected, in the limit $h \to 0$ we obtain the same result of [199].

The numerical validation of the critical-point prediction is discussed in the following section. Comparisons between theory and simulations for other choices of the model parameters are reported in 5.7.2.

As expected, in the limit of small handling times ($h \ll 1$), where $J(x) \sim x$, our results recover the phase diagram of the linear GLV model [186].

The solution of Eq. (5.44) is shown Figure 5.3 as a function of the different control parameters of the model. As a function of γ, the qualitative behavior of the critical line between UFP and MA remains consistent with the standard GLV, but we observe that incorporating a saturating non-linear response enlarges the region of stability of the system. Moreover, the greater the handling time, meaning that the non-linear response saturates at lower abundances, the greater the stability. We also note that, differently from the case $J(x) = x$, the critical line delineating the UFP phase is not horizontal in the μ-σ space. The presence of a non-linear saturating response allows us to explore in detail the region $\mu > 0$ of cooperative communities, which is inaccessible in the linear GLV due to the non-physical UG phase. As shown in panels b,c of Figure 5.3, our results indicate that the UFP region is larger in cooperative communities, which can thus be considered more stable than competitive ($\mu < 0$) ones.

5.5.2 Numerical characterization of multiple attractor phases

We performed extensive simulations to characterize the phases that are present beyond the unique fixed-point region. We introduce two phenomenological order parameters to characterize the long-time behavior of the dynamics. Following [226] we consider

$$v = \frac{\langle \langle x_i(t)^2 \rangle_T - \langle x_i(t) \rangle_T^2 \rangle_S}{\langle \langle x_i(t) \rangle_T^2 \rangle_S} \tag{5.45}$$

and

$$d = \frac{\langle\langle (x_i(t) - x_i'(t))^2\rangle_S\rangle_T}{\langle\langle x_i(t)\rangle_S^2\rangle_T}, \tag{5.46}$$

where $\langle\cdot\rangle_S$ is the average over the different populations, $\langle\cdot\rangle_T$ is the average over the last 5% time steps of the trajectories and x_i' is the population of the i-th species obtained by re-running the process with the same interaction matrix, but different initial conditions. The parameter v characterizes the volatility of the dynamical trajectory at stationarity, while the parameter d characterizes the distance between runs with the same interaction matrix and different initial conditions. In the UFP phase, we expect both $v = 0$ and $d = 0$ since the system invariably converges to a stable fixed point, which is unique and independent of the initial conditions. In the MA phase, we can have both $v > 0$ and $d > 0$ if the dynamics is volatile or $v = 0$ and $d > 0$ if the system displays multiple and linearly stable fixed points.

A similar characterization can be obtained by introducing more rigorous order parameters. The stability of the attractors can be taken into account by computing the Maximum Lyapunov Exponent

$$\text{MLE} = \lim_{t\to\infty} \lim_{d_0\to 0} \frac{1}{t} \ln \frac{d_t}{d_0}, \tag{5.47}$$

where d_0 is a small perturbation of the trajectory at the initial time $t = 0$ and d_t is the separation of the unperturbed and perturbed trajectories after time t. We computed it numerically by implementing the algorithm proposed in [45].

To quantify the volatility of the system, we introduce the dimension of activity, a measure commonly used in theoretical neuroscience to assess the number of degrees of freedom that are effectively engaged in the dynamics [261]. It is defined as

$$D = \frac{1}{S} \frac{\text{Tr}(C)^2}{\text{Tr}(C^2)}, \tag{5.48}$$

where C is the covariance matrix of the species abundance time-series. The prefactor $1/S$ ensures that D remains bounded between 0 and 1. The numerical results for the introduced order parameters are shown in Figure 5.4 as a function of the interaction symmetry γ. As expected, the parameters v and D exhibit a similar behavior, as well as the maximum Lyapunov exponent (MLE) and the parameter d. We note that, although a correspondence between v and D might be expected, the fact that they behave almost as linear transformations of each other in the MA I phase is not obvious, as the former quantifies the average volatility of species abundances, whereas the latter captures the number and structure of principal modes in the dynamics. Exploring their relationship could provide a useful framework for investigating the dynamical behavior of the multiple-attractor phase in Generalized Lotka-Volterra models, which we leave for future work.

From now on, we will consider only the dimension of activity D and the Maximum Lyapunov Exponent MLE for our considerations. Starting from the fully asymmetric case $\gamma = -1$ and moving towards the fully symmetric case $\gamma = 1$, the system undergoes a sharp transition from the UFP phase to the MA phase, which is well predicted by Eq. (5.44). Within the MA phase, we identify a region where both D and MLE remain non-zero, characterizing the MA I phase (shown in Figure 5.1). As the system approaches a higher degree of symmetry, it displays less volatility, leading to a decrease in D, which eventually reaches zero, marking the transition to the MA II phase (also shown in Figure 5.1). We determine the transition between MA I and MA II numerically, identifying it as the value of γ at which D equals its value at the sharp transition from UFP to MA. We note that the exact values of D and the MLE are influenced by the choice of the migration term λ. However, this

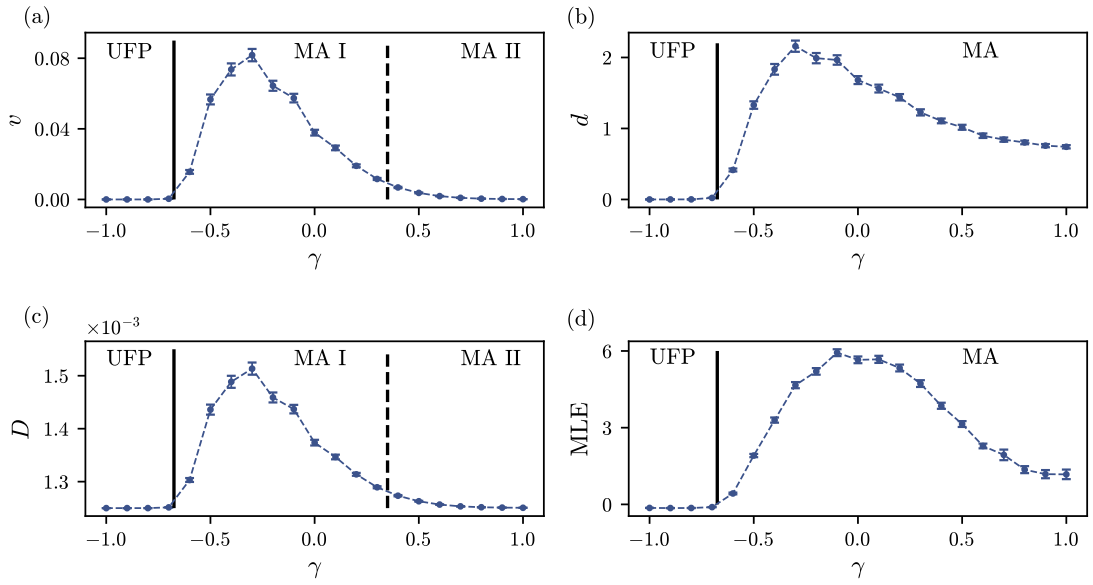

Figure 5.4: Comparison of the order parameter evaluated along a projection of the phase diagram, obtained fixing $\mu = -3$, $\sigma = 5$, $h = 0.1$ and varying γ. Each point is obtained as the average over 225 realizations of the interaction matrix with 800 species. The solid line marks the separation of between the Unique Fixed Point phase and the Multiple Attractors phase and is determined from the self-consistent condition Eq. (5.44). The dashed line marks the separation between the qualitatively different behaviors in the multiple attractors phase and is determined approximately.

dependence does not affect the validity of the arguments presented in this section. A numerical analysis of this effect is provided in Appendix 5.7.2, Fig. 5.7.

5.6 Discussion

In this chapter, we have studied the effect of introducing a saturating non-linear response in the generalized Lotka-Volterra model with quenched interactions in order to remove the non-physical unbounded phase of the model. In particular, we have chosen a Monod-like function, so to keep the model as simple as possible while ensuring that the system remains bounded. Interestingly, the simplicity of the model allows for analytical solutions of the SAD and for the fraction of extinct species that are close, but not the same, as the one obtained in the GLV model without saturating response.

A non-trivial effect of introducing the saturating response is the possibility of exploring the MA phase as a function of this interaction symmetry parameter γ, which shows the emergence of two types of dynamic behaviors: a region where chaotic dynamics with high species turnover is observed (MA I) and another region where species undergoes only small fluctuations in their population dynamics, with few (rare) switching events. The transitions between the two phases cannot be detected analytically through a linear stability analysis, but they have been characterized numerically through simulations by introducing two phenomenological order parameters: the volatility of the dynamic trajectory at stationarity v, and the distance between runs with the same interaction matrix and different initial conditions d. The MA I phase has been defined as the one

having $v > 0$ and $d > 0$, while the MA II phase has $v = 0$ and $d > 0$. This result has also been validated using an alternative approach based on the Maximum Lyapunov Exponent (MLE), the classic measure of the sensitivity of a dynamical system to initial conditions and on the "dimension of activity" D, a metric commonly used in theoretical neuroscience, which quantifies the number of degrees of freedom effectively involved in the dynamics. As expected, the parameters v and D exhibit a similar behavior, as well as MLE and d.

The transition observed as the symmetry parameter γ increases from -1 to 1 offers significant insight into the role of interaction symmetry in shaping the system's dynamic regime. For large enough interactions heterogeneity (σ), our results reveal a sharp transition from the unique fixed-point (UFP) phase to the MA II with low volatility, passing through the MA I phase (high-dimensional and chaotic dynamic). This suggests that symmetry in the interaction matrix can serve as a control parameter, tuning the system between qualitatively distinct dynamical behaviors. This progressive reduction in dynamical complexity with increasing symmetry highlights a key organizing principle: higher symmetry leads to less volatile dynamics. This stabilization is likely attributable to the existence of a Lyapunov function at $\gamma = 1$, which enhances stability in the vicinity of the symmetric limit.

5.7 Appendix

5.7.1 Stable solution of stationary equation

Starting from Eq. (5.18) we note that there is a trivial solution $x^* = 0$, and possible other solutions can be obtained solving the equation

$$1 - x^* + \gamma\sigma^2\chi J(x^*) + \mu Q^* + \eta^* = 0, \tag{5.49}$$

with $J(x^*) = x^*/(1 + hx^*)$. Finally we have a second degree polynomial equation in x^*. The solutions are

$$x^* = \frac{h\xi - y \pm \sqrt{(h\xi - y)^2 + 4h\xi}}{2h}, \tag{5.50}$$

where we have introduced $\xi = 1+\mu Q^*+\eta^*$ and $y = 1-\gamma\sigma^2\chi$. The latter can be shown to be always non-negative $y \geq 0$ as confirmed by numerical inspection. Since we want $x^* >= 0$ we need $\xi > 0$ to have at least one feasible solution. Given that, and the fact that $\sqrt{(h\xi - y)^2 + 4h\xi} > |h\xi - y|$ we find that the only non-trivial stationary solution is the one with the plus in Eq. (5.50). We also want to consider the case in which $h \to 0$ where Eq. (5.50) is ill-defined when we take the plus sign. To regularize it, it is sufficient to multiply numerator and denominator by $h\xi - y - \sqrt{(h\xi - y)^2 + 4h\xi}$. The final result for the stationary solution is

$$x^* = \frac{-2\xi}{h\xi - y - \sqrt{(h\xi - y)^2 + 4h\xi}} H[\xi]. \tag{5.51}$$

5.7.2 Additional figures

In this appendix we present a more detailed comparison between theoretical predictions and numerical simulations for different parameter choices of the model, focusing on the SAD in Figure 5.5 and on the transition between the Unique Fixed Point and Multiple Attractors in Figure 5.6. We also investigate the effects of the migration term λ on the computation of the dimensionality of activity in Figure 5.7.

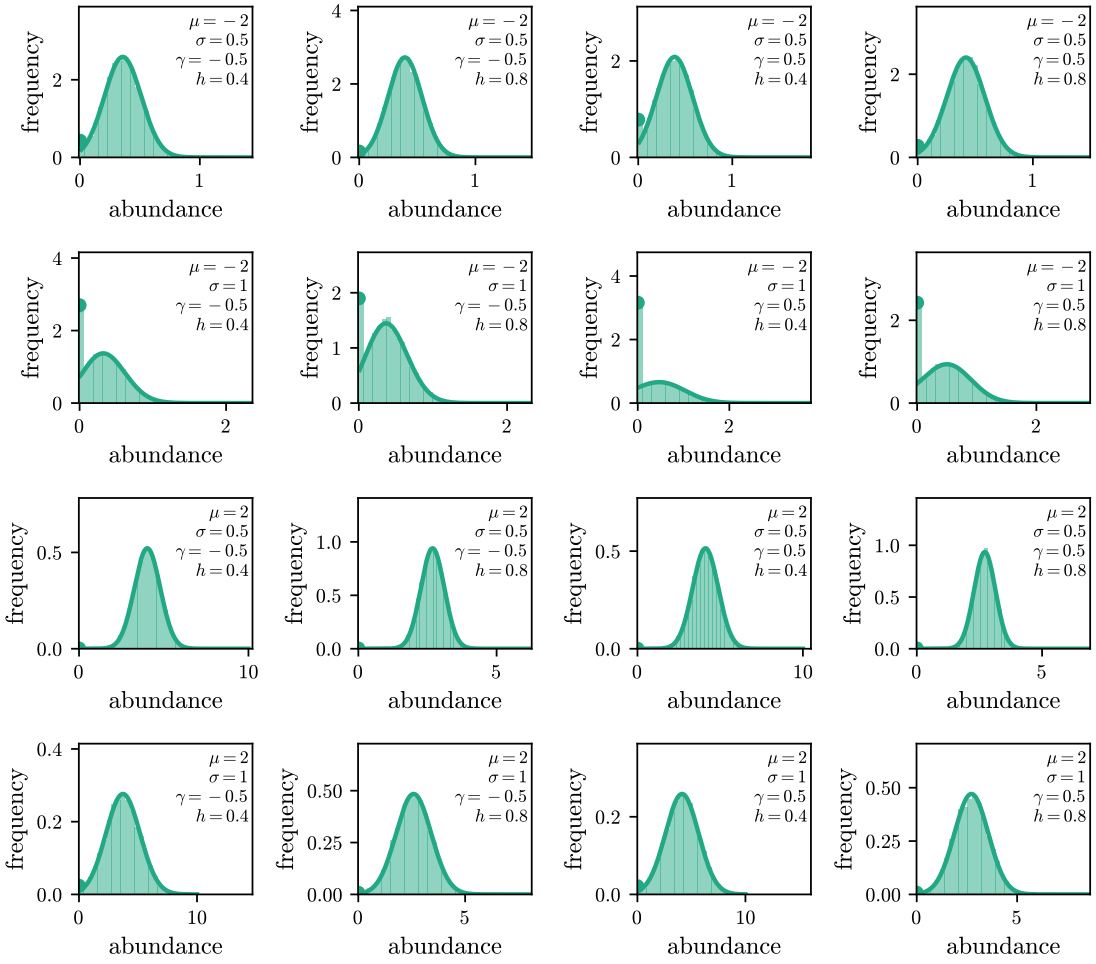

Figure 5.5: Species Abundance Distribution for different combinations of the control parameters of the model. Comparison between the theoretical species abundance distribution and the histogram of the stationary samples obtained from 10 simulations with 1000 species. The values x^* from the simulations are averaged over the last 5% of the trajectories that last for a total simulation time of 100.

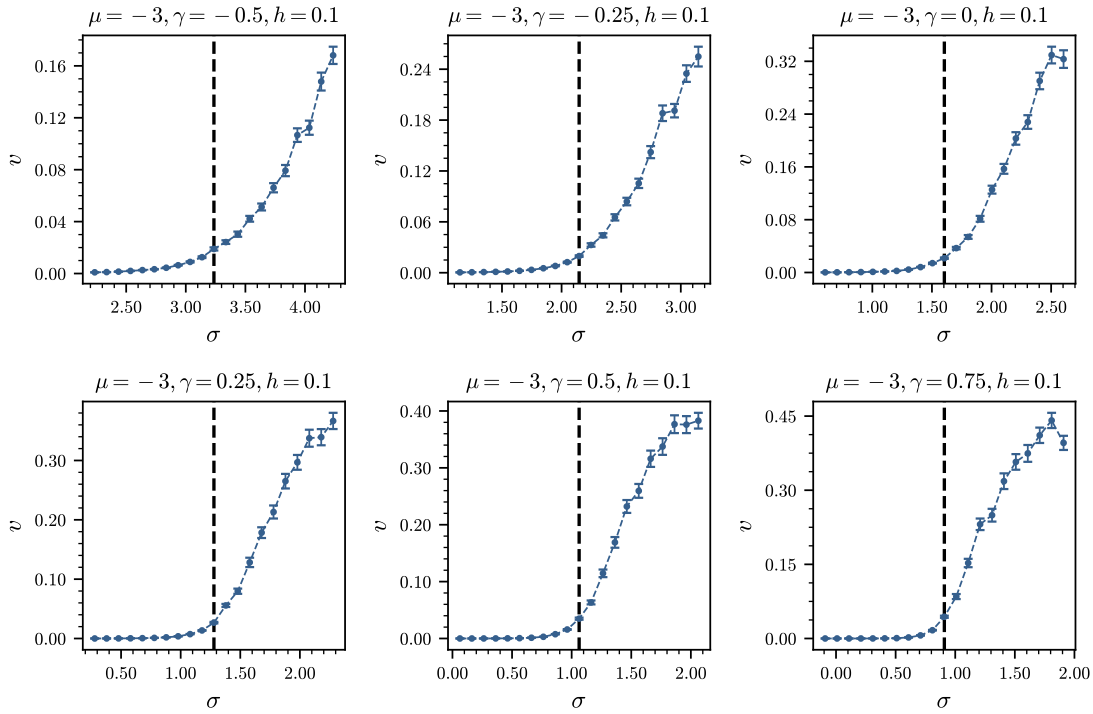

Figure 5.6: Numerical validation of critical-point prediction. Comparison between the critical interaction strength σ predicted by solving Eq. (5.44) self-consistently for different values of the symmetry parameter γ, with $\mu = -3$ and $h = 0.1$ held fixed. Numerical validation is performed by computing the volatility parameter v defined in Eq. (5.45). Each point is obtained as the average over 225 realizations of the interaction matrix with 1000 species.

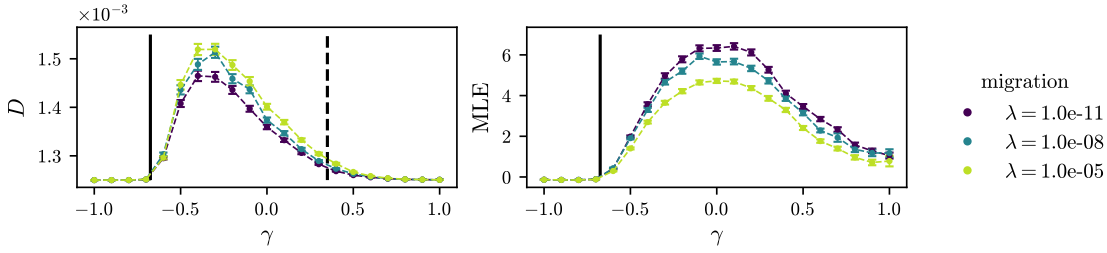

Figure 5.7: Comparison of the Dimension of activity (D) and Maximum Lyapunov Exponent (MLE) evaluated along a projection of the phase diagram, obtained fixing $\mu = -3$, $\sigma = 5$, $h = 0.1$ and varying γ, for different values of the migration term λ. Each point is obtained as the average over 225 realizations of the interaction matrix with 800 species. The solid line marks the separation between the Unique Fixed Point phase and the Multiple Attractors phase and is determined by the self-consistent condition Eq. (5.44). The dashed line marks the separation between the qualitatively different behaviors in the multiple attractors phase and is determined approximately.

Chapter 6

Disordered generalized Lotka-Volterra equations with time delays

Questo capitolo è dedicato ai miei genitori, che ancora non si capacitano del fatto che qualcuno mi abbia pagato per studiare disordine e ritardo.

Time delays are a ubiquitous and critical feature of complex systems, shaping their dynamics across fields from ecology to neuroscience. However, most theoretical analyses either neglect them or focus on low-dimensional models, as incorporating memory effects into high-dimensional systems is a considerable analytical challenge. To overcome this issue, we extend Dynamical Mean-Field Theory to incorporate time delays into high-dimensional random dynamical systems and render this analysis feasible. Applying this framework to the disordered generalized Lotka-Volterra equations with delayed interactions, we uncover a rich dynamical phase diagram emerging from the complex interplay of non-linearity and memory effects. Our methodological advances allow us to derive analytical conditions for the onset of the distinct dynamical regimes and characterize their dynamical properties in terms of ecologically interpretable parameters, such as community competitiveness and diversity. We find that memory effects can generate persistent and nearly synchronous oscillations in species abundances in sufficiently competitive communities. Moreover, we further show that when intraspecific interactions are delayed or reciprocal interspecific interactions are negatively correlated, time delays alone can induce chaotic behavior, contrasting with single-species models where delays typically lead only to periodic fluctuations. The analytical techniques developed are broadly applicable to any high-dimensional random dynamical system with time delays, with direct relevance to ecological, epidemiological, neural, and social complex systems.

6.1 Introduction

Interactions in real-world complex systems are inherently delayed due to the finite velocity of signal propagation, dynamical feedbacks, and a variety of other mechanisms [140, 143, 193]. In biological

This chapter is based on: Francesco Ferraro et al. "Synchronization and chaos in complex ecological communities with delayed interactions". In: *arXiv preprint arXiv:2503.21551* (2025). As a co-first author, I shared equal responsibility for designing and conducting the theoretical and numerical analyses and preparing the text and figures.

neural networks, electrochemical signals propagate on timescales ranging from 1 to 100 ms. These delays are comparable to the typical synaptic processing timescale of around 10 ms and thus play a central role in shaping neural computation [108, 164]. In ecological communities, population interactions are similarly delayed, for example, due to maturation times [35, 121]. An increase in predator abundance effectively reduces prey growth only after a time lag determined by the time it takes predators to reach hunting maturity. More generally, the effective dynamics of components in complex systems embedded in heterogeneous environments naturally develops memory through feedback mechanisms, an ubiquitous feature in statistical physics customarily analyzed through projection operator methods [101, 228].

Despite their prevalence, time delays are typically neglected in the analysis of complex systems. The fundamental reason is that delayed dynamics inhabit an infinite-dimensional phase space, which significantly impedes analytical progress [73]. Consequently, studies that incorporate time delays generally focus on low-dimensional models with few interacting components [68, 121] or on purely numerical analyses [253]. Yet, even in these simplified settings, delays can dramatically alter system dynamics, inducing sustained oscillations and chaos, or stabilizing otherwise unstable fixed points [33, 68].

Existing analytical approaches to high-dimensional complex systems with delays [111, 252, 275, 321] face fundamental limitations. They are mainly based on random matrix theory [224], which provides insight into the stability of such systems but remain restricted to the linear regime and cannot capture the non-linear dynamics that emerge beyond the onset of instability. This leaves a comprehensive theoretical framework for high-dimensional non-linear delayed dynamics still lacking. This gap is particularly problematic, as many real-world complex systems operate in non-equilibrium steady states far from a linear regime [56, 88, 128].

To address this gap, we develop an analytical framework for studying high-dimensional complex systems with delayed interactions in the non-linear domain. Our methodological advances are based on an extension of DMFT that is able to accommodate time delays. We build on established techniques from low-dimensional delayed systems and adapt them to the DMFT setting, introducing crucial modifications to account for the stochastic and self-consistent nature of the resulting equations. This approach allows to investigate analytically the dynamical phases of non-linear high-dimensional disordered systems with memory effects.

Our framework is broadly applicable, and we exemplify it in this chapter by studying the effect of time delays on the dynamical behavior of complex ecosystems beyond the linear regime. Specifically, we analyze the GLV equations with random and delayed interactions. Owing to our methodological advances, we find this model to display a rich set of dynamical phases. We identify a phase in which sufficiently competitive ecological communities spontaneously develop synchronized population oscillations. We derive analytical conditions for this transition and characterize the properties of the resulting oscillations. In ecosystems with intraspecific delayed interactions or structured interaction networks, we additionally uncover a regime of delay-induced chaos. Through an extensive sensitivity analysis, we assess the robustness of these findings and discuss their ecological implications.

Our results provide fundamental insights into the role of memory in high-dimensional complex systems, with implications extending well beyond ecology. The analytical framework developed in this work applies broadly to any complex system with time delays and enables the systematic study of memory effects in neural networks [91], epidemiological models [190], economic systems [156], and social networks [154], where delayed interactions are known to play a pivotal role.

This chapter is organized as follows: in Section 6.2 we show how delay effects generally arise; in Section 6.3 we give a short introduction to delay differential equations; in Section 6.4 we derive

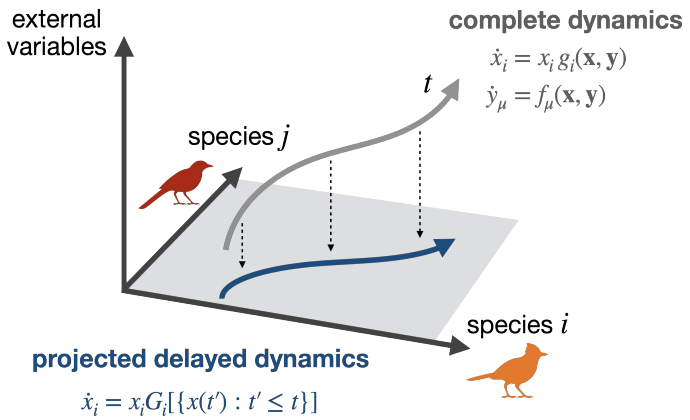

Figure 6.1: Schematic illustration of the projection mechanism for the dynamics of a community embedded in a broader ecosystem. The state of the system is characterized by the abundances of the community species x_i and additional ecological variables y_μ. These external variables represent environmental factors such as abiotic resources or environmental conditions. The full dynamical system is described by $\dot{x}_i = x_i g_i(\boldsymbol{x}, \boldsymbol{y})$ and $\dot{y}_\mu = f_\mu(\boldsymbol{x}, \boldsymbol{y})$. By integrating out the y_μ variables, an effective dynamical framework for the species abundances is derived, yielding a reduced description in the x-subspace given by $\dot{x}_i = x_i G_i[\{x(t') : t' \leq t\}]$. This effective dynamics encapsulates the influence of the environmental variables as memory effects, where species interactions are mediated through time-delayed kernels. In Appendix 6.10.1 the projection procedure is performed explicitly assuming a dynamics for the external variables close to equilibrium.

DMFT for delayed interactions; in Section 6.5 we study the GLV equations with discrete delay and in Section 6.6 with distributed delay; in Section 6.7 we study the case of delayed intraspecific interactions; in Section 6.8 we study the case of correlated interactions; we conclude with a summary of the results and possibilities for further research. In Chapter 7 the same methodologies are applied to a random neural network model.

6.2 Dynamic environments lead to delayed interactions

We begin by illustrating how time delays naturally emerge when reciprocal feedbacks between components of a complex system and their environment are taken into account. Although we focus on ecological communities for clarity of presentation, this mechanism is fundamentally generic and applies whenever a complex system operates in a heterogeneous environment [101, 228].

We consider a complex ecosystem whose dynamics is described by the abundances or biomass densities of species in a community of interest, denoted as x_i ($i = 1, \ldots, S$), alongside R additional ecological variables, y_μ ($\mu = 1, \ldots, R$), see Figure 6.1. These additional variables represent external factors, such as abiotic resources, environmental conditions, or species that do not belong to the focal community. We aim to derive a reduced dynamics for the S species that accounts in an effective way for the R variables, under the assumption that the latter lie outside our primary scope of interest. This assumption may be motivated either by the lack of direct experimental access to these variables or by their marginal relevance in the modeling of the ecosystem.

The dynamics of the species abundances and the other variables can generally be described by

$$\begin{aligned} \dot{x}_i &= x_i g_i(\boldsymbol{x}, \boldsymbol{y}), \\ \dot{y}_\mu &= f_\mu(\boldsymbol{x}, \boldsymbol{y}). \end{aligned} \tag{6.1}$$

This dynamics generalizes many well-known models of community ecology. For instance, if the variables y_μ are interpreted as resources, Eq. (6.1) includes, among others, niche models [288] and MacArthur's consumer-resource model [28].

We assume a linear, mass-action dependence of the growth rates $g_i(\boldsymbol{x}, \boldsymbol{y})$ on species abundances, as in the GLV equations, and a linear dependence on the environmental variables, as in consumer-resource models. Integrating out the external variables yields a closed equation for the community variables that includes a noise term, that we ignore, and delayed interactions between species:

$$\dot{x}_i(t) = r_i x_i(t) \left[1 + \sum_{j=1}^{S} \int_0^\infty d\tau \, K_{ij}(\tau) x_j(t-\tau) \right]. \tag{6.2}$$

The appearance of a memory kernel after projecting the dynamics of a large interacting system onto a reduced number of degrees of freedom is a well-known mechanism in statistical physics [101, 228]. In Appendix 6.10.1 we perform this procedure explicitly assuming a dynamics for the external variables close to equilibrium. As discussed there, this derivation illustrates how non-monotonic memory kernels may result from integrating out multiple external variables. We further note that non-monotonic delays can also emerge from multistep spatial coarse-graining [235, 252].

From now on, we set $r_i = 1$ equal for all species to streamline the notation. Additionally, the memory kernels are taken to be functionally equivalent up to a multiplicative constant, meaning

$$K_{ij}(\tau) = \alpha_{ij} K(\tau). \tag{6.3}$$

For simplicity, we also assume that intraspecific interactions have identical and unit carrying capacity. These choices simplify analytical results while maintaining the core of the discussion. The general case of species-specific growth rates, functionally different $K_{ij}(\tau)$, and species-specific carrying capacities is considered separately, see Appendix 6.10.7. Anticipating the results, these simplifications do not alter our conclusions. We also assume that intraspecific interactions are instantaneous. The effect of intraspecific delays is discussed in Section 6.7. As usual, we assume that α_{ij} are independent and identically distributed with

$$\begin{aligned} \text{mean}(\alpha_{ij}) &= \mu/S, \\ \text{var}(\alpha_{ij}) &= \sigma^2/S. \end{aligned} \tag{6.4}$$

In Section 6.8 the generalization to reciprocally-correlated interactions is considered.

6.3 Delay differential equations for pedestrians

Before turning our attention to the GLV equations with time delays, we first consider a single-species DDE. The techniques required to analyze this simpler equation are fundamentally the same as those employed later for the GLV equations. For definiteness, let us consider the delayed logistic equation, also known as Hutchinson's equation [11]:

$$\dot{x}(t) = x(t) \left[1 - x(t-\tau) \right]. \tag{6.5}$$

By proper rescaling we have set the growth rate and the carrying capacity to unity. The equation must be supplemented with an initial condition $x(t) = \phi(t)$ for t in $[-\tau, 0]$. We note that the initial condition is not a single point, but a function. This indicates that the phase space is not one-dimensional, as the scalar variable might suggest, but rather infinite-dimensional. This infinite dimensionality is the primary obstacle to analytical progress in DDEs.

Regarding the existence, uniqueness, and regularity of solutions for DDEs like Eq. (6.5), we note that once an initial function is given, the DDE for $x(t)$ reduces to a forced ODE for t in $[0, \tau]$. Consequently, standard existence and uniqueness theorems for ODEs apply on this interval. After a solution $x(t)$ is established on $[0, \tau]$, the procedure is iterated on $[\tau, 2\tau]$, and so forth. We note that solutions generally gain regularity as t increases, but derivative discontinuities might persist at integer multiples of the delay τ as a consequence of the discrete delay.

The notions of equilibrium and stability extend straightforwardly from the ordinary to the delayed case. An equilibrium x^* is defined as a constant solution of the DDE. An equilibrium is stable if solutions starting close to it, meaning that $|x(t) - x^*|$ is sufficiently small for all t in $[-\tau, 0]$, remain close to it for all $t > 0$. An equilibrium is asymptotically stable if solutions starting within a sufficiently small neighborhood eventually converge to x^*.

The specific DDE in Eq. (6.5) has two equilibria, $x^* = 0$ and $x^* = 1$. Small perturbations from $x^* = 0$ satisfy $\delta\dot{x}(t) = \delta x(t)$, indicating that this equilibrium is unstable. The dynamics of small perturbations around $x^* = 1$ is instead

$$\delta\dot{x}(t) = -\delta x(t - \tau). \tag{6.6}$$

We seek solutions of the form $\delta x(t) = e^{\lambda t}$. The eigenvalues λ are roots of the characteristic equation:

$$\lambda + e^{-\lambda\tau} = 0. \tag{6.7}$$

By linearization theory, the equilibrium is asymptotically stable if and only if all roots of Eq. (6.7) have negative real parts [21]. Intuitively, this is because the general solution to the linearized equation is a superposition of these characteristic exponentials, and stability requires that all these modes decay. Eq. (6.7) is transcendental, and its roots can be expressed in terms of the Lambert W-function [80] as $\lambda_k = W_k(-\tau)/\tau$. This equation has an infinite number of solutions, each corresponding to a different branch of the W-function, which reflects the infinite dimensionality of the DDE.

One observes that for small τ all roots of Eq. (6.7) have negative real part. However, as the delay increases, a pair of complex conjugate eigenvalues crosses the imaginary axis. This crossing marks the onset of instability, where the linearization displays diverging oscillatory solutions. This linear instability typically induces persistent limit cycles in the original non-linear DDE. To determine the critical delay we search for purely imaginary eigenvalues $\lambda = i\omega$ (with $\omega > 0$):

$$i\omega + e^{-i\omega\tau} = 0. \tag{6.8}$$

Taking the real part gives $\cos\omega\tau = 0$, which implies $\omega\tau = \pi/2$, while taking the imaginary part yields $\omega = 1$. Thus, for $0 < \tau < \pi/2$ all solutions of Eq. (6.7) have negative real part, and at $\tau = \pi/2$ a pair of complex eigenvalues cross the stability line.

To sum up, in the DDE Eq. (6.5), for $\tau < \pi/2$ the equilibrium $x^* = 1$ is asymptotically stable, while for $\tau > \pi/2$ it is unstable, and periodic solutions bifurcate from it. We will show that a similar phenomenology takes place in the GLV equations.

To conclude, we note that while scalar first-order DDEs with monotone negative feedback like Hutchinson's equation typically display only stable fixed points or limit cycles [121], chaos is not precluded in scalar DDEs generally. The standard textbook example is the Mackey-Glass equation [43, 48]:

$$\dot{x}(t) = -bx(t) + \frac{ax(t-\tau)}{1+x(t-\tau)^n}, \tag{6.9}$$

which is known to display chaotic attractors for example for $a = 0.2$, $b = 0.1$, $n = 10$, and $\tau > 16.8$.

6.4 Dynamical Mean-Field Theory for delayed interactions

To derive the DMFT equation for disordered systems with delayed interactions, one can employ generating functional methods [289], although the same results could be obtained with the dynamical cavity method [61, 211]. The procedure is a straightforward generalization of the usual method [199, 289], so we only state the result. The DMFT equation associated to Eq. (6.2) is

$$\dot{x}(t) = x(t)\left[1 - x(t) + \mu \int_0^\infty d\tau K(\tau)\langle x(t-\tau)\rangle + \sigma\eta(t)\right]. \tag{6.10}$$

The Gaussian noise $\eta(t)$ has zero mean and correlations given by

$$\langle \eta(t)\eta(t')\rangle = \int_0^\infty d\tau \int_0^\infty d\tau' K(\tau)K(\tau')\langle x(t-\tau)x(t'-\tau')\rangle. \tag{6.11}$$

For instantaneous interactions, the phase diagram of the model is the one previously discussed, see Section 1.2.1. The model exhibits a region where species abundances invariably converge to a unique fixed point (UFP). As σ increases, a transition occurs to a phase characterized by multiple attractors (MA). When μ or σ exceed a critical threshold, an unbounded growth (UG) phase emerges, in which a subset of species experiences population divergence in finite time.

Here, the simultaneous presence in the DMFT equation Eq. (6.10) of an infinite-dimensional phase space, noise, self-consistency relations, and memory kernels renders the analysis of this system highly non-trivial. To better understand the interplay between these various elements, we will first consider a discrete memory kernel and allow for heterogeneity in the interactions. Afterward, we will consider a more general class of kernels and derive our analytical results in the homogeneous, $\sigma = 0$ limit. Finally, we will investigate the effect of delayed self-regulation and a minimal structure in the interactions on the resulting community dynamics.

6.5 Discrete delays induce persistent synchronization

We first consider the case in which interactions among species are delayed by a fixed, discrete temporal delay τ, which is identical across all species pairs. This corresponds to considering a delta-function memory kernel. We assume that intraspecific interactions are purely instantaneous. The general case of delayed intraspecific interactions is analyzed in Section 6.7. The GLV equations with discrete delay and heterogeneous interactions then read

$$\dot{x}_i(t) = x_i(t)\left[1 - x_i(t) + \sum_{j\neq i} \alpha_{ij} x_j(t-\tau)\right]. \tag{6.12}$$

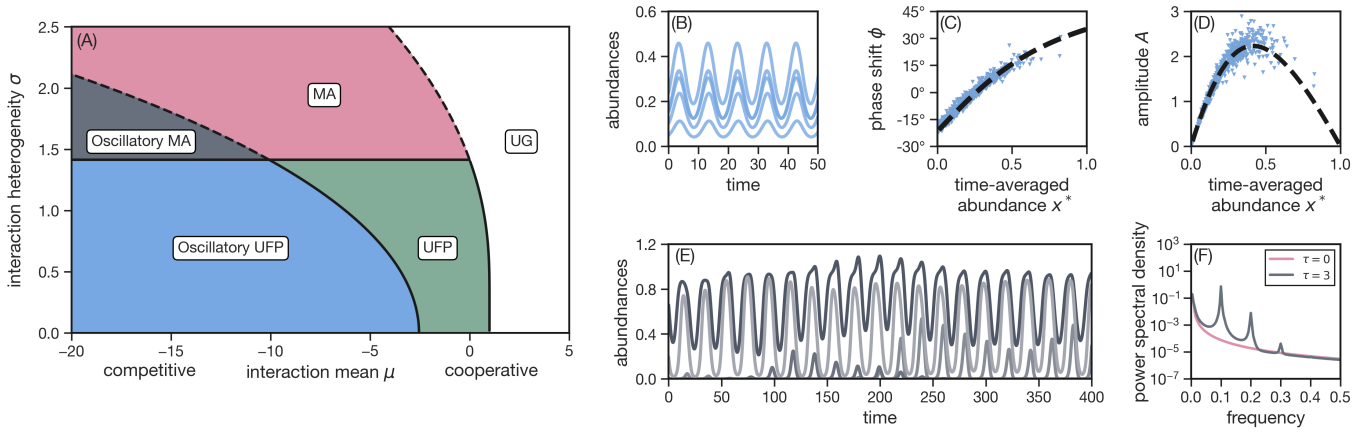

Figure 6.2: Phases of generalized Lotka-Volterra equations with discrete delay. Panel (A): Phase diagram of the generalized Lotka-Volterra equations with a discrete delay $\tau = 3$. Along the unique fixed-point (UFP) and multiple attractors (MA) phases, also observed for $\tau = 0$, two new oscillatory phases emerge if competition in the community is high enough, that is, when μ is sufficiently negative. The line separating the oscillatory phases and the non-oscillatory ones is obtained numerically. The unbounded growth (UG) phase is instead unaffected by the delay. Panel (B): Typical dynamics in the Oscillatory UFP phase. All the species fluctuate around a unique fixed point. Only a subset of the species composing the community is shown. Panels (C-D): Phase shift ϕ and relative amplitude A of oscillations of species abundances in the Oscillatory UFP phase. Triangles are obtained by numerical simulations, while the black line is given by Eq. (6.16). Panel (E): Typical dynamics in the Oscillatory MA phase. At difference with Oscillatory UFP, there is no unique fixed-point structure around which these oscillations occur. Only a subset of the species composing the community is shown. Panel (F): Comparison between the power spectral densities in the Oscillatory MA phase in the case of instantaneous and delayed interactions. Upon turning on a sufficiently large delay, equally-spaced peaks appear due to the oscillations in species abundances.

Figure 6.2 illustrates the dynamical phases of Eq. (6.12) as a function of the parameters μ and σ at a fixed value of delay τ. As in the case of instantaneous interactions, a UFP phase and an MA phase are present. The line separating the two is not affected by the presence of the delay (see Appendix 6.10.2). At the same time, two new dynamical phases emerge under sufficiently strong competition, that is, when μ is lower than a critical value, which decreases upon increasing σ. These phases, which we term Oscillatory UFP and Oscillatory MA, are characterized by persistent and almost synchronous oscillations, as depicted in Figure 6.2B and 6.2E.

In the Oscillatory UFP phase, species abundances oscillate periodically and indefinitely. This limit-cycle behavior is reached for any initial condition of the community and is stable to perturbations. The time-averaged abundances in this phase are the unique fixed-points of the GLV dynamics (see Appendix 6.10.3). In particular, these time-averaged abundances are distributed as a truncated Gaussian distribution, as in the UFP phase. In the Oscillatory MA phase, species abundances also display persistent oscillations but, as it happens in the MA phase, there is no stable fixed-point structure around which these oscillations occur. In both oscillatory phases, species abundances exhibit oscillations that are nearly synchronized.

The transition between the UFP and MA phases and their oscillatory counterparts takes place via a loss of linear stability via a pair conjugate eigenvalues with non-zero imaginary part. This is a well-documented behavior in delayed differential equations, where the critical point at which a fixed point loses stability is known as a Hopf bifurcation [121]. Since the fixed-point structure is

substantially simpler in the UFP phase, our analysis will focus on the transition line between this phase and the Oscillatory UFP one.

To understand the details of this phase transition, we consider the dynamics of the DMFT equation in the low-heterogeneity regime [282]. This approximation simplifies considerably the analysis. At leading order in σ the DMFT equation in the case of a discrete delay is approximated by (see Section 1.2.2.5)

$$\dot{x}(t) = x(t)\left[1 - x(t) + \mu\langle x(t-\tau)\rangle + \sigma z\langle x(t-\tau)\rangle\right], \tag{6.13}$$

where z is a quenched random Gaussian variable with zero mean and unit variance. We emphasize that this approximation is based solely on a low-heterogeneity expansion of the noise term in the DMFT equation, and as a consequence we expect it to be applicable not only to GLV equations, but also to a broad class of disordered dynamical systems [63, 71, 230, 308]. Although this approximation is technically valid only for small σ, it captures qualitatively, but also quantitatively, the dynamical behavior of the community for all values of σ, as we will show.

For $\tau = 0$ the stable equilibrium of Eq. (6.13) is $x^*(z) = \max[0, 1 + (\mu + \sigma z)\langle x^*\rangle]$. The loss of stability occurs only through the positive equilibrium, since the zero equilibrium, when stable at $\tau = 0$, retains stability for all $\tau > 0$. We thus study the dynamics of small perturbations $\delta x(t)$ around the non-zero equilibrium. We assume a solution of the linearized dynamics of the form

$$\delta x(t) = c(z)e^{\lambda t}. \tag{6.14}$$

Importantly, we are making the ansatz that the eigenvalue λ does not depend on the species, meaning it does not depend on z in our approximation. Generally, it is not expected that all degrees of freedom display the same eigenvalue, given the presence of a spectral bulk. Indeed, such an ansatz determines a spectral outlier. Since destabilization is due to such an outlier (see Appendix 6.10.8), this approach will capture the correct stability line between the UFP and Oscillatory UFP phases. As explicitly shown in Eq. (6.14), we allow for a species-dependent amplitude and phase shift, encoded in a complex $c(z)$. Since the linear equation is homogeneous, we can arbitrary normalize $c(z)$. We choose the absolute value $A(z)$ and the phase shift $\phi(z)$ as implicitly defined by $A(z)e^{i\phi(z)} = c(z)/\langle c(z)\rangle$, such that it results that $\langle A(z)e^{i\phi(z)}\rangle = 1$. The eigenvalue equation is then

$$\lambda = x^*(z)\left[-1 + (\mu + \sigma z)A(z)^{-1}e^{-i\phi(z)}e^{-\lambda\tau}\right]. \tag{6.15}$$

The equilibrium $x^*(z)$ is asymptotically stable if all solutions of Eq. (6.15) have negative real parts, and a change in the stability occurs when the leading eigenvalue becomes purely imaginary [138]. Therefore, to determine the critical line in the μ-σ plane separating the UFP and the Oscillatory UFP phases, we seek solutions of the form $\lambda = i\omega$. Imposing this leads to (see Appendix 6.10.4)

$$\begin{aligned} \phi(z) &= -\omega\tau - \arctan(\omega/x^*(z)), \\ A(z) &= \left[1 + (\omega/x^*(z))^2\right]^{-1/2}(\mu + \sigma z). \end{aligned} \tag{6.16}$$

Eq. (6.16) gives the phase shift and the amplitude of the oscillations of each non-extinct species at the critical line as a function of z or, by inverting $x^*(z)$, as a function of their time-averaged abundances. This is shown in Figure 6.2C and 6.2D. As anticipated, Eq. (6.16), obtained analytically for low heterogeneity, is in good agreement with numerical simulations even for large σ. In this regime, the approximation predicts the trend of the oscillation phase shifts and amplitudes as a function of the mean abundances, although it does not capture a dispersion around this trend.

Our results show that the phase shifts of oscillations depend on the species mainly through their time-averaged abundances. Moreover, they do so only in a weak manner. As a consequence, the overall dynamics of the community displays coherent oscillations that are nearly synchronous. Interestingly, species with larger abundances tend to anticipate the dynamics, exhibiting positive phase shifts. This means that more abundant species reach their peak populations slightly before the average trend of the community.

At the same time, we observe a non-monotonic dependence of the relative amplitudes of oscillations and the average abundances. In particular, species with intermediate abundances exhibit the largest oscillation amplitudes, while both rare and highly dominant species display relatively smaller amplitudes. This suggests that species with moderate abundances are more sensitive to delayed interactions, resulting in more pronounced oscillatory behavior compared to very rare or highly abundant species. We also note that species with higher mean abundances show a greater dispersion from the trend given by Eq. (6.16).

To determine the critical delay at which oscillations appear and the corresponding critical frequency, we use the fact that $\phi(z)$ and $A(z)$ by definition satisfy $\langle A(z)e^{i\phi(z)}\rangle = 1$. Taking the real and imaginary parts gives two equations that yield the critical τ and ω. These read

$$\begin{aligned} \cos\omega\tau &= \int_{-\infty}^{\infty} Dz \frac{(\mu+\sigma z)x^*(z)^2}{\omega^2 + x^*(z)^2}, \\ \sin\omega\tau &= -\int_{-\infty}^{\infty} Dz \frac{(\mu+\sigma z)\omega x^*(z)}{\omega^2 + x^*(z)^2}, \end{aligned} \tag{6.17}$$

where $Dz = (2\pi)^{-1/2}e^{-z^2/2}dz$ is the Gaussian measure. Eq. (6.17) can be solved numerically at a fixed value of τ to obtain the critical line separating the UFP and Oscillatory UFP phases in μ-σ space. We can compare this analytical transition line with the one obtained from numerical simulations of the GLV equation defined in Eq. (6.12), which is the one shown in Figure 6.2A. The two lines display the same qualitative trend and also coincide quantitatively up to intermediate values of heterogeneity (see Appendix 6.10.5). Our result is thus that more heterogeneous communities need a greater competition in order to sustain persistent oscillations, as we qualitatively explain in 6.10.6. We note that at present our analysis does not establish whether a phase transition occurs between the MA and Oscillatory MA phases, or if the transition consists in a smooth crossover.

Through a comprehensive sensitivity analysis, we confirm that the phase of coherent oscillations persists when considering a large class of extensions of the model considered here (see Appendix 6.10.7). These extensions include species-specific growth rates and carrying capacities, heterogeneous interaction delays, sparse interaction networks, and a finite number of species. We attribute the robustness of the phase diagram to the fact that oscillations emerge from the crossing of the stability line of a pair of outlier eigenvalues in the Jacobian spectrum, which is numerically illustrated in the 6.10.8. Moreover, as shown in 6.10.7.5, even when a non-linear response function is considered in the GLV equations, oscillations do not arise at any level of cooperation in the community.

6.6 Distributed delays also induce persistent synchronization

In the previous section, we focused on the case in which the memory kernel is a delta function, which models the delay as an impulsive feedback from the past state of the system. However, in the effective community dynamics given by Eq. (6.2), interactions are generally mediated by a distributed memory kernel $K(\tau)$.

To focus on the impact of a distributed delay rather than the heterogeneity of interactions, in this section, we analyze the simplified case of homogeneous interactions. When the system is homogeneous, the dynamics of each species can be found by setting $\sigma = 0$ in the DMFT equation:

$$\dot{x}(t) = x(t)\left[1 - x(t) + \mu \int_0^\infty d\tau K(\tau) x(t-\tau)\right]. \tag{6.18}$$

As in the case of discrete delays, we investigate the dynamics of small perturbations around the equilibrium abundance. The perturbation analysis leads to the eigenvalue equation

$$\lambda = x^* \left[-1 + \mu \hat{K}(\lambda)\right], \tag{6.19}$$

where $\hat{K}(\lambda)$ is the Laplace transform of the memory kernel. For concreteness, we consider a Gamma-distributed kernel

$$K(\tau) = \frac{\beta^{-\alpha}}{\Gamma(\alpha)} \tau^{\alpha-1} e^{-\tau/\beta}, \tag{6.20}$$

where $\alpha, \beta > 0$ are fixed parameters. To determine the phase transition in stability, as before, we search for solutions with purely imaginary eigenvalues. We find that for $\alpha > 1$ and for

$$\beta > \sin\frac{\pi}{2\alpha} \cdot \left(\cos\frac{\pi}{2\alpha}\right)^{-(\alpha+1)}, \tag{6.21}$$

there exists a value of the average interaction strength μ below which oscillations emerge. This is given by the function

$$\mu(\alpha, \beta) = \frac{\left(1 + \beta^2\omega^2\right)^{\alpha/2}}{\cos(\alpha \arctan(\beta\omega))}, \tag{6.22}$$

where the frequency of oscillations at criticality can be determined by solving the equation

$$\omega = \frac{\sin(\alpha \arctan(\beta\omega))}{(1 + \beta^2\omega^2)^{\alpha/2} - \cos(\alpha \arctan(\beta\omega))} \tag{6.23}$$

(see Appendix 6.10.9 for details). It can be shown $\mu(\alpha, \beta) < -1$. These results are illustrated in Figure 6.3, which reports the phase diagram as a function of the mean and coefficient of variation of the Gamma-distributed kernel.

Therefore, the same behavior found in the case of a discrete delay is also present in the distributed case. In conditions of sufficiently strong competition, the community displays persistent and coherent oscillations in species abundances. This happens if memory effects are sufficiently localized in the past, precisely if the coefficient of variation (defined as the ratio between the standard deviation and the mean of the distributed kernel) is lower than 1 and its mean exceeds a certain threshold. Although in the homogeneous limit oscillations are perfectly synchronous, introducing heterogeneity in the interactions slightly perturbs this synchronicity. Upon increasing σ, first an Oscillatory UFP phase and subsequently an Oscillatory MA phase are found. The heterogeneous case is not investigated here, although the techniques employed previously in the discrete delay case could be extended to the case of a distributed kernel.

In the limit $\alpha = 1$, the Gamma function simplifies to an exponential. In this case, the eigenvalues always have a negative real part. Consequently, neither an Oscillatory UFP nor an Oscillatory MA phase is found, and the long-time phase diagram is identical to the instantaneous case. This result is consistent with the theory of delay differential equations, where exponential kernels are

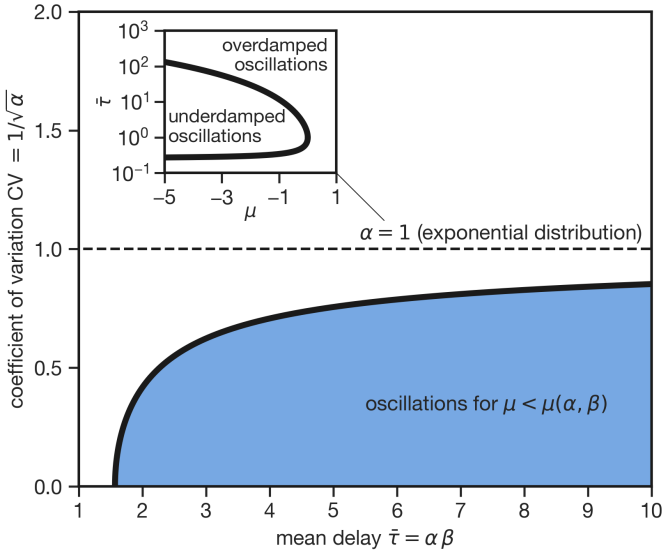

Figure 6.3: Phase diagram of generalized Lotka-Volterra equations with distributed delay and homogeneous interactions. Main: Phase diagram as a function of the mean delay and the coefficient of variation of a Gamma-distributed kernel. When CV ≥ 1, sustained oscillations do not appear. In contrast, when the memory effects are sufficiently localized in the past, precisely if CV < 1, oscillations can emerge if the mean delay memory exceeds a certain threshold and if the community is sufficiently competitive (shaded blue region). Inset: The case of an exponentially decaying memory kernel, which can display overdamped or underdamped oscillations during the relaxation to equilibrium.

known as "weak kernels", which do not generally destabilize fixed points [121]. The absence of oscillatory phases for exponential delays reflects the fact that such kernels heavily weight recent history, effectively smoothing out the destabilizing effects of time delays.

Still, for an exponentially decaying memory kernel, we can precisely identify the boundary between two distinct phases during the relaxation of the community to equilibrium. In the underdamped phase, at least one eigenvalue has a non-zero imaginary part, leading to oscillatory behavior during relaxation. In contrast, the overdamped phase is characterized by all eigenvalues being real and negative, resulting in non-oscillatory dynamics. The critical line separating these two regimes is (see Appendix 6.10.10)

$$1 - 2\mu + \mu^2 - 2\bar{\tau} + 6\mu\bar{\tau} - 4\mu^2\bar{\tau} + \bar{\tau}^2 = 0, \tag{6.24}$$

where $\bar{\tau}$ is the characteristic time of the exponential kernel (see inset of Figure 6.3).

6.7 Delayed intraspecific interactions induce both synchronization and chaos

In the previous sections we considered ecological communities in which only interspecific interactions were delayed. However, ecological mechanisms such as maturation times or resource renewal generally lead to memory effects also in intraspecific interactions. Moreover, as Eq. (6.2) shows, integrating out environmental variables also induces delays in species self-regulation. In this section we therefore relax the assumption of instantaneous intraspecific interactions and consider the case in which these are also delayed.

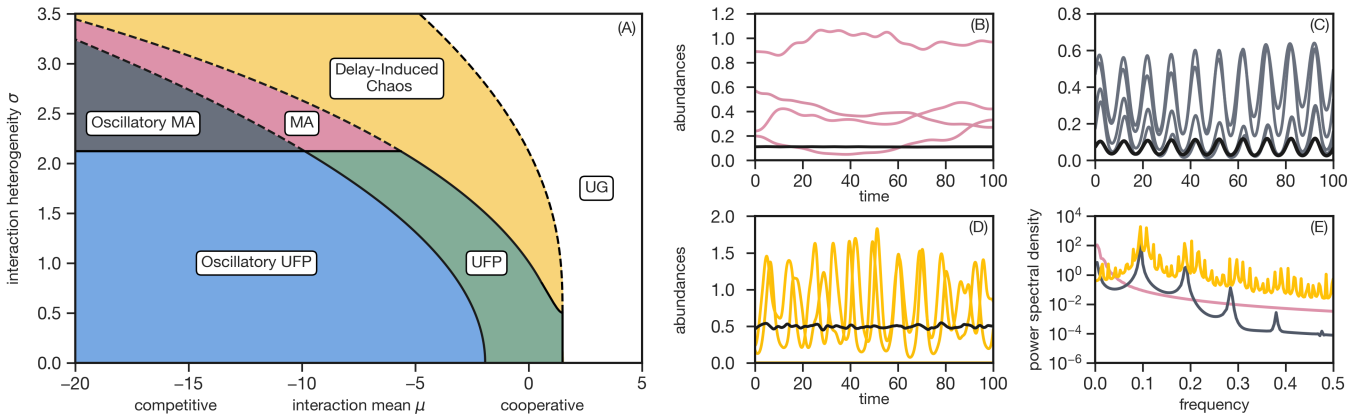

Figure 6.4: Phase diagram of generalized Lotka-Volterra equations with delayed intraspecific interactions. Panel (A): Phase diagram of the generalized Lotka-Volterra equations with a discrete delay $\tau = 3$ and an intensity of delayed intraspecific interactions $u = -0.5$. In addition to the phases observed without delayed intraspecific interactions ($u = 0$), an additional phase of delay-induced chaos emerges. Panel (B): An example of the dynamics in the MA phase. Only a subset of the species composing the community is shown. In this phase the dynamics takes place on slow timescales and the instantaneous mean abundance is constant. Panel (C): An example of the dynamics in the Oscillatory MA phase. Only a subset of the species composing the community is shown. In this phase species abundances additionally display nearly synchronized oscillations and the mean oscillates periodically. Panel (D): An example of the dynamics in the phase of delay-induced chaos. Only a subset of the species composing the community is shown. Species abundances in this phase exhibit irregular and aperiodic fluctuations and the mean fluctuates. Panel (E): Comparison between the power spectral densities in the MA, Oscillatory MA, and delay-induced chaos phases.

For simplicity of presentation, we consider only discrete delays, although the techniques from Section 6.6 could be extended to the case of delayed intraspecific interactions. We assume each species has self-regulation with both instantaneous and delayed contributions, with the delay identical across all species and equal to that of interspecific interactions. The community dynamics is then described by

$$\dot{x}_i(t) = x_i(t)\left[1 - x_i(t) + u x_i(t-\tau) + \sum_{j\neq i} \alpha_{ij} x_j(t-\tau)\right], \tag{6.25}$$

where $u < 1$ sets the strength of memory effects in self-regulation. For $u = 0$ we recover the case of Section 6.5.

The resulting phase diagram is shown in Figure 6.4. For $u \neq 0$, Eq. (6.25) displays both Oscillatory UFP and Oscillatory MA phases, which are qualitatively similar to those found for $u = 0$. The line in μ-σ space separating the UFP and Oscillatory UFP phases can be found by a straightforward extension of the method employed for $u = 0$ (see Appendix 6.10.11).

Interestingly, unlike the case of instantaneous intraspecific interactions, Eq. (6.25) exhibits a phase of delay-induced chaos for $u < 0$. Here, species abundances fluctuate irregularly and aperiodically as a consequence of delayed interactions (see Figure 6.4B). The power spectrum in this regime exhibits regularly spaced peaks, similar to those seen in the Oscillatory MA phase, but with interlaced lower peaks (see Figure 6.4C).

To locate the exact transition line between the UFP and delay-induced chaotic phases, we perform

a linear stability analysis. The procedure is the standard one [71, 199], see also Section 1.2.2.2, although here not employed to detect the transition from the UFP phase to the MA phase. We add a small-amplitude white noise $\xi(t)$ to the DMFT equation associated to Eq. (6.25) as

$$\dot{x}(t) = x(t)\Big[1 - x(t) + ux(t-\tau) + \mu\langle x(t-\tau)\rangle + \sigma\eta(t) + \xi(t)\Big], \tag{6.26}$$

and study the resulting fluctuations about the fixed point, $\delta x(t) = x(t) - x^*$. We find that $\langle \delta x(t)\delta x(t')\rangle = \delta C(t-t')$, where the transform $\delta C(\omega)$ of this function is found to be

$$\delta C(\omega) = \frac{B(\omega)}{1 - \sigma^2 B(\omega)}, \tag{6.27}$$

where the function $B(\omega)$ is

$$B(\omega) = \langle \left| \frac{i\omega}{x^*(z)} + 1 - ue^{-i\omega\tau} \right|^{-2} \rangle. \tag{6.28}$$

We see that the perturbations diverge whenever the denominator of Eq. (6.27) vanishes. This occurs when there exists a ω for which

$$\sigma^2 B(\omega) = 1. \tag{6.29}$$

For $u < 0$, there exists a critical line in μ-σ space satisfying Eq. (6.29), and on this line ω maximizes $B(\omega)$. The resulting transition line is exact for the UFP and delay-induced chaos boundary, but can be analytically continued to yield an approximate boundary between the MA and delay-induced chaos phases. As before, our analysis cannot currently conclude whether the transitions between the high-heterogeneity phases are analytic or not.

We note that although the MA, Oscillatory MA, and delay-induced chaos phases are all chaotic, they exhibit qualitatively distinct dynamics, as illustrated in Figure 6.4. The dynamics in the MA phase takes place on slow timescales, the instantaneous mean abundance is constant, and its power spectrum is monotone. In the Oscillatory MA phase species abundances additionally display nearly synchronized oscillations, the mean abundance oscillates periodically, and the power spectrum displays pronounced peaks at characteristic frequencies. Finally, the dynamics in the delay-induced chaos phase occurs on much shorter timescales and significantly larger amplitudes, which leads to a fluctuating mean for a finite number of species, and the power spectrum exhibits multiple nested peaks.

Our results thus reveal an additional pathway to chaotic dynamics in complex ecological communities, arising from the presence of time delays rather than from high ecological heterogeneity. Unlike the case of synchronization, we do not propose a qualitative mechanism underlying the onset of chaos. Future work will characterize this chaotic regime more precisely, for example by computing the Lyapunov spectra or the effective dimensionality of collective activity.

6.8 Negatively-correlated reciprocal interspecific interactions also induce synchronization and chaos

Until now, we have considered in this chapter a complex ecological community with interactions taken as uncorrelated random variables. In this section, we relax this assumption by considering a correlation between reciprocal interactions. As usual, we examine the case in which

$$\text{corr}(\alpha_{ij}, \alpha_{ji}) = \gamma. \tag{6.30}$$

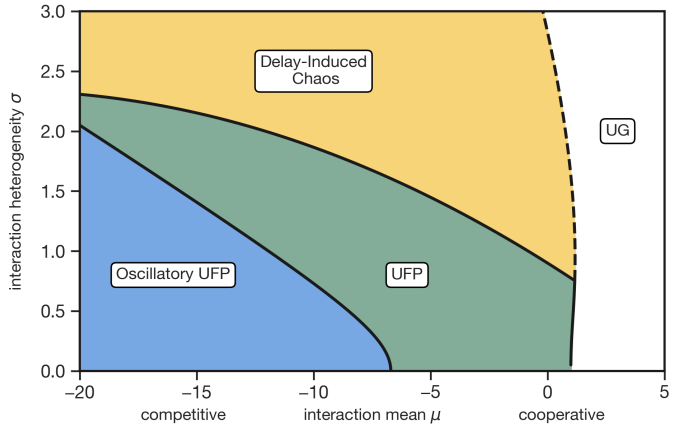

Figure 6.5: Phase diagram of generalized Lotka-Volterra equations with negatively-correlated reciprocal interactions. Phase diagram of generalized Lotka-Volterra equations with a discrete delay $\tau = 2$ and correlation $\gamma = -0.5$ between reciprocal species interactions. The phase diagram is similar to the one obtained with delayed intraspecific interactions.

Considering for simplicity the case of a discrete delay, the DMFT equation generalizes to

$$\dot{x}(t) = x(t)\left[1 - x(t) + \mu\langle x(t-\tau)\rangle + \sigma\eta(t) + \gamma\sigma^2 \int_0^{t-\tau} dt' G_\tau(t,t')x(t'-\tau)\right]. \tag{6.31}$$

A correlation structure in the interactions thus enters the DMFT description as a memory kernel, which is given self-consistently by

$$G_\tau(t,t') = \frac{\delta\langle x(t-\tau)\rangle}{\delta\sigma\eta(t')}. \tag{6.32}$$

The phase diagram of Eq. (6.31) is shown in Figure 6.5. For $\gamma \neq 0$ it displays oscillatory phases, which are qualitatively similar to those found for $\gamma = 0$.

Additionally, for $\gamma < 0$, we observe the presence of a phase of delay-induced chaos. The onset of this phase can be understood through a linear stability analysis analogous to the one presented in Section 6.7. We study fluctuations around the fixed point after the introduction of small-amplitude noise. In the same notation as before, the critical line satisfies $\sigma^2 B(\omega) = 1$, where now

$$B(\omega) = \langle \left| \frac{i\omega}{x^*(z)} + 1 - \gamma\sigma^2 G(\omega) e^{-2i\omega\tau} \right|^2 \rangle, \tag{6.33}$$

and $G(\omega)$ is the transform of the response Eq. (6.32) in the stationary limit.

To proceed, one would need the explicit form of the response function $G(\omega)$, which, however, is not easily accessible since it results from the underlying non-linear dynamics. To overcome this limitation, we approximate $G(t)$ as an exponentially decaying function, a simple ansatz for the system's relaxation near a stable fixed point, see also Section 1.2.2.1. The amplitude and timescale of this exponential are fixed by [211]

$$G(0) = \langle x^*(z)\rangle \tag{6.34}$$

and

$$\int_0^\infty dt G(t) = \chi, \tag{6.35}$$

where both $\langle x^*(z)\rangle$ and χ can be computed from the UFP assumption. This leads to

$$G(\omega) = \frac{\langle x^*(z)\rangle\chi}{\langle x^*(z)\rangle + i\chi\omega}. \tag{6.36}$$

This approximation yields predictions that closely match the numerical results (see Appendix 6.10.12). We underline that this approximation does not rely on any specific feature of the GLV dynamics and should therefore be broadly applicable to describe disordered dynamical systems with reciprocally correlated interactions near stable fixed points.

The resulting phase diagram is therefore similar to that obtained for delayed intraspecific interactions: in both cases, delayed feedback can give rise to both oscillatory and chaotic dynamics. Notably, and in contrast with results on the linear stability analysis of ecosystems [153], we observe that negatively correlated reciprocal interactions can destabilize the system and drive it into a chaotic phase. As in the previous case, we do not provide an intuitive explanation for why the interplay between correlation and delay can lead to chaos. In this context, we note that even in the linear case these two ingredients interact in non-trivial and counterintuitive ways [321]. We note that the presence of a phase of delay-induced chaos actually suppresses the other two chaotic phases, the MA and Oscillatory MA phases. At present, we offer no mechanism behind this phenomenon.

6.9 Discussion

In this chapter, we developed an analytical framework that enables the systematic analysis of high-dimensional non-linear systems with memory effects. We showed how DMFT can be extended to incorporate time delays, allowing for the dimensionality reduction of randomly interacting systems. Building on this reduction, we demonstrated how techniques from low-dimensional delay differential equations can be adapted to the stochastic and self-consistent setting of DMFT. This, in turn, makes it possible to analytically describe the dynamical behavior exhibited by complex systems in terms of key macroscopic parameters.

We exemplified our framework by studying the effect of time delays on the dynamics of complex ecological communities, a setting in which memory effects frequently arise through a variety of mechanisms. Within the context of generalized Lotka-Volterra equations with random and delayed interactions, our methodology revealed a remarkably rich set of dynamical behaviors emerging from the interplay of non-linearity, memory, and high dimensionality. We identified a phase in which sufficiently competitive communities spontaneously exhibit persistent and nearly synchronous oscillations. We derived analytical expressions for the transition to this regime, as well as for the oscillation frequency, amplitudes, and phase displacements. We also uncovered the presence of a phase of delay-induced chaos in ecological communities with structured interactions. This feature arises from the high-dimensional setting we considered, as time delays in time-continuous single-species models typically produce only limit-cycle behavior [121].

Our method offers several advantages over previous analytical approaches. Random matrix theory techniques [111, 252, 275, 321] cannot always be applied, as the instantaneous and delayed Jacobian matrices generally do not commute. This is the case, for example, of the generalized Lotka-Volterra equations we considered. Moreover, even when applicable, random matrix theory can at most delineate stability boundaries, without revealing the nature of dynamics beyond these transitions. In contrast, our framework provides a complete analytical characterization of both the transition points and the properties of the resulting dynamical phases.

A few important assumptions underlie our method, and relaxing them in future research could yield valuable insights. Firstly, we assumed a deterministic dynamics, but introducing noise [113, 229, 322, 323] can profoundly influence the properties of ecosystems, as highlighted by neutral theory [174]. Moreover, extending our framework to account for more complex interaction structures [268, 299, 312], including higher-order interactions and structured topologies, could reveal an even broader range of dynamical behaviors. Given that even minimal structural modifications significantly alter our phase diagrams, such extensions are likely to produce a richer phenomenology. While these directions present considerable technical challenges, addressing them in future work could substantially deepen our understanding of high-dimensional delayed systems.

Overall, the techniques presented here represent a significant methodological advance for understanding memory effects in complex systems. Limit cycles and chaos are not unique to the ecological setting we studied, but are ubiquitous features of high-dimensional, time-delayed, and non-linear systems. The mathematical structure underlying these behaviors, and correspondingly the techniques developed in this work, extend well beyond ecology. Moreover, both the approximations we introduced do not apply only to GLV systems, but are expected to be applicable to the broad class of disordered dynamical systems amenable to a DMFT formulation.

Our work could be relevant, for example, in the analysis of neural networks with transmission delays, epidemiological models with incubation periods, and economic systems with decision lags, providing a general toolkit for understanding the interplay between memory effects and high-dimensionality in disordered systems. Future research could leverage these methods to investigate time-delayed effects in any domain in which memory plays a pivotal role. In Chapter 7 the same methodologies are applied to a random neural network model.

6.10 Appendix

6.10.1 Emergence of delay effects from interaction with external variables

The dynamics of the community species and the external variables are set by Eq. (6.1). We assume that the dynamics settles at steady-state values x_i^* and y_μ^*. We posit that the growth rates $g_i(\boldsymbol{x}(t), \boldsymbol{y}(t))$ depend linearly on the species variables and we also expand them linearly around the equilibrium of the external variables. This yields

$$g_i(\boldsymbol{x}(t), \boldsymbol{y}(t)) = \sum_{j=1}^{S} a_{ij} x_j(t) + \sum_{\mu=1}^{R} b_{i\mu}(y_\mu(t) - y_\mu^*). \tag{6.37}$$

We further suppose that the dynamics of species in the community induce only a small perturbation in the dynamics of the external variables. This assumption allows a linear expansion of the dynamics of the external variables around the equilibrium values. We get

$$\dot{y}_\mu(t) = -r_\mu(y_\mu(t) - y_\mu^*) + \sum_{j=1}^{S} c_{\mu j}(x_j(t) - x_j^*). \tag{6.38}$$

Each $y_\mu(t)$ relaxes to equilibrium on a timescale r_μ^{-1} in the absence of the community species. For simplicity we consider a diagonal dynamics in the external dynamics, although the approach easily generalizes without this restriction. At long times, the explicit solution of Eq. (6.38) for given $x_i(t)$

is

$$y_\mu(t) = y_\mu^* + \int_0^\infty d\tau e^{-r_\mu \tau} \sum_{j=1}^{S} c_{\mu j}(x_j(t-\tau) - x_j^*). \tag{6.39}$$

This is where delay effects originate. Substituting this solution into the dynamics of the community gives a closed equation for the species abundances $x_i(t)$. The result is Eq. (6.2), where the macroscopic parameters are related to the microscopic ones as

$$\begin{aligned} r_i &= -\sum_{j=1}^{S}\sum_{\mu=1}^{R} \frac{1}{r_\mu} b_{i\mu} c_{\mu j} x_j^*, \\ K_{ij}(\tau) &= \frac{1}{r_i}\left[a_{ij}\delta(\tau) + \sum_{\mu=1}^{R} e^{-r_\mu \tau} b_{i\mu} c_{\mu j} \right]. \end{aligned} \tag{6.40}$$

Notably, if $\boldsymbol{x}$ represent consumers and $\boldsymbol{y}$ resources, $b_{i\mu}$ are positive and $c_{\mu j}$ are negative, which implies that the effective interaction kernel $K_{ij}(\tau)$ has a negative sign, describing a competitive community. Moreover, a larger uptake rate $b_{i\mu}$ for the species i results in a faster growth rate in the effective dynamics. Furthermore, we notice that the weight $b_{i\mu}c_{\mu j}$ of each exponential in Eq. (6.40) can assume both positive and negative values, depending on the nature of the interactions between species and external variables. As a consequence, the sum of these exponentials can produce non-monotonic kernels $K_{ij}(\tau)$.

6.10.2 Delay does not affect transition line between UFP and MA phases

We follow the approach of [199], see also Section 1.2.2.2. We add small white noise $\xi(t)$ to the DMFT equation with discrete delay:

$$\dot{x}(t) = x(t)\left[1 - x(t) + \mu\langle x(t-\tau)\rangle + \sigma\eta(t) + \xi(t)\right], \tag{6.41}$$

and study the resulting fluctuations $\delta x(t) = x(t) - x^*$ about a fixed point. We denote by $v(t)$ the first-order term in the noise, that is, $\eta(t) = \eta^* + v(t)$. Self-consistently we obtain that $\langle v(t)v(t')\rangle = \langle \delta x(t-\tau)\delta x(t'-\tau)\rangle$. We note, importantly, that at stationarity there is no dependence on τ in the noise $v(t)$, since in this limit $\langle \delta x(t-\tau)\delta x(t'-\tau)\rangle = \langle \delta x(t)\delta x(t')\rangle$. We can then follow the same steps as in [199] and find that the critical value of interaction heterogeneity above which perturbations do not decay is $\sigma = \sqrt{2}$. This means that the transition between the UFP and MA phases happens at the same point as in the instantaneous case, $\tau = 0$. This reasoning generalizes in straightforward way to the case of distributed delay, delayed intraspecific interactions ($u \neq 0$), or structured interactions ($\gamma \neq 0$).

6.10.3 Equivalence of time-averaged and equilibrium abundances

For any non-extinct, oscillating species i, we divide both sides of the GLV equation by $x_i(t)$ and take the time average. Since the mean of the left-hand side vanishes and $K(\tau)$ is normalized to 1, we get

$$0 = 1 - \overline{x}_i + \sum_j \alpha_{ij}\overline{x}_j, \tag{6.42}$$

where $\overline{x}_i$ is the mean abundance of species i over one oscillation period T. For non-extinct species, Eq. (6.42) match those describing the equilibrium values x_i^*. Assuming a unique equilibrium, it

follows that the time-averaged abundances and the equilibrium ones are equivalent. We notice that this argument crucially depends on the oscillation period being identical across species and on the linearity of the interaction term in $x_j(t)$.

6.10.4 Critical behavior for discrete delay

To locate the Hopf bifurcation of Eq. (6.15) we search for solutions of the eigenvalue equation in the form $\lambda = i\omega$

$$i\omega = x^*(z)\left[-1 + (\mu + \sigma z)A(z)^{-1}e^{-i\phi(z)}e^{-i\omega\tau}\right]. \tag{6.43}$$

To make calculations less cumbersome we choose for $A(z)$ and $\phi(z)$ the parametrization $-\infty < A(z) < \infty$ and $-\pi/2 < \phi(z) + \omega\tau < \pi/2$. Separating the real and imaginary part of Eq. (6.43) yields

$$\begin{aligned}(\mu + \sigma z)A(z)^{-1}\cos(\phi(z) + \omega\tau) &= 1,\\ (\mu + \sigma z)A(z)^{-1}\sin(\phi(z) + \omega\tau) &= -\omega/x^*(z),\end{aligned} \tag{6.44}$$

which are solved by Eq. (6.16). Using the fact that $\phi(z)$ and $A(z)$ by definition satisfy $\langle A(z)e^{i\phi(z)}\rangle = 1$, Eq. (6.17) follows by straightforward manipulations.

Although Eq. (6.17) needs to be solved numerically in general, an exact solution can be obtained when the interactions are homogeneous, that is, for $\sigma = 0$. This leads to the the critical delay and frequency in the homogeneous limit:

$$\begin{aligned}\tau &= \omega^{-1}\arccos\left(1/\mu\right),\\ \omega &= [(\mu+1)/(\mu-1)]^{1/2}.\end{aligned} \tag{6.45}$$

τ_c has a minimum in $\pi/2$ for an infinitely competitive system, $\mu = -\infty$. In other words, the oscillatory phases appear only if $\tau > \pi/2$.

6.10.5 Comparison between analytical and numerical critical line for discrete delay

In the main text we derived the critical line separating the UFP and Oscillatory UFP phases employing an approximated low-heterogeneity DMFT equation. In Figure 6.6 we show the exact critical line, obtained from numerical simulations, and compare it with the approximated one. As discussed in the main text, the two lines coincide at low values of the heterogeneity σ, as expected. Upon increasing σ the numerical simulations indicate that a greater competition is needed in the community to present sustained oscillations than what is predicted by our approximation. Nevertheless, the two lines present the same qualitative behavior.

6.10.6 Qualitative explanation for emergence of synchronization

We provide here an intuitive picture explaining the appearance of synchronization in communities in which competition is sufficiently high. The core idea is that while self-interactions are stabilizing, time delays introduce a feedback of the community from its past state. The relative strength of these two effects is μ, in the limit of long delays. Thus perturbations are amplified if $|\mu| > 1$. For $\mu > 1$ this leads to unbounded growth, while for $\mu < -1$ this yields sustained oscillations.

Let us consider for simplicity the case of a discrete delay with instantaneous intraspecific interactions, with community dynamics set by Eq. (6.12). We start by considering the homogeneous,

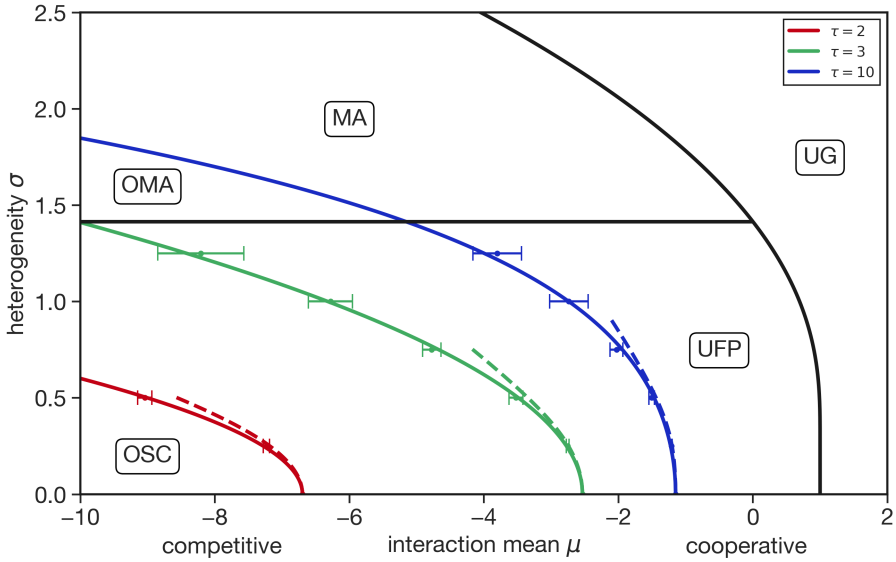

Figure 6.6: Exact and approximated critical line for GLV with discrete delay. Phase diagram comparing the critical lines for various values of τ obtained through the approximated DMFT (dashed lines) and from numerical simulations (solid lines). The error bars indicate numerical uncertainty due to the finite size $S = 1000$ of the community. The solid line is obtained as a polynomial fourth-order fit of the numerical points.

$\sigma = 0$ limit. The dynamics of each species in the community can be found by setting $\sigma = 0$ in the DMFT equation, which yields

$$\dot{x}(t) = x(t)\left[1 - x(t) + \mu x(t-\tau)\right]. \tag{6.46}$$

For $\tau = 0$ the positive equilibrium $x^* = 1/(1-\mu)$ is stable. We consider a small perturbation at $t = 0$ around this equilibrium (see Figure 6.7). The resulting linear dynamics of each species will be

$$\delta\dot{x}(t) = x^*\left[-\delta x(t) + \mu\delta x(t-\tau)\right]. \tag{6.47}$$

This equation shows the interplay between intraspecific regulation and interspecific mutualism or competition. It is straightforward to show that for large τ the dynamics will return to the equilibrium for $|\mu| < 1$ and will diverge from it for $|\mu| > 1$.

To see this explicitly, let us consider a large time delay τ and denote by $\delta x_0(t)$ the dynamics on $0 < t < \tau$, by $\delta x_1(t)$ the dynamics on $\tau < t < 2\tau$, and so on. Since for $t < 0$ we are assuming that $\delta x(t) = 0$, it follows that $\delta\dot{x}_0(t) = -x^*\delta x_0(t)$, whose solution is $\delta x_0(t) = e^{-x^*t}\delta x(0)$. Since we are assuming a large τ, the initial condition on each subsequent interval will then be $\delta x_{n+1}(0) \approx 0$ and the dynamics will be

$$\delta\dot{x}_{n+1}(t) = x^*\left[-\delta x_{n+1}(t) + \mu\delta x_n(t)\right]. \tag{6.48}$$

By integrating Eq. (6.48) on $0 < t < \tau$, using $\delta x_{n+1}(0) \approx 0$ and $\delta x_{n+1}(\tau) \approx 0$, we see that

$$\int_0^\tau dt\delta x_{n+1}(t) = \mu\int_0^\tau dt\delta x_n(t), \tag{6.49}$$

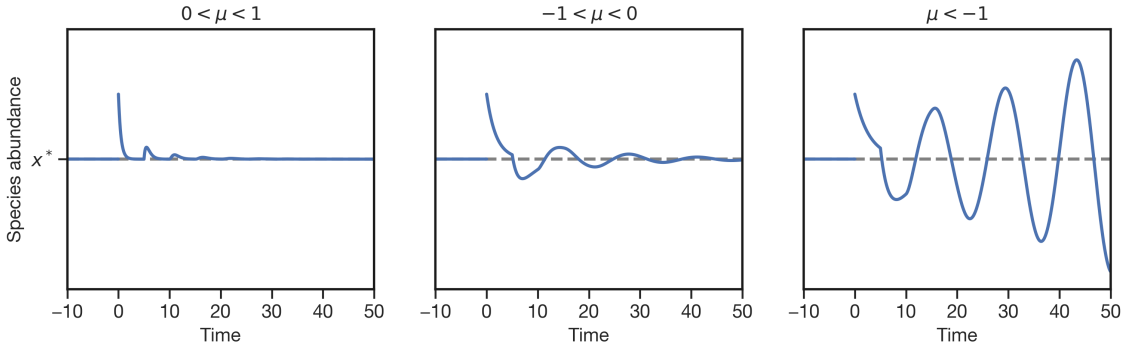

Figure 6.7: Qualitative explanation for emergence of synchronization in competitive communities

and thus conclude that the perturbation will grow as $\mu^n \delta x(0)$. Alternatively, it is a simple exercise to solve iteratively Eq. (6.48) and show for example that the resulting maximum has value $\approx \mu^n \delta x(0)$ for large n.

The resulting dynamics is thus the one illustrated in Figure 6.7. For $|\mu| > 1$ perturbations do not decay and the non-linear response kicks in. For $\mu > 1$ this leads to unbounded growth (not shown in the figure), while for $\mu < -1$ this yields sustained oscillations. For finite values of τ, a more precise estimation is needed to obtain the value of μ which leads to sustained oscillations. Upon increasing the community diversity σ, one can expect that the asymmetry in species dynamics will lead to a greater value of competition μ being required in order to maintain the regime of sustained oscillations. In order to arrive at this conclusion in a definite manner, one needs a more careful analysis, which is the one performed in the main text. We also note that that introducing heterogeneity in interactions generally stabilizes fixed points [311, 312], which is consistent with our findings.

One may speculate whether introducing a functional response, which allows values of $\mu > 1$ without leading to unbounded growth, can give rise to oscillations also in cooperative communities. This is not the case since, as shown below in Appendix 6.10.7.5, as introducing a functional response yields an effective μ_{eff} always smaller than 1.

6.10.7 Sensitivity analysis

In order to support our ecological implications, we perform an extensive sensitivity analysis by considering a number of extensions of the model discussed in the main text. We find that the oscillatory phases persist with the same qualitative properties in all cases considered.

6.10.7.1 Species-specific growth rates

In the main text, we assumed identical growth rates for all species in the ecological community. Here, we relax this assumption, demonstrating that even with species-specific growth rates, the results remain qualitatively consistent. Specifically, when the community is sufficiently competitive and the time delay is large enough, persistent and coherent oscillations still appear in species abundances. This finding indicates that the fact that species abundances oscillate with the same frequency is not simply an artifact of assigning the same timescale to all species. For simplicity, we

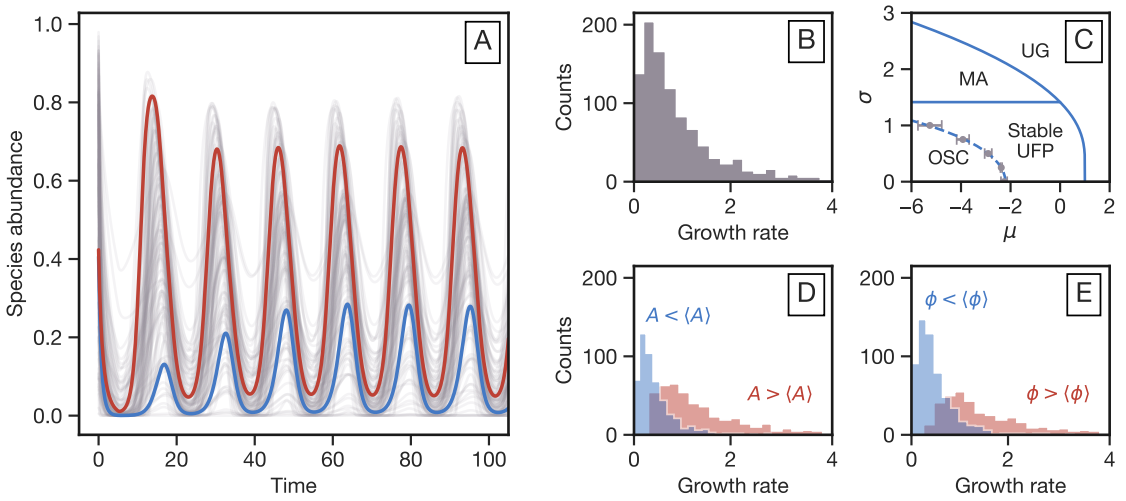

Figure 6.8: Effects of species-specific intrinsic growth rates on the dynamics of species abundances. (A) Coherent oscillations of species abundances observed in the Oscillatory UFP phase. (B) Distribution of intrinsic growth rates r_i sampled from a lognormal distribution with $\langle r \rangle = 1$ and $\mathrm{Var}(r) = 1$. (C) Numerical phase diagram showing the boundaries between different dynamical regimes as a function of μ and σ. The diagram is qualitatively similar to the phase diagram shown in the main text, despite the variability in growth rates. (D) Distribution of oscillation amplitudes and (E) phase shifts as a function of intrinsic growth rate r_i for fixed $\mu = -4$ and $\sigma = 0.5$ in the Oscillatory UFP phase. Species with higher intrinsic growth rates tend to oscillate with greater amplitudes and are phase-advanced compared to others, indicating a positive correlation between growth rate and oscillation characteristics.

consider GLV dynamics with discrete delay:

$$\dot{x}_i(t) = r_i x_i(t) \left[1 - x_i(t) + \sum_{j \neq i} \alpha_{ij} x_j(t - \tau) \right], \tag{6.50}$$

where r_i represents the intrinsic growth rate of species i in the absence of interactions with other species. Analytical results are involved with non-equal growth rates so we focus on numerical simulations. We draw r_i from a lognormal distribution with $\mathrm{mean}(r) = 1$ and $\mathrm{var}(r) = 1$ (Figure 6.8, inset B) and set the time delay to $\tau = 5$. The resulting numerical phase diagram (Figure 6.8, inset C) qualitatively agrees with the phase diagram shown in the main text. For all values of μ and σ in the Oscillatory UFP phase, we find that the oscillations remain coherent (Figure 6.8, inset A). We then fix $\mu = -4$ and $\sigma = 0.5$ and analyze the distribution of amplitudes and phase shifts in the Oscillatory UFP phase in more detail (Figure 6.8, insets D and E). We observe a correlation between both amplitude and phase shift with the intrinsic growth rate: species with higher growth rates oscillate, on average, with greater amplitudes and lead in phase relative to others. This pattern holds true for other values of μ and σ as well.

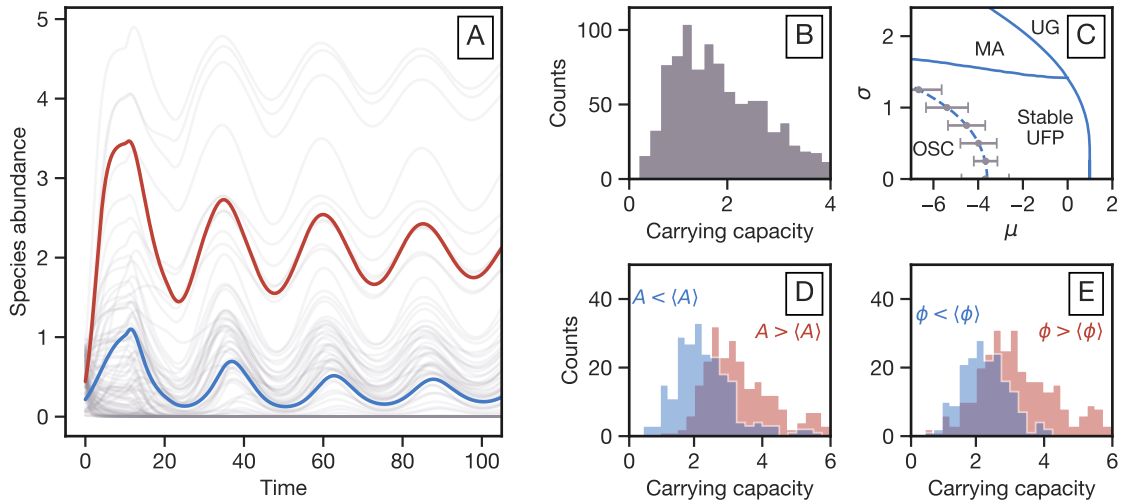

Figure 6.9: Effects of species-specific carrying capacities on community dynamics. (A) Temporal evolution of community abundances showing coherent oscillations across species in the Oscillatory UFP phase. (B) Distribution of carrying capacities K_i sampled from a lognormal distribution with mean $\langle K \rangle = 2$ and variance $\mathrm{Var}(K) = 2.5$. (C) Numerical phase diagram depicting the dynamical regimes as a function of μ and σ. (D) Distribution of oscillation amplitudes and (E) phase shifts as functions of carrying capacity K_i for fixed $\mu = -4$ and $\sigma = 0.5$. Species with higher carrying capacities exhibit larger oscillation amplitudes and are phase-advanced relative to others.

6.10.7.2 Species-specific carrying capacities

In the same spirit as the previous section, we extend the GLV equation with discrete delay to incorporate species-specific carrying capacities:

$$\dot{x}_i(t) = \frac{x_i(t)}{k_i}\left[k_i - x_i(t) + \sum_{j \neq i} \alpha_{ij} x_j(t-\tau)\right], \tag{6.51}$$

where k_i represents the carrying capacity of species i and defines its steady-state population in the absence of interactions. We focus on numerical results for this generalized model, drawing the carrying capacities k_i from a lognormal distribution with $\mathrm{mean}(k) = 2$ and $\mathrm{var}(K) = 2.5$ (see Figure 6.9, inset B). The time delay is set to $\tau = 10$. The resulting numerical phase diagram, presented in Figure 6.9, inset C, shows that the oscillatory phase persists. For all tested values of μ and σ within the oscillatory phase, we observe that the oscillations remain coherent, with species abundances oscillating with identical frequency (Figure 6.9, inset A). We then fix $\mu = -4$ and $\sigma = 0.5$ to examine the distribution of oscillation amplitudes and phase shifts in greater detail (Figure 6.9, insets D and E).

6.10.7.3 Interaction-specific kernels

In the main text, we have considered the interaction memory kernel to be decoupled as $K_{ij}(\tau) = \alpha_{ij} K(\tau)$, implying that the shape of the memory term is independent of specific interactions. However, as discussed in the main text, in general the kernel may vary across interaction pairs. Therefore, we extend here the model by considering $K_{ij}(\tau) = \alpha_{ij}\delta(\tau - \tau_{ij})$, so that each interaction

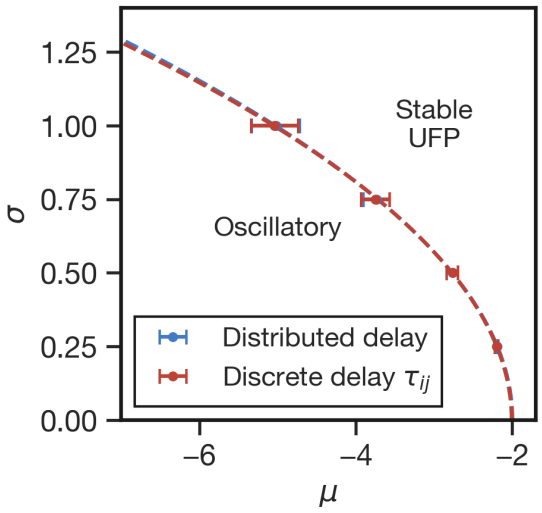

Figure 6.10: The Role of Interaction-Specific Kernels. Phase diagram comparing the boundary between oscillatory and fixed-point phases for two types of interaction delays: (i) a unique, distributed kernel applied uniformly across all species pairs, modeled by a Gamma distribution (blue), and (ii) interaction-specific kernels with discrete delays, each delay independently drawn from the same Gamma distribution as the distributed kernel (red). The alignment of phase boundaries indicates the equivalence of the two settings.

occurs with a specific discrete delay, τ_{ij}. In this formulation, the dynamics is then given by:

$$\dot{x}_i(t) = x_i(t)\left[1 - x_i(t) + \sum_{j\neq i} \alpha_{ij} x_j(t-\tau_{ij})\right], \tag{6.52}$$

where the delays τ_{ij} are drawn from an arbitrary distribution. This approach introduces heterogeneity in the interaction delays, accounting for variability in how different species influence each other over time. Remarkably, by sampling τ_{ij} from a Gamma distribution, as considered in the GLV model with distributed delay, numerical analysis of the phase diagram reveals that this case is equivalent to the GLV model with distributed delay. The resulting numerical phase diagrams, shown in Figure 6.10, exhibit perfect agreement between the two cases. This finding implies that the system's emergent behavior remains consistent whether the interaction kernel is the same across all species pairs and distributed in time, or whether it is interaction-specific and discrete. The mapping between random and distributed delays is established rigorously in Chapter 7.

6.10.7.4 Sparse interactions

Another assumption in the main text is that all species interact with each other, which is a considerable simplification of natural ecosystems. Here, we extend the model to incorporate sparse interactions, where only a subset of potential interactions is present. Specifically, we introduce a finite connectivity C in the interaction matrix α_{ij}, such that $\alpha_{ij} = 0$ with probability $1 - C$. This means that, on average, each species interacts with only a fraction C of the total species, reflecting ecological communities where not all species interact directly. The introduction of sparsity modifies the model parameters without altering the overall behavior observed in the fully connected case. The effective mean interaction strength is rescaled to $\mu = C\langle\alpha_{ij}\rangle$, and the interaction variance becomes $\sigma^2 = C\mathrm{Var}(\alpha_{ij})$, as shown in Figure 6.11.

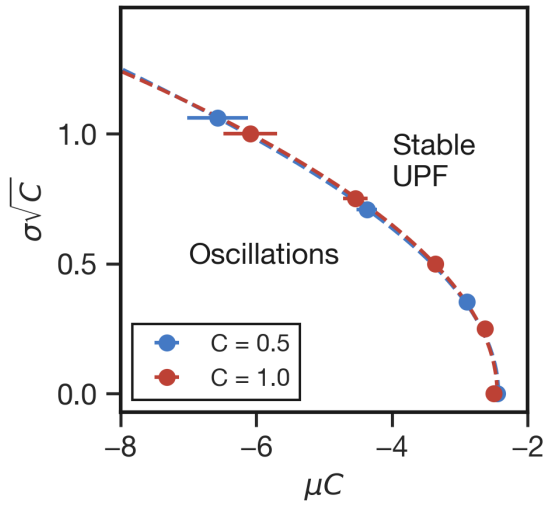

Figure 6.11: The Role of Sparsity in Species Interactions. Phase diagram showing the boundary between oscillatory and fixed-point phases for two levels of connectivity: $C = 0.5$ (blue) and $C = 1.0$ (red). With appropriate rescaling of the mean and variance of interactions, the phase boundaries align, illustrating that sparsity does not alter the quantitative nature of the phase transition.

6.10.7.5 Non-linear functional response

In the main text, we showed that delayed interactions can induce persistent and coherent oscillations if the ecological community is sufficiently competitive, precisely if $\mu < -1$. This is due to the fact that if $|\mu| > 1$ the interaction of the community with itself in the past gets amplified. Given that for $\mu > 1$ the GLV equations display unbounded growth in the species abundances, this leaves only the competitive regime $\mu < -1$ for the appearance of sustained oscillations. The presence of unbounded growth is a known feature of the GLV equations, in which a linear functional response is assumed [186, 226]. Thus, the possibility that oscillations could also appear in cooperative communities with $\mu > 1$ is still open in scenarios where a saturating functional response is assumed. Indeed, a regime in which species abundances grow indefinitely is non-physical, as one would expect the effect of one species on the growth of another to saturate in this limit In previous sections we focused on the GLV dynamics with a linear functional response, known as Holling type I in the ecological literature [15, 16, 251]. Here, we extend the previous results by considering two classes of functional response and will show that, oscillations do not occur in a cooperative community, regardless of the cooperation strength $\mu > 0$. This supports the claim that the phenomenon of persistent oscillations in the case of delayed interactions is truly only present in competitive communities.

Local functional response

A possible functional response consists in a function $J(x)$ which modifies the GLV equations as follows [300, 331], see also Chapter 5:

$$\dot{x}_i(t) = x_i(t)\left[1 - x_i(t) + \sum_{j\neq i} \alpha_{ij} J(x_j(t-\tau))\right]. \tag{6.53}$$

We refer to this function as local functional response, as it applies only to the interacting species x_j. $J(x)$ can be any increasing and bounded function. A possible form, which is similar to the Holling

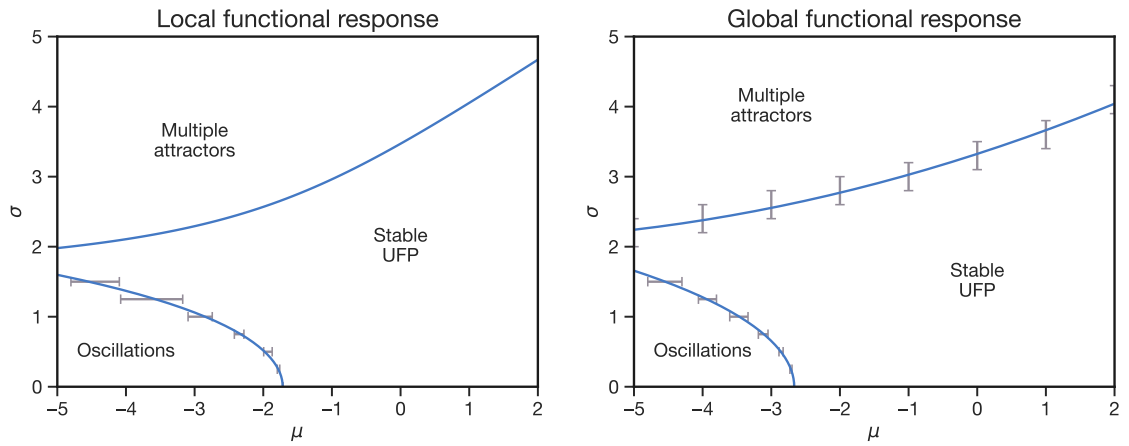

Figure 6.12: Phase diagram with functional response. Left: Phase diagram with a local functional response $J(x) = 2x/(2+x)$ and for $\tau = 10$. The line separating the UFP and Oscillatory UFP phases is obtained numerically, with error bars showing the uncertainty due to the finite size $S = 500$ of the community. The line separating the UFP and MA phases is obtained analytically (procedure detailed Chapter 5). Right: Phase diagram with a global functional response $g(x) = 2x/(2+|x|)$ and $\tau = 10$. The lines separating the three phases are obtained numerically.

type II functional response [15, 16, 251], is

$$J(x) = \frac{ax}{a+x}, \tag{6.54}$$

where $a > 0$ is the value of the response at saturation. The DMFT equation associated to Eq. (6.53) can be derived following the lines of [300, 331] and it reads

$$\dot{x}(t) = x(t)\left[1 - x(t) + \mu\langle J(x(t-\tau))\rangle + \sigma\eta(t)\right], \tag{6.55}$$

where the correlation of the Gaussian noise is $\langle \eta(t)\eta(t')\rangle = \langle J(x(t-\tau))J(x(t'-\tau))\rangle$.

We first consider the case of homogeneous interactions, that is, $\sigma = 0$. As usual, the system becomes homogeneous and all species follow the same dynamics given by

$$\dot{x}(t) = x(t)\left[1 - x(t) + \mu J(x(t-\tau))\right]. \tag{6.56}$$

The positive equilibrium, which satisfies $1 - x^* + \mu J(x^*) = 0$, is always stable at $\tau = 0$ for any choice of $J(x)$. The linearization around this equilibrium is

$$\delta\dot{x}(t) = x^*\left[-\delta x(t) + \mu J'(x^*)\delta x(t-\tau)\right]. \tag{6.57}$$

This is the same linearization as in the case of a linear functional response previously considered, although with an effective interaction strength $\mu_{\text{eff}} = \mu J'(x^*)$. Importantly, the stability of x^* for $\tau = 0$ implies $\mu_{\text{eff}} < 1$. We can follow the same steps as in the linear case and conclude that when $-1 < \mu_{\text{eff}} < 1$ no oscillation appear for any value of the delay, while when $\mu_{\text{eff}} < -1$ there exists a critical τ_c for which persistent oscillations appear as $\tau > \tau_c$. However, given that $J' > 0$ since we assume the functional response to be increasing, μ and μ_{eff} have the same sign. We therefore conclude that no persistent oscillations can appear for any $\mu > 0$, that is, if the community is mostly cooperative. Of course, the condition $\mu_{\text{eff}} < -1$ for the existence of a critical τ_c in competitive

communities can yield a μ that can be both smaller or greater than $\mu = -1$, depending on the specific choice of $J(x)$.

Given the results discussed before in the case of a linear functional response, we expect heterogeneity in the interactions to not qualitatively change the results at $\sigma = 0$. We do not present analytical results, although they could be obtained in a similar way to the linear case, and we only report numerical results for a specific choice of the functional response. Figure 6.12 shows that the oscillatory phase is not affected by the functional response, which instead eliminate the unbounded growth phase. Moreover, it shows that oscillations are present only in a competitive regime.

Global functional response

An alternative to the previously considered local functional response is a response function $g(x)$ in the GLV equations with discrete delay which acts on the whole interaction term [226]

$$\dot{x}_i(t) = x_i(t) \left[1 - x_i(t) + g \left(\sum_{j \neq i} \alpha_{ij} x_j(t - \tau) \right) \right] . \tag{6.58}$$

We refer to $g(x)$ as global response function and we assume it to be bounded and increasing. A possible choice, similar to a Holling type II functional response, is

$$g(x) = \frac{ax}{a + |x|}, \tag{6.59}$$

where $a > 0$ is again the value of the response at saturation. The DMFT equation associated to Eq. (6.58) can be derived following the lines of [226] and it reads

$$\dot{x}(t) = x(t) \left[1 - x(t) + g \left(\mu \langle x(t - \tau) + \sigma \eta(t) \rangle \right) \right] , \tag{6.60}$$

where the autocorrelation of the Gaussian noise is $\langle \eta(t) \eta(t') \rangle = \langle x(t - \tau) x(t' - \tau) \rangle$.

We first consider the case of homogeneous interactions. In this limit the community becomes homogeneous, all species behave identically and follow the dynamics given by Eq. (6.60) after setting $\sigma = 0$:

$$\dot{x}(t) = x(t) \left[1 - x(t) + g(\mu x(t - \tau)) \right] . \tag{6.61}$$

The positive equilibrium, which satisfies $1 - x^* + g(\mu x^*) = 0$, is always stable at $\tau = 0$ for any choice of $g(x)$. Linearizing around this equilibrium yields

$$\delta \dot{x}(t) = x^* \left[-\delta x(t) + \mu g'(\mu x^*) \delta x(t - \tau) \right] . \tag{6.62}$$

This is the same linearization as in the case of a linear functional response previously considered, although with an effective interaction strength $\mu_{\text{eff}} = \mu g'(\mu x^*)$. The stability of x^* at $\tau = 0$ implies $\mu_{\text{eff}} < 1$. Since $g' > 0$, following the same reasoning as in the case of a local functional response, we arrive at the same conclusion that no persistent oscillations can appear for any delay in the interactions in cooperative ecological communities.

Given the results discussed before in the case of a linear functional response, we expect heterogeneity in the interactions to not qualitatively change the results obtained for $\sigma = 0$. We do not present analytical results and we only report numerical results for a specific choice of functional response in Figure 6.12.

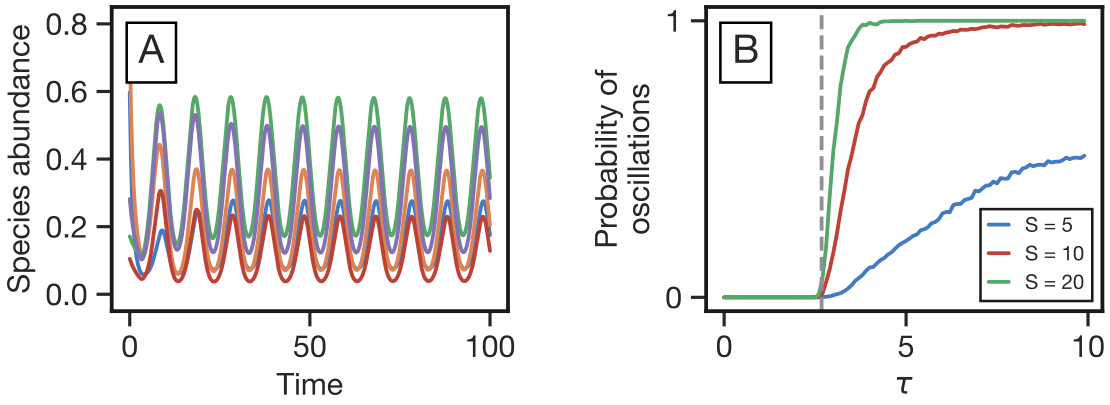

Figure 6.13: Finite number of species. (A) Coherent oscillations of species abundances observed in the oscillatory phase, for a system composed of 5 species. (B) Probability that the species abundance oscillates as a function of τ, for different number of species, given the parameters $\mu = -4$, $\sigma = 0.5$. The vertical dashed grey line represents the critical τ_c computed in the infinite species limit.

6.10.7.6 Finite-size effects

The results discussed in the main text are strictly valid in the limit infinite number of species in the community. However, Figure 6.13 inset A shows that the oscillatory regime also occurs in a system with a small number of species. In this case, given μ and σ, the uncertainty in determining the critical τ increases as shown in Figure 6.13, inset B.

6.10.8 Numerical eigenspectrum

We show here an example of the spectrum of the GLV equation obtained numerically.

The eigenvalues λ of a general DDE with a single discrete delay τ are the roots of the generalized eigenvalue equation

$$\det(-\lambda I + A_0 + A_1 e^{-\lambda\tau}) = 0. \tag{6.63}$$

Here A_0 and A_1 are the instantaneous and retarded Jacobian respectively. In the case of the GLV equation Eq. (6.12) these are given by

$$\begin{aligned} A_{0,ij} &= \left(1 - 2x_i^* + \sum_j \alpha_{ij} x_j^*\right) \delta_{ij} \\ A_{0,ij} &= x_i^* \alpha_{ij} \end{aligned} \tag{6.64}$$

where the equilibria x_i^* are those reached in the UFP phase or the time-averages in the Oscillatory UFP phase. A method to find the generalized eigenvalues leverages the fact the the DDE can be rewritten as a hyperbolic PDE, and as such the infinitesimal generator of the PDE has the same spectrum of the DDE of interest. This infinitesimal generator can be found numerically for example by spectral methods, and specifically we employ code (3) of [134].

The result is shown in Figure 6.14. The spectrum shows that the oscillations arise when a pair of outliers cross the stability threshold. We also note that the accumulation of the bulk around the origin is due to extinct species. This gives an explanation of the robustness of the phase diagram to

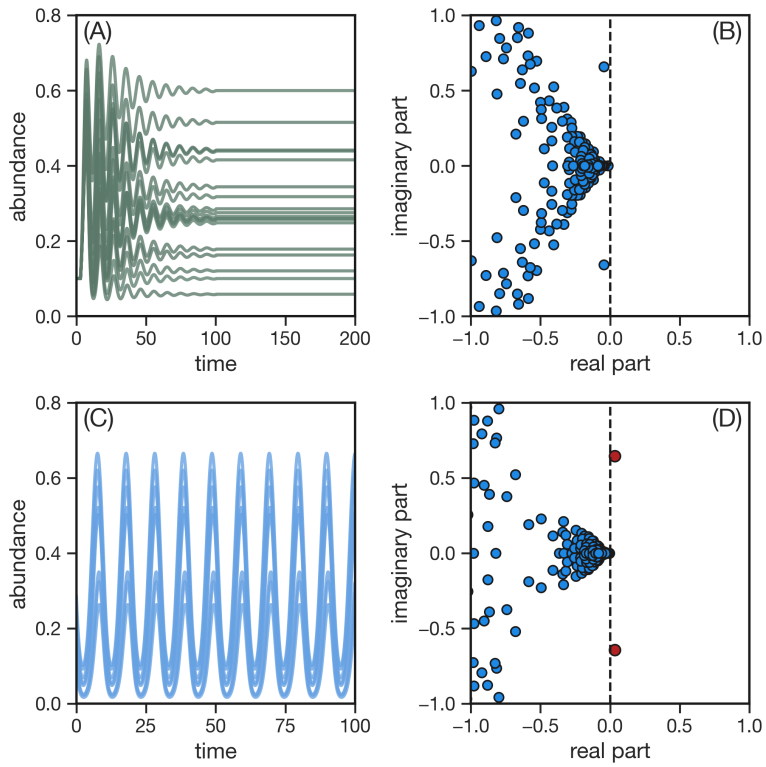

Figure 6.14: Comparison of numerical eigenspectra. Panel (A): Representative dynamics of a subset of species in the UFP phase. Panel (B): Numerical eigenspectrum of the corresponding delayed linearized system around the steady state, showing a bulk and two stable outliers. The vertical dashed line indicates the stability threshold. Panel (C): Representative dynamics of a subset of species in the oscillatory UFP phase. Panel (D): Numerical eigenspectrum of the corresponding delayed linearized system around the time-averaged abundances. Here, the outliers (highlighted in red) cross the stability threshold, triggering a Hopf instability that gives rise to oscillatory dynamics.

various modifications considered, as we do not expect these to significantly alter the mechanism by which these oscillations arise.

6.10.9 Critical behavior for gamma-distributed delay

The Laplace transform of the Gamma-distributed kernel defined in Eq. (6.20) is

$$\hat{K}(\lambda) = (1 + \beta\lambda)^{-\alpha}. \tag{6.65}$$

To locate the Hopf bifurcation we search for purely imaginary solutions, $\lambda = i\omega$ of the eigenvalue equation Eq. (6.19). This yields

$$i\omega = x^* \left[-1 + \mu\rho^{-\alpha} e^{-i\alpha\theta} \right], \tag{6.66}$$

where we defined $\rho = (1 + \beta^2\omega^2)^{1/2}$ and $\theta = \arctan(\beta\omega)$. Separating the real and imaginary parts we get

$$\begin{aligned} \mu\rho^{-\alpha}\cos(\alpha\theta) &= 1, \\ x^*\mu\rho^{-\alpha}\sin(\alpha\theta) &= -\omega. \end{aligned} \tag{6.67}$$

We divide the second equation by the first one obtaining

$$\omega = -x^* \tan\left(\alpha \arctan \beta\omega\right). \tag{6.68}$$

A non-zero solution exists only for $\alpha > 1$. In this case, solving Eq. (6.67) for μ and then employing $x^* = 1/(1-\mu)$ leads to the closed equation for the critical ω Eq. (6.23). With ω we then obtain the equation for the critical μ for example by solving Eq. (6.67), which gives Eq. (6.22). We get the condition for the existence of a critical μ in α-β space by requiring that the critical μ is physical, that is, $\mu < 1$. The condition on β at fixed α is that β is larger than the critical value given by Eq. (6.21).

6.10.10 Over- and underdamped regimes for exponetially-distributed delay

In the case $\alpha = 1$ the Gamma distribution is an exponential. Renaming $\beta = \tau$ its scale, the eigenvalue equation is

$$\lambda = x^* \left(-1 + \frac{\mu}{1+\lambda\tau}\right), \tag{6.69}$$

which is a second-order equation. By direct inspection $\mathrm{Re}(\lambda) < 0$ for all values of the parameters, so that there is no critical value of τ for which a Hopf bifurcation takes place, consistently with previous results. By setting its discriminant to zero we get the critical line Eq. (6.24) separating the regions in μ-τ space in which eigenvalues are purely real and the region in which they develop also an imaginary part. This yields the line between underdamped and overdamped regimes after a perturbation of the equilibrium abundances.

6.10.11 Emergence of oscillations for negative intraspecific interactions

The critical line separating the UFP and Oscillatory UFP phases is given, at low values of the heterogeneity σ, by the following generalization of Eq. (6.17):

$$\begin{aligned} \cos\omega\tau &= \int_{-\infty}^{\infty} \frac{Dz(\mu+\sigma z)C_u(\omega\tau)}{C_u(\omega\tau)^2 + (\omega/x^*(z) + S_u(\omega\tau))^2}, \\ \sin\omega\tau &= -\int_{-\infty}^{\infty} \frac{Dz(\mu+\sigma z)(\omega/x^*(z) + S_u(\omega\tau))}{C_u(\omega\tau)^2 + (\omega/x^*(z) + S_u(\omega\tau))^2}, \end{aligned} \tag{6.70}$$

where $C_u(\omega\tau) = 1 - u\cos\omega\tau$, $S_u(\omega\tau) = u\sin\omega\tau$, and the fixed point is now $x^*(z) = \max[0, (1 + (\mu+\sigma z)\langle x^*\rangle)/(1-u)]$.

6.10.12 Analytical and numerical critical line for negatively-correlated interactions

In the main text we derived the critical line separating the UFP and delay-Induced Chaos phases employing an approximated response function $G(t)$ in the DMFT equation with negatively-correlated reciprocal interactions. In Figure 6.15 we show the critical line obtained from numerical simulations, and compare it with the approximated one. The two lines present the same qualitative behavior.

6.10.13 Inclusion of immigration in delayed DMFT and effect on dynamics

We indicate here how the addition of immigration can be included in the delayed DMFT framework and perform some preliminary numerical exploration of the resulting dynamics.

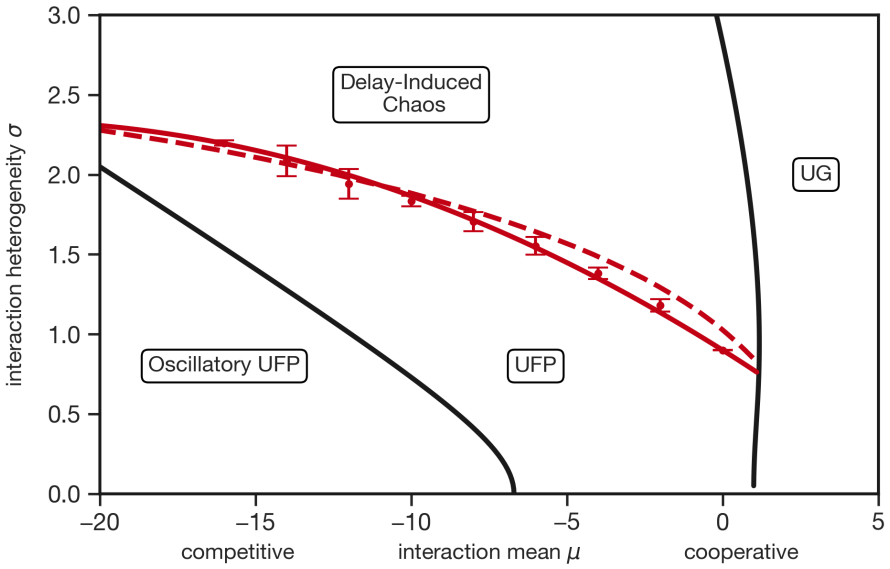

Figure 6.15: Exact and approximated critical line for GLV with discrete delay and negatively correlated-correlated reciprocal interactions. Phase diagram comparing the critical lines obtained through the approximated response function $G(t)$ (dashed line) and from numerical simulation (solid line). The error bars indicate numerical uncertainty due to the finite size $S = 1000$ of the community. The solid line is obtained as a polynomial second-order fit of the numerical points.

For illustration purposes, consider the simplest GLV equation with discrete delay and an immigration term λ which is constant for all species

$$\dot{x}_i(t) = x_i(t)\left[1 - x_i(t) + \sum_{j\neq i} \alpha_{ij} x_j(t-\tau)\right] + \lambda. \tag{6.71}$$

One can follow the derivation presented in this Appendix with very little modifications and arrive at the following modified DMFT equation

$$\dot{x}(t) = x(t)\left[1 - x(t) + \mu\langle x(t-\tau)\rangle + \sigma\eta(t)\right] + \lambda. \tag{6.72}$$

For the various extensions considered in the main text the DMFT equation can be derived in a similar way. For example when interactions are reciprocally correlated Eq. (6.31) generalizes in the presence of immigration to

$$\dot{x}(t) = x(t)\left[1 - x(t) + \mu\langle x(t-\tau)\rangle + \sigma\eta(t) + \gamma\sigma^2 \int_0^{t-\tau} dt' G_\tau(t,t') x(t'-\tau)\right] + \lambda. \tag{6.73}$$

Thus immigration can be included in a straightforward way into the delayed DMFT framework.

When λ is small in comparison to the other parameters, as customarily assumed, it has a negligible effect on the transition boundaries. Therefore, all the phase diagrams presented in this work are robust to the addition of a weak immigration term.

Numerically, we performed numerical simulations in all three chaotic phases with weak immigration and illustrative examples are reported in Figure 6.16. In the UFP phase dynamics is

completely unaffected. In the chaotic Oscillatory MA phase, the synchronized oscillations persist with similar amplitude and frequency. In the MA phase immigration does not qualitatively alter the chaotic dynamics. Also in the delay-induced chaos phase, the high-frequency oscillations and large-amplitude fluctuations remain unchanged. In all three chaotic phases, the spectrum is virtually unaffected by the presence of the immigration term.

In summary, immigration can be straightforwardly incorporated into the delayed DMFT framework and, when weak, does not significantly affect either the phase boundaries or the qualitative dynamics within each phase.

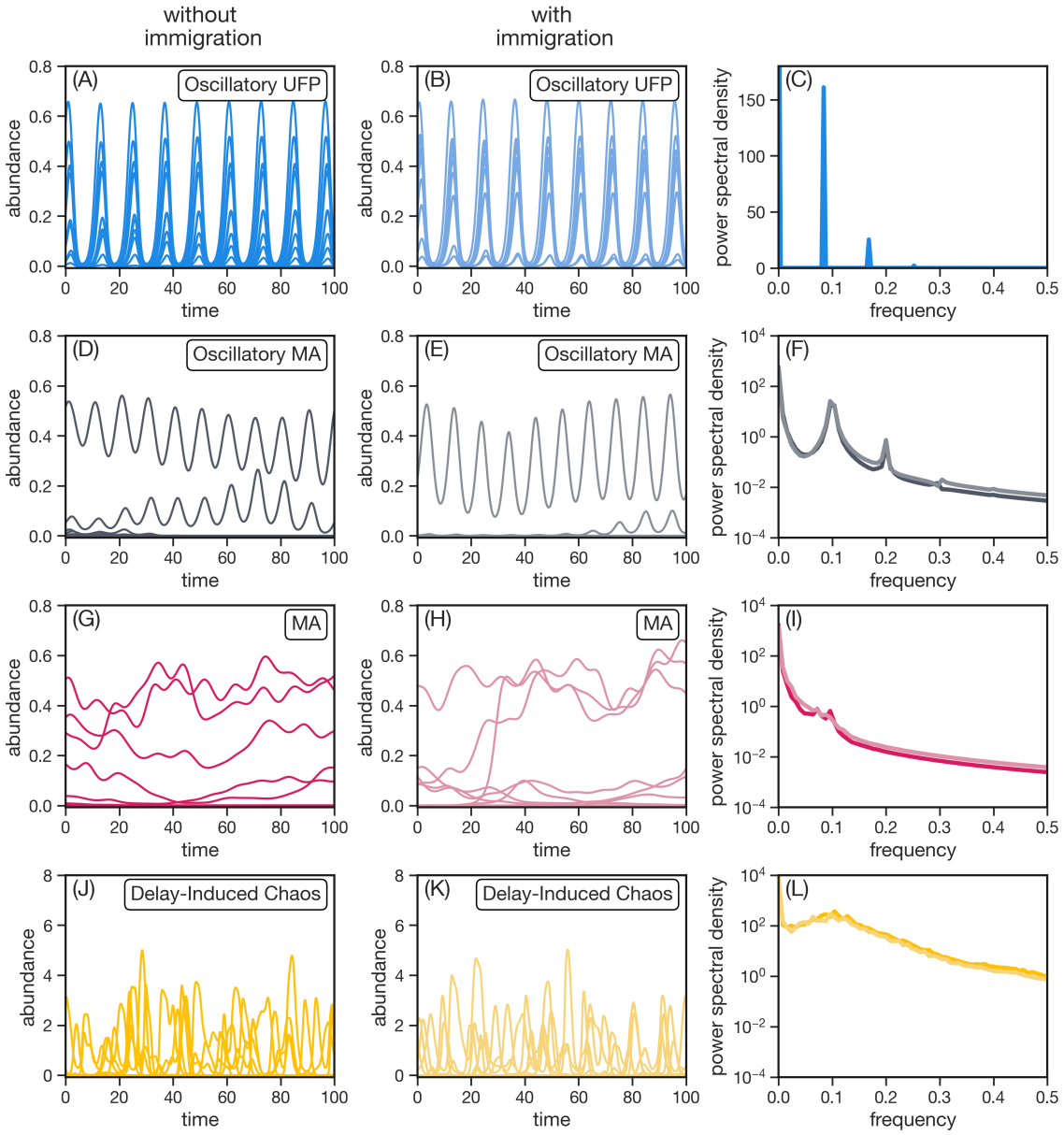

Figure 6.16: Comparison of dynamical regimes with and without immigration. Panels (A-C): Oscillatory UFP phase. Panels (D-F): Oscillatory MA phase. Panels (G-I): MA phase. Panels (J-L): Delay-Induced Chaos phase. For each regime, panels on the left show representative species trajectories without immigration, while the central panels include a small immigration rate ($\lambda = 10^{-9}$) added to the GLV dynamics. The right panels display the corresponding power spectral densities, which show no substantial differences.

Chapter 7

Disordered neural network model with time delays

To demonstrate the generality of the methods developed in Chapter 6, this chapter investigates a disordered neural network with delayed interactions, departing slightly from the general ecological focus of the thesis. Recurrent neural networks provide a powerful framework for modeling biological circuits and designing artificial learning systems. In both neural and neuromorphic recurrent dynamics, however, interactions are inevitably constrained by finite transmission speeds and communication latencies, introducing time delays that can qualitatively reshape the networks behavior. Yet, theoretical understanding of the impact of time delays on the collective dynamics of high-dimensional networks remains limited. Here, we address this gap by deriving the complete phase diagram of a random neural network with delayed interactions. We identify a competition between disorder-driven chaos, governed by a static bulk instability, and delay-induced synchronization, produced by an unstable spectral outlier. Notably, we find that sufficiently strong delayed feedback can suppress chaos, moving the dynamics into a stable synchronized state. We further establish an exact mapping between disordered dynamical systems with random delays and those with distributed delays, extending the applicability of our framework well beyond the context of neural dynamics. Finally, we show that delays fundamentally reshape information processing by redistributing memory capacity toward longer timescales.

7.1 Introduction

High-dimensional systems can display a diverse range of macroscopic behavior, as exemplified in an ecological context in previous chapters. Similarly, large-scale neural networks exhibit rich emergent behavior arising from the collective interactions of their constituent units [49, 122, 141, 150, 213]. In this context, random recurrent neural networks serve as fundamental null models for biological circuits [63, 84, 144, 158, 173, 202] and constitute important paradigms for artificial learning systems, such as reservoir computing [103, 110, 136, 139, 151], as well as providing a theoretical lens for high-dimensional learning in layered architectures [127, 131, 182, 183].

While these systems are widely studied in the case of instantaneous interactions, physical and

This chapter is based on an article currently being prepared in collaboration with Christian Grilletta, Emanuele Pigani, Samir Suweis and Luca Taffarello. As the first author, I was responsible for designing conducting the theoretical and numerical analyses and preparing the text and figures.

biological constraints inevitably impose transmission lags [92, 135, 198]. This is relevant for both biological networks and neuromorphic hardware implementations, where finite signal propagation and communication latencies are intrinsic. However, these time delays render the phase space infinite-dimensional, which limits the theoretical understanding of such systems [48, 64, 74, 167]. Furthermore, in biological systems such as the cortex, these delays are not uniform but exhibit significant heterogeneity across different regions and connections [157, 249]. Consequently, the interplay between network heterogeneity and transmission lags, and the resulting emergent behavior and computational capabilities, remain largely unexplored [117, 120, 193, 220].

In this work, we address this gap by building upon the extensions of Random Matrix Theory (RMT) [111, 252, 275, 321] and Dynamical Mean-Field Theory (DMFT) to time-delayed dynamics introduced in Chapter 6. We derive the complete phase diagram of random networks with delayed interactions. In inhibition-dominated networks, delays destabilize the quiescent fixed point, inducing a phase of globally synchronized activity via a Hopf bifurcation. Conversely, when synaptic heterogeneity is high, the system transitions to a chaotic state, similarly to the instantaneous case. A linear stability analysis reveals that the macroscopic dynamics is determined by the competition between the spectral bulk and the outliers. In particular, when the delayed outlier is sufficiently dominant, the system synchronizes in regions where the instantaneous dynamics would be chaotic, indicating that delayed feedback can effectively suppress chaos.

We further prove an exact mapping between networks with random delays and those with distributed delays. This equivalence, which holds for random interactions and does not rely on the linearity of the dynamics or the independence of units, significantly broadens the applicability of our framework to general disordered systems with heterogeneous time delays.

Beyond their impact on stability and collective dynamics, we demonstrate that interaction delays also critically affect how information is represented over time. We study information processing in delayed random networks by quantifying their ability to retain and access past inputs. We show that delays redistribute memory across timescales, shifting it toward longer lags. This establishes a direct link between delay-controlled dynamics and information-processing performance in random recurrent networks.

This chapter is organized as follows: in Section 7.2 we introduce the model; in Section 7.3 we derive its phase diagram; in Section 7.4 we extend it to non-uniform delays; in Section 7.5 we study the information processing capabilities; we conclude with a discussion of the results and perspective for further research.

7.2 Model

We analyze the dynamics for the synaptic current $x_i(t)$ of a network of N neurons [63, 173, 283]:

$$\dot{x}_i(t) = -x_i(t) + \sum_{j \neq i} J_{ij}\phi(x_j(t-\tau)). \tag{7.1}$$

Here τ denotes a signal transmission delay which, for now, is assumed uniform across all neuron pairs. The matrix J_{ij} sets the synaptic coupling strengths. The nonlinear transfer function $\phi(x)$ is characterized by a gain $g = \phi'(0)$ and saturates to ± 1 at large values of its argument. While the analytics remain general, we consider $\phi(x) = \tanh(gx)$ in numerical simulations.

The zero fixed point $x_i = 0$ is stable for sufficiently weak couplings and short delays. Small

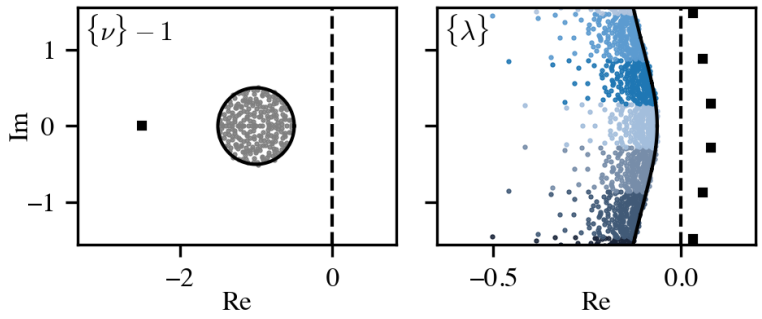

Figure 7.1: Spectral properties and delay-induced instability. Left: Example of eigenvalues at the zero fixed point for instantaneous dynamics ($\tau = 0$), featuring a circular bulk (circles) and a spectral outlier (square). Right: Corresponding spectrum for the delayed dynamics ($\tau > 0$), obtained from Eq. (7.3). Colors indicate different branches of the Lambert W-function. The dashed vertical line marks the stability boundary. In this example, while the zero fixed point is stable under the instantaneous dynamics, the delay drives the outliers across the stability boundary. This crossing triggers a Hopf bifurcation, leading to collective oscillations in the delayed dynamics.

fluctuations $\delta x_i(t)$ around this fixed point follow the linearized dynamics

$$\delta \dot{x}_i(t) = -\delta x_i(t) + \sum_{j \neq i} J_{ij} g \delta x_j(t - \tau). \tag{7.2}$$

Let ν denote an eigenvalue of J_{ij} and u its corresponding eigenvector. Inserting the ansatz $\delta x_i(t) = u_i e^{\lambda t}$ into the linearized dynamics we obtain the eigenvalue equation of Eq. (7.2) [64, 111, 252]

$$\lambda = -1 + \nu g e^{-\lambda \tau}. \tag{7.3}$$

This equation is solved by $\lambda_k = -1 + W_k(\nu g \tau e^{\tau})/\tau$, where W_k denotes the k-th branch of the Lambert W-function [80]. Since the delay term renders the phase space infinite-dimensional, the system admits an infinity of modes λ_k for each eigenvalue ν, indexed by k.

We focus on random networks in which the synaptic weights J_{ij} are independent and identically distributed variables, with statistics

$$\begin{aligned} \text{mean}(J_{ij}) &= \mu/N, \\ \text{var}(J_{ij}) &= \sigma^2/N. \end{aligned} \tag{7.4}$$

The eigenvalues ν are uniformly distributed within a disk of radius σ centered at the origin, together with an outlier at $(\mu, 0)$. Figure 7.1 illustrates the spectrum of the time-delayed neural network.

7.3 Phase diagram

The zero fixed point can lose stability via the crossing of the instability boundary of either the delayed outlier or the delayed bulk. The resulting phase diagram is summarized in Figure 7.2 and comprehensively derived below.

A sufficiently negative mean interaction μ drives the leading delayed eigenvalue associated to the outlier across the imaginary axis. This crossing marks a Hopf bifurcation, which leads

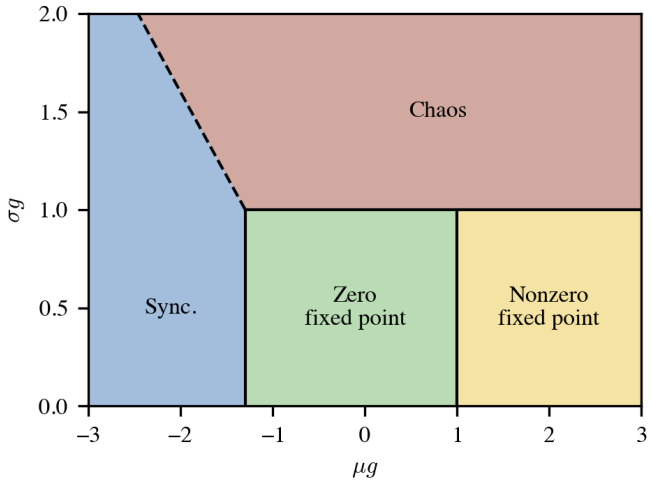

Figure 7.2: Dynamical phase diagram. The delayed neural dynamics exhibit four regimes as a function of the coupling statistics μ, σ and gain g for fixed delay (here $\tau = 3$): a stable zero fixed point, a stable nonzero fixed point, collective synchronization, and chaos. The transitions to the nonzero fixed point and chaos are governed by static instabilities at $\mu g = 1$ and $\sigma g = 1$, respectively. In contrast, the boundary between the trivial fixed point and synchronization depends on τ and is given by Eq. (7.5). The boundary between synchronization and chaos arises from the competition between the delayed outlier and bulk and is approximately given by Eq. (7.7), see also Figure 7.3.

to sustained oscillations in the non-linear neural dynamics. We locate the stability boundary by substituting the ansatz $\lambda = i\omega$ into Eq. (7.3) for the outlier $\nu = \mu$. This yields the critical frequency and delay:

$$\begin{aligned} \omega &= \sqrt{(\mu g)^2 - 1}, \\ \tau &= \omega^{-1} \arccos(1/\mu g). \end{aligned} \tag{7.5}$$

For a fixed delay τ, Eq. (7.5) determines the critical mean coupling μ marking the onset of synchronization. Importantly, this threshold is independent of the disorder parameter σ. We can characterize the resulting oscillatory state using DMFT. The network exhibits perfect phase synchronization in this regime, see Appendix 7.7.2. At criticality, oscillation amplitudes A_i are Gaussian-distributed with relative variance

$$\frac{\mathrm{var}(A_i)}{\mathrm{mean}(A_i)^2} = \frac{\sigma^2}{\mu^2 - \sigma^2}, \tag{7.6}$$

see Appendix 7.7.3. The dynamics become exactly solvable in the strong coupling limit $\mu \to -\infty$, see Appendix 7.7.4.

If the mean interaction μ is positive enough, the leading delayed eigenvalue associated to the outlier crosses the stability boundary along the real axis, yielding a pitchfork bifurcation [86, 173, 248]. We locate the transition point by setting $\lambda = 0$ in Eq. (7.3) for $\nu = \mu$. This results in the critical threshold $\mu g = 1$. Notably, this boundary is independent of the delay τ. This non-zero state can be comprehensively characterized employing again DMFT, see Appendix 7.7.5.

Instantaneous networks transition to chaos when the synaptic heterogeneity σ exceeds a critical threshold [63]. This occurs when the bulk spectrum destabilizes, which induces a proliferation of unstable modes. We observe the same mechanism in the presence of delay. The rightmost edge

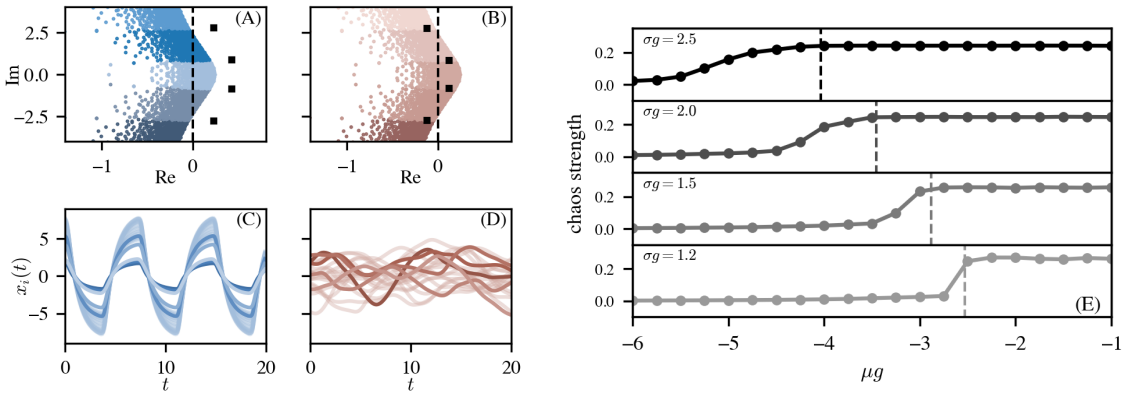

Figure 7.3: Competition between synchronization and chaos. (A, C) Synchronization phase ($\sigma g = 2.5$, $\mu g = -6$). The real part of the leading delayed outlier is greater than that of the bulk edge, driving the system into periodic oscillations. (B, D) Chaotic phase ($\sigma g = 2.5$, $\mu g = -2$). The bulk instability dominates, resulting in aperiodic fluctuations. (E) Transition from synchronization to chaos. A phenomenological parameter quantifying chaos strength is plotted as a function of μg for fixed values of σg. Vertical lines indicate the theoretical boundary where the real parts of the outlier and bulk coincide, as given by Eq. (7.7). These correspond to the dashed line in Figure 7.2. The theoretical boundary is in excellent agreement with the point at which synchronization starts to suppress chaos. Further details for panel E are provided in Appendix 7.7.7. In all panels $\tau = 3$.

of the coupling matrix spectrum lies at $\nu = \sigma$. The corresponding Lyapunov exponent satisfies $\lambda = -1 + \sigma g e^{-\lambda\tau}$. Searching for oscillatory solutions $\lambda = i\omega$ forces $\omega = 0$. This yields the static instability condition $\lambda = 0$. We thus recover the critical boundary $\sigma g = 1$. In Appendix 7.7.6 we extend the reasoning of [63] to the delayed dynamics to rigorously confirm the onset of chaos above this threshold, independently of τ.

For sufficiently negative mean interaction μ and high heterogeneity σ, both the delayed outlier and the bulk spectrum become unstable. We determine the resulting behavior by analyzing the competition between these unstable modes. If the real part of the outlier exponent exceeds that of the bulk edge, the system synchronizes. Conversely, if the bulk instability is dominant, chaos appears. Explicitly, the critical boundary is given by the condition

$$W_0(\sigma g \tau e^{\tau}) = \mathrm{Re}[W_0(\mu g \tau e^{\tau})], \tag{7.7}$$

where W_0 denotes the principal branch of the W-function. Albeit approximate, this linear analysis around the unstable zero fixed point yields results in excellent agreement with numerical simulations, see Figure 7.3 and Appendix 7.7.7 for further details. Interestingly, we observe that a sufficiently dominant delayed outlier can drive the system into stable synchronization even when $\sigma g > 1$, where the bulk is unstable and the instantaneous dynamics would be chaotic.

7.4 Random and distributed delays

We now extend our analysis to networks with heterogeneous interaction delays, considering the dynamics

$$\dot{x}_i(t) = -x_i(t) + \sum_{j \neq i} J_{ij}\phi(x_j(t - \tau_{ij})). \tag{7.8}$$

The delays τ_{ij} are drawn independently from a probability density function $K(\tau)$. While the mapping between random and distributed delays is generally approximate unless the dynamics is linear or non-interacting [162, 176, 234], in the case of random interactions the problem simplifies considerably. We show in Appendix 7.7.8 using DMFT that Eq. (7.8) is equivalent to the distributed delay model

$$\dot{x}_i(t) = -x_i(t) + \sum_{j\neq i} J_{ij} \int_0^\infty d\tau K(\tau)\phi(x_j(t-\tau)). \tag{7.9}$$

We emphasize that this equivalence is not specific to neural dynamics, suggesting a general simplification for a broad class of disordered systems with heterogeneous delay times.

The distributed formulation allows a comprehensive analysis of Eq. (7.8). Employing Eq. (7.9), the eigenvalue Eq. (7.3) generalizes to

$$\lambda = -1 + \nu g \hat{K}(\lambda), \tag{7.10}$$

where $\hat{K}(\lambda)$ denotes the Laplace transform of the delay distribution $K(\tau)$. The synchronization boundary is determined by $i\omega = -1 + \mu g \hat{K}(i\omega)$ and thus depends on the specific shape of the delay distribution. In contrast, the static instabilities describing the transition to the non-trivial fixed point and to chaos are governed by the condition $\lambda = 0$. Since the distribution is normalized, $\hat{K}(0) = 1$ for any $K(\tau)$. Consequently, the critical boundaries $\mu g = 1$ and $\sigma g = 1$ remain identical to the uniform delay case. We conclude that the phase diagram in Figure 7.2 is structurally robust to delay heterogeneity.

7.5 Information processing

In recurrent networks, temporal information is stored in the evolving activity state through the history dependence of the dynamics. Since interaction delays modify the dynamical properties of recurrent networks, as demonstrated in the previous sections, they are expected to play a crucial role in the resulting processing capabilities of temporal signals. To quantify how delays affect information processing, we analyze the memory curve $m(s)$, which measures how accurately an input signal $z(t)$ can be decoded from the network state at time $t + s$ using a linear readout. Following [202], each neuron is driven by Gaussian white noise:

$$\dot{x}_i(t) = -x_i(t) + \sum_{j\neq i} J_{ij}\phi(x_j(t-\tau_{ij})) + \xi_i(t), \tag{7.11}$$

where $\langle \xi_i(t)\xi_j(t')\rangle = 2\Delta^2\delta_{ij}\delta(t-t')$. The target signal is defined as the population-averaged drive $z(t) = N^{-1}\sum_{i=1}^N \xi_i(t)$. For a given time lag $s > 0$, $z(t)$ is decoded from network activity at time $t + s$ by $\hat{z}(t) = \sum_{i=1}^K w_i x_i(t+s)$ over $K \leq N$ units. Choosing the weights w_i that minimize the relative mean-squared error $\langle[\hat{z}(t) - z(t)]^2\rangle / \langle z(t)^2\rangle$ between the signal and readout, the memory curve can be expressed as [96]

$$m(s) = \frac{\langle \mathbf{x}(t+s)z(t)\rangle^T \langle \mathbf{x}(t)\mathbf{x}(t)^T\rangle^{-1} \langle \mathbf{x}(t+s)z(t)\rangle}{\langle z(t)^2\rangle}, \tag{7.12}$$

where $\mathbf{x}(t) = (x_1(t), \ldots, x_K(t))^T$ collects the activities of the K readout units and we assume stationary dynamics. Neglecting off-diagonal elements of the covariance $\langle \mathbf{x}\mathbf{x}^T\rangle$, an approximation accurate for sparse readouts ($K \ll N$) [152], and using self-averaging in the thermodynamic limit so

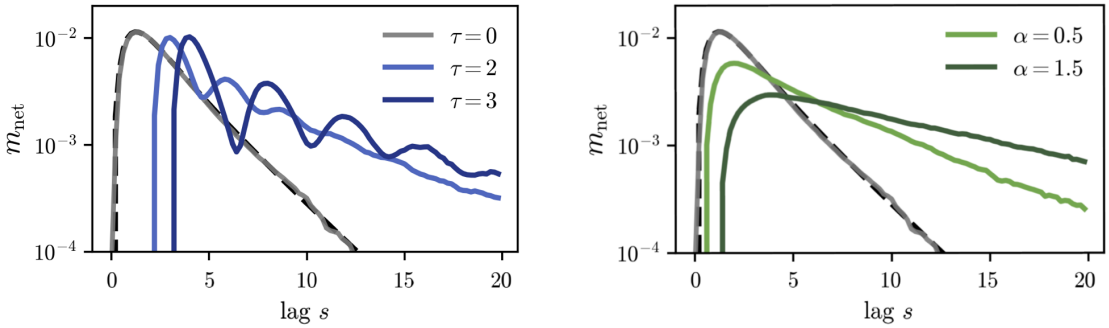

Figure 7.4: Reshaping of memory capacity by time delays. Left: Network contribution to the sequential memory $m_{\text{net}}(s)$ for uniform discrete delays. Increasing the delay τ shifts the memory capacity to longer time lags s and creates resonance peaks at integer multiples of τ. Right: Network memory for heterogeneous Gamma-distributed delays with varying shape parameter α at fixed $\theta = 3.0$. Heterogeneity in transmission times suppresses the resonance peaks observed in the discrete case, resulting in a broad, smooth memory profile that retains information over extended timescales. Parameters: $\sigma = 1.7$, $\mu = 0$, $g = 1$ and $\Delta = 1$. For these parameters, the driven dynamics is expected to be locally expansive yet non-chaotic [202].

that single-neuron variances can be replaced by their population average $c_0 = N^{-1}\sum_{i=1}^{N}\langle x_i(t)^2\rangle$, Eq. (7.12) reduces to

$$m(s) = \frac{1}{c_0\langle z(t)^2\rangle}\sum_{i=1}^{K}\langle x_i(t+s)z(t)\rangle^2. \tag{7.13}$$

At short lags, $m(s)$ is dominated by a local single-unit contribution due to leaky integration. Indeed, for the uncoupled dynamics $\dot{x} = -x + \xi$, each unit acts as a first-order linear filter of the drive, so that $\langle x_i(t+s)z(t)\rangle$ decays exponentially with s. Since $m(s)$ depends on the squared cross-correlation, this yields $m_{\text{single}}(s) \propto e^{-2s}$ [202]. To isolate the interesting contribution to the memory generated by recurrent interactions, we subtract this baseline and define

$$m_{\text{net}}(s) = m(s) - m_{\text{single}}(s). \tag{7.14}$$

Figure 7.4 shows numerical results for $m_{\text{net}}(s)$ in networks with uniform delays and heterogeneous (Gamma-distributed) delays, compared with the instantaneous case ($\tau = 0$), where an analytical prediction is available [202]. Delays reshape the memory profile: $m_{\text{net}}(s)$ is suppressed at short lags and redistributed over a wider range of lags, indicating that recurrent interactions retain information about the input history over longer timescales. Across both uniform and heterogeneous delays, increasing the mean interaction delay (larger τ, or larger shape α at a fixed scale θ, respectively) shifts $m_{\text{net}}(s)$ toward larger lags. For uniform delays, $m_{\text{net}}(s)$ emerges at $s \approx \tau$, consistent with the time required for the input to propagate through delayed recurrent connections. Subsequent recirculation of the drive generates echoes spaced by τ and hence oscillations in $m_{\text{net}}(s)$. In contrast, for heterogeneous delays, the spread in arrival times suppresses oscillations and produces a smoother, broader $m_{\text{net}}(s)$ whose large-lag tail is supported by the subset of long-delay interactions.

7.6 Discussion

Our results establish that time delays can fundamentally reshape the collective dynamics of high-dimensional neural networks. Employing extended RMT and DMFT accommodating delayed

interactions, we uncovered a rich phase diagram governed by the interplay between two distinct instability mechanisms: the disorder-driven static instability of the spectral bulk, which induces chaos, and the delay-induced Hopf instability of the spectral outlier, which drives synchronization. We are able to precisely describe the emergent dynamical behavior in terms of the statistical properties of the coupling matrix.

The mapping established between random and distributed delays demonstrates that the phase diagram is structurally robust to heterogeneity in time delays. Moreover, this equivalence extends beyond neural dynamics to a broad class of high-dimensional disordered systems subject to heterogeneous delays.

Functionally, our analysis reveals that delays not only reshape neural dynamics but can impact information processing capabilities. We demonstrated that delays redistribute the network's memory capacity toward longer timescales. This mechanism allows the system to maintain traces of past inputs well beyond the characteristic relaxation time of individual units. Consequently, delays may serve as a crucial computational resource that enables the integration of temporal features over extended windows.

From a broader perspective, these results offer new insights into the design and control of physical learning systems. In neuromorphic hardware and photonic computing where communication latencies are intrinsic, our framework provides the theoretical tools to predict stability boundaries and emergent collective states. Ultimately, this work bridges the gap between abstract theoretical modeling and the physical reality of networks with finite signal propagation speeds.

7.7 Appendix

7.7.1 Dynamical Mean-Field Theory for delayed random networks

While RMT methods are able to locate linear stability boundaries, we resort to DMFT to describe the dynamical behavior in the various phases displayed by the neural network model. DMFT was extended to accommodate delayed interactions in ecological dynamics in Chapter 6. A straightforward adaptation of the calculation presented in [308] shows that the DMFT equation for the neural dynamics Eq. (7.1) is

$$\dot{x}(t) = -x(t) + \mu\langle\phi(x(t-\tau))\rangle + \sigma\eta(t), \tag{7.15}$$

where $\eta(t)$ is Gaussian noise with zero mean and correlations

$$\langle\eta(t)\eta(t')\rangle = \langle\phi(x(t-\tau))\phi(x(t-\tau))\rangle. \tag{7.16}$$

Linearizing the DMFT equation around the zero fixed point gives

$$\delta\dot{x}(t) = -\delta x(t) + \mu g\langle\delta x(t-\tau)\rangle + \sigma g\delta\eta(t), \tag{7.17}$$

where $\delta\eta(t)$ is zero-mean Gaussian noise with

$$\langle\delta\eta(t)\delta\eta(t')\rangle = \langle\delta x(t-\tau)\delta x(t'-\tau)\rangle. \tag{7.18}$$

7.7.2 Perfect synchronicity in oscillatory phase

We demonstrate here that in the oscillatory region all neurons oscillate in perfect synchronicity, with no phase shift between them. It is convenient to employ the usual low-heterogeneity approximation

of Eq. (7.17), see Section 1.2.2.5 for details:

$$\delta\dot{x}(t) = -\delta x(t) + \mu g\langle\delta x(t-\tau)\rangle + \sigma g z\langle\delta x(t-\tau)\rangle. \tag{7.19}$$

We assume a solution of this linearized dynamics of the form

$$\delta x(t) = c(z)e^{i\omega t}. \tag{7.20}$$

We are making the ansatz that the frequency ω is the same for all neurons, meaning it does not depend on z in our approximation, but we allow for neuron-dependent amplitude and phase shift, encoded in a complex $c(z)$. Inserting the ansatz Eq. (7.20) into Eq. (7.19), and normalizing the amplitude and phase shift as $A(z)e^{i\phi(z)} = c(z)/\langle c(z)\rangle$, we obtain

$$i\omega = -1 + (\mu + \sigma z)gA(z)^{-1}e^{-i\phi(z)}e^{-i\omega\tau}. \tag{7.21}$$

Separating the real and imaginary part of this equation yields

$$\begin{aligned}(\mu + \sigma z)A(z)^{-1}\cos(\phi(z) + \omega\tau) &= 1,\\ (\mu + \sigma z)A(z)^{-1}\sin(\phi(z) + \omega\tau) &= -\omega.\end{aligned} \tag{7.22}$$

Dividing the second by the first gives $\tan(\phi(z)+\omega\tau) = -\omega$, which implies $\phi(z) = -\omega\tau - \arctan\omega$. Since $\phi(z)$ does not actually depend on z, we conclude that there is no phase difference in neuron oscillations.

7.7.3 Amplitude properties in oscillatory phase

Following the previous section, we assume a solution of the linearized dynamics Eq. (7.17) in which all neurons have identical frequency and phase shift, but display a neuron-dependent amplitude:

$$\delta x(t) = c[\delta\eta]e^{i\omega t}. \tag{7.23}$$

Here $c[\delta\eta]$ is a real number dependent on the specific realization of the noise $\delta\eta$. Within this assumption, we read from Eq. (7.18) that the correlation of the linearized noise satisfies

$$\langle\delta\eta(t)\delta\eta(t')\rangle = \langle c[\delta\eta]^2\rangle e^{i\omega(t-\tau)}e^{i\omega(t'-\tau)}. \tag{7.24}$$

Defining z as a zero-mean unit-variance Gaussian variable, we observe that the following ansatz

$$\delta\eta(t) = \langle c(z)^2\rangle^{1/2}e^{\lambda(t-\tau)}z, \tag{7.25}$$

yields the correlations Eq. (7.24). Since $\delta\eta(t)$ is Gaussian, it implies that we equivalently insert Eq. (7.25) in Eq. (7.17). Inserting the ansatz Eq. (7.23) into Eq. (7.15), and normalizing the amplitude as $A(z) = c(z)/\langle c(z)\rangle$, gives

$$i\omega = -1 + (\mu g + \sigma g\langle A(z)^2\rangle^{1/2}z)A(z)^{-1}e^{-i\omega\tau}. \tag{7.26}$$

After separating the real and imaginary part and straightforward manipulations we obtain

$$A(z) = 1 + \frac{\sigma}{\mu}\langle A(z)^2\rangle^{1/2}z. \tag{7.27}$$

From this equation we infer that oscillations Gaussian distributed, with statistics given by Eq. (7.6) of the main text. From this result one can for instance obtain the fraction of neurons that oscillate in phase opposition, which is given by

$$\frac{1}{2}\mathrm{erfc}\left(\frac{\sqrt{\mu^2-\sigma^2}}{\sqrt{2}\sigma}\right). \tag{7.28}$$

7.7.4 Exact solution for large negative interaction mean

The neural oscillations can be exactly described in the limit $\mu \to -\infty$. The key observation is that the amplitudes of oscillations of $x_i(t)$ are approximately proportional to μ [64]. Therefore, in the limit $\mu \to -\infty$ the amplitude of the DMFT process $x(t)$ diverges. Correspondingly, the response field becomes a step function, that is $\phi(x(t)) = s(t)$ with

$$s(t) = \begin{cases} -1 & -T/2 < t < 0 \\ 1 & 0 < t < T/2 \end{cases}, \tag{7.29}$$

where T is the period of oscillations. Consequently, Eq. (7.16) reads $\langle \eta(t)\eta(t') \rangle = s(x(t-\tau))s(x(t'-\tau))$. Following a reasoning similar to the one in Appendix 7.7.3, this relation implies that the DMFT noise can be equivalently described as $\eta(t) = zs(t-\tau)$, where z is a zero-mean, unit-variance Gaussian variable. In Fourier-series space the step function Eq. (7.29) is

$$s_n = \begin{cases} 0 & n \text{ even} \\ -2i/n\pi & n \text{ odd} \end{cases}, \tag{7.30}$$

and the DMFT equation, after shifting by τ, reads

$$i\omega n x_n = -x_n + (\mu + \sigma z)s_n. \tag{7.31}$$

Consequently, we obtain the exact solution of the DMFT process $x(t)$ as

$$x_n = \begin{cases} 0 & n \text{ even} \\ 2i(\mu + \sigma z)/\pi n(1 + i\omega n) & n \text{ odd} \end{cases}. \tag{7.32}$$

In particular the amplitude of oscillations is given by

$$\begin{aligned} x(0) &= \frac{2i(\mu + \sigma z)}{\pi} \sum_{n \text{ odd}} \frac{1}{n(1 + i\omega n)} \\ &= (\mu + \sigma z) \tanh(T/4). \end{aligned} \tag{7.33}$$

(this $\tanh$ is unrelated to the activation function). It remains to find the period T of oscillations. To obtain it, we notice that the DMFT equation

$$\dot{x}(t) = -x(t) + (\mu + \sigma z)s(t - \tau) \tag{7.34}$$

implies that

$$x(T/2) - x(0) = \int_0^{T/2} dt e^{-T/2+t}(\mu + \sigma z)s(t - \tau). \tag{7.35}$$

Since $x(0) = x(T/2) = 0$, this integral vanishes. Evaluating the integral and solving for T yields the period of oscillations, which is given by

$$T = 2\tau + 2\log(2 - e^{-\tau}). \tag{7.36}$$

7.7.5 Statistics of non-zero fixed point phase

As discussed in the main text, for $\mu g > 1$ the dynamics settles into one of two non-trivial fixed points symmetric under $x \to -x$. The statistics of each one of the fixed points can be found by using the DMFT Eq. (7.15) in the stationary limit:

$$x^*(z) = \mu M + \sigma\sqrt{q}z, \tag{7.37}$$

where

$$\begin{aligned} M &= \langle \phi(x^*(z)) \rangle, \\ q &= \langle \phi(x^*(z))^2 \rangle. \end{aligned} \tag{7.38}$$

More explicitly, these self-consistencies read

$$\begin{aligned} M &= \int \frac{e^{-z^2/2}}{\sqrt{2\pi}} \phi(\mu M + \sigma\sqrt{q}z), \\ q &= \int \frac{e^{-z^2/2}}{\sqrt{2\pi}} \phi(\mu M + \sigma\sqrt{q}z)^2. \end{aligned} \tag{7.39}$$

These self-consistencies can solved at a given values of μ and σ to obtain M and q and thus the statistics of the non-zero fixed point.

7.7.6 Transition to chaos for unstable bulk

We show here that for when the bulk becomes unstable a transition to chaos takes place. Consider for simplicity the case $\mu = 0$. Assuming the system reaches a time-invariant stationary state, we see that the average in Eq. (7.16) can be shifted by τ, giving $\langle \eta(t)\eta(t') \rangle_{\rm st} = \langle \phi(x(t))\phi(x(t')) \rangle_{\rm st} = C_{\rm st}(t - t')$. Define $\Delta(t) = \langle x(t)x(0) \rangle_{\rm st}$. By rewriting the DMFT Eq. (7.15) as $\sigma\eta(t) = \dot{x}(t) + x(t)$ and by averaging the product $\sigma^2\eta(t)\eta(t')$ we see that the correlation satisfies $-\ddot{\Delta}(t) + \Delta(t) = \sigma^2 C_{\rm st}(t)$. From here, one can follow the same steps as [63] and arrive at the conclusion that for $\sigma g > 1$ the neural dynamics is chaotic.

7.7.7 Quantification of the synchronization-chaos transition

We detail here the phenomenological order parameter used in Figure 7.3E to distinguish between synchronized and chaotic dynamics. We rely on the observation that in the synchronized phase all neurons exhibit identical shape of oscillations, differing only by a scaling factor. This property allows us to discriminate synchronization from chaos by a simple analysis of the dynamics without resorting to Lyapunov exponents or the dimension of activity, which are computationally demanding to compute especially in the context of delayed dynamics.

For each data point in Figure 7.3E, we simulate a network of $N = 1000$ neurons for a coupling matrix with the given statistics μ and σ. The initial conditions $x_i(0)$ are drawn randomly. The simulation is run for a total duration of $T = 400$, discarding the initial transient up to $T = 300$ to ensure stationarity. We consider the absolute values of the trajectories, normalized by their respective maximum amplitudes:

$$y_i(t) \equiv \frac{|x_i(t)|}{\max_t |x_i(t)|}. \tag{7.40}$$

In a perfectly synchronized state, the functions $y_i(t)$ are identical across all i. We quantify deviations from this situation by computing the instantaneous average over all neurons

$$\overline{y(t)} \equiv \frac{1}{N}\sum_{i=1}^{N} y_i(t) \tag{7.41}$$

and the squared residuals for each neuron:

$$z_i(t) \equiv \left[y_i(t) - \overline{y(t)}\right]^2. \tag{7.42}$$

The "chaos strength" plotted in Figure 7.3E is the average of these residuals over all neurons and time steps:

$$\text{chaos strength} \equiv \frac{1}{NT}\sum_{i,t} z_i(t). \tag{7.43}$$

The final curve in Figure 7.3E is obtained by averaging this metric over 10 independent realizations of the random coupling matrix for value of μ and σ.

In the synchronized phase, $y_i(t) = \overline{y(t)}$ for all i, and this parameter vanishes. In the fully chaotic regime this parameter instead saturates at a plateau. As shown in Figure 7.3E, the theoretical boundary coincides with the point where the chaos strength begins to deviate from its saturation level, marking the onset of synchronization.

7.7.8 Equivalence between random and distributed delays

We prove here that neural dynamics with random delays can be equivalently described with the DMFT equation associated to neural dynamics with non-random distributed delay. This holds in the case in which neural interactions are random. Consider Eq. (7.8) of the main text and define the random processes

$$\xi_i(t) = \sum_k J_{ik}\phi(x_k(t-\tau_{ik})). \tag{7.44}$$

Since we assume the coupling matrix and the delays to be independent, their second moment will be

$$\begin{aligned}\langle \xi_i(t)\xi_j(t')\rangle &= \sum_{kl}\langle J_{ik}J_{jl}\phi(x_k(t-\tau_{ik}))\phi(x_l(t'-\tau_{jl}))\rangle \\ &= \int_0^\infty d\tau \int_0^\infty d\tau' K(\tau)K(\tau')\sum_{kl}\langle J_{ik}J_{jl}\phi(x_k(t-\tau))\phi(x_l(t'-\tau'))\rangle.\end{aligned} \tag{7.45}$$

From here, one can proceed with standard cavity arguments [61, 211]. In particular, $\xi_i(t)$ will be independent Gaussian processes with connected autocorrelation

$$\langle \xi_i(t)\xi_i(t')\rangle_c = \int_0^\infty d\tau \int_0^\infty d\tau' K(\tau)K(\tau')\langle \phi(x_i(t-\tau))\phi(x_i(t'-\tau'))\rangle. \tag{7.46}$$

Consequently, the dynamics of a representative neuron $x(t)$ will follow the DMFT Eq. (7.15), where now

$$\langle \eta(t)\eta(t')\rangle = \int_0^\infty d\tau \int_0^\infty d\tau' K(\tau)K(\tau')\langle \phi(x(t-\tau))\phi(x(t'-\tau'))\rangle. \tag{7.47}$$

Following a straightforward adaptation of the methods of [309], we see that the DMFT Eq. (7.15) where $\eta(t)$ has statistics given by Eq. (7.47) is also the DMFT equation associated to the neural dynamics Eq. (7.9) of the main text. In conclusion, as mentioned in the main text, in the case of random interactions there is an exact mapping between dynamics with random delays and distributed delays.

Conclusions

In this thesis, we studied disordered models of ecological communities, introduced and briefly reviewed in Chapter 1. At their core, disordered models circumvent the need for detailed parameterization by assuming that interaction strengths and other unknowns are randomly drawn from probability distributions characterized by a limited number of statistical properties. The interest in disordered ecological models was historically initiated in the context of the complexity-stability debate [31, 98], but it remains highly relevant today. A first reason is that disordered models generate testable empirical predictions [31, 186, 199, 271, 281]. If these match empirical observations, it suggests that a disordered perspective is informative and possibly sufficient, without the need for fine-grained biological and ecological characterization. Furthermore, they serve as null models upon which explicit features can be added and their distinct effects quantified [195, 296, 312, 311]. In this way, one can isolate the precise consequences of any specific element to community stability, structure, and dynamics.

It is important to highlight the fundamental difference between disordered and neutral approaches [106, 119, 147, 174] to the modeling of ecological communities. While both approaches provide an essentially null description of communities, neutral models assume all species are ecologically identical, with community properties resulting purely from stochasticity rather than interactions. In contrast, disordered models assume explicitly interacting species, and consequently niche variation, although in a simplified statistically equivalent manner. Neutral models, treating all species as functionally identical, cannot detail the consequences of heterogeneous species interactions and niche variability, including the effect of competition [294, 316, 329] or the appearance of alternative stable states [186, 247, 271].

Because the use of non-linear disordered models in community ecology is a relatively recent development, early work understandably relied on simplifying assumptions to establish baseline behavior [65, 186, 196, 199]. However, as reviewed in Sections 1.3 and 1.4, an expanding body of literature is actively building upon foundational models to incorporate greater biological and ecological realism and detail its impact on community properties. In this spirit, in this thesis we aimed to relax the assumption of a strict separation of timescales, which results in perfectly quenched and instantaneous interactions, as well as the assumption that reciprocal effects between species are purely linear. This was motivated by the ecological facts that environmental fluctuations continuously reshape interactions [170, 204, 222, 305, 306, 324], that a variety of mechanisms inevitably introduce delays in species interactions [35, 98, 121], and that reciprocal effects between species abundances are bound to saturate at high densities [25, 226, 240]. By integrating these specific features into simple models, we sought to isolate and study their specific effects in high-dimensional communities.

We first analyzed the impact of time-varying interactions on community properties. More specifically, in Chapters 2 and 3, we introduced stochastically fluctuating interactions into a linear

model. This approach was motivated by a surprising gap in the literature. Despite the ubiquity of temporal fluctuations [116, 118, 124, 155, 259, 304], a systematic understanding of how they affect the stability of complex systems was lacking [4, 36, 52, 105, 206, 227, 237]. The framework we considered can be seen as an extension of May's classic model, reviewed in Section 1.1, to the non-static case. We employed the linear model to investigate the relationship between complexity and stability in the presence of fluctuating interactions. Notably, as detailed in Section 3.3, we found that time-variability can stabilize complexity even beyond May's static bound, where the instantaneous Jacobian would predict instability. This supports the general principle that temporal fluctuations can lead to more stable complex systems than their static counterparts. Furthermore, our findings indicate that static criteria may be insufficient for determining the stability of generic complex systems. Our results align with recent literature demonstrating that noise stabilizes diversity in metacommunity models [327, 328].

To investigate the effect of time-varying interactions on community properties beyond stability, in Chapter 4 we introduced stochastically fluctuating interactions into the generalized Lotka-Volterra equations. We found that variability in interactions promotes coexistence, as detailed in Section 4.5, and generates abundance distributions that better match experimental data, as detailed in Section 4.6. This latter finding is consistent with a core tenet of neutral theory, demonstrating that stochasticity generally produces broader and more realistic abundance distributions [106, 147, 174]. Overall, the results of these chapters support the implication that temporal variability in interactions is a functional component of ecosystem persistence. This indicates that moving beyond static approximations might be relevant for developing more accurate and predictive models of ecological communities.

Another limitation of simplified disordered community models is the presence of a non-physical phase characterized by unbounded growth in species abundances, as described in Section 1.2.1.3. To resolve this, in Chapter 5 we introduced a saturating response into the generalized Lotka-Volterra equations. While a similar approach was taken in [226], our formulation permits slightly improved analytical tractability. This modification eliminates the divergent behavior inherent to models assuming strictly linear interactions. The introduction of a saturating response further allows for the exploration of communities with highly cooperative and heterogeneous interactions, as detailed in Sections 5.4 and 5.5. We found that the degree of symmetry between reciprocal interactions can move the system between qualitatively distinct dynamical behaviors. More specifically, an increase in symmetry drives the system into a regime characterized by lower volatility.

In Chapter 6, we relaxed the assumption of perfectly instantaneous interactions within complex communities. This approach was motivated by the fact that various ecological mechanisms introduce time delays comparable to the timescale of population dynamics [35, 98, 121]. We found that delays can induce both periodic and aperiodic fluctuations, as detailed in Sections 6.5, 6.6, 6.7 and 6.8. This finding provides a theoretical mechanism for population cycles as an alternative to multiple fixed points or non-dissipative predator-prey interactions. Notably, we also demonstrated that under certain structural conditions, delays alone are sufficient to induce chaotic behavior in high-dimensional ecological models. This result contrasts with single-species models, where delays typically only generate limit-cycle behavior [121]. Broadly, these results help clarify the specific conditions under which time delays induce complex dynamical behavior in species-rich heterogeneous communities.

The findings presented in these chapters were obtained via suitable extensions of Dynamical Mean-Field Theory [50, 58, 61] to accommodate stochastic and delayed interactions. Importantly, these extensions are essentially model-agnostic, making them generally applicable for analyzing the effects of time-varying interactions and time delays in any complex system amenable to a disordered

formulation [260, 267]. To demonstrate this, in Chapter 7 we employed these methods to examine the role of time delays in a model of neural dynamics [63, 64, 173]. Our results establish that time delays can fundamentally reshape the collective behavior of high-dimensional networks. We highlighted the critical role of the interaction mean, a parameter typically neglected in standard analyses of random networks. We found that a sufficiently negative interaction mean induces a phase of global and perfect synchronicity, capable of suppressing disorder-driven chaos.

Overall, the analytical techniques developed in this thesis are applicable well beyond the specific models considered here. Future work could employ these methods to explore the impact of time-varying and delayed interactions across the cornucopia of contexts in which a disordered systems perspective is informative [61, 260, 267]. In this sense, the work presented in this thesis ultimately contributes a set of analytical tools designed to help theoreticians gain a deeper understanding of both ecological communities and complex systems in general.

Vito Volterra: scientist, patriot, antifascist

Muoiono gli imperi, ma i teoremi di Euclide conservano eterna giovinezza.
Empires die, but Euclid's theorems retain eternal youth.
– Vito Volterra (epitaph)

The work presented in this thesis owes much, among others, to the pioneering contributions of the Italian mathematician Vito Volterra to the field of mathematical ecology. Here, I would like to humbly pay homage not only to his scientific achievements, but also to his historical and civic stature. I am partly motivated in doing this by the fact that since the 2010s nationalist and populist parties have decisively entered the political mainstream worldwide. These movements have frequently cast doubt on pluralism and weakened trust in liberal institutions, all in the name of a unified national will. Particularly concerning is that, in several cases, such parties draw popular support from an ambiguous attitude toward their neofascist roots, and share with them the same authoritarian tendencies. In many cases, they adopt anti-scientific and anti-environmentalist positions, which threaten to undermine the very tools needed to address today's urgent global challenges. For these reasons, I believe it is worthwhile remembering the ideals and actions of a citizen and academic who, in lieu of difficult decisions, maintend his integrity, as an exemplary reminder that scientific authority carries not only intellectual influence but also moral responsibility. Volterra was the most influential Italian mathematician of his generation, yet his influence extended well beyond mathematics, into the scientific and civic life of his country. Though a moderate for his whole life, even conservative in his loyalty to the King, he stood openly against the authoritarian regime that was trying to impose its laws on the world of knowledge, fully aware of the risks such a stance carried. He paid for his resistance with isolation and the loss of honors, in the country to which he patriotically contributed so much.

Vito Volterra was born on May 3, 1860, in Ancona. At that time, the city was still part of the Papal States. A couple of months after his birth, during incursion of troops claiming the annexion of the city to the Kingdom of Italy, a bomb detonated near the Volterra home. The explosion destroyed the cradle of the infant Vito but, miraculously, the child survived unharmed. He was the only son of Abramo Volterra and Angelica Almagià, both of Jewish descent. Tragedy struck the family when Abramo died in 1862, when Vito was only two years old, which left the family in difficult financial

---

Sources for this appendix: Rita Levi-Montalcini. *Senz'olio contro vento*. Baldini & Castoldi, 1996; Judith R Goodstein. *The Volterra chronicles: the life and times of an extraordinary mathematician, 1860-1940*. Vol. 31. American Mathematical Society, 2007; Angelo Guerraggio and Giovanni Paoloni. *Vito Volterra*. Springer-Verlag, 2010; Annalisa Capristo. "Volterra, Fascism, and France". In: *Science in Context* 28.4 (2015), pp. 637–674

circumstances. Despite these challenges, young Vito displayed an uncommon curiosity and a precocious inclination towards mathematics. At the age of nine, he observed that the oscillations produced by a twisted string are isochronous. At eleven years old, he began self-studying Bertrand's *Traité d'arithmétique* and Legendre's *Eléments de géométrie*. At thirteen, Vito read Verne's *From the Earth to the Moon* and proposed himself to compute, for fun, the trajectory of the wagon-rocket which in the book is launched from Florida under the gravitational influence from Earth and the Moon. He resorted to partitioning time in small intervals, such that in each one of them the force could be considered constant and the motion of the wagon could then be constructed as a collection of parabolic arcs. When he was fourteen, once again without a teacher, he plunged into Bertrand's first volume of *Traité de calcul différentiel et de calcul intégral*, which deals with differential calculus. Without any apparent access to any work on integral calculus, such as the second volume of the *Traité*, he discovered while computing centers of gravity and momenta of inertia of rigid bodies that these could be determined by means of an operation which consisted in the inversion of differentiation.

His family remained concerned with practical considerations. However, he was undeterred in becoming a mathematician, displaying a stubbornness that would accompany him in later developments. Fortunately, with the help of a physics professor and a relative who recognized the outstanding potential of the young Vito, he convinced his family to allow him to pursue his vocation. In the fall of 1879, Volterra sat for the competitive entrance examination for the Scuola Normale Superiore in Pisa, which he passed with distinction. While still a student in Pisa, he wrote his first original papers. In a first one, he demonstrated the existence of a "pointwise discontinuous function [...] which in a given interval is not capable of integration." In a second one, he showed the existence of functions "whose derivatives are not capable of integration." These results addressed open questions posed by Dini and were crucial to the development of rigorous calculus. Volterra graduated in physics in 1882 with a thesis on hydrodynamics written under the supervision of Enrico Betti. Volterra never again addressed questions related to the foundations of mathematics, as he subsequently turned his attention to more applied topics.

After his graduation, Volterra began his professional career in Pisa as an assistant to Betti. In 1883, just a year later, he was appointed professor of rational mechanics there, and he would subsequently hold chairs in mathematical physics and graphic statics. He remained in Pisa for ten years following his graduation. During this decade Volterra displayed a remarkable breadth of intellectual output, publishing no fewer than twenty papers dedicated to mathematical physics. His research spanned a vast array of topics, including potential theory and hydrodynamics, as well as the emerging field of elasticity. He also addressed complex problems in electrochemistry, optics, and electrodynamics. Most significantly, this period marked the early development of functional analysis. Volterra initiated the systematic study of functionals, laying the foundations for the field. In all his theoretical work, he consistently highlighted the deep connections between abstract mathematical concepts and their applications to physical contexts.

Volterra's talents soon started to gain recognition by the Italian academic establishment, far beyond the confines of Pisa. In 1887, the Società dei XL awarded him the gold medal for mathematics. The following year, he was nominated corresponding member of the prestigious Accademia dei Lincei. During this period, he also cemented his standing within the Circolo Matematico di Palermo, and was appointed a Knight of the Order of the Crown of Italy in 1891. Upon the death of Enrico Betti in 1892, he was elected dean of the faculty of sciences at the University of Pisa and succeeded him as the director of the influential journal *Nuovo Cimento*.

Beginning with the academic year 1893-1894, the young professor transferred from Pisa to the

University of Turin. During this period, Volterra made his most profound contributions to analysis. He was the first to elaborate a general theory of integral equations, motivated by dynamics of fresh waters. He investigated the existence and uniqueness of their solutions and presented a general method for solving them. His time in Turin was also marked by a fierce academic dispute, which became a significant distraction for Volterra. He engaged in a controversy with Giuseppe Peano, the rising star of analysis in Turin, debating on matters regarding the rotation of the Earth and the motion of its poles. Despite this local conflict, his international reputation continued to soar. He participated in the inaugural International Congress of Mathematicians in Zurich in 1897. Three years later, he was invited to deliver a plenary lecture at the 1900 Congress in Paris. This invitation served as a definitive acknowledgment of his scientific authority. In these years, he also forged deep connections with the French mathematical community, meeting figures such as Émile Borel and Henri Lebesgue.

In 1900, Volterra secured, not without significant maneuvering of academic politics, a professorship in Rome. It is important to note that a chair there represented one of the highest acknowledgments of professional success at the time. Indeed, since 1870, the policies of successive Italian governments had aimed to promote Rome not just as the political center, but as the undisputed scientific and cultural capital of a unified Italy. This professional triumph also coincided with a major event in his private life. After a brief engagement lasting only a month, Volterra married Virginia Almagià. This union was the successful result of a long-standing matchmaking plan orchestrated by Volterra's mother and her wealthy cousin, who was Virginia's father. She would remain a constant and supportive figure by his side throughout his life. Shortly after his arrival in Rome, Volterra was invited to deliver the official inaugural lecture for the 1901–1902 academic year. In it, he illustrated the potential new applications of mathematics to economics and biology.

The first decade of the 1900s was the period in which Volterra started to build up his public image and fame, both in Italy and abroad. His influence extended well beyond mathematics and into civic life. In 1904, he received a government mandate to oversee the reorganization of the institutes for higher technical education in Turin. In 1905, Volterra was nominated senator of the Kingdom of Italy by prime minister Giolitti. In this period he also assumed leadership roles in the scientific community, as he was elected president of the Italian Physical Society for the 1906-1908 term. Furthermore, he played a central organizing role in the 1908 International Congress of Mathematicians held in Rome. He had insisted strongly on bringing the event to Italy. At stake was not merely the location of the congress, but Italy's placement in the global hierarchy of mathematics. The goal was to secure the third place in the ranking of world mathematics, following France and Germany. The prestige of the congress was such that King Vittorio Emanuele III attended the opening ceremony, departing only after Volterra's inaugural lecture had concluded. This event cemented Volterra's strong ties with the Italian political elite, leading to his widespread recognition as the undisputed leader of the scientific community and its primary representative before the political powers.

Within the Italian scientific movement at the beginning of the century, he was the figure most acutely aware of the political stakes involved in scientific organization. This vision materialized in his fundamental contribution in the founding of the Italian Society for the Progress of Sciences (SIPS). The SIPS served a dual purpose. Internally, it provided an opportunity for democratic convergence among scientists to offset the dangers of excessive specialization. Externally, it aimed at presenting Italian science to the general public and political powers. Volterra's inaugural discourse was farsighted. It included a lucid analysis of the relationship between science and society in Italy at the turn of the twentieth century. He believed that scientific progress to be essential for civil

progress. It is also worth noting that the SIPS encouraged a certain degree of participation by women, an innovative aspect that was far from negligible for the time.

Amidst these civic commitments, he continued his research, mainly on the theory of elasticity. He introduced the concept of distortions, and also developed the theory of what he called "hereditary phenomena". Classical mechanics assumes that the state of a system depends only on its present conditions. Volterra challenged this assumption by introducing a new class of equations combining the properties of both differential and integral calculus, in order to account for memory effects in physical materials. The attentive reader will recognize these as the precursors to what are now called delay differential equations. I find it particularly interesting that Chapter 6 of this thesis owes therefore, in a sense, a threefold debt to Volterra, drawing upon his work for the foundational concept of mathematical ecology and for the specific form of the Lotka-Volterra equations (discussed later), as well as for the inclusion of the delay term to model memory in species interactions.

As war clouds gathered over Europe, Volterra became increasingly engaged with the political crisis facing the continent. He had opposed Italy's colonial campaign in Libya and, when World War I broke out in 1914, firmly rejected Italy's association with the Central Powers. Instead, he advocated for intervention on the side of the Allies, interpreting the conflict as a continuation of the Risorgimento and a defense of liberal and constitutional values. Deeply troubled by German militarism, he reacted with dismay to the *Manifesto of the Ninety-Three*, which he condemned as a betrayal of scientific internationalism. He consequently joined efforts to mobilize intellectuals in support of the Allies cause. This period of uncertainty ended in May 1915, when Italy declared war on Austria. Throughout the crisis, Volterra's actions reflected a synthesis of patriotism, political engagement, and commitment to the European scientific community.

Volterra did not limit his contribution to civil mobilization. Following a request for voluntary enlistment, he was commissioned and assigned to the Central Institute of Aeronautics in 1914. He was tasked with calculating firing tables (sets of numerical data used by artillery crews to aim weapons so that projectiles strike a specific target) for cannons that were intended to be mounted on dirigibles. This project was controversial because the prevailing opinion held that the muzzle flash would ignite the hydrogen gas of the airship at the moment of firing. Volterra dedicated himself to this problem for over a year, obviously with the rigorous methodology of a mathematical physicist. He first established and solved the differential equations governing the general ballistic problem. He then outlined methods for constructing the trajectories and finally computed the required firing tables. Volterra personally validated these theoretical models: despite being 59 years old at the time, he insisted to climb into the nacelle of the first dirigible equipped with the cannon to verify his calculations during a trial at the airfield of Campi Bisenzio. This act of personal courage, along with other risks taken during his service, earned him a promotion to the rank of Captain and the War Cross for military valor. Volterra's wartime scientific contributions extended beyond ballistics. Based on a proposal of his, the military developed a specialized meteorological service to support aerial and artillery operations, an initiative that evolved into what is today the Meteorological Service of the Italian Air Force.

During the war the nature of military conflict had changed irrevocably. Following the chlorine gas attacks by Germany at Ypres in 1915, society at large realized that science had become a critical factor in military capability. In response, Volterra championed the institution of an Office of Inventions and Research in 1917, mirroring similar initiatives in England, France, and the US, and was named as its director. In this capacity, he increasingly became the central pivot in the triangle of Italian science-industry-military, working to channel academic research into practical applications for the war effort. After the war ended, inspired by the model of the National Research

Council in the US and driven by a vision of creating research centers that would collaborate on a supranational level, he proposed a permanent Italian equivalent. This project culminated in the founding of the National Research Council in 1923, and Volterra served as its first president. This presidency was actually flanked by his presidency of the Accademia dei Lincei, the oldest and most prestigious scientific academy in Italy. Furthermore, under his important guidance, the Italian Mathematical Union was established in 1922. Volterra is also credited with a significant role in the initial conception and scientific direction of the monumental Treccani's *Enciclopedia Italiana*.

Volterra leveraged his international reputation to secure funding for young talent. Through his involvement with the International Education Board, the global operating arm of the Rockefeller Foundation, he facilitated an important exchange program. This initiative allowed numerous Italian and foreign scholars to gain fundamental experience in research centers and laboratories abroad. It included mathematicians such as Bruno de Finetti and André Weil. Even more significantly for the history of physics, Volterra secured fellowships for rising stars like Enrico Fermi, enabling his critical residency at Lorentz's laboratory in Leiden.

October 28, 1922 marked the day of the March on Rome, with Mussolini's militants entering the capital. Despite the ill-timed optimism of prime minister Luigi Facta ("Nutro fiducia che tutto andrà nel migliore dei modi"), this signaled the beginning of a dramatic turn of events for both Italy and Volterra. Shortly thereafter, King Vittorio Emanuele III charged Mussolini with constituting a new government. Volterra viewed the political situation with deep worry and harbored no sympathy for Mussolini's movement. However, in this initial phase, while personally opposed to the new government, he resigned himself to the reality of the situation. A loyal monarchist, Volterra remained faithful to the institutions of the state. In his official capacity, he therefore adopted a line of cautious collaboration with the government that the King had authorized. He attempted to strictly separate his personal political opinions from his institutional duties, hoping to safeguard the scientific organizations under his care.

The first major clash between Volterra and the Fascist regime arose over the educational reforms proposed by the minister of public education Giovanni Gentile. Drawing upon the philosophical framework of Benedetto Croce, Gentile sought to reshape the Italian educational system. The design for the school system in the Gentile reform was driven by two primary objectives. First, he aimed to establish classical humanities as the exclusive pedagogical foundation for the nation's future ruling elite. Second, he intended to enforce a rigid social stratification by channeling students from lower socio-economic backgrounds into vocational tracks with severely restricted access to higher education. Under this system, the Liceo Classico was elevated to the pinnacle of secondary education and the only path that granted access to all university faculties. In contrast, scientific and technical institutes were relegated to a secondary tier, signaling that scientific knowledge was considered culturally inferior to philosophical and literary studies. The reform also overhauled the university system. Among other centralizing measures, it revoked the autonomy of universities to elect their own rectors, who were henceforth to be nominated directly by the Ministry. Volterra viewed these changes as a direct assault on the dignity of scientific culture and the autonomy of academic institutions. He mounted a vigorous defense against the legislation, utilizing every platform available to him. As a senator and the serving president of the Accademia dei Lincei, he became the vocal leader of the opposition, arguing that a modern nation could not prosper by marginalizing scientific education. Despite his authoritative protests and the concerns of the scientific community, the reform was passed in 1923. The effects of this infamous reform persist, often as a grotesque caricature, in the structure, values, and implicit hierarchies of the Italian educational system today, more than a century later.

In the second half of 1924, Volterra followed the deteriorating political situation with increasing alarm. This year marked the definitive crisis of the liberal state and the transformation of Fascism from a parliamentary coalition into an open dictatorship. The brutal kidnapping and murder of Giacomo Matteotti in June 1924 removed any lingering doubts: Fascism represented the end of the constitutional order Volterra had sworn to uphold. In the Senate, Volterra joined the opposition. He was one of only 21 senators who cast a vote of no confidence against the government. His opposition moved from the parliament to the public square the following year. When Giovanni Gentile published the *Manifesto of the Fascist Intellectuals*, Volterra immediately signed the counter-statement, the *Manifesto of the Anti-Fascist Intellectuals* drafted by Benedetto Croce. The regime retaliated by dismantling his institutional power. Mussolini promoted the creation of the Accademia d'Italia, a new, lavishly funded institution designed to gather regime-friendly intellectuals and delegitimize the historic Accademia dei Lincei, which was seen as a bastion of liberal independence. Sensing the political climate, Volterra did not seek a second term as president of the Lincei when his mandate expired in 1926. The purge continued in 1927 when Guglielmo Marconi succeeded Volterra as the president of the National Research Council. Marconi, who would also assume the presidency of the Accademia d'Italia in 1930, became the symbol of the new "fascist science".

By 1928, the police had opened a personal dossier on Volterra, classifying him as politically suspect. Scrutiny of his affairs reached the highest level. At the end of 1928, when Volterra submitted a routine request for a passport to attend scientific conferences, the authorization was not handled by low-level bureaucrats. The document granting the "Sì" to his request bears the characteristic initial "M", that marked the matters directly acted on by the Duce. This surveillance tightened over time, and from April 1930 onwards his private correspondence was placed under systematic control.

The definitive rupture arrived with the decree of August 28, 1931. This law obligated all tenured and contracted university professors to swear an oath of allegiance using a new specific formula. It explicitly required them not only to be faithful to the King, but to swear loyalty to the Fascist regime, and to dedicate their teaching to "forming citizens who are industrious, upright, and devoted to the Nation and to the Fascist Regime". Volterra fully understood the gravity of this demand. He knew that refusing meant facing immediate social downfall, financial loss, and professional ostracism. Yet he could not compromise his conscience to save his chair. In a resolute act of moral courage, he refused to utter the oath. He was one of only 12 professors out of a total of over 1200 in all of Italy who dared to say no. On December 31, 1931, Volterra was formally dismissed from service and invited to request his pension. Thus ended his teaching career in the Italian university system, a distinguished tenure that had lasted nearly fifty years. The persecution did not stop at the university level. The regime enacted a reform of cultural institutions in 1933 to complete the process of "fascistisation". This extended the obligation to swear allegiance to Fascism to the members of all Academies. In June 1934, Volterra was once again invited to take the oath, and he once again refused. The consequence was immediate: he was expelled from all Italian academies, including the Accademia dei Lincei, the very institution he had once led with distinction.

Despite the mounting political turmoil and his increasing isolation from public life, Volterra was able to make a final contribution that would, by itself, secure his place in the history of twentieth-century science. In 1925, his son-in-law Umberto D'Ancona presented him with a puzzling statistical anomaly discovered while analyzing fish market data from the Adriatic Sea. D'Ancona had observed that during World War I, when fishing activity was drastically reduced, the composition of the catch changed in an unexpected way. While one might intuitively expect all fish populations to increase when fishing stops, D'Ancona noted a relative surge in the abundances of

predator species and a decline in the prey species. Intrigued by this, Volterra formulated a pair of non-linear differential equations modeling the dynamics between a predator and a prey population. From this model, Volterra derived three laws of population dynamics. The most relevant is the third one, which posits that a reduction in the effective growth rate of both species, such as that caused by industrial fishing, ultimately increases the average population of the prey and decreases the average population of the predators. The converse is therefore also true: when the fishing stops, the ecosystem reverts to a state that favors the predators. This mathematical insight provided the explanation for the wartime surge in Adriatic predators and effectively founded the field of mathematical ecology. After reading Volterra's 1926 article in *Nature*, the American mathematician and physical chemist Alfred James Lotka recognized similarities between their equations and results. He wrote a letter to the editor, to which Volterra replied. Volterra conceded the priority of Lotka's work but highlighted some differences. From that point on, the model became universally known as the Lotka-Volterra equations which, in their generalized multi-species extension, form the foundation of the work presented in this thesis

Meanwhile, in July 1938, the Fascist government officially inaugurated its anti-Jewish politics with the publication of the *Manifesto of Race*. This was followed in August by a mandatory census of the Jewish population. Volterra was required to fill out these personal data forms. In response to the question "Do you belong to the Jewish race on your father's side?" he wrote: "The Volterra family, which has never moved from Italy and whose ancestors can be traced to earlier than 1400, has always professed the Israelite religion.". For the question "Do you belong to the Jewish race on your mother's side?" he wrote: "The Almagià family, whose ancestors have resided in Italy for centuries, have always professed the Israelite religion and they originate from the Iberian peninsula.".

Volterra died in Rome on October 11, 1940. Surveillance accompained him even in death. A police phonogram reported: "This morning at 4:30 in his home in Via in Lucina 17 the Senator Volterra Vito son of Abramo of the Jewish race has died". The private funeral took place in Ariccia, near Rome, where Volterra and his family had spent their summers for decades. The entire local population attended to pay their respects. No representatives from the government attended, nor did anyone from the cultural institutions he had once presided over. There were no official commemorations, with the sole exception of a ceremony held one year after his death at the Vatican Academy. On October 16, 1943, a German truck arrived at Via in Lucina 17 to collect him and transport him to Auschwitz. The fact that he had died three years earlier had escaped the civil registry clerks who had handed over the list of Jews to the SS. His lifelong partner Virginia had been warned by friends and managed to reach safety the day before. It is hard to believe Volterra would have been persuaded to do the same. Disdainful of danger and hampered by difficulty in walking, we can only imagine he would have stubbornly refused to abandon his home on Via in Lucina and his vast, beloved library.

Bibliography

[1] Alfred J Lotka. “Contribution to the theory of periodic reactions”. In: *The Journal of Physical Chemistry* 14.3 (1910), pp. 271–274.

[2] Alfred J Lotka. “Analytical note on certain rhythmic relations in organic systems”. In: *Proceedings of the National Academy of Sciences* 6.7 (1920), pp. 410–415.

[3] Alfred J Lotka. “Contribution to the general kinetics of material transformations”. In: *Proceedings of the American Academy of Arts and Sciences* 55.3 (1920), pp. 137–153.

[4] Alfred J Lotka. “Note on moving equilibra”. In: *Proceedings of the National Academy of Sciences* 7.6 (1921), pp. 168–172.

[5] Vito Volterra. “Fluctuations in the abundance of a species considered mathematically”. In: *Nature* 118.2972 (1926), pp. 558–560.

[6] Alfred J Lotka and Vito Volterra. “Fluctuations in the abundance of a species considered mathematically”. In: *Nature* 119.2983 (1927). Correspondence, pp. 12–13.

[7] Vito Volterra. “Variazioni e fluttuazioni del numero d’individui in specie animali conviventi”. In: *Memorie del Reale Comitato Talassografico Italiano* 131 (1927), pp. 1–142.

[8] Mark Kac. “On the average number of real roots of a random algebraic equation”. In: *Proceedings of the London Mathematical Society* (1943).

[9] George Neville Watson. *A Treatise on the Theory of Bessel Functions*. 2nd. Cambridge University Press, 1944.

[10] Stephen O Rice. “Mathematical analysis of random noise”. In: *The Bell System Technical Journal* 24.1 (1945), pp. 46–156.

[11] G Evelyn Hutchinson et al. “Circular causal systems in ecology”. In: *Ann. NY Acad. Sci* 50.4 (1948), pp. 221–246.

[12] J. Monod. “The Growth of Bacterial Cultures”. In: *Annu. Rev. Microbiol.* 3 (1949), p. 371.

[13] Robert MacArthur. “Fluctuations of animal populations and a measure of community stability”. In: *ecology* 36.3 (1955), pp. 533–536.

[14] Charles S Elton. *The ecology of invasions by animals and plants*. Methuen and Co., 1958.

[15] Crawford S Holling. “Some characteristics of simple types of predation and parasitism1”. In: *The canadian entomologist* 91.7 (1959), pp. 385–398.

[16] Crawford S Holling. “The components of predation as revealed by a study of small-mammal predation of the European Pine Sawfly1”. In: *The canadian entomologist* 91.5 (1959), pp. 293–320.

[17] G Evelyn Hutchinson. “Homage to Santa Rosalia or why are there so many kinds of animals?” In: *The American Naturalist* 93.870 (1959), pp. 145–159.

[18] David Pimentel. “Species diversity and insect population outbreaks”. In: *Annals of the entomological society of America* 54.1 (1961), pp. 76–86.

[19] AL Turnbull and Donald A Chant. “The practice and theory of biological control of insects in Canada”. In: *Canadian journal of zoology* 39.5 (1961), pp. 697–753.

[20] H Zwölfer. “Untersuchungen über die Struktur von Parasitenkomplexen bei einigen Lepidopteren 1”. In: *Zeitschrift für Angewandte Entomologie* 51.1-4 (1962), pp. 346–357.

[21] Kenneth L Cooke. “Differential—difference equations”. In: *International symposium on nonlinear differential equations and nonlinear mechanics*. Elsevier. 1963, pp. 155–171.

[22] A. Macfadyen. *Animal ecology: aims and methods*. Pitman and Sons, 1963.

[23] P. DeBach. *Biological Control of Insect Pests and Weeds*. Reinhold Publishing Corporation, 1964. ISBN: 9780412074509.

[24] Jean Ginibre. “Statistical ensembles of complex, quaternion, and real matrices”. In: *Journal of Mathematical Physics* 6.3 (1965), pp. 440–449.

[25] C. S. Holling. “The Functional Response of Predators to Prey Density and its Role in Mimicry and Population Regulation”. In: *Memoirs Entomol. Soc. Canada* 97 (1965), p. 5.

[26] NG Hairston et al. “The relationship between species diversity and stability: an experimental approach with protozoa and bacteria”. In: *Ecology* 49.6 (1968), pp. 1091–1101.

[27] Richard Levins. *Evolution in changing environments: some theoretical explorations*. 2. Princeton University Press, 1968.

[28] Robert MacArthur. “Species packing and competitive equilibrium for many species”. In: *Theoretical Population Biology* 1.1 (1970), pp. 1–11.

[29] Robert Harding Whittaker. “Communities and ecosystems.” In: (1970).

[30] Milton Abramowitz and Irene A Stegun. *Handbook of Mathematical Functions with Formulas, Graphs, and Mathematical Tables. National Bureau of Standards Applied Mathematics Series 55. Tenth Printing*. ERIC, 1972.

[31] Robert M May. “Will a large complex system be stable?” In: *Nature* 238.5364 (1972), pp. 413–414.

[32] Paul Cecil Martin, Eric D Siggia, and Harvey A Rose. “Statistical dynamics of classical systems”. In: *Physical Review A* 8.1 (1973), p. 423.

[33] Robert M May. “Time-delay versus stability in population models with two and three trophic levels”. In: *Ecology* 54.2 (1973), pp. 315–325.

[34] James A Estes and John F Palmisano. “Sea otters: their role in structuring nearshore communities”. In: *Science* 185.4156 (1974), pp. 1058–1060.

[35] John Maynard-Smith. *Models in ecology*. Cambridge university press, 1974.

[36] Daniel B Botkin and Matthew J Sobel. “Stability in time-varying ecosystems”. In: *The American Naturalist* 109.970 (1975), pp. 625–646.

[37] Martin L Cody and Jared M Diamond. *Ecology and evolution of communities*. Harvard University Press, 1975.

[38] Robert M May and Warren J Leonard. “Nonlinear aspects of competition between three species”. In: *SIAM journal on applied mathematics* 29.2 (1975), pp. 243–253.

[39] R Bausch, Hans-Karl Janssen, and Ho Wagner. “Renormalized field theory of critical dynamics”. In: *Zeitschrift fur Physik B Condensed Matter* 24.1 (1976), pp. 113–127.

[40] Hans-Karl Janssen. “On a Lagrangean for classical field dynamics and renormalization group calculations of dynamical critical properties”. In: *Zeitschrift für Physik B Condensed Matter* 23.4 (1976), pp. 377–380.

[41] B. S. Goh. “Global Stability in Many-Species Systems”. In: *The American Naturalist* 111.977 (Jan. 1977), pp. 135–143. ISSN: 0003-0147. DOI: 10.1086/283144.

[42] Pierre C Hohenberg and Bertrand I Halperin. “Theory of dynamic critical phenomena”. In: *Reviews of Modern Physics* 49.3 (1977), p. 435.

[43] Michael C Mackey and Leon Glass. “Oscillation and chaos in physiological control systems”. In: *Science* 197.4300 (1977), pp. 287–289.

[44] C De Dominicis. “Dynamics as a substitute for replicas in systems with quenched random impurities”. In: *Physical Review B* 18.9 (1978), p. 4913.

[45] Giancarlo Benettin et al. “Lyapunov characteristic exponents for smooth dynamical systems and for Hamiltonian systems; a method for computing all of them. Part 1: Theory”. In: *Meccanica* 15 (1980), pp. 9–20.

[46] Haim Sompolinsky and Annette Zippelius. “Dynamic theory of the spin-glass phase”. In: *Physical Review Letters* 47.5 (1981), p. 359.

[47] Peter Yodzis. “The stability of real ecosystems”. In: *Nature* 289.5799 (1981), pp. 674–676.

[48] J Doyne Farmer. “Chaotic attractors of an infinite-dimensional dynamical system”. In: *Physica D: Nonlinear Phenomena* 4.3 (1982), pp. 366–393.

[49] John J Hopfield. “Neural networks and physical systems with emergent collective computational abilities.” In: *Proceedings of the national academy of sciences* 79.8 (1982), pp. 2554–2558.

[50] Haim Sompolinsky and Annette Zippelius. “Relaxational dynamics of the Edwards-Anderson model and the mean-field theory of spin-glasses”. In: *Physical Review B* 25.11 (1982), p. 6860.

[51] Chi-Tsong Chen. *Linear system theory and design*. Saunders college publishing, 1984.

[52] Joel E Cohen and Charles M Newman. “The stability of large random matrices and their products”. In: *The Annals of Probability* (1984), pp. 283–310.

[53] John J Hopfield. “Neurons with graded response have collective computational properties like those of two-state neurons.” In: *Proceedings of the national academy of sciences* 81.10 (1984), pp. 3088–3092.

[54] Stuart L Pimm. “The complexity and stability of ecosystems”. In: *Nature* 307.5949 (1984), pp. 321–326.

[55] Vyacheslav L Girko. “Circular law”. In: *Theory of Probability & Its Applications* 29.4 (1985), pp. 694–706.

[56] Ilya Prigogine and Grégoire Nicolis. “Self-organisation in nonequilibrium systems: towards a dynamics of complexity”. In: *Bifurcation analysis* (1985), pp. 3–12.

[57] Michael E Soulé. “What is conservation biology?” In: *BioScience* 35.11 (1985), pp. 727–734.

[58] Kurt Binder and A Peter Young. “Spin glasses: Experimental facts, theoretical concepts, and open questions”. In: *Reviews of Modern physics* 58.4 (1986), p. 801.

[59] M Mézard, G Parisi, and MA Virasoro. “SK Model: The Replica Solution without Replicas.” In: *Europhys. Lett* 1.2 (1986), pp. 77–82.

[60] Peter Jung and Peter Hänggi. “Dynamical systems: a unified colored-noise approximation”. In: *Physical review A* 35.10 (1987), p. 4464.

[61] Marc Mézard, Giorgio Parisi, and Miguel Angel Virasoro. *Spin glass theory and beyond: An Introduction to the Replica Method and Its Applications*. Vol. 9. World Scientific Publishing Company, 1987.

[62] Hans Juergen Sommers et al. “Spectrum of large random asymmetric matrices”. In: *Physical review letters* 60.19 (1988), p. 1895.

[63] Haim Sompolinsky, Andrea Crisanti, and Hans-Jurgen Sommers. “Chaos in random neural networks”. In: *Physical review letters* 61.3 (1988), p. 259.

[64] CM Marcus and RM Westervelt. “Stability of analog neural networks with delay”. In: *Physical Review A* 39.1 (1989), p. 347.

[65] H Rieger. “Solvable model of a complex ecosystem with randomly interacting species”. In: *Journal of Physics A: Mathematical and General* 22.17 (1989), p. 3447.

[66] Kirk O Winemiller. “Must connectance decrease with species richness?” In: *The American Naturalist* 134.6 (1989), pp. 960–968.

[67] Peter Chesson. “MacArthur’s consumer-resource model”. In: *Theoretical Population Biology* 37.1 (1990), pp. 26–38.

[68] K Gopalsamy, MRS Kulenović, and G Ladas. “Environmental periodicity and time delays in a “food-limited” population model”. In: *Journal of Mathematical Analysis and Applications* 147.2 (1990), pp. 545–555.

[69] Philip H Warren. “Variation in food-web structure: the determinants of connectance”. In: *The American Naturalist* 136.5 (1990), pp. 689–700.

[70] H Eissfeller and M Opper. “New method for studying the dynamics of disordered spin systems without finite-size effects”. In: *Physical review letters* 68.13 (1992), p. 2094.

[71] Manfred Opper and Sigurd Diederich. “Phase transition and 1/f noise in a game dynamical model”. In: *Physical review letters* 69.10 (1992), p. 1616.

[72] Leticia F Cugliandolo and Jorge Kurchan. “Analytical solution of the off-equilibrium dynamics of a long-range spin-glass model”. In: *Physical Review Letters* 71.1 (1993), p. 173.

[73] Yang Kuang. *Delay differential equations*. Academic press New York, 1993.

[74] Pierre Baldi and Amir F Atiya. “How delays affect neural dynamics and learning”. In: *IEEE Transactions on Neural Networks* 5.4 (1994), pp. 612–621.

[75] Leticia F Cugliandolo, Jorge Kurchan, and Giorgio Parisi. “Off equilibrium dynamics and aging in unfrustrated systems”. In: *Journal de Physique I* 4.11 (1994), pp. 1641–1656.

[76] Peter Häunggi and Peter Jung. “Colored noise in dynamical systems”. In: *Advances in chemical physics* 89 (1994), pp. 239–326.

[77] Josef Hofbauer. “Heteroclinic cycles in ecological differential equations”. In: *Equadiff 8* (1994), pp. 105–116.

[78] David Tilman and John A Downing. “Biodiversity and stability in grasslands”. In: *Nature* 367.6461 (1994), pp. 363–365.

[79] Peter C De Ruiter, Anje-Margriet Neutel, and John C Moore. “Energetics, patterns of interaction strengths, and stability in real ecosystems”. In: *Science* 269.5228 (1995), pp. 1257–1260.

[80] Robert M Corless et al. “On the Lambert W function”. In: *Advances in Computational mathematics* 5.1 (1996), pp. 329–359.

[81] Jorge Kurchan and Laurent Laloux. “Phase space geometry and slow dynamics”. In: *Journal of Physics A: Mathematical and General* 29.9 (1996), p. 1929.

[82] Rita Levi-Montalcini. *Senz'olio contro vento*. Baldini & Castoldi, 1996.

[83] Wilson J Rugh. *Linear system theory*. Prentice-Hall, Inc., 1996.

[84] Carl Van Vreeswijk and Haim Sompolinsky. “Chaos in neuronal networks with balanced excitatory and inhibitory activity”. In: *Science* 274.5293 (1996), pp. 1724–1726.

[85] Martin Krupa. “Robust heteroclinic cycles”. In: *Journal of Nonlinear Science* 7.2 (1997), pp. 129–176.

[86] Enrique Nestor Miranda, Damián H Zanette, and Demian Reidel. “Statistical properties of random asymmetrical neural networks”. In: *Physica A: Statistical Mechanics and its Applications* 241.3-4 (1997), pp. 481–492.

[87] Josef Hofbauer and Karl Sigmund. *Evolutionary games and population dynamics*. Cambridge university press, 1998.

[88] Nigel Goldenfeld and Leo P Kadanoff. “Simple lessons from complexity”. In: *science* 284.5411 (1999), pp. 87–89.

[89] Jef Huisman and Franz J Weissing. “Biodiversity of plankton by species oscillations and chaos”. In: *Nature* 402.6760 (1999), pp. 407–410.

[90] John N Thompson. “The evolution of species interactions”. In: *Science* 284.5423 (1999), pp. 2116–2118.

[91] Sabri Arik. “Stability analysis of delayed neural networks”. In: *IEEE Transactions on Circuits and Systems I: Fundamental Theory and Applications* 47.7 (2000), pp. 1089–1092.

[92] Kwabena A. Boahen. “Point-to-Point Connectivity Between Neuromorphic Chips Using Address Events”. In: *IEEE Transactions on Circuits and Systems II: Analog and Digital Signal Processing* 47.5 (2000), pp. 416–434.

[93] Peter Chesson. “Mechanisms of maintenance of species diversity”. In: *Annual review of Ecology and Systematics* 31.1 (2000), pp. 343–366.

[94] Kevin Shear McCann. “The diversity–stability debate”. In: *Nature* 405.6783 (2000), pp. 228–233.

[95] Sandra Diaz and Marcelo Cabido. “Vive la différence: plant functional diversity matters to ecosystem processes”. In: *Trends in ecology & evolution* 16.11 (2001), pp. 646–655.

[96] H. Jaeger. *Short term memory in echo state networks*. 2001.

[97] Michel Loreau et al. "Biodiversity and ecosystem functioning: current knowledge and future challenges". In: *science* 294.5543 (2001), pp. 804–808.

[98] Robert M May. *Stability and complexity in model ecosystems*. Princeton university press, 2001.

[99] Per Jesper Sjöström, Gina G Turrigiano, and Sacha B Nelson. "Rate, timing, and cooperativity jointly determine cortical synaptic plasticity". In: *Neuron* 32.6 (2001), pp. 1149–1164.

[100] Evan Weiher and Paul Keddy. *Ecological assembly rules: perspectives, advances, retreats*. Cambridge University Press, 2001.

[101] Robert Zwanzig. *Nonequilibrium statistical mechanics*. Oxford university press, 2001.

[102] Hassan K Khalil and Jessy W Grizzle. *Nonlinear systems*. Vol. 3. Prentice hall Upper Saddle River, NJ, 2002.

[103] Wolfgang Maass, Thomas Natschläger, and Henry Markram. "Real-time computing without stable states: A new framework for neural computation based on perturbations". In: *Neural computation* 14.11 (2002), pp. 2531–2560.

[104] Jenny M Schmid-Araya et al. "Connectance in stream food webs". In: *Journal of Animal Ecology* (2002), pp. 1056–1062.

[105] Michio Kondoh. "Foraging adaptation and the relationship between food-web complexity and stability". In: *Science* 299.5611 (2003), pp. 1388–1391.

[106] Igor Volkov et al. "Neutral theory and relative species abundance in ecology". In: *Nature* 424.6952 (2003), pp. 1035–1037.

[107] James H Brown et al. "Toward a metabolic theory of ecology". In: *Ecology* 85.7 (2004), pp. 1771–1789.

[108] Gyorgy Buzsaki and Andreas Draguhn. "Neuronal oscillations in cortical networks". In: *science* 304.5679 (2004), pp. 1926–1929.

[109] Yan V Fyodorov. "Complexity of Random Energy Landscapes, Glass Transition, and Absolute Value¡? format?¿ of the Spectral Determinant of Random Matrices". In: *Physical review letters* 92.24 (2004), p. 240601.

[110] Herbert Jaeger and Harald Haas. "Harnessing nonlinearity: Predicting chaotic systems and saving energy in wireless communication". In: *science* 304.5667 (2004), pp. 78–80.

[111] Viktor K Jirsa and Mingzhou Ding. "Will a large complex system with time delays be stable?" In: *Physical review letters* 93.7 (2004), p. 070602.

[112] R Kupferman, Grigorios A Pavliotis, and Andrew M Stuart. "Itô versus Stratonovich white-noise limits for systems with inertia and colored multiplicative noise". In: *Physical Review E* 70.3 (2004), p. 036120.

[113] Bernardo Spagnolo, Davide Valenti, and Alessandro Fiasconaro. "Noise in ecosystems: a short review". In: *arXiv preprint q-bio/0403004* (2004).

[114] Pasquale Calabrese and Andrea Gambassi. "Ageing properties of critical systems". In: *Journal of Physics A: Mathematical and General* 38.18 (2005), R133.

[115] Till Daniel Frank. *Nonlinear Fokker-Planck equations: fundamentals and applications*. Springer, 2005.

[116] K-I Goh, B Kahng, and D Kim. “Nonlocal evolution of weighted scale-free networks”. In: *Physical Review E—Statistical, Nonlinear, and Soft Matter Physics* 72.1 (2005), p. 017103.

[117] Alex Roxin, Nicolas Brunel, and David Hansel. “Role of delays in shaping spatiotemporal dynamics of neuronal activity in large networks”. In: *Physical review letters* 94.23 (2005), p. 238103.

[118] Alessandro Scirè, Idán Tuval, and Víctor M Eguíluz. “Dynamic modeling of the electric transportation network”. In: *Europhysics Letters* 71.2 (2005), p. 318.

[119] Sandro Azaele et al. “Dynamical evolution of ecosystems”. In: *Nature* 444.7121 (2006), pp. 926–928.

[120] Axel Hutt and Fatihcan M Atay. “Effects of distributed transmission speeds on propagating activity in neural populations”. In: *Physical Review E—Statistical, Nonlinear, and Soft Matter Physics* 73.2 (2006), p. 021906.

[121] Shigui Ruan. “Delay differential equations in single species dynamics”. In: *Delay differential equations and applications*. Springer, 2006, pp. 477–517.

[122] Elad Schneidman et al. “Weak pairwise correlations imply strongly correlated network states in a neural population”. In: *Nature* 440.7087 (2006), pp. 1007–1012.

[123] Eric W Weisstein. “Generalized hypergeometric function”. In: *MathWorld-A Wolfram Web Resource* (2006).

[124] Changsong Zhou and Jürgen Kurths. “Dynamical weights and enhanced synchronization in adaptive complex networks”. In: *Physical review letters* 96.16 (2006), p. 164102.

[125] Yan V Fyodorov and H-J Sommers. “Classical particle in a box with random potential: exploiting rotational symmetry of replicated Hamiltonian”. In: *Nuclear Physics B* 764.3 (2007), pp. 128–167.

[126] Judith R Goodstein. *The Volterra chronicles: the life and times of an extraordinary mathematician, 1860-1940*. Vol. 31. American Mathematical Society, 2007.

[127] Robert Legenstein and Wolfgang Maass. “Edge of chaos and prediction of computational performance for neural circuit models”. In: *Neural networks* 20.3 (2007), pp. 323–334.

[128] Roberto Luzzi, ÁR Vasconoellos, and J Galvao Ramos. “Non-equilibrium statistical mechanics of complex systems: An overview”. In: *La Rivista del Nuovo Cimento* 30 (2007), pp. 95–157.

[129] Brian J McGill et al. “Species abundance distributions: moving beyond single prediction theories to integration within an ecological framework”. In: *Ecology letters* 10.10 (2007), pp. 995–1015.

[130] Anje-Margriet Neutel et al. “Reconciling complexity with stability in naturally assembling food webs”. In: *Nature* 449.7162 (2007), pp. 599–602.

[131] Ali Rahimi and Benjamin Recht. “Random features for large-scale kernel machines”. In: *Advances in neural information processing systems* 20 (2007).

[132] Igor Volkov et al. “Patterns of relative species abundance in rainforests and coral reefs”. In: *Nature* 450.7166 (2007), pp. 45–49.

[133] Elisa Benincà et al. “Chaos in a long-term experiment with a plankton community”. In: *Nature* 451.7180 (2008), pp. 822–825.

[134] Elias Jarlebring. “Some numerical methods to compute the eigenvalues of a time-delay system using MATLAB”. In: *The delay e-letter* 2 (2008), p. 155.

[135] Luis A. Plana et al. “An On-Chip and Inter-Chip Communications Network for the SpiNNaker Massively-Parallel Neural Net Simulator”. In: *Proceedings of the Second ACM/IEEE International Symposium on Networks-on-Chip (NoCS 2008)*. 2008, pp. 215–216.

[136] Mantas Lukoševičius and Herbert Jaeger. “Reservoir computing approaches to recurrent neural network training”. In: *Computer science review* 3.3 (2009), pp. 127–149.

[137] Johan Rockström et al. “A safe operating space for humanity”. In: *nature* 461.7263 (2009), pp. 472–475.

[138] S Ruan. “On Nonlinear Dynamics of Predator-Prey Modelswith Discrete Delay”. In: *Mathematical Modelling of Natural Phenomena* 4.2 (2009), pp. 140–188.

[139] David Sussillo and Larry F Abbott. “Generating coherent patterns of activity from chaotic neural networks”. In: *Neuron* 63.4 (2009), pp. 544–557.

[140] Fatihcan M Atay. *Complex time-delay systems: theory and applications*. Springer, 2010.

[141] Dante R Chialvo. “Emergent complex neural dynamics”. In: *Nature physics* 6.10 (2010), pp. 744–750.

[142] Angelo Guerraggio and Giovanni Paoloni. *Vito Volterra*. Springer-Verlag, 2010.

[143] Wolfram Just et al. “Delayed complex systems: an overview”. In: *Philosophical Transactions of the Royal Society A: Mathematical, Physical and Engineering Sciences* 368.1911 (2010), pp. 303–304.

[144] Michael Monteforte and Fred Wolf. “Dynamical entropy production in spiking neuron networks in the balanced state”. In: *Physical review letters* 105.26 (2010), p. 268104.

[145] Terence Tao and Van Vu. “Random matrices: Universality of ESDs and the circular law”. In: *The Annals of Probability* 38.5 (2010), pp. 2023–2065.

[146] Andrew G Haldane and Robert M May. “Systemic risk in banking ecosystems”. In: *Nature* 469.7330 (2011), pp. 351–355.

[147] Stephen P Hubbell. “The unified neutral theory of biodiversity and biogeography”. In: *The unified neutral theory of biodiversity and biogeography*. Princeton University Press, 2011.

[148] Kevin S McCann. “Food webs”. In: *Food Webs*. Princeton University Press, 2011.

[149] Camilo Mora et al. “How many species are there on Earth and in the ocean?” In: *PLoS biology* 9.8 (2011), e1001127.

[150] Thierry Mora and William Bialek. “Are biological systems poised at criticality?” In: *Journal of Statistical Physics* 144.2 (2011), pp. 268–302.

[151] Taro Toyoizumi and Larry F Abbott. “Beyond the edge of chaos: Amplification and temporal integration by recurrent networks in the chaotic regime”. In: *Physical Review E—Statistical, Nonlinear, and Soft Matter Physics* 84.5 (2011), p. 051908.

[152] Taro Toyoizumi and Larry F Abbott. “Beyond the edge of chaos: Amplification and temporal integration by recurrent networks in the chaotic regime”. In: *Physical Review E—Statistical, Nonlinear, and Soft Matter Physics* 84.5 (2011), p. 051908.

[153] Stefano Allesina and Si Tang. “Stability criteria for complex ecosystems”. In: *Nature* 483.7388 (2012), pp. 205–208.

[154] Wei Chen, Wei Lu, and Ning Zhang. “Time-critical influence maximization in social networks with time-delayed diffusion process”. In: *Proceedings of the AAAI Conference on Artificial Intelligence*. Vol. 26. 1. 2012, pp. 591–598.

[155] Dan Hu, David Cai, and Aaditya V. Rangan. “Blood Vessel Adaptation with Fluctuations in Capillary Flow Distribution”. In: *PLOS ONE* 7.9 (Sept. 2012), pp. 1–13.

[156] Carlo Bianca, Massimiliano Ferrara, and Luca Guerrini. “The time delays’ effects on the qualitative behavior of an economic growth model”. In: *Abstract and applied analysis*. Vol. 2013. 1. Wiley Online Library. 2013, p. 901014.

[157] Roberto Caminiti, Filippo Carducci, Claudia Piervincenzi, et al. “Diameter, length, speed, and conduction delay of callosal axons in macaque monkeys and humans: comparing data from histology and magnetic resonance imaging diffusion tractography”. In: *The Journal of Neuroscience* 33.36 (2013), pp. 14501–14511.

[158] Guillaume Lajoie, Kevin K Lin, and Eric Shea-Brown. “Chaos and reliability in balanced spiking networks with temporal drive”. In: *Physical Review E—Statistical, Nonlinear, and Soft Matter Physics* 87.5 (2013), p. 052901.

[159] Michel Loreau and Claire De Mazancourt. “Biodiversity and ecosystem stability: a synthesis of underlying mechanisms”. In: *Ecology letters* 16 (2013), pp. 106–115.

[160] Henrique Miguel Pereira et al. “Essential biodiversity variables”. In: *Science* 339.6117 (2013), pp. 277–278.

[161] Samir Suweis et al. “Emergence of structural and dynamical properties of ecological mutualistic networks”. In: *Nature* 500.7463 (2013), pp. 449–452.

[162] Tobias Brett and Tobias Galla. “Gaussian approximations for stochastic systems with delay: chemical Langevin equation and application to a Brusselator system”. In: *The Journal of chemical physics* 140.12 (2014).

[163] Charles K Fisher and Pankaj Mehta. “The transition between the niche and neutral regimes in ecology”. In: *Proceedings of the National Academy of Sciences* 111.36 (2014), pp. 13111–13116.

[164] Wulfram Gerstner et al. *Neuronal dynamics: From single neurons to networks and models of cognition*. Cambridge University Press, 2014.

[165] Si Tang, Samraat Pawar, and Stefano Allesina. “Correlation between interaction strengths drives stability in large ecological networks”. In: *Ecology letters* 17.9 (2014), pp. 1094–1100.

[166] Uwe C Täuber. *Critical dynamics: a field theory approach to equilibrium and non-equilibrium scaling behavior*. Cambridge University Press, 2014.

[167] Huaguang Zhang, Zhanshan Wang, and Derong Liu. “A comprehensive review of stability analysis of continuous-time recurrent neural networks”. In: *IEEE Transactions on Neural Networks and Learning Systems* 25.7 (2014), pp. 1229–1262.

[168] Tommaso Biancalani, Lee DeVille, and Nigel Goldenfeld. “Framework for analyzing ecological trait-based models in multidimensional niche spaces”. In: *Physical Review E* 91.5 (2015), p. 052107.

[169] Annalisa Capristo. “Volterra, Fascism, and France”. In: *Science in Context* 28.4 (2015), pp. 637–674.

[170] Francesca Fiegna et al. “Evolution of species interactions determines microbial community productivity in new environments”. In: *The ISME journal* 9.5 (2015), pp. 1235–1245.

[171] Yann Hautier et al. “Anthropogenic environmental changes affect ecosystem stability via biodiversity”. In: *Science* 348.6232 (2015), pp. 336–340.

[172] Alex James et al. “Constructing random matrices to represent real ecosystems”. In: *The American Naturalist* 185.5 (2015), pp. 680–692.

[173] Jonathan Kadmon and Haim Sompolinsky. “Transition to chaos in random neuronal networks”. In: *Physical Review X* 5.4 (2015), p. 041030.

[174] Sandro Azaele et al. “Statistical mechanics of ecological systems: Neutral theory and beyond”. In: *Reviews of Modern Physics* 88.3 (2016), p. 035003.

[175] Yan V Fyodorov and Boris A Khoruzhenko. “Nonlinear analogue of the May- Wigner instability transition”. In: *Proceedings of the National Academy of Sciences* 113.25 (2016), pp. 6827–6832.

[176] Marcella M Gomez et al. “Stability of systems with stochastic delays and applications to genetic regulatory networks”. In: *SIAM journal on applied dynamical systems* 15.4 (2016), pp. 1844–1873.

[177] Dominique Gravel, François Massol, and Mathew A Leibold. “Stability and complexity in model meta-ecosystems”. In: *Nature communications* 7.1 (2016), p. 12457.

[178] Jacopo Grilli, Tim Rogers, and Stefano Allesina. “Modularity and stability in ecological communities”. In: *Nature communications* 7.1 (2016), p. 12031.

[179] John A Hertz, Yasser Roudi, and Peter Sollich. “Path integral methods for the dynamics of stochastic and disordered systems”. In: *Journal of Physics A: Mathematical and Theoretical* 50.3 (2016), p. 033001.

[180] Claire Jacquet et al. “No complexity–stability relationship in empirical ecosystems”. In: *Nature communications* 7.1 (2016), p. 12573.

[181] Alexander Kuczala and Tatyana O Sharpee. “Eigenvalue spectra of large correlated random matrices”. In: *Physical Review E* 94.5 (2016), p. 050101.

[182] Ben Poole et al. “Exponential expressivity in deep neural networks through transient chaos”. In: *Advances in neural information processing systems* 29 (2016).

[183] Samuel S Schoenholz et al. “Deep information propagation”. In: *arXiv preprint arXiv:1611.01232* (2016).

[184] Shaopeng Wang and Michel Loreau. “Biodiversity and ecosystem stability across scales in metacommunities”. In: *Ecology letters* 19.5 (2016), pp. 510–518.

[185] György Barabás, Matthew J Michalska-Smith, and Stefano Allesina. “Self-regulation and the stability of large ecological networks”. In: *Nature ecology & evolution* 1.12 (2017), pp. 1870–1875.

[186] Guy Bunin. “Ecological communities with Lotka-Volterra dynamics”. In: *Physical Review E* 95.4 (2017), p. 042414.

[187] Jacopo Grilli et al. “Higher-order interactions stabilize dynamics in competitive network models”. In: *Nature* 548.7666 (2017), pp. 210–213.

[188] Rohit Jain and KL Sebastian. “Diffusing diffusivity: a new derivation and comparison with simulations”. In: *Journal of Chemical Sciences* 129.7 (2017), pp. 929–937.

[189] Andrew D. Letten, Po-Ju Ke, and Tadashi Fukami. “Linking Modern Coexistence Theory and Contemporary Niche Theory”. In: *Ecological Monographs* 87.2 (2017), pp. 161–177.

[190] Meghdad Saeedian et al. “Memory effects on epidemic evolution: The susceptible-infected-recovered epidemic model”. In: *Physical Review E* 95.2 (2017), p. 022409.

[191] Mikhail Tikhonov and Remi Monasson. “Collective phase in resource competition in a highly diverse ecosystem”. In: *Physical review letters* 118.4 (2017), p. 048103.

[192] Gang Yan, Neo D Martinez, and Yang-Yu Liu. “Degree heterogeneity and stability of ecological networks”. In: *Journal of the Royal Society Interface* 14.131 (2017), p. 20170189.

[193] Serhiy Yanchuk and Giovanni Giacomelli. “Spatio-temporal phenomena in complex systems with time delays”. In: *Journal of Physics A: Mathematical and Theoretical* 50.10 (2017), p. 103001.

[194] Madhu Advani, Guy Bunin, and Pankaj Mehta. “Statistical physics of community ecology: a cavity solution to MacArthur’s consumer resource model”. In: *Journal of Statistical Mechanics: Theory and Experiment* 2018.3 (2018), p. 033406.

[195] Matthieu Barbier et al. “Generic assembly patterns in complex ecological communities”. In: *Proceedings of the National Academy of Sciences* 115.9 (2018), pp. 2156–2161.

[196] Giulio Biroli, Guy Bunin, and Chiara Cammarota. “Marginally stable equilibria in critical ecosystems”. In: *New Journal of Physics* 20.8 (2018), p. 083051.

[197] Dylan Craven et al. “Multiple facets of biodiversity drive the diversity–stability relationship”. In: *Nature ecology & evolution* 2.10 (2018), pp. 1579–1587.

[198] Mike Davies et al. “Loihi: A Neuromorphic Manycore Processor with On-Chip Learning”. In: *IEEE Micro* 38.1 (2018), pp. 82–99.

[199] Tobias Galla. “Dynamically evolved community size and stability of random Lotka-Volterra ecosystems (a)”. In: *Europhysics Letters* 123.4 (2018), p. 48004.

[200] Mark Newman. *Networks*. Oxford university press, 2018.

[201] Jannis Schuecker, Sven Goedeke, and Moritz Helias. “Optimal sequence memory in driven random networks”. In: *Physical Review X* 8.4 (2018), p. 041029.

[202] Jannis Schuecker, Sven Goedeke, and Moritz Helias. “Optimal sequence memory in driven random networks”. In: *Physical Review X* 8.4 (2018), p. 041029.

[203] Lewi Stone. “The feasibility and stability of large complex biological networks: a random matrix approach”. In: *Scientific reports* 8.1 (2018), pp. 1–12.

[204] Masayuki Ushio et al. “Fluctuating interaction network and time-varying stability of a natural fish community”. In: *Nature* 554.7692 (2018), pp. 360–363.

[205] Ada Altieri and Silvio Franz. “Constraint satisfaction mechanisms for marginal stability and criticality in large ecosystems”. In: *Physical Review E* 99.1 (2019), p. 010401.

[206] Vasilis Dakos et al. “Ecosystem tipping points in an evolving world”. In: *Nature ecology & evolution* 3.3 (2019), pp. 355–362.

[207] Kevin Liautaud et al. “Superorganisms or loose collections of species? A unifying theory of community patterns along environmental gradients”. In: *Ecology letters* 22.8 (2019), pp. 1243–1252.

[208] Robert Marsland III et al. “Available energy fluxes drive a transition in the diversity, stability, and functional structure of microbial communities”. In: *PLoS computational biology* 15.2 (2019), e1006793.

[209] Pankaj Mehta et al. “Constrained optimization as ecological dynamics with applications to random quadratic programming in high dimensions”. In: *Physical Review E* 99.5 (2019), p. 052111.

[210] José Moran and Jean-Philippe Bouchaud. “May’s instability in large economies”. In: *Physical Review E* 100.3 (2019), p. 032307.

[211] Felix Roy et al. “Numerical implementation of dynamical mean field theory for disordered systems: Application to the Lotka–Volterra model of ecosystems”. In: *Journal of Physics A: Mathematical and Theoretical* 52.48 (2019), p. 484001.

[212] Chuan Yan and Zhibin Zhang. “Impacts of consumer–resource interaction transitions on persistence and long-term interaction outcomes of random ecological networks”. In: *Oikos* 128.8 (2019), pp. 1147–1157.

[213] Yasaman Bahri et al. “Statistical mechanics of deep learning”. In: *Annual review of condensed matter physics* 11.1 (2020), pp. 501–528.

[214] Joseph W Baron and Tobias Galla. “Dispersal-induced instability in complex ecosystems”. In: *Nature communications* 11.1 (2020), p. 6032.

[215] Wenping Cui, Robert Marsland III, and Pankaj Mehta. “Effect of resource dynamics on species packing in diverse ecosystems”. In: *Physical review letters* 125.4 (2020), p. 048101.

[216] Itay Dalmedigos and Guy Bunin. “Dynamical persistence in high-diversity resource-consumer communities”. In: *PLoS computational biology* 16.10 (2020), e1008189.

[217] Lana Descheemaeker and Sophie De Buyl. “Stochastic logistic models reproduce experimental time series of microbial communities”. In: *Elife* 9 (2020), e55650.

[218] Jacopo Grilli. “Macroecological laws describe variation and diversity in microbial communities”. In: *Nature communications* 11.1 (2020), p. 4743.

[219] Paulo R Guimaraes Jr. “The structure of ecological networks across levels of organization”. In: *Annual Review of Ecology, Evolution, and Systematics* 51.1 (2020), pp. 433–460.

[220] Jonathan Kadmon, Jonathan Timcheck, and Surya Ganguli. “Predictive coding in balanced neural networks with noise, chaos and delays”. In: *Advances in neural information processing systems* 33 (2020), pp. 16677–16688.

[221] Jeffrey C Magee and Christine Grienberger. “Synaptic plasticity forms and functions”. In: *Annual review of neuroscience* 43 (2020), pp. 95–117.

[222] Leonardo Pacciani-Mori et al. “Dynamic metabolic adaptation can promote species coexistence in competitive microbial communities”. In: *PLoS computational biology* 16.5 (2020), e1007896.

[223] Michael T Pearce, Atish Agarwala, and Daniel S Fisher. “Stabilization of extensive fine-scale diversity by ecologically driven spatiotemporal chaos”. In: *Proceedings of the National Academy of Sciences* 117.25 (2020), pp. 14572–14583.

[224] Marc Potters and Jean-Philippe Bouchaud. *A first course in random matrix theory: for physicists, engineers and data scientists*. Cambridge University Press, 2020.

[225] Felix Roy et al. "Complex interactions can create persistent fluctuations in high-diversity ecosystems". In: *PLoS computational biology* 16.5 (2020), e1007827.

[226] Laura Sidhom and Tobias Galla. "Ecological communities from random generalized Lotka-Volterra dynamics with nonlinear feedback". In: *Physical Review E* 101.3 (2020), p. 032101.

[227] Meng-Yu Tian et al. "Estimating the nonlinear effects of an ecological system driven by Ornstein-Uhlenbeck noise". In: *Chaos, Solitons & Fractals* 136 (2020), p. 109788.

[228] Michael te Vrugt and Raphael Wittkowski. "Projection operators in statistical mechanics: a pedagogical approach". In: *European Journal of Physics* 41.4 (2020), p. 045101.

[229] Ada Altieri et al. "Properties of equilibria and glassy phases of the random lotka-volterra model with demographic noise". In: *Physical Review Letters* 126.25 (2021), p. 258301.

[230] Joseph W Baron. "Consensus, polarization, and coexistence in a continuous opinion dynamics model with quenched disorder". In: *Physical Review E* 104.4 (2021), p. 044309.

[231] AR Batista-Tomás, Andrea De Martino, and Roberto Mulet. "Path-integral solution of MacArthur's resource-competition model for large ecosystems with random species-resources couplings". In: *Chaos: An Interdisciplinary Journal of Nonlinear Science* 31.10 (2021).

[232] Eran Bouchbinder et al. "Low-frequency vibrational spectrum of mean-field disordered systems". In: *Physical Review B* 103.17 (2021), p. 174202.

[233] Wenping Cui, Robert Marsland III, and Pankaj Mehta. "Diverse communities behave like typical random ecosystems". In: *Physical Review E* 104.3 (2021), p. 034416.

[234] Philip Doldo and Jamol Pender. "A note on the interpretation of distributed delay equations". In: *arXiv preprint arXiv:2106.11413* (2021).

[235] Deepak Gupta et al. "Effective resource competition model for species coexistence". In: *Physical review letters* 127.20 (2021), p. 208101.

[236] SMJ Khadem, NH Siboni, and SHL Klapp. "Transport and phase separation of active Brownian particles in fluctuating environments". In: *Physical Review E* 104.6 (2021), p. 064615.

[237] Yvonne Krumbeck et al. "Fluctuation spectra of large random dynamical systems reveal hidden structure in ecological networks". In: *Nature Communications* 12.1 (2021), p. 3625.

[238] Anne E Magurran. "Measuring biological diversity". In: *Current Biology* 31.19 (2021), R1174–R1177.

[239] Leonardo Pacciani-Mori et al. "Constrained proteome allocation affects coexistence in models of competitive microbial communities". In: *The ISME Journal* 15.5 (2021), pp. 1458–1477.

[240] Gian Marco Palamara, José A Capitán, and David Alonso. "The stochastic nature of functional responses". In: *Entropy* 23.5 (2021), p. 575.

[241] Nikos E Papanikolaou et al. "Predators' Functional Response: Statistical Inference, Experimental Design, and Biological Interpretation of the Handling Time". In: *Frontiers in Ecology and Evolution* (2021), p. 749.

[242] Pierfrancesco Urbani. “Disordered high-dimensional optimal control”. In: *Journal of Physics A: Mathematical and Theoretical* 54.32 (2021), p. 324001.

[243] Qianna Xu et al. “Consistently positive effect of species diversity on ecosystem, but not population, temporal stability”. In: *Ecology Letters* 24.10 (2021), pp. 2256–2266.

[244] Ada Altieri and Giulio Biroli. “Effects of intraspecific cooperative interactions in large ecosystems”. In: *SciPost Physics* 12.1 (2022), p. 013.

[245] Joseph W Baron et al. “Eigenvalues of random matrices with generalized correlations: A path integral approach”. In: *Physical Review Letters* 128.12 (2022), p. 120601.

[246] Giulia Garcia Lorenzana and Ada Altieri. “Well-mixed Lotka-Volterra model with random strongly competitive interactions”. In: *Physical Review E* 105.2 (2022), p. 024307.

[247] Jiliang Hu et al. “Emergent phases of ecological diversity and dynamics mapped in microcosms”. In: *Science* 378.6615 (2022), pp. 85–89.

[248] Yu Hu and Haim Sompolinsky. “The spectrum of covariance matrices of randomly connected recurrent neuronal networks with linear dynamics”. In: *PLoS computational biology* 18.7 (2022), e1010327.

[249] Jean-Didier Lemaréchal, Maciej Jedynak, Lena Trebaul, et al. “A brain atlas of axonal and synaptic delays based on modelling of cortico-cortical evoked potentials”. In: *Brain* 145.5 (2022), pp. 1653–1667.

[250] Alessandro Manacorda and Francesco Zamponi. “Gradient descent dynamics and the jamming transition in infinite dimensions”. In: *Journal of Physics A: Mathematical and Theoretical* 55.33 (2022), p. 334001.

[251] Gian Marco Palamara, José A Capitán, and David Alonso. “The implicit assumptions of classic functional responses and their multi-species extensions”. In: *bioRxiv* (2022), pp. 2022–07.

[252] Emanuele Pigani et al. “Delay effects on the stability of large ecosystems”. In: *Proceedings of the National Academy of Sciences* 119.45 (2022), e2211449119.

[253] Meghdad Saeedian et al. “Effect of delay on the emergent stability patterns in generalized Lotka–Volterra ecological dynamics”. In: *Philosophical Transactions of the Royal Society A* 380.2227 (2022), p. 20210245.

[254] Ion Santra, Urna Basu, and Sanjib Sabhapandit. “Effect of stochastic resetting on Brownian motion with stochastic diffusion coefficient”. In: *Journal of Physics A: Mathematical and Theoretical* 55.41 (2022), p. 414002.

[255] Yogev Yonatan et al. “Complexity–stability trade-off in empirical microbial ecosystems”. In: *Nature Ecology & Evolution* 6.6 (2022), pp. 693–700.

[256] Thibaut Arnoulx de Pirey and Guy Bunin. “Aging by near-extinctions in many-variable interacting populations”. In: *Physical Review Letters* 130.9 (2023), p. 098401.

[257] Joseph W Baron et al. “Breakdown of random-matrix universality in persistent Lotka-Volterra communities”. In: *Physical Review Letters* 130.13 (2023), p. 137401.

[258] Gérard Ben Arous, Paul Bourgade, and Benjamin McKenna. “Exponential growth of random determinants beyond invariance”. In: *Probability and Mathematical Physics* 3.4 (2023), pp. 731–789.

[259] Annalisa Caligiuri et al. “Lyapunov exponents for temporal networks”. In: *Physical Review E* 107.4 (2023), p. 044305.

[260] Patrick Charbonneau et al. *Spin glass theory and far beyond: replica symmetry breaking after 40 years*. World Scientific, 2023.

[261] David G Clark, LF Abbott, and Ashok Litwin-Kumar. “Dimension of activity in random neural networks”. In: *Physical Review Letters* 131.11 (2023), p. 118401.

[262] Jules Fraboul, Giulio Biroli, and Silvia De Monte. “Artificial selection of communities drives the emergence of structured interactions”. In: *Journal of Theoretical Biology* 571 (2023), p. 111557.

[263] Paul R Garabedian. *Partial differential equations*. Vol. 325. American Mathematical Society, 2023.

[264] Enrique Rozas Garcia, Mark J Crumpton, and Tobias Galla. “Niche overlap and Hopfield-like interactions in generalized random Lotka-Volterra systems”. In: *Physical Review E* 108.3 (2023), p. 034120.

[265] Alessandro Lonardi et al. “Infrastructure adaptation and emergence of loops in network routing with time-dependent loads”. In: *Physical Review E* 107.2 (2023), p. 024302.

[266] Giorgio Nicoletti et al. “Emergent encoding of dispersal network topologies in spatial metapopulation models”. In: *Proceedings of the National Academy of Sciences* 120.46 (2023), e2311548120.

[267] Giorgio Parisi. “Nobel lecture: Multiple equilibria”. In: *Reviews of Modern Physics* 95.3 (2023), p. 030501.

[268] Lyle Poley, Joseph W Baron, and Tobias Galla. “Generalized Lotka-Volterra model with hierarchical interactions”. In: *Physical Review E* 107.2 (2023), p. 024313.

[269] Katherine Richardson et al. “Earth beyond six of nine planetary boundaries”. In: *Science advances* 9.37 (2023), eadh2458.

[270] Valentina Ros and Yan V Fyodorov. “The high-dimensional landscape paradigm: Spin-glasses, and beyond”. In: *Spin Glass Theory and Far Beyond: Replica Symmetry Breaking After 40 Years*. World Scientific, 2023, pp. 95–114.

[271] Valentina Ros et al. “Generalized lotka-volterra equations with random, nonreciprocal interactions: The typical number of equilibria”. In: *Physical Review Letters* 130.25 (2023), p. 257401.

[272] Valentina Ros et al. “Quenched complexity of equilibria for asymmetric generalized lotka–volterra equations”. In: *Journal of Physics A: Mathematical and Theoretical* 56.30 (2023), p. 305003.

[273] Marcello Seppi et al. “Emergent Functional Organization of Gut Microbiomes in Health and Diseases”. In: *Biomolecules* 14.1 (2023), p. 5.

[274] John J Wiens. “How many species are there on Earth? Progress and problems”. In: *PLoS biology* 21.11 (2023), e3002388.

[275] Yuguang Yang et al. “Time delays modulate the stability of complex ecosystems”. In: *Nature Ecology & Evolution* 7.10 (2023), pp. 1610–1619.

[276] Guim Aguadé-Gorgorió, Alexander RA Anderson, and Ricard Solé. “Modeling tumors as complex ecosystems”. In: *iScience* 27.9 (2024).

[277] Guim Aguadé-Gorgorió et al. “A taxonomy of multiple stable states in complex ecological communities”. In: *Ecology Letters* 27.4 (2024), e14413.

[278] Fabián Aguirre-López. “Heterogeneous mean-field analysis of the generalized Lotka–Volterra model on a network”. In: *Journal of Physics A: Mathematical and Theoretical* 57.34 (2024), p. 345002.

[279] Imane Akjouj et al. “Complex systems in ecology: a guided tour with large Lotka–Volterra models and random matrices”. In: *Proceedings of the Royal Society A* 480.2285 (2024), p. 20230284.

[280] Ada Altieri and Marco Baity-Jesi. “An introduction to the theory of spin glasses”. In: *Encyclopedia of Condensed Matter Physics (Second Edition)*. Second Edition. Oxford: Academic Press, 2024, pp. 361–370.

[281] Thibaut Arnoulx de Pirey and Guy Bunin. “Many-species ecological fluctuations as a jump process from the brink of extinction”. In: *Physical Review X* 14.1 (2024), p. 011037.

[282] Sandro Azaele and Amos Maritan. “Generalized Dynamical Mean Field Theory for Non-Gaussian Interactions”. In: *Physical Review Letters* 133.12 (2024), p. 127401.

[283] Giovanni Ballarin, Lyudmila Grigoryeva, and Juan-Pablo Ortega. “Memory of recurrent networks: Do we compute it right?” In: *Journal of Machine Learning Research* 25.243 (2024), pp. 1–38.

[284] Emmy Blumenthal, Jason W Rocks, and Pankaj Mehta. “Phase Transition to Chaos in Complex Ecosystems with Nonreciprocal Species-Resource Interactions”. In: *Physical Review Letters* 132.12 (2024), p. 127401.

[285] José Camacho-Mateu et al. “Sparse species interactions reproduce abundance correlation patterns in microbial communities”. In: *Proceedings of the National Academy of Sciences* 121.5 (2024), e2309575121.

[286] Can Chen, Xu-Wen Wang, and Yang-Yu Liu. “Stability of ecological systems: A theoretical review”. In: *Physics Reports* 1088 (2024), pp. 1–41.

[287] Luca Cocconi et al. “The OU2 process: characterising dissipative confinement in noisy traps”. In: *New Journal of Physics* 26.10 (2024), p. 103016.

[288] Wenping Cui, Robert Marsland III, and Pankaj Mehta. “Les Houches Lectures on Community Ecology: From Niche Theory to Statistical Mechanics”. In: *ArXiv* (2024).

[289] Tobias Galla. “Generating-functional analysis of random Lotka-Volterra systems: A step-by-step guide”. In: *arXiv preprint arXiv:2405.14289* (2024).

[290] Giulia Garcia Lorenzana, Ada Altieri, and Giulio Biroli. “Interactions and migration rescuing ecological diversity”. In: *PRX Life* 2.1 (2024), p. 013014.

[291] Ian A Hatton et al. “Diversity begets stability: Sublinear growth and competitive coexistence across ecosystems”. In: *Science* 383.6688 (2024), eadg8488.

[292] Yizhou Liu, Jiliang Hu, and Jeff Gore. “Ecosystem stability relies on diversity difference between trophic levels”. In: *Proceedings of the National Academy of Sciences* 121.50 (2024), e2416740121.

[293] Emil Mallmin, Arne Traulsen, and Silvia De Monte. “Chaotic turnover of rare and abundant species in a strongly interacting model community”. In: *Proceedings of the National Academy of Sciences* 121.11 (2024), e2312822121.

[294] Stav Marcus, Ari M Turner, and Guy Bunin. “Local and extensive fluctuations in sparsely interacting ecological communities”. In: *Physical Review E* 109.6 (2024), p. 064410.

[295] Onofrio Mazzarisi and Matteo Smerlak. “Complexity-stability relationships in competitive disordered dynamical systems”. In: *Physical Review E* 110.5 (2024), p. 054403.

[296] Marc Mézard. “Spin glass theory and its new challenge: structured disorder”. In: *Indian Journal of Physics* (2024).

[297] Egbert H van Nes et al. “A tiny fraction of all species forms most of nature: Rarity as a sticky state”. In: *Proceedings of the National Academy of Sciences* 121.2 (2024), e2221791120.

[298] Jong Il Park et al. “Incorporating heterogeneous interactions for ecological biodiversity”. In: *Physical Review Letters* 133.19 (2024), p. 198402.

[299] Laura Sidhom and Tobias Galla. “Higher-order interactions in random Lotka-Volterra communities”. In: *arXiv preprint arXiv:2409.10990* (2024).

[300] Samir Suweis et al. “Generalized lotka-volterra systems with time correlated stochastic interactions”. In: *Physical Review Letters* 133.16 (2024), p. 167101.

[301] Thibaut Arnoulx de Pirey and Guy Bunin. “Critical behavior of a phase transition in the dynamics of interacting populations”. In: *SciPost Physics* 18.2 (2025), p. 051.

[302] Matthieu Barbier. “Disordered systems in community ecology: a tutorial”. In: (2025).

[303] Matthieu Barbier, Guy Bunin, and Mathew A Leibold. “Getting more by asking for less: linking species interactions to species co-distributions in metacommunities”. In: *Peer Community Journal* 5 (2025).

[304] Annalisa Caligiuri, Tobias Galla, and Lucas Lacasa. “Characterizing the dynamics of unlabeled temporal networks”. In: *Chaos: An Interdisciplinary Journal of Nonlinear Science* 35.5 (2025).

[305] Annalisa Caligiuri et al. “Time-varying ecological interactions characterise equilibrium and stability”. In: *arXiv preprint arXiv:2506.22123* (2025).

[306] Violeta Calleja Solanas, Ignasi Bartomeus, and Oscar Godoy. “Time-varying interactions drive species coexistence via rainfall variation”. In: *bioRxiv* (2025), pp. 2025–11.

[307] Alice Doimo et al. “Finite-size scaling of survival statistics in metapopulation models”. In: *Physical Review E* 111.6 (2025), p. 064415.

[308] Francesco Ferraro et al. “Exact solution of dynamical mean-field theory for a linear system with annealed disorder”. In: *Journal of Statistical Mechanics: Theory and Experiment* 2025.2 (2025), p. 023301.

[309] Francesco Ferraro et al. “Synchronization and chaos in complex ecological communities with delayed interactions”. In: *arXiv preprint arXiv:2503.21551* (2025).

[310] Juan Giral Martínez. “Symmetry-based approach to species-rich ecological communities”. In: *Physical Review E* 111.1 (2025), p. 014415.

[311] Juan Giral Martínez, Matthieu Barbier, and Silvia De Monte. “Interplay of structured and random interactions in complex ecosystems dynamics”. In: *PLOS Computational Biology* 21.12 (2025), e1013786.

[312] Juan Giral Martínez, Silvia De Monte, and Matthieu Barbier. “Stabilization of macroscopic dynamics by fine-grained disorder in many-species ecosystems”. In: *Phys. Rev. E* 112 (3 2025), p. 034305.

[313] Akshit Goyal, Jason W Rocks, and Pankaj Mehta. “Universal niche geometry governs the response of ecosystems to environmental perturbations”. In: *PRX Life* 3.1 (2025), p. 013010.

[314] Deepak Gupta and Sabine HL Klapp. “Non-equilibrium fluctuations in a harmonic trap with annealed stochastic stiffness”. In: *Journal of Statistical Mechanics: Theory and Experiment* 2025.10 (2025), p. 103204.

[315] Jiliang Hu et al. “Transition from global stability to multiple attractors in microcosms”. In: (2025).

[316] Tommaso Jack Leonardi, Amos Maritan, and Sandro Azaele. “Griffiths phase emerging from strong mutualistic disorder in high-dimensional interacting systems”. In: *arXiv preprint arXiv:2509.24692* (2025).

[317] Fernando L Metz. “Dynamical mean-field theory of complex systems on sparse directed networks”. In: *Physical Review Letters* 134.3 (2025), p. 037401.

[318] Jacopo Pasqualini et al. “Microbiomes Through The Looking Glass: Linking Species Interactions to Dysbiosis through a Disordered Lotka-Volterra Framework”. In: *eLife* (2025).

[319] Thibaut Arnoulx de Pirey. “Self-organized criticality in complex model ecosystems”. In: *arXiv preprint arXiv:2512.06961* (2025).

[320] Lyle Poley, Tobias Galla, and Joseph W Baron. “Interaction networks in persistent Lotka-Volterra communities”. In: *Physical Review E* 111.1 (2025), p. 014318.

[321] Bo-Wei Qin et al. “Reordered hierarchical complexity in ecosystems with delayed interactions”. In: *PNAS Nexus* 4.7 (2025), pgaf214.

[322] Davide Zanchetta, Amos Maritan, and Sandro Azaele. “Modeling postdisturbance empirical patterns in a forest ecosystem”. In: *Physical Review E* 112.4 (2025), p. 044408.

[323] Davide Zanchetta et al. “Emergence of ecological structure and species rarity from fluctuating metabolic strategies”. In: *PRX Life* 3.3 (2025), p. 033016.

[324] Pau Colom et al. “Three Decades of Butterfly–Plant Interaction Turnover Explained by Climate and Species Loss”. In: *Ecology Letters* 29.3 (2026), e70361.

[325] Francesco Ferraro et al. “Will a time-varying complex system be stable?” In: *arXiv preprint arXiv:2603.28464* (2026).

[326] Samantha Fournier and Pierfrancesco Urbani. “Chaos in high-dimensional dynamical systems with tunable non-reciprocity”. In: *arXiv preprint arXiv:2601.04702* (2026).

[327] James FD Henderson and Andreas Tiffeau-Mayer. “Fluctuating environments are sufficient to drive substantial variability in species abundance across locations”. In: *arXiv preprint arXiv:2603.02403* (2026).

[328] Amer Al-Hiyasat et al. “Spatiotemporal noise stabilizes unbounded diversity in strongly-competitive communities”. In: *arXiv preprint arXiv:2602.13423* (2026).

[329] Pablo Lechón-Alonso et al. “Robust coexistence in competitive ecological communities”. In: *Nature Communications* (2026).

[330] Tommaso Tonolo et al. “Generalized Lotka-Volterra model with sparse interactions: non-Gaussian effects and topological multiple-equilibria phase”. In: *PRX Life* 4.1 (2026), p. 013017.

[331] Marco Zenari et al. “Generalized Lotka-Volterra systems with quenched random interactions and saturating nonlinear response”. In: *Physical Review E* 113.2 (2026), p. 024206.

Funding information

I acknowledge financial support funded under the National Recovery and Resilience Plan (NRRP), Mission 4, Component 2 Investment 1.4 - Call for tender No. 3138 of 16 December 2021, rectified by Decree No. 3175 of 18 December 2021 of Italian Ministry of University and Research funded by the European Union - NextGenerationEU; Award Number: Project code CN00000033, Concession Decree No. 1034 of 17 June 2022 adopted by the Italian Ministry of University and Research, CUP C93C22002810006, Project title "National Biodiversity Future Center - NBFC". I additionally acknowledge financial support received from the Istituto Nazionale di Fisica Nucleare (INFN) Padova Division, Fondazione Alma Dal Co ETS, and Young Researchers of the Complex Systems Society (SECS grant).